2017-01-01

Material Behavior of Window 7 Carrier Panel Tiles and Thermal Pane Fragments Recovered from the Space Shuttle Columbia

Brenda Roseanne Arellano
University of Texas at El Paso, brarellano9@gmail.com

MATERIAL BEHAVIOR OF WINDOW 7 CARRIER PANEL TILES AND THERMAL PANE FRAGMENTS RECOVERED FROM THE SPACE SHUTTLE COLUMBIA

BRENDA R. ARELLANO

Doctoral Program in Materials Science and Engineering

APPROVED:

Stephen W. Stafford, Ph.D., Chair

Anupama B. Kaul, Ph.D.

Jorge Lopez, Ph.D.

Peter Golding, Ph.D.

Charles Ambler, Ph.D.
Dean of the Graduate School

Dedication

To my parents and sister.

MATERIAL BEHAVIOR OF WINDOW 7 CARRIER PANEL TILES AND THERMAL PANE FRAGMENTS RECOVERED FROM THE SPACE SHUTTLE COLUMBIA

by

BRENDA R. ARELLANO, B.S in Metallurgical and Materials Engineering

DISSERTATION

Presented to the Faculty of the Graduate School of

The University of Texas at El Paso

in Partial Fulfillment

of the Requirements

for the Degree of

DOCTOR OF PHILOSOPHY

Materials Science and Engineering

THE UNIVERSITY OF TEXAS AT EL PASO

May 2017

Acknowledgements

This dissertation could not have been completed without the support I have received from many people over the years. I would like to offer my sincere appreciation for the following people. To my advisor and dissertation chair, Dr. Stafford for his guidance, knowledge, and for allowing me to pursue research on a topic for which I am truly passionate. Thank you for your advice, support, and being available as I progressed through my research. I would also like to express my gratitude to Darren Cone who was a tremendous help throughout the development and completion of my project. Thank you for keeping your office door open and sharing your knowledge. Thank you to John "Danny" Olivas for bringing CASSMAR to UTEP and having the opportunity to make an important contribution to *Columbia*. I would also like to acknowledge NASA's *Columbia* Research and Preservation Office at KSC that provided our research group with access to the debris. I have a large appreciation for Dr. Kaul, Dr. Lopez, and Dr. Golding for serving as my dissertation committee. Special thanks to Dr. Lopez and Dr. Carlos Diaz Moreno from the Physics Department at UTEP for contributing to this work. I would also like to thank the Metallurgical, Materials, and Biomedical Engineering (MMBME) Department faculty especially during my undergraduate studies who have prepared me for my professional career. I will never forget my first research experiences under Dr. S.K. Varma, that prepared me for graduate school. To Miss Bea, thank you for caring about all metallurgy students, I appreciate all the advice you have given me throughout the years.

Lastly, I want to give my heartfelt thanks to additional people that have provided wonderful encouragement. To my parents who have supported me throughout the period of my education. To my sister, Roxy who has been my mentor, best friend, and my role model. To my friends, colleagues, and students I've gotten to know in the department; thank you for the conversations, advice, friendships, and laughter. I could not have done this without you all.

Abstract

Since the end of the space shuttle program, a new generation spacecraft has been developed to transport humans back into space. NASA's Orion will carry a crew beyond low-earth orbit and the exploration of Mars may be possible in the future. Space safety becomes significant with human spaceflight and the risks are high. However, aerospace materials may provide opportunities to prevent future disasters. When the space shuttle *Columbia* disintegrated during re-entry in 2001, thousands of debris were collected for analysis. In contrast, when the Challenger space shuttle broke apart in 1986, all shuttle debris were buried. These tragic disasters are reminders of the importance of proper material selection and the concern of their performance in service. This research focused on investigating the effects of the debris recovered from the *Columbia* space shuttle after re-entry and break-up. Many of the components encountered unforeseen extreme temperatures, vibrations, and high stresses. The *Columbia* debris contained unique characteristics that have yet to be examined and the components for this study are the thermal protection system (TPS) carrier panel tiles and the thermal pane glass from the starboard orbiter Window 7. The alterations endured by the debris was studied through forensic materials characterization to investigate material interactions, material degradation, and thermal consequences. These materials played an essential role in the operation of the orbiter as they protected the underlying structural materials of the shuttle and underwent extreme temperatures. The methods and procedures for analyzing the debris included non-destructive and destructive evaluations. Non-destructive evaluations involved visual inspection, photographic documentation, 3D modeling, and surface elemental composition. The destructive analysis consisted of sectioning, scanning electron microscopy, energy dispersive spectroscopy, X-ray diffraction, and X-ray photoelectron spectroscopy. The results obtained revealed metallic and oxide formations, flow trajectory, and the presence of other space shuttle materials. Determining the conditions of the debris after break-up is valuable because new developments for future manned spacecraft will require TPS. These materials must be continued to be studied aggressively to provide risk assessment for future missions. The findings

of this investigation will identify the alterations on the debris and determine if these TPS materials are reliable for future spacecraft.

Table of Contents

List of Tables

List of Figures

Chapter 1: Introduction

Spaceflight disasters are moments that remind engineers and scientists about the risks of traveling to space. The *Columbia* space shuttle disaster was one of the most tragic events in spaceflight history. The shuttle broke apart while entering earth's atmosphere on February 1, 2003, taking the lives of the STS-107 crew. The *Columbia* Accident Investigation Board (CAIB) was formed to obtain data from the shuttle and analysis of the recovered debris. Many pieces of the shuttle were found throughout Texas and Louisiana and the reconstruction team was able to determine a timeline of events of the accident. The CAIB declared that the cause of failure was a piece of insulating foam that broke off the external tank after launch. It struck the leading edge of the left wing allowing super-heated gasses to enter and melt the wing from the inside out during the shuttle's return to Earth's atmosphere. After the wing was destroyed, the shuttle lost control while spinning and broke a part due to aerodynamic forces and thermal stresses.

The *Columbia* space shuttle had left a large impact on the aerospace community and the focus of this work was to study the recovered debris with the intention to prevent future material related spaceflight accidents. One recommendation from the CAIB report insisted on further examination of techniques to prevent structural failure of the crew module caused by thermal degradation. More information on the debris should be provided for future vehicles carrying a crew.

The thermal protection system of hypersonic traveling vehicles is crucial to shield the vehicle and payload from the extreme temperatures encountered during re-entry. Extreme aerodynamic temperatures during high-speed flight cause elevated temperatures that may affect the structural components of the vehicle. The role of the TPS is to preserve the temperatures of the structural components of the vehicle within operational limits to prevent failures. NASA used TPS technology for the space shuttle program that allowed for a reusable spacecraft carrying payloads and astronauts. The debris obtained from the space shuttle *Columbia* after the accident provides the opportunity to determine the ways spacecraft materials respond to off-nominal conditions of re-entry.

The debris analyzed included the carrier panel tiles and thermal pane fragments belonging to the starboard orbiter window seven of *Columbia*. The analysis will determine the ways these materials responded to the extreme conditions of re-entry. The research will begin with an overview of thermal protection systems, experimental methods, results, and discussion. After a thorough investigation, having preformed materials forensic characterization techniques, identification of the possible sources of depositions will be explained.

1.1 *Columbia* Disaster

The first orbiter to be flown into space during NASA's space shuttle program was the *Columbia* space shuttle that first launched in 1981 [1]. The shuttle went on to complete 27 missions and operated for 22 years up until the STS-107 final mission. It was a science mission that the crew of seven aboard *Columbia* were set to research. The shuttle was launched on January 16, 2003 from the Kennedy Space Center and it was not known at the time that a debris strike occurred on the external tank just after launching. At 81.7s several pieces of debris detached from the external tank and struck the reinforced carbon-carbon panels of the left wing. The seven crew members went on to conduct microgravity research and experiments for commercial payloads. The mission lasted 15 days and as *Columbia* was returning to the atmosphere on February 1, 2003, the orbiter disintegrated. Hot atmospheric gasses entered the thermal protection system of the leading edge of the left wing causing melting of the aluminum frame leading to the breakup.

After the incident, the *Columbia* Accident Investigation Board (CAIB) gathered all material and data to investigate the accident. Fallen debris was recovered from east Texas to west Louisiana. Approximately 85,000 pieces of debris were found and sent to the *Columbi*a debris hangar at the Kennedy Space Center. The reconstruction team pieced the found debris together based on their locations and in the end, 38% of the shuttle was recovered. After gathering the debris, it was confirmed that the breach occurring on the wing allowed heat to enter the wing causing it to weaken. Failure of the wing took place

followed by a loss of control of the orbiter and the final breakup. The debris analysis became a large part of the CAIB and provided clues to the events that took place during the accident by modeling, mechanical testing, and other analytical techniques.

Figure 1.1 The *Columbia* debris recovered and laid out to where the pieces were on the Orbiter [1].

Because the orbiter experienced extreme temperatures, hypersonic velocities, and exposure to high altitudes; studying these effects of orbital materials can provide insights onto how aerospace materials react under such conditions. Commercial spaceflight companies are continuing their pursuit of space research, re-supply missions to the International Space Stations, or determined to visit Mars in the future. To keep producing reliable transportation vehicles, the way aerospace materials fail under extreme conditions must be studied aggressively. Space safety measures may also be improved.

1.2 Objectives

The aim of this research is to examine the material effects of a component of the shuttle to determine how the material reacted under unforeseen extreme environments. The *Columbia* debris contains unique characteristics that have yet to be thoroughly examined and the component of the study is the overhead window seven located directly above the crew module. The thermal protection system of the window will be the focus of research along with the remaining protective outer glass thermal pane. These two materials played a large role in protecting the orbiter because they experienced extreme temperatures and protected the underlying structural materials of the shuttle. The re-entry effects that will be examined include;

1. investigating materials interactions
2. material degradation
3. evidence of thermal consequences

The analysis will include identifying and quantifying a number of deposits using forensic materials characterization. Damage to the carrier panel tiles and thermal pane fragments will be determined through a non-destructive evaluation. Investigating the existence of metallic and non-metallics will provide more insights regarding flow trajectory, sequencing of deposit events, and the possible presence of other materials used on the space shuttle. Characterizing the materials behavior is needed to understand the TPS subsystem response to a minor or major breach. The results obtained from this investigation will identify the alterations on the debris and determine if these TPS materials are reliable for future spacecraft.

1.3 Overview of Dissertation

Additional background for the thermal protection system and thermal glass panes will be discussed in Chapter 2 along with past studies on these materials. Chapter 3 contains the experimental procedures performed in this investigation that include visual inspection, surface elemental analysis, and destructive analysis. The first phase of this research involved a non-destructive evaluation to assess the condition of

the as-received component. A preliminary analysis was conducted where Chapter 5 includes a sectioning procedure for the TPS, removal of a carrier panel, analysis of the unaffected loaned samples, analysis of glass shards, and Window 8 TPS results. The results and discussion is presented on Chapter 6 which includes all results obtained from the characterization techniques. A final chapter describing the conclusions of the research are discussed on Chapter 7.

Chapter 2: Literature Review

The materials that make up thermal protection systems for hypersonic spacecraft have much improved since the first shuttle, *Columbia*. New TPS materials were later introduced however, the TPS became a highly important part of the design process of spacecraft. This chapter will provide insights on how the TPS for the space shuttle program was developed and the materials chosen for TPS. A few studies were conducted on shuttle TPS along with the fabrication of new TPS materials.

2.1 Thermal Protection System and the Shuttle

The first re-usable commercial spacecraft was NASA's space shuttle that consisted of a large cargo capacity and transporting humans into space. The space shuttle program was responsible for the building of the International Space Station (ISS), launching satellites and allowed for a variety of research experiments. The shuttle was a multipurpose engineering marvel and was a success for space technology for the U.S. The space shuttle consisted of a reusable shuttle orbiter, solid rocket boosters, and an external tank. It was designed to be a round trip vehicle that was capable of carrying payloads up to 50,000 pounds with a crew. A reusable space shuttle required the orbiter to be shielded with a thermal protection system (TPS). Earlier spacecraft such as Mercury, Gemini, and Apollo used ablative heat shields [2]. The ablative heat shields dissipate incoming high heat fluxes by an endothermic process that ultimately leads to a loss and depletion of the ablative material itself [3] [4]. Rather than ablation, the shuttle was fitted with a TPS that dissipated heat.

The thermal protection system used in the shuttle program proved to be successful in reusability and protection of the orbiters. The space shuttle orbiter required a protective coating for aerodynamic heating therefore, the TPS was designed to perform as a radiator, a reflector, and an insulator. The orbiter was fitted by a thermal insulation system that consists of various materials in different configurations to protect the shuttle and crew. It was developed to be reusable, able to withstand high-temperature re-entry heating, and extremely cold temperatures at the night phase. Additionally, decreasing the weight of the

space shuttle was critical and required light materials able to be repaired at a low-cost. The re-entry temperatures the obiter's external surface experienced up to 1648°C (3000°F) [2] [5] [6] thus, a thermal protection system demanded a light aerodynamic surface while protecting the orbiter's metal skin.

2.1.1 Thermal Protection System Development

During 1970 and 1973, NASA developed various technologies for thermal protection that resulted in the selection of low-density ceramic tiles bonded to a lightweight structure [2]. A skin-stringer 2024-T6 aluminum aircraft structure [7] [8] that could withstand 350°F for the shuttle's orbiter skin was chosen and a silica-based insulation material for thermal protection. NASA used this material to manufacture heat-resistant tiles and other coatings to protect the shuttle's airframe. The thermal protection shield was sectioned into various smaller tiles to be tailored to the orbiter's structure. Areas such as the nose cap and wing leading edges experienced the highest heating temperatures thus utilizing several different types of thermal protection materials. Three major materials were designed for *Columbia* to include [9] [10] [11] [5];

1. Reinforced Carbon-Carbon (RCC)
2. Low and High-Temperature Reusable Surface Insulation Tiles (LRSI and HRSI)
3. Felt Reusable Surface Insulation (FRSI) blankets

These materials would be placed on different areas of the orbiter depending on their weight, temperature limits, and durability. The tiles were individually numbered and consisted of a time-consuming placement and replacement. Generally, these materials had high-emissivity coatings for maximum rejection of incoming convective heat through radiative heat transfer based on the temperatures of the orbiter. Figure 2.1 shows the typical re-entry temperature variations of the surfaces of the orbiter recorded from STS-1 to STS-5 [12]. Other design considerations consisted of enduring launch acoustics, structural deflection created by aerodynamic loads, low temperatures of space while on orbit, and other natural environments [7]. The shape of the TPS could not be altered in any way for repeated missions, weather thermal shocks, or gradients.

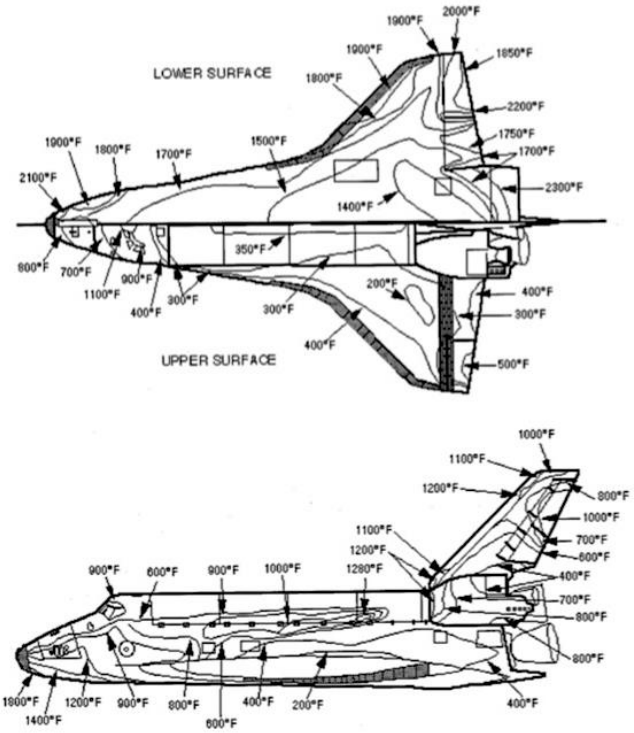

Figure 2.1 Surface temperatures experienced by the space shuttle during re-entry [12] [10].

The black or white tiles seen on the upper or lower surfaces of the space shuttle, protected the Orbiter against temperatures of 1200 and 2500°F [12] [10] [9]. The High-Temperature Reusable Insulation (HRSI) tiles contained a black borosilicate glass coating with maximum emissivity. The Low-Temperature Reusable Insulation (LRSI) tiles possessed a white coating with high thermal reflectivity for thermal control. Both HRSI and LRSI tiles are made up of 99.7% pure amorphous silica fibers that were light weight and heat resistant [10] [9]. The FRSI blankets were made up of a nylon felt material with a white silicone elastomer for waterproofing. Silica contains the chemical formula of SiO_2 and it is an oxide of silicon. Approximately 31,000 tiles were used on *Columbia* covering 70% of the surface [7]. The leading edges and the nose of the shuttle were protected by RCC panels as it is the hottest region during re-entry. The areas these TPS materials were placed on the shuttle are shown in Figure 2.2. HRSI tiles were used on the upper forward fuselage, windows, the whole underside of the vehicle where RCC is not used, portions of the OMS/RCS pods, leading and trailing edges of the vertical stabilizer, wing glove areas, elevon trailing edges next to the RCC on the upper wing surface, the base heat shield, interface with wing leading edge RCC, and upper body flap surface [6].

The HRSI and LRSI tiles were manufactured in blocks and machined to the desired shapes before the coating application. A fiber slurry is created, pressed, and sintered at a specific high temperature and duration for ceramic bonding [9] [10]. Rigidized blocks of the silica fibers are then cut to desired geometries. Either a white coating for LRSI tiles or a black coating for HRSI tiles was applied to the silica fiber substrate material.

The reaction-cured glass (RCG) coatings for the HRSI tiles are applied by spraying and are constructed of blended glass powders mixed with thickeners and pigments [13] [11] [14]. It contains powdered borosilicate glass with a black pigment (silicon tetraboride) for high-temperature emittance [9]. The coating is sprayed onto the individual tiles and heated that provides a waterproof glossy coating. These tiles were manufactured by Lockheed Missiles & Space Company designated as LI-900 with a bulk density of 9 pounds per cubic foot [2] [12] [7]. They were used to minimize thermal conductivity, weight, and maximum thermal shock resistance. A higher-strength material was developed later as the LI-2200 with 22 pounds per cubic foot bulk density [5]. Several advantages of utilizing silica tiles include excellent insulating properties due to the 93% of void. The low coefficient of thermal expansion obtained from amorphous silica and low modulus of the tiles removes thermal stress and thermal shock problems [4]. Silica also has a high-temperature resistance of above 1480°C (2700°F) for a small amount of time. The smooth aerodynamic surface and its performance provided a successful protection of the underlying structure throughout the shuttle program.

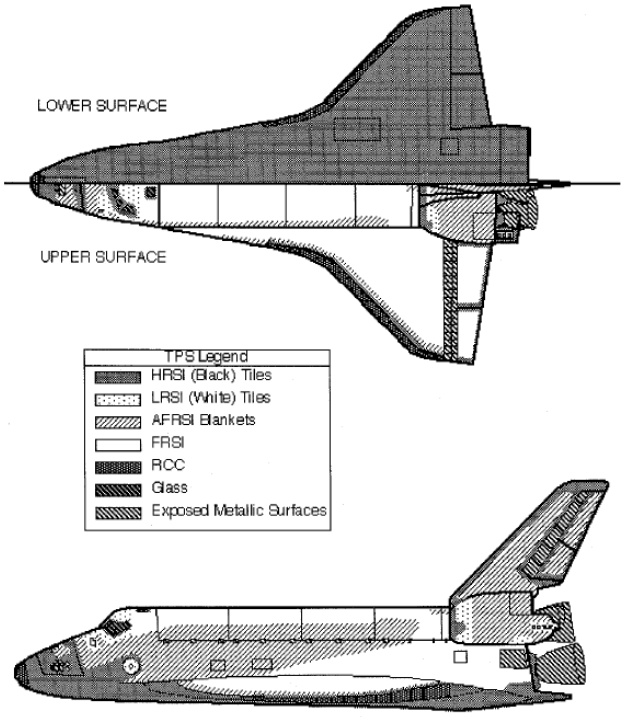

Figure 2.2 Various thermal protection system materials and their placement on the space shuttle [12] [9].

2.1.2 TPS Construction

The orbiter tiles consisted of four major pieces; a ceramic tile, a nylon felt mounting pad, filler material, and room-temperature vulcanizing (RTV) adhesives as demonstrated on Figure 2.3. The tiles were bonded to the orbiter using silicone adhesives because they remain flexible at low temperatures during the cold segments of orbit and maintain good bond strength at high temperatures during re-entry [5] [10] [12]. First, the tiles are bonded to a Strain Isolation Pad (SIP) comprised of a needled Nomex felt material before adhering to the aluminum airframe. They limit the vibration experienced during the ascent to orbit and thermal strains of the airframe. The inner mold line of the tile was densified before the SIP bonding, which allowed for the uniform distribution of the stress concentration loads at the tile-to-strain isolation pad interface. The gaps between the tiles were necessary because of the difference in thermal expansion properties between the tiles and the airframe. The gaps are allowed to expand and contract since the tiles contract much less than the airframe due to the difference in thermal expansion.

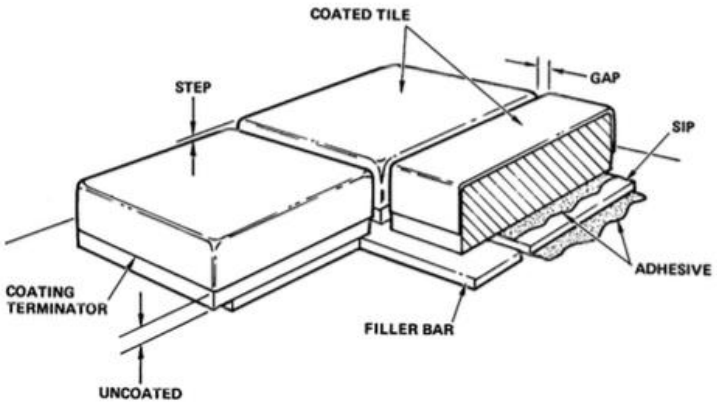

Figure 2.3 Typical configuration of the thermal protection system [4] [10].

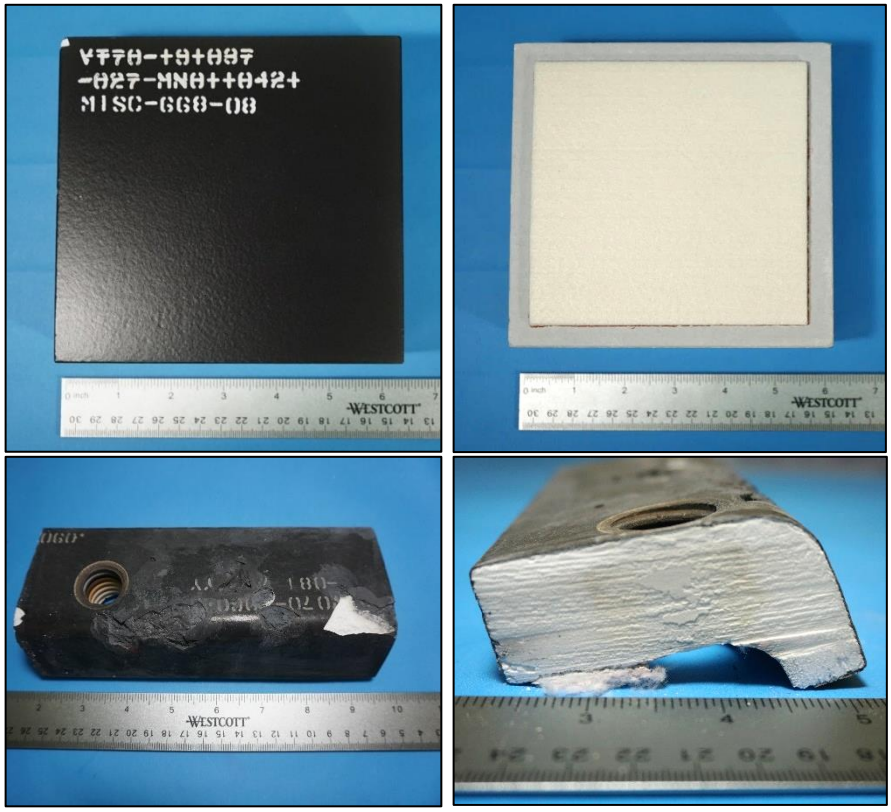

Figure 2.4 Exemplar HRSI tile used in the orbiter containing a black RCG coating and the underside of the tile shows the SIP. A carrier panel identical to those located at shuttle windows was also obtained. The cross-section is also presented after sectioning through the tile.

2.1.3 TPS Performance

Although the tiles were extremely brittle and could not withstand any loads, the thermal protection properties were excellent due to heat dissipation. This was a result of the coating that reradiated heat to

the atmosphere. The low diffusivity of the silica base material limited the remaining heat. Inspections were carried out to assess the condition of the tiles where the common flight outcomes included impact damage, gap filler damage, tile damage, tile slumping, thermal barrier damage, and window contamination/ impacts [1] [10] [9] [5]. Tile to tile gap heating also took place in several locations causing tile sidewall shrinkage, filler bar charring, and localized temperature gradients [9]. The TPS incorporated all shuttle materials and effectively protected the vehicle. There were no thermally induced failures during any flight during the beginning stages of the shuttle program [7]. The TPS reacted well to different weather conditions and debris damage from re-entry. The surface damages to the RSI tiles were in the forms of impacts, gouges, and coating chips that have occurred on all flights [1] [10] [9]. Although damages occurred during all flights, there were no severe damages.

However, the space shuttle TPS proved to be successful until the STS-107 accident in 2003 where the foam piece compromised the wing's TPS. The CAIB insisted on changes for material and design modifications, new inspections, material repairing, and training for the subsequent orbiters. New types of tiles replaced some areas of the HRSI tiles called fibrous refractory composite insulation (FRCI) [6]. They had higher strength from adding alumina and borosilicate fibers to the pure silica tile slurry. The black reaction cured class coating was compressed while curing to reduce the cracking sensitivity of the coating. They became 10% lighter than HRSI tiles and a tensile strength three times greater than HRSI tiles [15]. The service temperature was also improved by approximately 100°F higher than the HRSI tiles. Advanced flexible reusable surface insulation (AFRSI) was developed after *Columbia* [6]. It contained sewn composite quilted fabric insulation batting between two layers of white fabric and sews together to create a quilted blanket. Discovery and the Atlantis shuttle used AFRSI to replace the majority of LRSI tiles [6].

Today, spacecraft such as NASA's Orion contains a thermal protection system similar to the Apollo and Space Shuttle TPS [5]. The Johnson Space Center developed a TPS for the crew module of Orion that consists of coated tiles bonded to a SIP similar to those the space shuttle. The cone-shaped back shell is comprised of 970 black coated tiles that protected the space shuttle over three decades and 135 missions of returning from space [16]. Orion also travels at higher velocities compared to the space shuttle

at 20,000 miles per hour compared to 17,000 miles per hour. For this reason, continuing to study the re-entry behavior of the TPS becomes relevant [17].

2.1.4 Space Shuttle Windshields

A critical part of the TPS were the outer panes of the space shuttle windshields because they kept high re-entry temperatures away from the crew module and experienced the same environment as the vehicle. The crew module consisted of eleven windows (6 forward, 2 overhead, 1 side hatch, and 2 rearview [10]) and a total of eight windows were located above the flight deck as shown in Figure 2.5. All windows contained a similar construction of three panes; an internal pressure pane, redundant pressure pane, and a fused silica outer pane (Figure 2.6) [18] [19] [10]. The first pane from *Columbia* Windows 7 and 8 on the inner crew side is a thermally tempered aluminosilicate pressure pane to withstand the crew compartment pressure. Next, the second redundant pane is also made up of tempered aluminosilicate glass and is used for additional pressure containment. The outer pane or thermal pane attached to the forward fuselage provides the thermal protection of the crew module and is comprised of fused silica glass. The two overhead windows were identical to the six forward windows apart from the thickness. The inner and center panes were 0.45 of an inch thick and the outer pane is 0.68 of an inch thick. Windows 7 and 8 provided a viewing area of 20 by 20 inches.

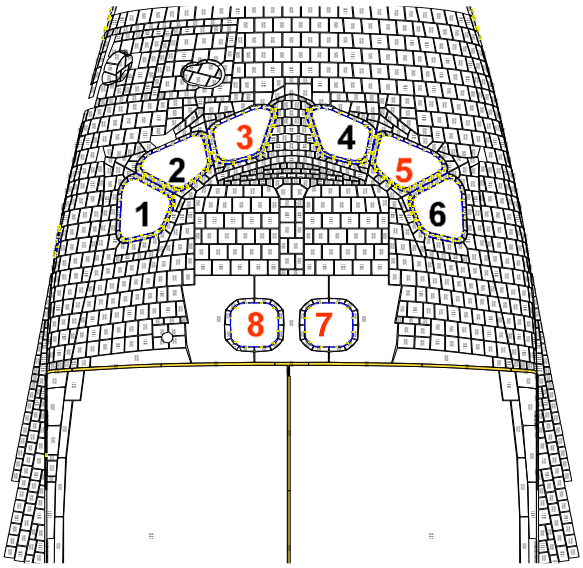

Figure 2.5 Window placements on the Orbiter with overhead Window 7 (starboard) and Window 8 (port) above the crew module [19].

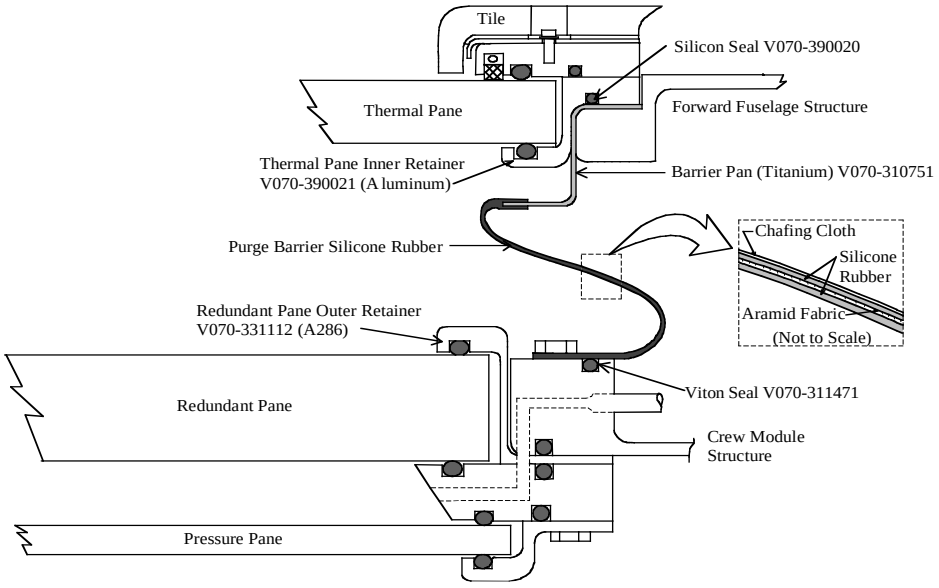

Figure 2.6. Typical construction of Shuttle windows illustrating three panes and tile placement [19].

The strength of the thermal pane is critical and must remain undamaged in order to provide thermal protection. Impacts or damages would eventually affect the window's strength. The eleven-crew module windows account for less than 1% of the orbiter, however; it has been reported that they contained the majority of the records in the orbiter impact data sheet [20]. The cause of this was the response of the fused silica material under hypervelocity conditions that permitted detection of small impact pits [21]. Contamination also occurred on the thermal pane during each flight. Forty-six shuttle windshields have been documented to have been replaced on flights up to STS-68 as result of impact pits [10] [22]. Several impacts on the crew module windows were examined and found to be micrometeoroid residues in the central pit regions [23] [22]. Many traces of impacts were manmade or of meteoric origin. The history of the remaining Window 7 thermal pane is also unknown, and any major anomalous features observed in this study, are assumed to have occurred after the accident.

2.1.5 Previous Analyses

Several *Columbia* components have been studied [1] however, microstructural examinations on TPS have been limited [24] [25]. Nonetheless, the shuttle windshields were first examined to determine the remnants deposited on the windows before and after *Columbia* took off. Fragments of the orbiter windows were collected for the analysis where distinct dark "char layer" was found to be present on

several thermal window panes [24] [19] [18]. All window panes contained this opaque layer and a few examples are shown in Figure 2.7 as a dull coating on the glass. Electron microscope imaging showed an adhered char layer on a Window 8 pane illustrated in Figure 2.8. The layer contained a variety of chemical compositions with an abundant aluminum weight percentage as a result of aluminum alloy oxidation. The alloys closest to the window frames were 2000 series aluminum alloys including 2219 and 7075 alloys [19]. Other elements detected were iron, copper, and oxygen. A sample was obtained from Window 7 where another distinct layer was present after the aluminum-rich layer. This high titanium region was directly applied to the glass and was made up of a Ti/Al mixture. Globules of silicon were also present with other metallic particles. The globules may have been silica droplets that make up the thermal protection system materials. The layered cross-section of the major elements detected is shown in Figure 2.9. Calcium was also found in large amounts but the origin of this element could not be determined. TEM analysis accompanied with EDS was used to confirm the three different phases seen on Window 8. A cross-sectional area is given in Figure 2.9 where the three variances in layered deposits are shown [2]. The three different layers were only present on orbiter Windows 7 and 8 at the exterior. The first inner layer on Figure 2.9 contained titanium dioxide (TiO_2) rutile form grains whereas the following outer layer was an aluminosilicate phase. The last porous layer was consistent with a 2000 series Al alloy composition. These layers were deposited from materials close to the window components. The titanium source may have been a result of orbital structural members which are made up of a Ti-6Al-4V alloy. A mechanism was suggested as the reason for the formation of the three depositions by a process of titanium combustion and plasma sprayed coating behavior [24].

Figure 2.7 Windows 4-6 frames with remaining thermal pane glass. Window 5 opaque thermal pane glass is also shown [19].

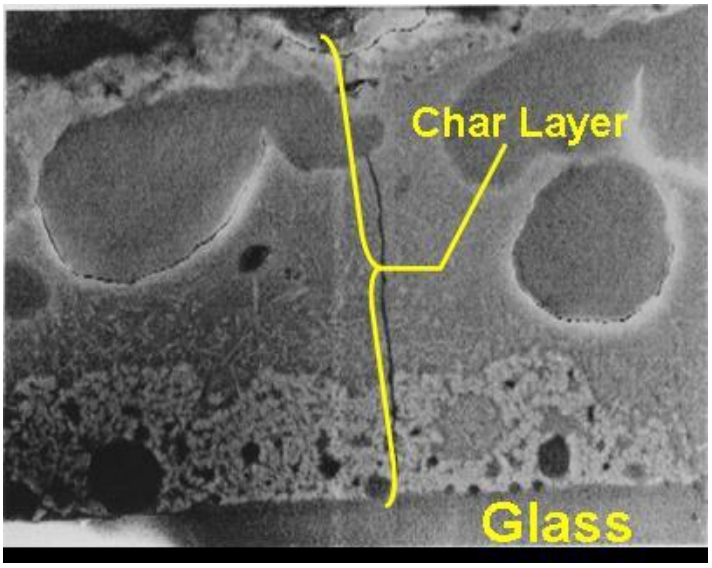

Figure 2.8. The morphology of a Window 8 thermal pane cross-section (500X) [19].

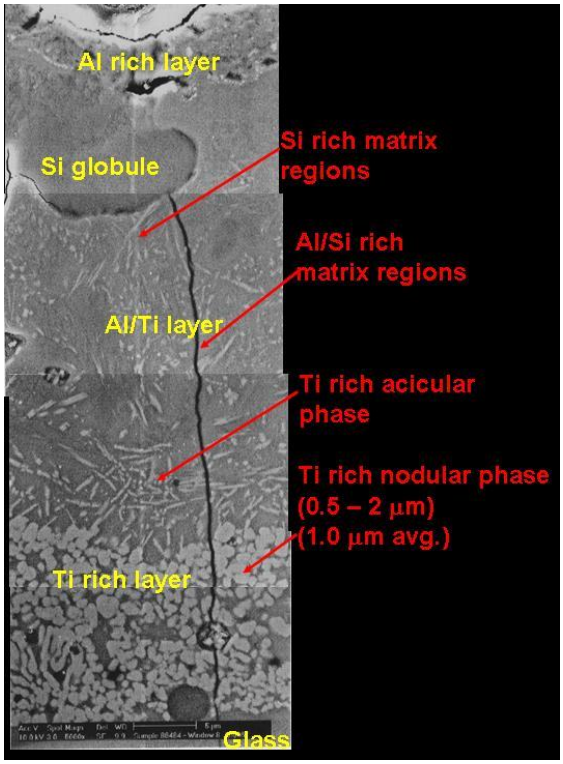

Figure 2.9 The layer structure of the char layer found on Window 8 [19].

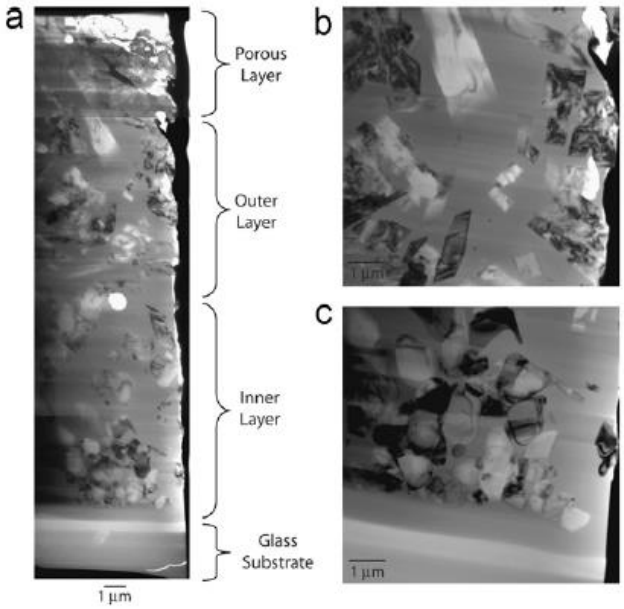

Figure 2.10 TEM bright field image of the window cross-sections showing the different structure in the cross-section [24].

2.1.6 Outcomes of the *Columbia* accident

As mentioned before the CAIB analyzed several recovered debris. The right wing and left wing debris showed that the left wing experienced high heat and aerodynamic forces while the right wing suffered from aerodynamic forces only. Several changes in the shuttle program were suggested in the CAIB report after the accident. The RCC panel of the left wing was the first component of the orbiter to fail. Tiles obtained from the lower left wing contained evidence of slumping or heat damage with erosion [1]. Deposits were also discovered on RCC debris where layered slag deposits were present in metallic and non-metallic forms. Other spherical deposits were also found and made up of an Inconel 718 alloy. This type of alloy could be found in the wing leading edge attachment fittings. There was also a difference in deposits found on the left and right wings. The deposits on the left wing were rough had evidence of insulation material. Figure 2.11 shows an example of a deposit found on the left wing on the RCC panel with Inconel 718 particles. This proves that extreme heating for long times occurred. No aluminum was detected on the slag layers. Other locations with deposits were thin and contained primarily aluminum and aluminum oxides mixed with A-286, Inconel, and Cerachrome (insulation material) [1]. The layers containing these deposits were not uniform. This assortment of metals indicates simultaneous melting and re-depositing of the components surrounding the wing. All results determined that the original breach occurred at the RCC panel 8 on the left wing.

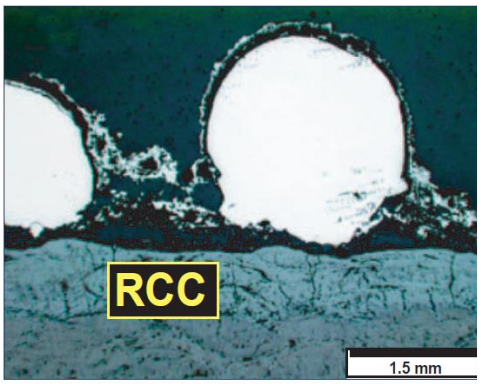

Figure 2.11 Spheroid deposits of Inconel 718 found on the surface of the RCC panel of the left wing [1].

Because of the findings of the accident and studying the TPS impact damages through all shuttle missions, several changes in the TPS were recommended by the CAIB. The new tile material of LI-2200 (22lb/ft^3) replaced the original LI-900 (9lb/ft^3) system [26] [2]. However, the higher density of the LI-2200 made the material heavier and was used in areas where additional strength was required. Other new materials were created by adding different fibers to silica. Aluminum borosilicate fiber was added and it provided a stronger and higher-temperature capability. Fibrous Refractory Composite Insulation (FRCI) and Alumina-Enhanced Thermal Barrier (AETB) were two types of these new materials. Previously mentioned, FRCI contained aluminum borosilicate fibers mixed with silica fibers that produced good thermal shock resistance [26]. Adding alumina in AETB materials enhanced the temperature capability and had excellent debris impact resistance [1] [27]. AETB was used in areas where small particles would damage tiles [2]. The RCG coating was also improved with a new coating that was developed for high-temperature rigid insulation also known as Toughened Uni-piece Fibrous Insulation (TUFI) [1] [2]. The uni-piece did not contain a coating or substrate, it had a gradual transition. It had improved impact resistance and was used in other space shuttles with great results [26]. It is used on an Alumina Enhanced Thermal Barrier (AETB) tile with excellent debris impact resistance [1] [27]. These were only placed in smaller areas of the orbiter. All improvements did reduce the weight of the orbiter, provided greater resistance to orbital debris, and increased mechanical properties.

New research developments in TPS include metallic TPS using a superalloy honeycomb TPS [28] [29] [27]proposed for the X-33 vehicle and a titanium multiwall TPS [30]. In the recent years, new novel materials have been developed to improve high-temperature resistance while maintaining a low weight. Materials such as ultra-high temperature ceramics (UHTCs) that possess high melting temperature, thermal shock resistance, great mechanical, and chemical stability at elevated temperatures [31] [32] [33] [34] [35]. Several examples include ZrB2-based ceramics for leading edges and nose cones for reusable hypersonic vehicles [32] [31]. Other contenders for UHTCs are hafnium, titanium, and zirconium with

different additives due to their high-temperature properties. Arc-jet testing of different configurations of ZrB2-based specimens showed good oxidation resistance at extreme temperatures [36]. Ceramic matrix composites (CMCs) also have excellent properties such as high heat resistance, resist up to 1600C, light-weight, low thermal expansion, and oxidation resistance [8] [37].

Chapter 3: Experimental Procedures

The component for this study was loaned by the *Columbia* Research and Preservation Office at the Kennedy Space Center. The starboard orbiter window located above the crew module was obtained in the as-received condition. The window contained two fastened carrier panels and one detached panel. The TPS for this experiment were directly attached to the panels along the window and fastened by pairs of screws. The remaining thermal pane fragments were also attached to the window including the window frame.

3.1 Non-Destructive Evaluation, NDE

Visual examination of Window 7 was essential in examining the as-is configuration of the component, determining dimensions, recognizing surface imperfections, locating alterations, deformation, and possible deposits. Along with photographic documentation, three-dimensional modeling was also performed to preserve the natural state of the window and retain a record of the window's dimensions. The PhotoModeler Scanner software was used to stitch a 3D image using photographs of the component by using an algorithm to generate dense point clouds form pairs of the images with textured surfaces. X-ray fluorescence (XRF) using an Olympus Innov-X Delta handheld analyzer was performed all along the window surfaces in order to semi-quantitatively identify the elemental species present and determine areas of interest. The surface of the desired area to be measured is irradiated by photons or charged particles of sufficient energy to cause its elements to emit or fluoresce their characteristic X-ray line spectra. The elements are identified by their spectral line energies and their intensities are related to the concentrations of elements for quantitative analysis (in weight percentages). XRF measurements were able to provide initial answers to existing depositions.

3.3 Sample Preparation

Based on the results from the non-destructive analysis, several areas were chosen for this investigation. The areas of interest consisted of removing carrier panel tile and thermal pane specimens. Metallography was performed to examine the morphology of tile cross-sections and identify damage. The process required samples to be sectioned, mounted, ground, and cleaned.

A sectioning technique was developed to extract samples directly from the tiles as each tile is attached to a window panel. A representative tile was used to determine the proper cutting tools. Several sectioning tools were tested to select the proper sectioning procedures to determine which cause damage and provide accurate dimensions. This sectioning technique was performed on the window's carrier panel tiles to extract samples for analysis. A carrier panel was first removed from the window frame to determine if sectioning would cause the surrounding areas to break. Several samples were obtained and re-sectioned to smaller pieces for equipment sizing requirements.

After all samples were sectioned, they were mounted in a two-part epoxy mount and ground to obtain an even cross-section with silicon carbide grit paper. Tile samples were ground from 600 to 1200 silicon carbide grit paper. This was done in order to reveal the TPS coating interface for SEM/EDS analysis. No alumina or diamond slurries were sued to prevent contamination of the porous TPS coating and fibers. After the grinding process, samples were ultrasonically cleaned with methanol.

3.4 Scanning Electron Microscopy, SEM

SEM was performed on all samples to study the tile surface morphology and tile cross-sections. Because of the non-conductive nature of the tile and glass, samples were required to be coated with a conductive element. The samples were sputter coated with a target material of Au/Pd to eliminate charging using a Gatan 682 Precision Etching Coating System. The tile surfaces were analyzed by SEM and TPS coating cross-sections were analyzed by SEM.

SEM was performed on all samples with a Hitachi S-4800 microscope equipped with EDS at the operating conditions of:

1. Accelerating voltage range of 10-20Kv
2. Probe current of 10-25 μA
3. Working distance of 8 to 15mm
4. EDS dwell time of 30s

A second SEM instrument was also used along with its energy dispersive spectrometer detector on the Hitachi TM-1000. The EDS system on this microscope only detects heavier elements and does not detect oxygen. Both instruments were used for analyzing all samples. Characterization was carried out on the samples using EDS (electron dispersive spectroscopy) with EDAX 5.21 Genesis Imaging and Mapping software. EDS is a qualitative and quantitative technique that provides information on the chemical composition of a sample in a point or area of a micrograph. EDS analysis was used to identify the elemental compositions of deposits present at the deposit scales. X-ray mapping was used to create individual element map of an image to determine the spatial distribution. X-ray maps are composed of recording the number of X-ray photons with their specific energy at each point for a pixel on a secondary or backscattered electron image. The X-ray beam rasters over the area to be mapped and collects the image information including the X-ray data. The final map consists of single element maps with different assigned colors. Element maps show the different phases in an SEM image. EDS spot readings were also performed. Samples were characterized by surface analysis, microstructural features of cross-sections, and elemental analysis.

3.5 X-Ray Diffraction, XRD

XRD was used to identify the compounds present in the carrier panel tiles and glass fragments. XRD analysis was conducted using a D8 Discovery X-Ray Diffractometer with a Cu Kα radiation using:

1. All samples used a scan rate of 5°/min

2. A 0.8mm slit on the X-ray source and a 8mm slit on the detector.
3. Voltage of 40KV
4. Current of 40mA

XRD measurements were taken on the surfaces of the tile samples in order to obtain compound information. One limitation of this technique is that XRD cannot identify amorphous materials, thus only characterizing crystalline materials. The International Center for Diffraction Data database for X-ray diffraction patterns provides the phase identifications of numerous crystalline materials. For this investigation, XRD was used for the identification and characterization of compounds based on the diffraction pattern. The basis of the XRD experiment involves an incident beam of monochromatic X-rays that interact with the material and the scattering of the X-rays from the atoms within the material. The scattering X-rays from crystalline materials go through constructive and destructive interference. When this occurs, the process of diffraction of X-rays meets the Bragg's Law criteria ($n\lambda=2d\sin\theta$) [38]. It is only satisfied by constructive interference. Bragg's Law relates the wavelength to the lattice spacing in a crystalline material and diffraction angle. The diffracted X-rays depend on the arrangement of the atoms in a crystal structure. Analyzing samples at different angles will produce all possible diffraction directions of the lattice are obtained.

3.6 X-Ray Photoelectron Spectroscopy, XPS

Information about a material's thin surface layer may lead to a further identification of surface deposits. X-ray Photoelectron Spectroscopy (XPS) is a surface sensitive quantitative technique to surface chemistry including identification of elements and their state [39] [40]. XPS works on the principal of the photoelectric effect where incoming electrons impact a surface and cause the core electrons to ionize and release photoelectrons. An analyzer measures the kinetic energy of electrons that escape from the top layers of the analyzed material. XPS is able to identify and measure concentrations of elements in the

surface as each element has a unique set of binding energies. XPS is equipped with ion sputter-etching capabilities to remove surface contaminants.

The surfaces of the sectioned TPS samples were analyzed to attempt to verify the deposits present. XPS analyses were carried out with a PHI 5600 spectrometer with a hemispherical energy analyzer, using magnesium (MgK_{α}) source of 1253.6 eV at 100 Watts. The measurements were carried out on the sample after argon sputtering exposure of 10 minutes at 25μA and $15x10^{-3}$ Pa. Additional test parameters used for all tests include:

1. The pressure in the analysis chamber during XPS analysis was in the low range of 10^{-9} Torr.
2. All spectra were recorded at 54° take off angle, the analyzed area being currently about 800 μm. All spectra were recorded with 1.0 eV step, 10 cycles, 40 sweeps and corrected using carbon signal (C1s) at 284.5 eV.
3. XPS spectra were analyzed using Casa-XPS software version2.3.12. The Shirley method was used for extracting the background necessary for curve fitting.

Chapter 4: Non-Destructive Evaluation

Previous data [24] [19] indicates that a deposition event occurred during re-entry and breakup of the *Columbia* space shuttle in different assortments. The char layer was identified on window glass samples in three distinct layers. One layer consisted of TiO_2 crystals, the second had TiO_2 mixed with mullite crystals, and a final layer of metallic aluminum. This deposition event is investigated on the TPS from the orbiter Window 7. The loaned *Columbia* component was obtained in the as-received condition. A forensic characterization of the carrier panel tiles and several glass fragments was performed and the results are reported in this section. The first phase of this investigation consists of a non-destructive evaluation to document the component's original state, obtain evidence of flow trajectory, and determine areas of interest.

4.1 Visual Examination and Photographic Documentation

The visual inspection was performed as part of the preliminary NDE examination to; establish and document the as-is configuration of the window assembly, determine the surface condition of the thermal carrier panel tiles and the thermal pane glass. The overall Window 7 components are shown in Figure 4.1, with a corresponding legend to depict the relative orientation with respect to the vehicle (Figure 2.5). The window is approximately $3\frac{1}{2}$feet long and $2\frac{3}{4}$feet tall and was originally attached to the forward fuselage of the orbiter. The first carrier panel tile was received detached from the window during the debris recovery. This is shown in Figure 4.1 as the first panel consisting of three HRSI tiles located on the forward (front) port (left) side of the window. The tiles were approximately 8 inches long and $3\frac{1}{2}$ inches wide. These carrier panel tiles are screwed into aluminum outer retainers to the window frame and face the outside of the shuttle. The sizing of the carrier panel tiles varied particularly the thickness of the tiles, as they were tailored to the curved shape of the orbiter. Figure 4.2 shows the rectangular carrier panels

located on the orbiter windows for comparison. The second carrier panel that remained on the window was the forward starboard (right) tiles. On the aft (below) end of the window, one panel is missing while panel 3 contains only one HRSI tile as shown in Figure 4.1. Under the carrier panels as described in Figure 2.6, are the opaque thermal pane remains of the outermost surviving layer of the window. The thermal pane is mostly removed while fractured pieces are located on the aft and the forward end of the window. Larger fragmented pieces of the glass are shown in location 4. A part of the window frame from the aluminum forward fuselage remains attached as shown.

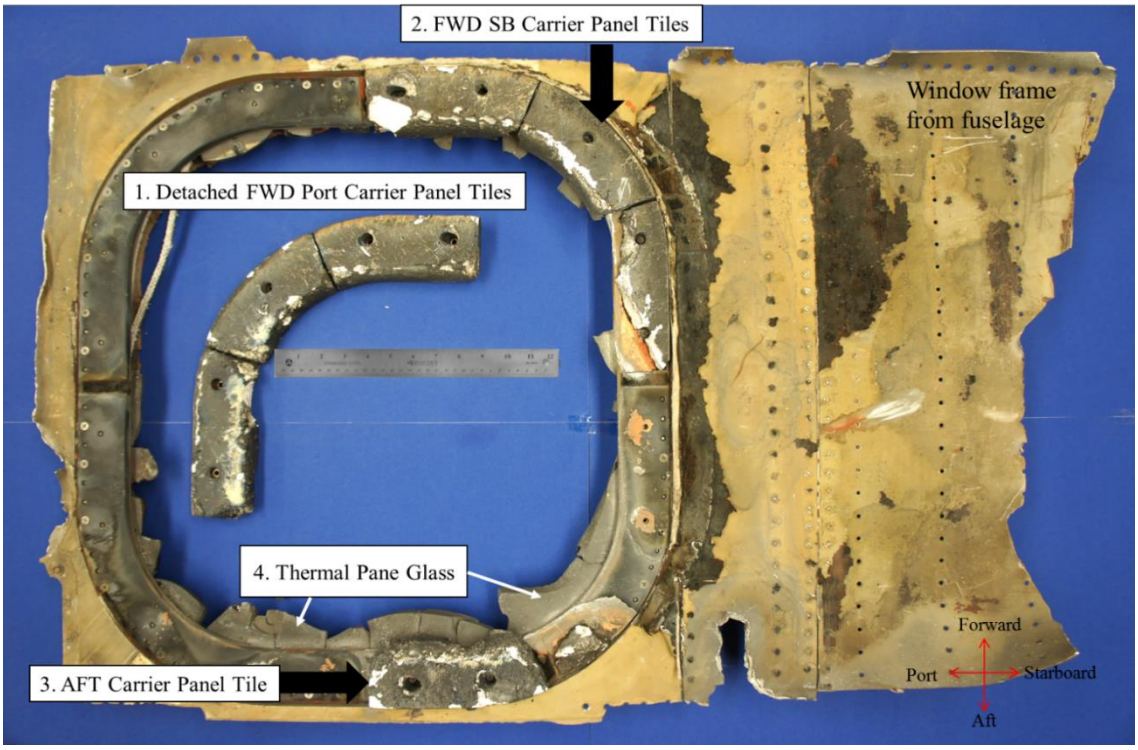

Figure 4.1 Recovered starboard Window 7 from the *Columbia* space shuttle.

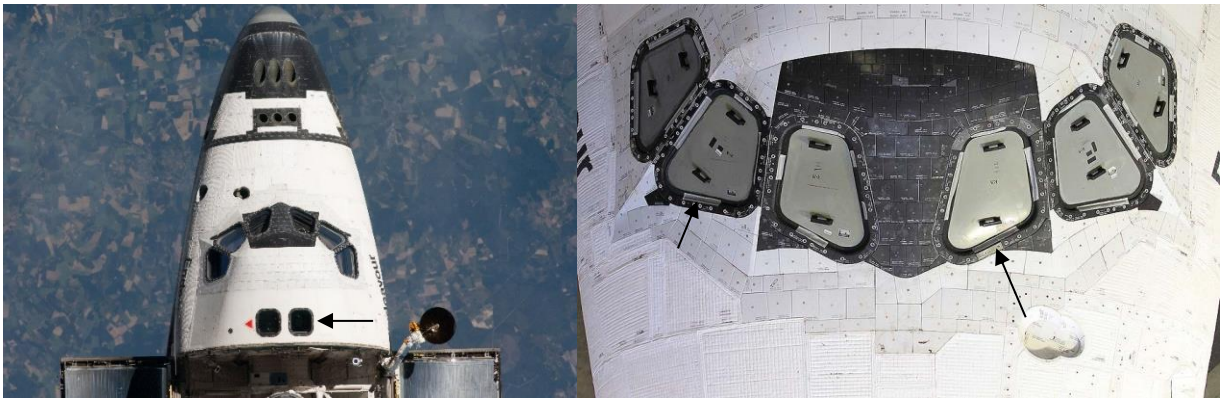

Figure 4.2 An example of HRSI carrier panel tiles located on the Orbiter windows.

Next, the individual carrier panels were examined with additional photographic documentation. The state of the first carrier panel tiles when placed on the window are shown in Figure 4.3. When comparing to original carrier panels (Figure 2.4), the surfaces of the tiles in this panel contained areas that exposed the inner silica fibers of the tiles. Several areas are pointed out in Figure 4.3 where the exposed areas are mostly located in the inner lip regions of the tiles. Several distinct areas are also shown in Figure 4.4a where several yellow and blue discolorations are present along the inner edge of the tile. The rest of the carrier panel contains surface scratches and brown discolorations as shown in Figure 4.4b. Evidence of slumping is also present along the holes used for threading in the direction shown. When looking at the inner sides of the tiles on Figure 4.4c, the black coating contains a glassy coat that is only found in the inner lip areas of the tiles. The inner areas or lip regions of the tiles all contained a porous surface with many pits. The black coating seems to be worn away and directionality can be determined to be occurring in the direction shown in Figure 4.4d. When looking at the yellow and blue discolorations, there are several splat-like metallic deposits shown in Figure 4.5a and b. These metallic features were only present in the forward port tiles.

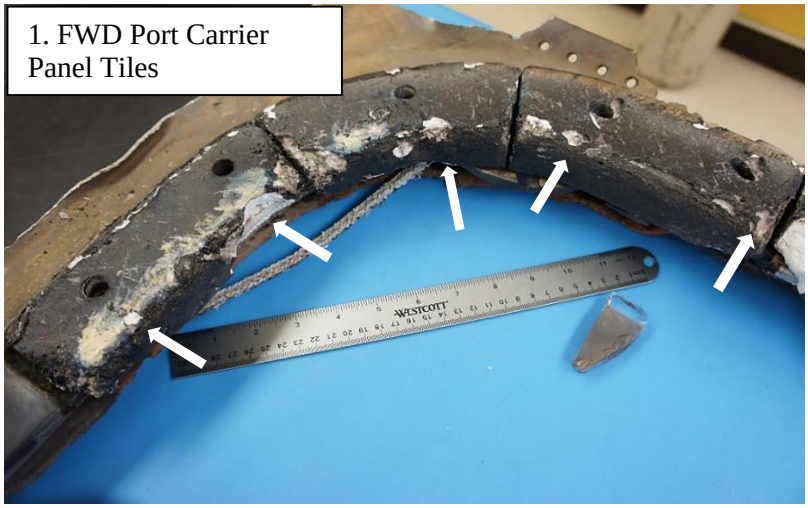

Figure 4.3 The forward port carrier panel tiles on Window 7. White arrows show areas with exposed silica material.

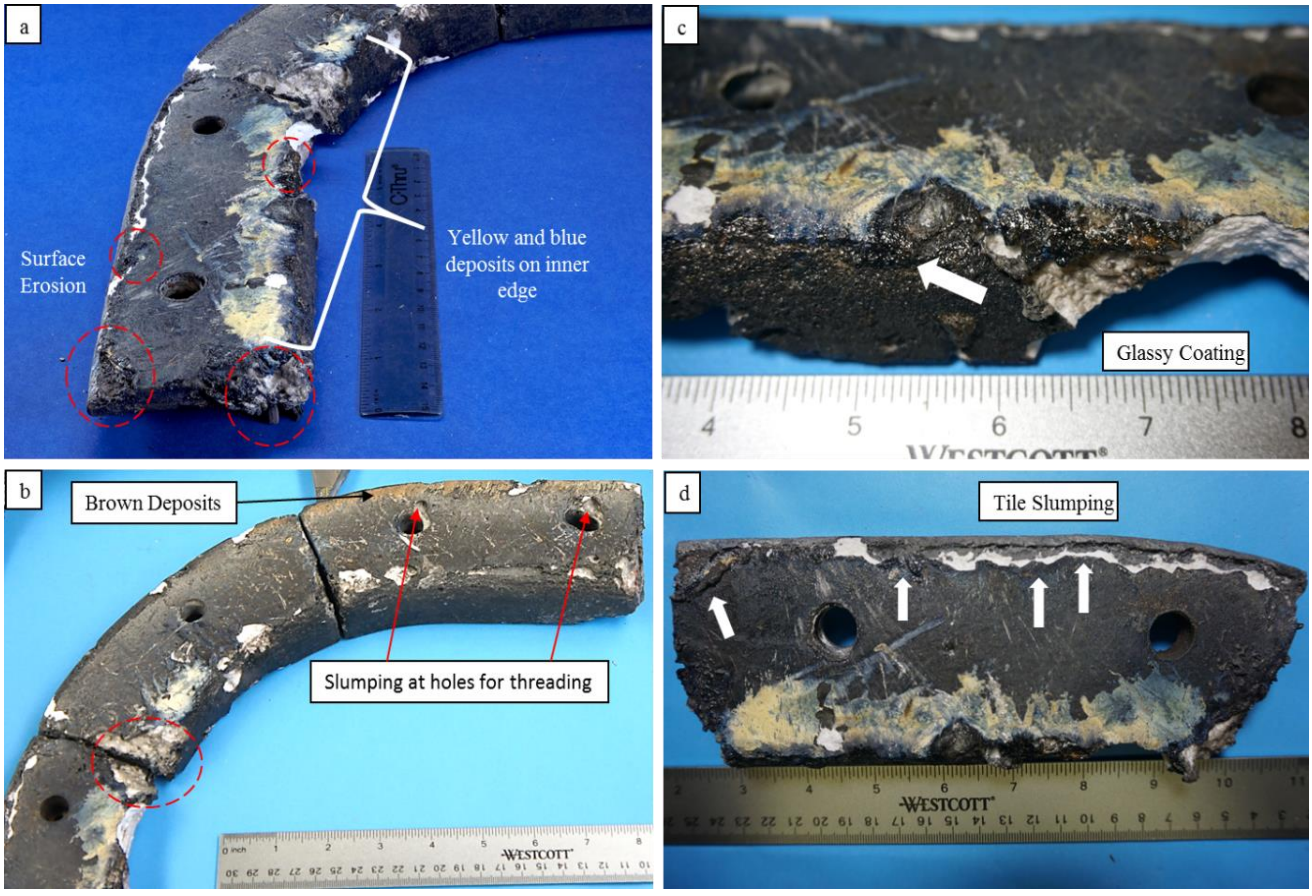

Figure 4.4 Several unique surface features seen on the FWD port carrier panel tile: (a) points out the deposits present and evidence of erosion, (b) shows the rest of the carrier panel tiles with similar features, and (d) shows tile slumping occurring from aft to forward.

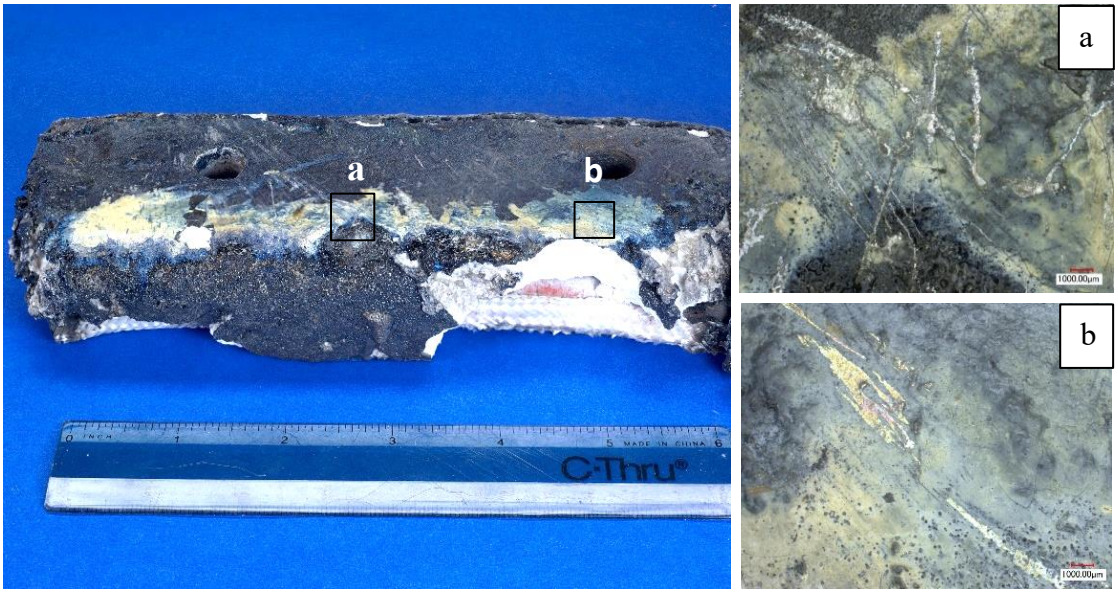

Figure 4.5. Digital microscope images of metallic splats on the yellow and blue deposits on two locations a and b.

The next carrier panel tile is shown in Figure 4.6 and it is located on the forward starboard side of the window. Similar to the previous carrier panel, all three tiles contained areas damage on the coating including large fractured areas with missing pieces as illustrated on Figure 4.6a. Many areas contained slumping that revealed the foam-like bulk material shown by the red arrows in Figure 4.6a and 4.6b. Severe melting of the coating occurred in one of the exposed holes for threading and began to expose the silica substrate. Flow trajectory may be suspected due to the directionality that is indicated by the coating peeling from the aft to forward direction. Other observations include several brown surface deposits were present on all surfaces, cracks at the coating, and indentations on the coating as shown in 4.6b. The inner lip areas also contained many pits and cracked areas. Slumping can also be distinguished in these areas as they contained exposed fibers and an apparent flow occurring from aft-to-forward.

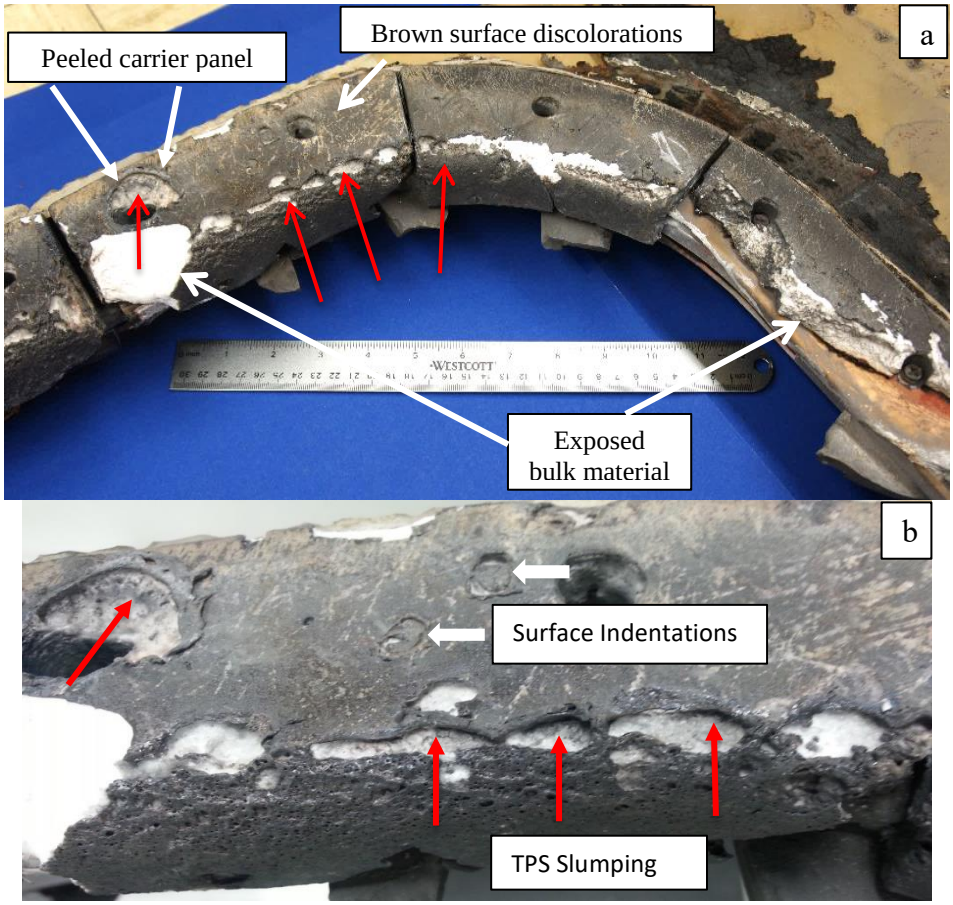

Figure 4.6 As-received forward starboard carrier panel tiles and surface characteristics (a and b). Red arrows represent suspected flow directions from re-entry plasma. Image (b) is a closeup of the first tile.

The aft tile shown in Figure 4.7 contained heavier degradation compared to the starboard and port side carrier panel tiles. Unlike the previous carrier panel, the aft tile contained several discolorations that were similar in hue to the port side carrier panel. Only one full carrier panel tile survived the accident. They are present in yellow and blue or a mixture of both. These were predominately located on the inner side of the tile as pointed out in Figure 4.7a. There are small holes on the coating that were barely visible. Both threading holes may also have experienced thermal conditions due to an apparent slumping damage of the coating in the directions shown. The slumping appears to begin at the very aft edge of the tile and began to melt the coating. The thermal panes can also be seen located under the aft tile and are not translucent but opaque. In addition, exposed areas of the inner silica are also present. Evidence of heavy erosion can be distinguished by the large deformations concentrated at the two locations illustrated by the

red circles (Figure 4.7b). Figures 4.7 c and d show two digital microscope images of several areas of the surface of the aft tile. Location c showed unique metallic deposits and d shows the mixture of discolorations.

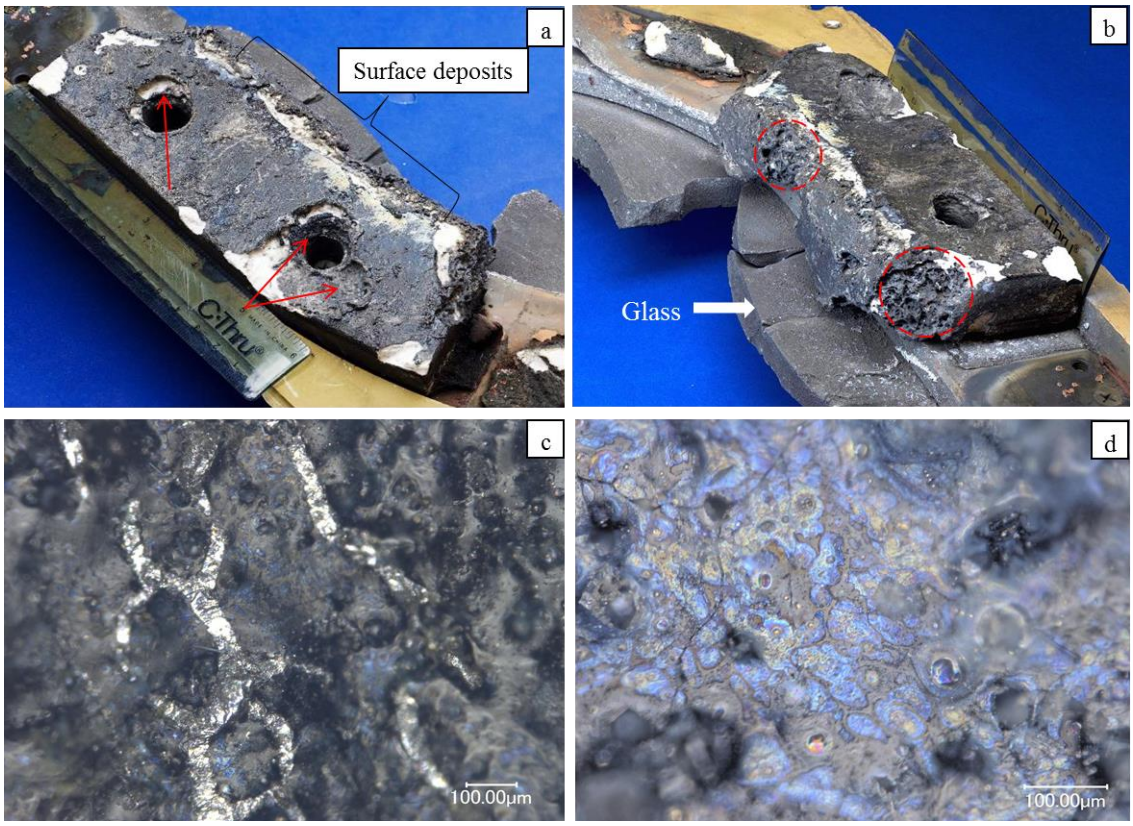

Figure 4.7 Attached tile aft of Window 7 with corresponding surface features. The blue and yellow surface deposits are shown in 16a and flow directionality is shown by the red arrows. Evidence of erosion and remaining thermal pane glass is presented on 16b. Digital microscope images of the surface deposits are shown in 16c and 16d.

4.1.1 3D Modeling

3-Dimensional modeling was performed in order to preserve the natural state of Window 7 without altering the physical evidence. Along with photographic documentation, a 3D modeling tool was used with PhotoModeler Scanner© software. The first step in the process was to take photographs of the desired component at different angles all around the component. After uploading several images, the software computed the position of points in 3D space by geometry using an algorithm to generate dense point clouds from pairs of photographs with textured surfaces to create a final 3D model. The 3D models of the

top and bottom surfaces of Window 7 are shown in Figure 4.8. The top model displays the aforementioned remaining carrier panel tiles located on Window 7. The modeling was done with the purpose of conserving and visually analyzing the debris evidence in a 360-degree view and to obtain original dimensions before any destructive analysis is completed.

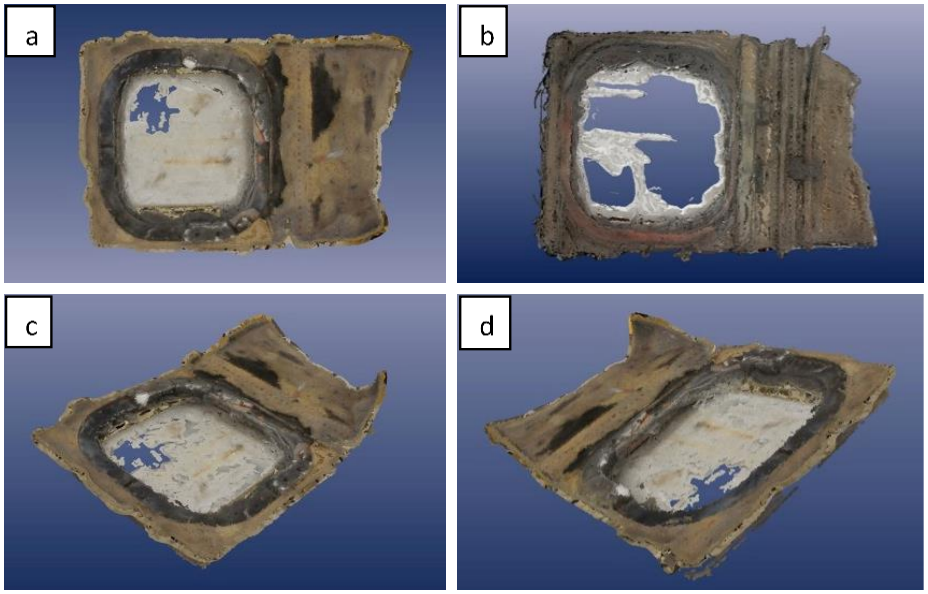

Figure 4.8 3D models of Window 7 showing (a,c,d) top view and (b) bottom side.

4.2 X-Ray Fluorescence, XRF

Due to the previous findings [24] that located three distinct deposits on thermal pane samples from Window 7 and 8, similar deposits may exist on the carrier panel tiles. A semi-quantitative technique was used to determine the elemental species present on the surfaces of the carrier panel tiles using a handheld X-ray fluorescence (XRF) analyzer. The XRF contained a 1-inch by 1-inch window for the surface measurements and a transparent grid was placed over the tiles to protect them from additional damage.

The remaining window frame from the fuselage in general contained an average of 25wt% aluminum, 17wt% copper, and 41wt% silicon. XRF measurements were obtained on the forward starboard carrier panel tile in the areas shown in Figure 4.9. The results in Table 4.1 show several elements were detected on the tile surfaces. The elements with the highest weight percentage detected were aluminum, silicon, iron, and titanium. Remarkably, the compositions of titanium were larger when comparing to the

percentages of aluminum. The largest weight percentage of titanium was 39.89wt% occurring in location 8. Other minor elements present at the tile surfaces include manganese, nickel, phosphorous, zinc, and zirconium.

Figure 4.9 Locations for XRF measurements of the forward starboard carrier panel tiles.

Table 4.1 XRF results of the forward starboard tile surfaces analyzed.

	Composition (wt%)								
Elements	**1**	**2**	**3**	**4**	**5**	**6**	**7**	**8**	**9**
Al	18.52	10.69	18.95	19.9	19.01	18.36	16.58	19.1	18.48
Cu	16.25	4.4	10.24	5.09	1.98	3.28	1.57	1.92	0.8
Fe	17.35	1.49	20.03	7.89	10.6	10.5	8.08	9.11	11.4
Mn	0.62							1.24	
Ni	4.58	0.54	2.3	0.96			0.61		1.07
P	2.22		3.87	4.43	5.25	5.39	3.57	4.61	4.63
S	1.86		2.39	5.13	4.38	3.79	5.96	2.47	2.71
Si	16.13	72.96	15.29	20.14	21.01	23.51	20.14	18.13	18.19
Ti	16.67	9.08	21.14	30	33.42	30.45	39.87	39.89	17.15
Zn	2.23	0.42	2.39	2.11	4.06			3.53	2.16
Zr	2.95	0.42	3.39	4.36		4.72	3.62		4.26

The next carrier panel tile also contained similar elemental compositions in the locations displayed in Figure 4.10. The areas measured include areas A-D to represent the outer areas of the tiles, while the sides close to the edges contained the colored deposits with areas 1-4. The XRF results of these areas are

shown in Table 4.2. Areas A-D contained consistent compositions of aluminum, silicon, and a range of 12-15wt% of titanium. Areas at the yellow and blue discolorations contained the largest weight percentages of titanium. The results are shown in areas 1-4 where locations 1 and 3 contained a presence of approximately 44 wt% titanium. Locations 2 and 4 had 30 and 35 wt% titanium. The primary elements detected were similar to the forward starboard tiles. A variation of silicon was observed to occur in areas where the yellow and blue deposits were present. The amount of silicon decreases at locations 1-4, while the silicon amounts are constant in areas A-D. The rest of the carrier panel shown in Figure 4.11 contained equivalent elemental compositions. The locations of the measurements are marked and the main elements present are shown. The primary elements of aluminum, silicon, and titanium had similar concentrations when compared to the previous carrier panel. The carrier panel tile in all areas had much lower concentrations of titanium than those pertaining to the yellow and blue deposits. Therefore, the deposits contained the highest relative amount of titanium compared to any other measured areas. The XRF results have proven that the areas to be sectioned will take place where significant unique deposits are found such as titanium and the degradation of tiles.

Figure 4.10 Forward port side detached tiles and corresponding XRF results on areas A-D and 1-4.

Table 4.2 XRF results of the starboard port side.

	Composition (wt%)							
Element	**A**	**1**	**B**	**2**	**C**	**3**	**D**	**4**
Al	20.27	15.72	20.57	29.17	18.55	15.99	24.45	29.45
Cu	0.33	0.63	0.48	1.1	0.46	0.25	0.8	1.55
Fe	2.85	2.08	2.75	1.25	1.87	1.64	1.56	1.37
Mn								0.21
Ni	0.12	0.14	0.07	0.05	0.08	0.09	0.08	0.05
P					0.21			
Si	61.1	36.88	63.14	33.05	66.47	36.76	58.97	37.12
Ti	14.88	44.09	12.47	35.06	11.92	44.84	13.75	29.9
Zn	0.13	0.17	0.14	0.11	0.11	0.13	0.12	0.1
Zr	0.34	0.29	0.38	0.213	0.33	0.31	0.27	0.24

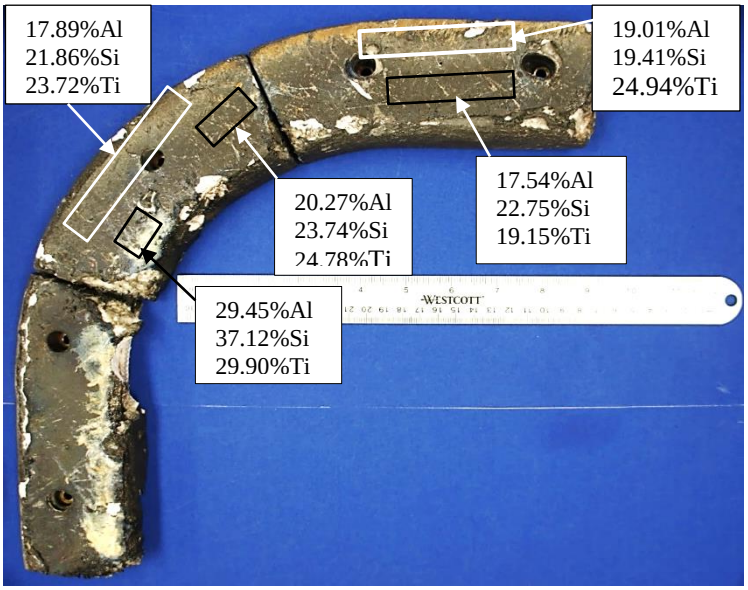

Figure 4.11 Completed elemental analysis results of the forward port side tile panel.

The attached aft tile just aft of the window frame also indicated the same primary elements, except with lower amounts of titanium ranging from 8-26 wt%. The locations of the XRF readings are shown in Figure 4.12 along with the major elements compositions. The yellow and blue deposits were also located on the aft tile near the inner edge, however they were unable to be analyzed by XRF since the deposits are in close proximity to the tile edge. The areas showed a continuous presence of titanium with the largest

amount being 35 wt% appearing at the outer edge of the tile as shown. The amount of titanium appears to increase from the forward to the port side of the tile. Additional examination of the deposits will provide a more accurate elemental analysis due to the severe degradation present.

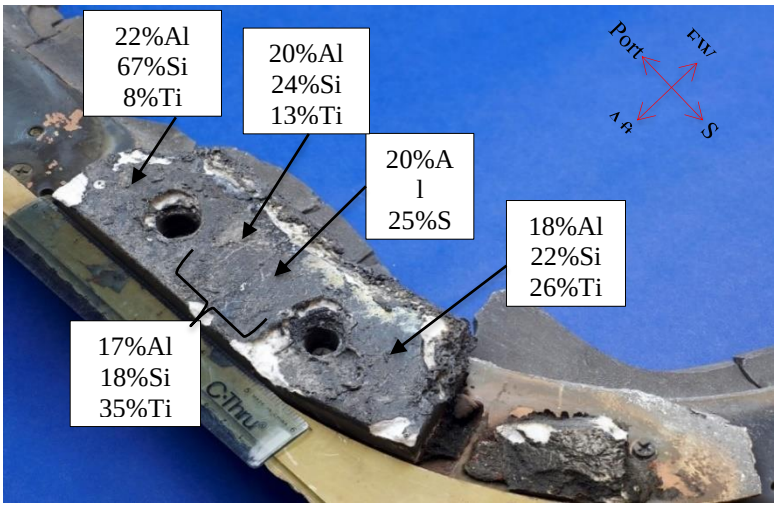

Figure 4.12 Aft tile with selected elemental analysis results of several locations with primary elemental species.

Finally, three thermal pane glass fragments were analyzed on locations at the forward and aft sides of Window 7 (Figure 4.13 a-c). On the aft locations, they contained a variety of major elements with different compositions in Figure 4.13c and 4.13d. The broken thermal pane glass located on the forward side (4.13b) contained a very large amount of silicon at 79.88 wt% while the other two contained much less. Thus, all fragments analyzed possessed various amounts of high elements and the presence of titanium was not as high compared to the percentage found on the carrier panel tiles. It is important to note that the handheld XRF analyzer is not able to distinguish multiple layers, if they exist. Consequently, destructive analysis must be performed in order to obtain detailed composition information.

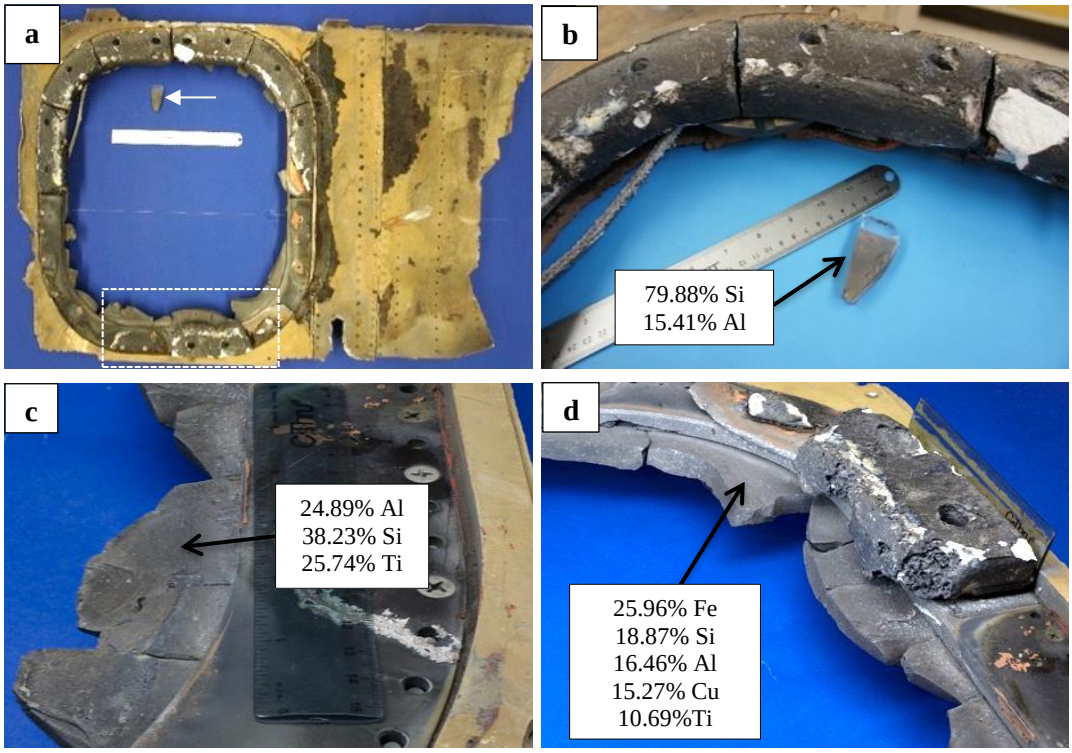

Figure 4.13 XRF locations and corresponding results of the main elements detected pertaining to thermal pane glass fragments located on the forward and aft portion of window 7 as indicated in a. Fractured fragment in forward side is shown on b, while letters c and d are measurements obtained from the aft region.

4.3 Non-Destructive Evaluation Summary

Upon receiving the window component and its materials, no previous servicing history was available. As a result, it was assumed that any anomalous features did not exist on the carrier panels or thermal panes before the accident. NDE analysis was performed to evaluate several properties of the window such as; examining the as-received condition, dimension, recognizing surface imperfections that could adversely affect the materials, located types of alterations, and locate evidence of deposits. Because the materials making up the shuttle experienced off-nominal conditions upon re-entry, it was necessary to conduct an elemental analysis of all surfaces. Photographic inspection and documentation highlighted the surface degradation effects experienced by carrier panel tiles and thermal pane glass after re-entry. The directionality of the suspected plasma flow of tiles was also observed, in several different directions on each tile frame. The plasma flow from the re-entry environment may have affected the surface of the tiles

by causing depositions and slumping of the black coating. The slumping appears to be severe on the exposed holes that are used for threading the carrier panel tiles to the window frame. Many other areas with evidence of slumping occurred and all had the inner silica material exposed. The 3D modeling results provided a record of the original state of Window 7 and will be helpful in obtaining original dimensions before any sectioning is done. The elemental analysis provided essential information about the major and trace elements present on the surface of tiles. Since many of the components near the tiles are rich in silicon, other major elements were identified at larger weight percentages. For example, the major elements with highest weight percentages that were detected were aluminum, titanium, and silicon throughout all tiles. The XRF results determined that the colored surface deposits had the largest amount of titanium therefore, the behavior of titanium will initially be investigated. In most cases, the amounts of titanium were preferentially higher at inner edges of the tiles, and decrease to the top edge of the tiles. Since titanium was often the highest percentage of several areas that contained smaller percentages of aluminum, it is important to thoroughly investigate the behavior of titanium since it is used in other structural and substructural components in the space shuttle. It is possible that a component that was located directly near Window 7 may have played a role in the deposits found on the carrier panel tiles (Figure 4.14). Two payload bay latch rollers along with a portion of the existing bulkhead frame contained evidence of heavy erosion. The rollers are made up of a Ti-6Al-4V alloy and are covered with a nickel-based superalloy that may have been the source of the titanium detected by XRF. An analysis of the depositions will confirm their identity and source. The thermal pane fragments contained a variety of different elements and fractures. Fractography and further examination of the opaque “char layer” will determine the sequence of events. In order to confirm these non-destructive findings, a destructive analysis must be carried out for elemental analysis and compound examination.

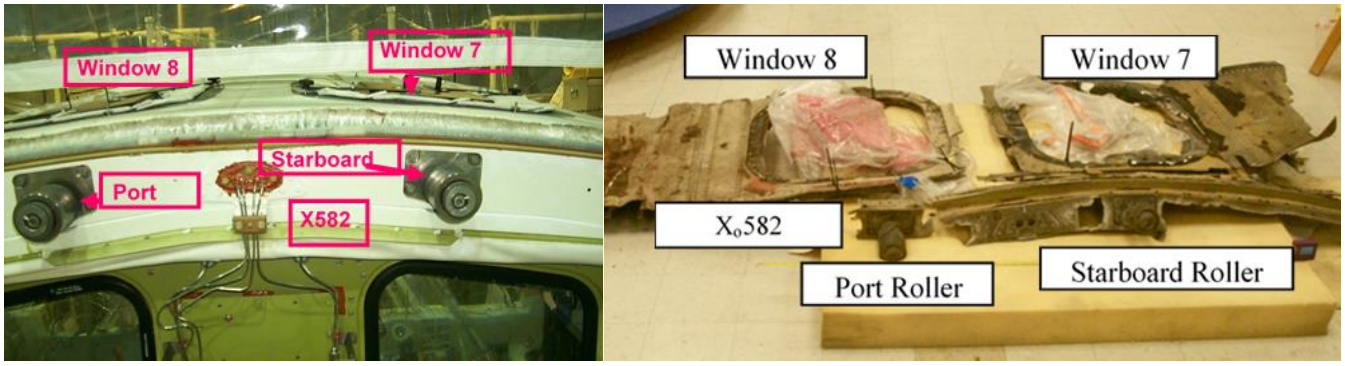

Figure 4.14 Left image depicts the unaffected bulkhead rollers and shuttle windows. Right image shows the X_o582 bulkhead with bay door latch rollers locations with respect to *Columbia's* windows.

4.4 Areas of Interest

Several areas were selected as a result of the preliminary non-destructive evaluation outcomes. Samples were chosen from all carrier panel tiles located on Window 7. The areas are shown in Figure 4.15 with carrier panels 1-3. Areas of interest were samples 1-4. Sample 1 was obtained to characterize the colored deposits with metallic splats. This area was also obtained to confirm surface XRF measurements and to verify the amounts of titanium present. The following sectioned area is located on the forward starboard tile as sample 2. The area was to study any deposition formation and examine the inner sides of the tiles as XRF could not measure small edges. This area also contained a large percentage of titanium. The aft tile was also selected since the tile is nearest to the two payload bay bulkhead latch rollers, and the specific areas gathered are shown in Figure 4.15. The yellow and blue discolorations that make up sample 3, were necessary to determine if they contain similar chemical signature as those seen on the forward port side carrier panel. Sample 4 also chosen as it contained metallic deposits and to investigate traces of the surrounding materials are present. All samples were essential as they embodied all directions of Window 7 and facilitated investigating plasma flow directionality from re-entry.

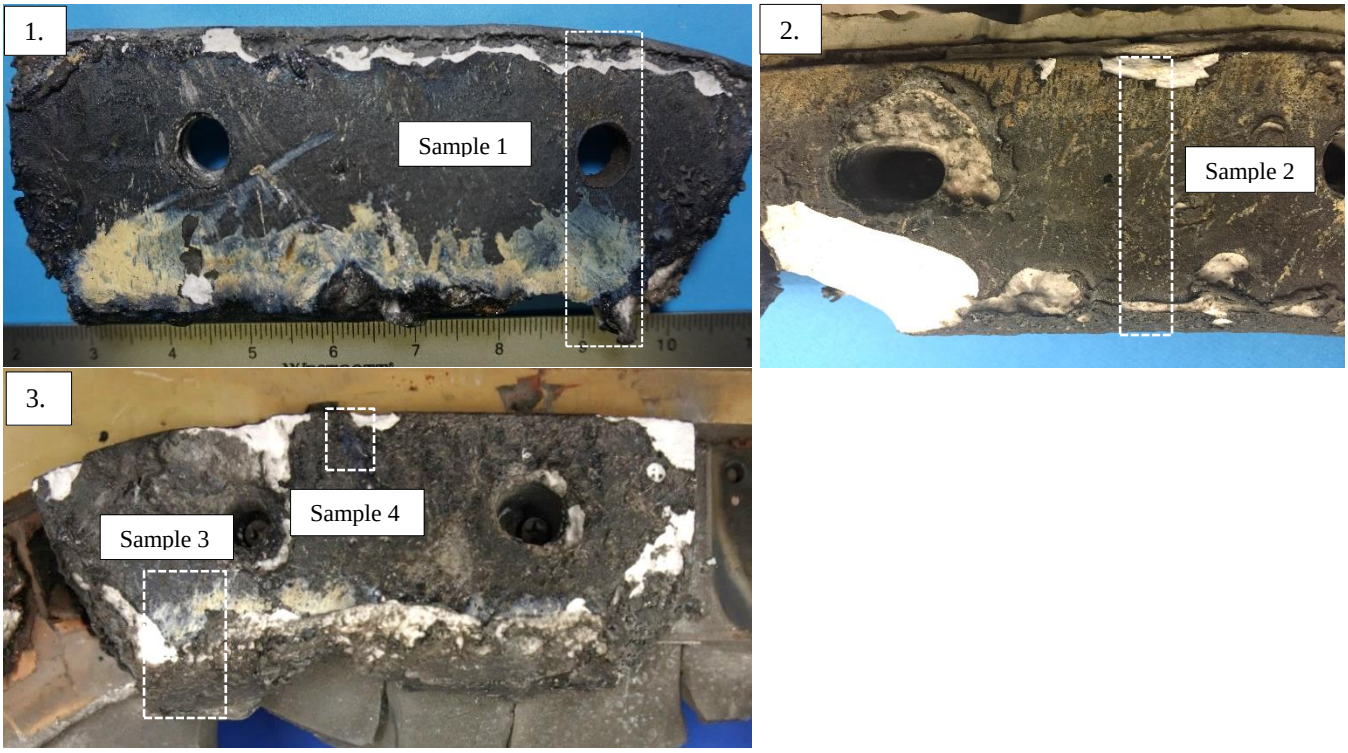

Figure 4.15 Selected areas for experiment with sectioning guides for each carrier panel tile. Sample 1 corresponds to the forward port side, sample 2 is from the forward starboard side, and samples 3 and 4 are located in the aft tile.

The thermal pane glass fragments that were collected from the window structure consist of a thermal pane fragment positioned in the forward area and smaller glass fragments from Window 7. The separated glass fragment in Figure 4.16 was chosen for this analysis because characterization of the thermal pane cross-section was necessary to compare the formed deposits to those belonging to the carrier panel tiles. The smaller collected glass shards from Window 7 were also used to determine if layering exists since XRF is not capable to discern separate layers of a deposit. The smaller glass fragments were needed for microscopic evaluation due to their dark coloration. The smaller glass samples were also mounted in a two-part epoxy mount and was ground from 80-1200SiC grit until a cross-section was obtained.

Chapter 5: Preliminary Analysis

5.1 Sectioning Procedure

In order to study the deposits on the carrier panel tiles, sectioning of several areas for obtaining samples was carried out. The exemplar thermal protection system tile and carrier panel tile were used to determine the proper sectioning tools and techniques. The sectioning plan consisted of photographic documentation before sectioning, sectioning utilizing a variety of tools, and final results with recommended cutting tools. All sectioning methods were performed dry without the use of lubricants to prevent contamination of the coating and silica fibers of the tiles. The sectioning began by cutting two large cross-sections followed by smaller sized cross-sections. It was determined that the RCG coating required its own sectioning tool as it is much harder than the fibrous silica. The saw that provided the best results without creating a substantial amount of coating debris was a Dremel tool with a diamond blade at a low speed setting. The saws that were successful in sectioning the silica cross-section were thin jeweler's saws and a hacksaw blade. The results also revealed that a hacksaw blade provided best results for sectioning larger geometries of the tile. The felt pad also required its own sectioning tool of a heavy-duty razor blade to cut through the felt successfully.

Next, the carrier panel exemplar was sectioned into one-half inch pieces in width and sectioning was begun on the inner lip area first to minimize stresses. The Dremel tool continued to perform best for the RCG coating as did the jeweler and hacksaw blades for the silica material. Figure 5.1 a shows the sectioning procedure of cutting through the coating with the Dremel tool followed by the fine saw through the silica cross-section on Figure 5.1b. The cross-sections of the carrier panel tile are shown in Figure 5.1c with a successful thin specimen on Figure 5.1d. Additionally, the felt pad on the carrier panel exemplar was very thin therefore; the jeweler's saws and hacksaw were capable of cutting through the felt material with minimal material loss. Based on these results, the recommended sectioning material and technique are:

1. Sectioning RCG coating first with rotary Dremel Tool
2. Cross-sections of silica material must be sectioned with 32 TPI hacksaw blade or a fine jeweler's saws
3. Sectioning of Nomex felt pad with heavy duty razor blade

The method for sectioning the thermal pane glass was to first encapsulate a glass fragment with similar geometries of the separated fragment (Figure 4.13b) using a two-part epoxy mount. The sample was then ground in order to analyze the cross-section of the glass for chemical analysis. The thermal pane glass was not sectioned as the glass thickness was too large for most cutting tools. Thus, smaller glass shards were selected in the analysis to facilitate sample preparation and technical equipment size requirements.

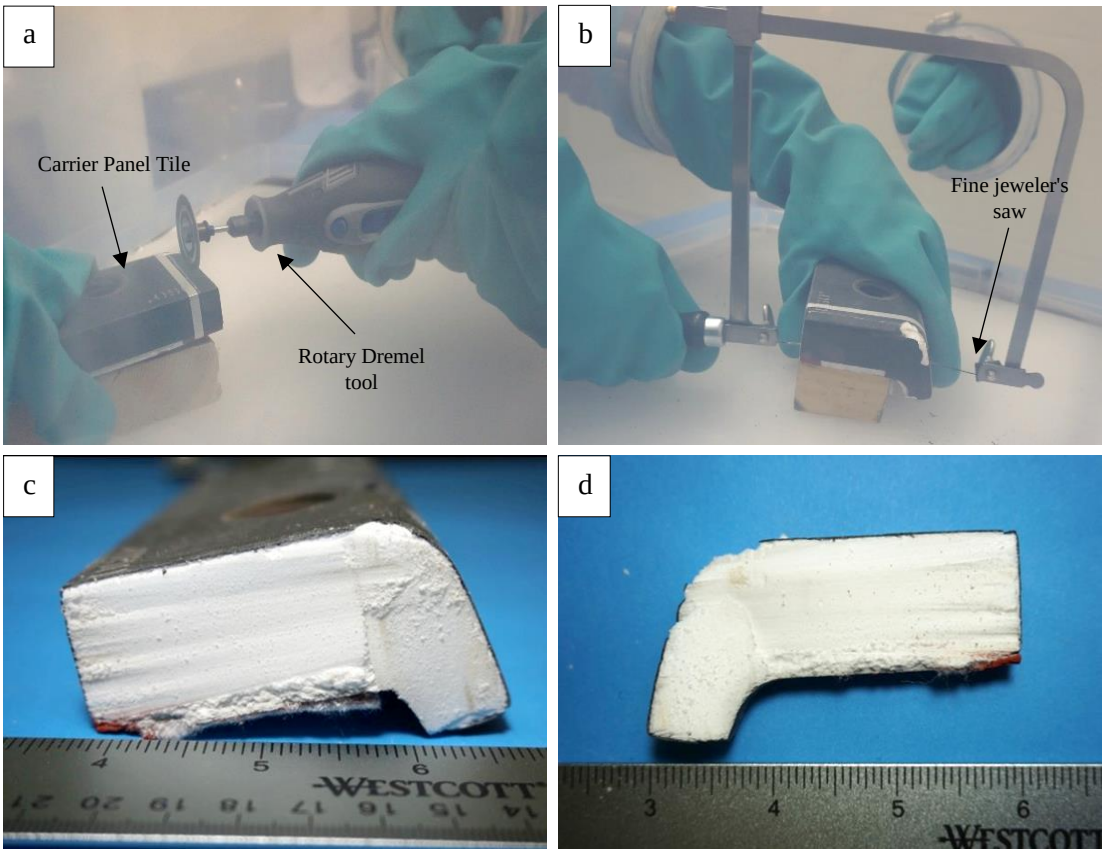

Figure 5.1 Examples of sectioning procedure of Dremel tool sectioning of coating (a) and jeweler's saw cutting the foam-like silica. Areas (c) and (d) show the aftermath of sectioning with these tools.

5.2 Removal of Carrier Panel Tile

Given that the forward port side carrier panel contained the most evidence for depositions as demonstrated in Figures 4.5 and 4.10, the tile was removed from the frame. This was in particularly due to the carrier panel being attached to Window 7 and to determine the most favorable way of sectioning areas within the carrier panel. The tile was removed by using a heavy-duty razor blade and a hacksaw blade to detach. Figure 5.2 shows the tile after its removal and the underside of the tile contained several areas of burned Nomex felt pad.

Figure 5.2 Forward port side carrier panel tile with legend after removal and underside of tile (right).

5.3 Exemplar Tile Study

Two HRSI TPS tiles were loaned to represent a sample control which did not contain any surface deposits or damages. As the service history of the window carrier panel tiles is unknown, it is assumed that the tiles contained minimal damages and the unaffected tiles would provide sampling for comparison. Several samples were sectioned as the tiles were too large for several experiments. After receiving these samples, they were analyzed with several characterization tools. The results are discussed in this section.

5.3.1 X-Ray Diffraction

XRD was used to first characterize the exemplar TPS sample as the set up and sample configuration did not require special material preparation. The analysis revealed the type of phases present at a specific area measured. Several data sets were used to accurately distinguish the phases present on the unaffected tile. Figure 5.3 indicates the types of phases present on the coating of the exemplar sample.

Silicon oxides of SiO_2 and $Si_{34}O_{68}$ were detected including major peaks of C, SiC, and Zn. The compounds present are consistent with tile materials of silica fibers and borosilicate coating. The source of Zn found in the sample may have originated from a primer used for corrosion protection for aluminum structures. The CAIB also reported that there was contamination from a zinc primer used on the launch pad structure [1] [2]. It was also stated that the primer may be removed from rain conditions or heat exposure.

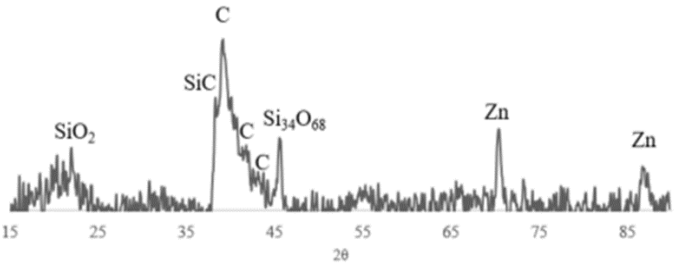

Figure 5.3 XRD pattern of the as-received unaffected carrier panel tile surface.

5.3.2 Scanning Electron Microscopy

The loaned exemplar tiles were observed through SEM initially, to assess the morphology of the surface and cross-section. The sample was used to represent a TPS sample as a control to compare with future measurements. The surface of the as-received unaffected tile is shown in Figure 5.4 where the coating appeared to be uniform and no other deposits were observed. Several silica fibers were present as a result of contamination from sectioning the tile. EDS measurements were conducted and show that the average surface composition mostly contained silicon. The EDS spectra on Figure 5.4 also detected copper as the sample contained conductive tape for reducing sample charging. The microstructure of the unaffected tile sample when mounted and polished at the cross-section, consisted of the silica fibrous base material with the TPS borosilicate coating. Figure 5.5 shows the location of the coating and bulk material. The TPS coating thickness was consistent with approximately 450μm (0.045cm). Images a and b show the coating adhered to the bulk material. When analyzing the exemplar tile through EDS, the X-ray maps

are shown in Figure 5.6. The spectra obtained on the entire cross-section of the sample contained major peaks of oxygen, silicon, carbon, and minor peaks of chlorine and potassium. The carbon map shows it is located on the epoxy coating area and the encased fine silica powder in the mount. Oxygen and silicon maps show that they are concentrated on the TPS coating. However, several fibers were not fully encased in the mounting material and thus confirm the fibers to be rich in silicon. Two minor elements of potassium and chlorine were also detected and are dispersed through the cross-section.

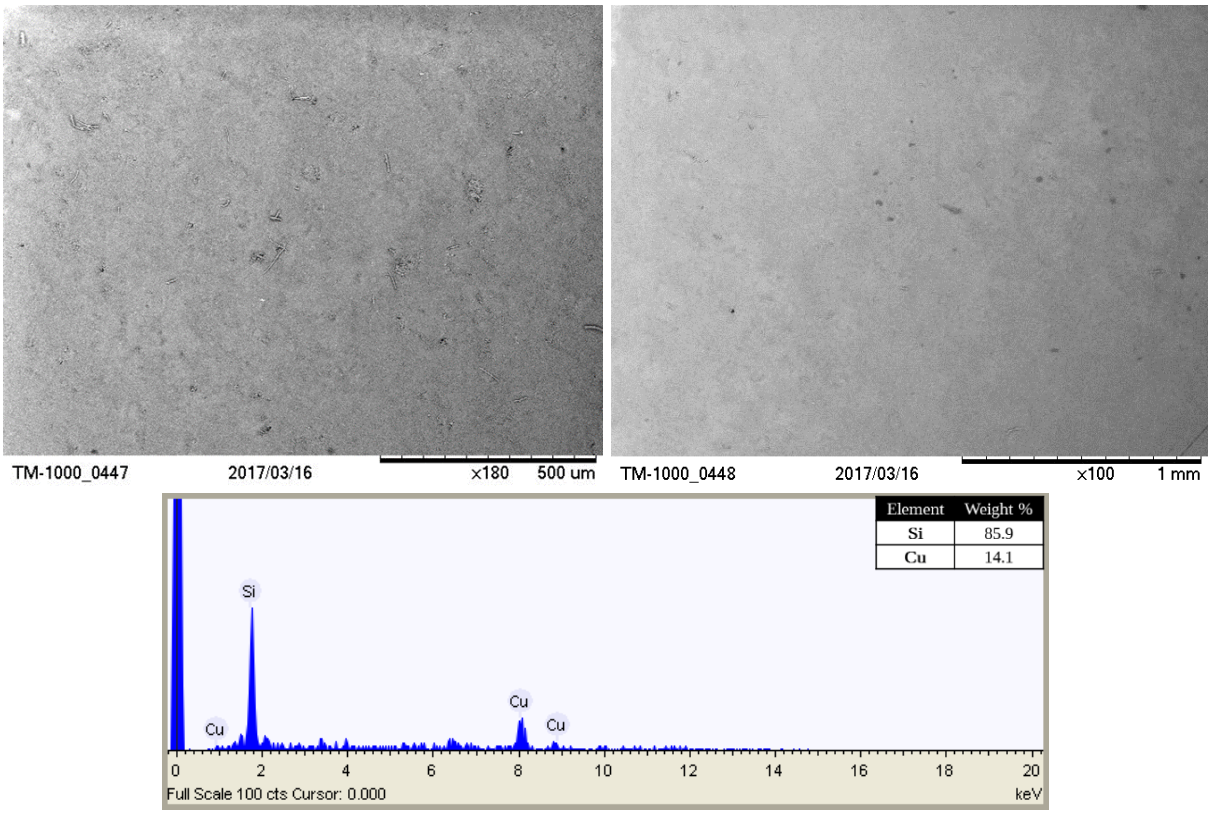

Figure 5.4 Surface SEM images for the loaned as-received exemplar tile with the average surface EDS composition.

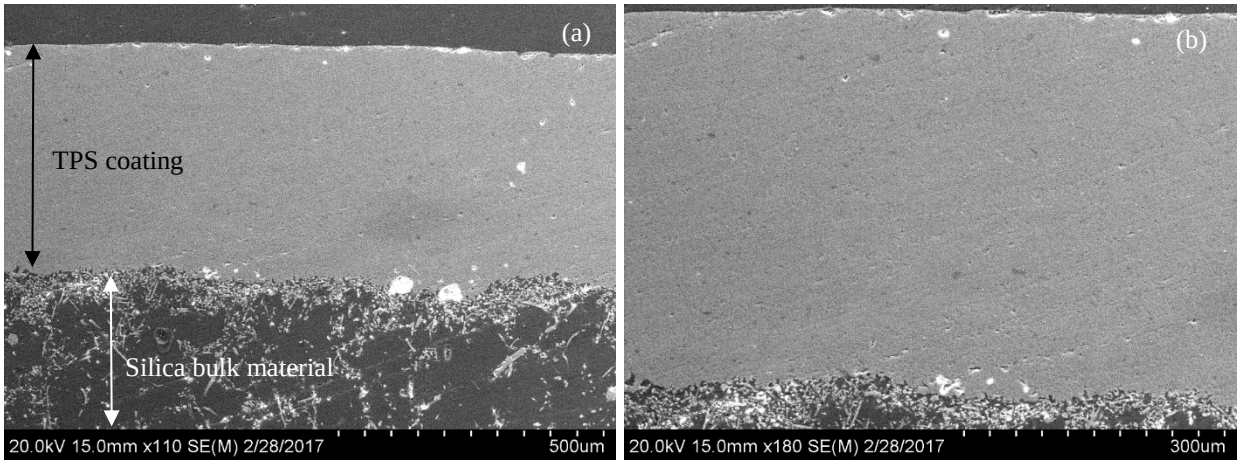

Figure 5.5 SEM micrographs of two typical cross-sections of the exemplar TPS not used for the shuttle.

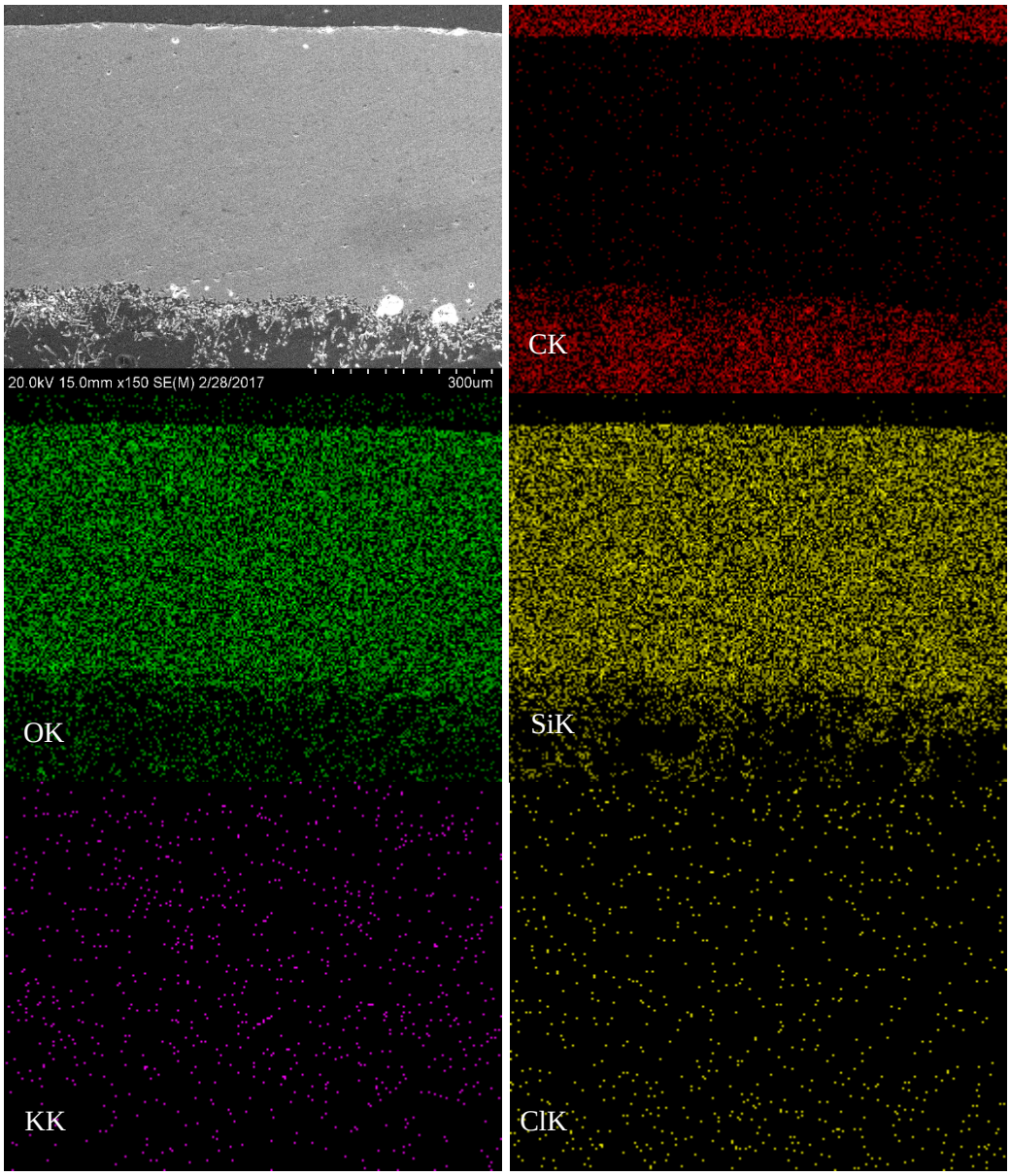

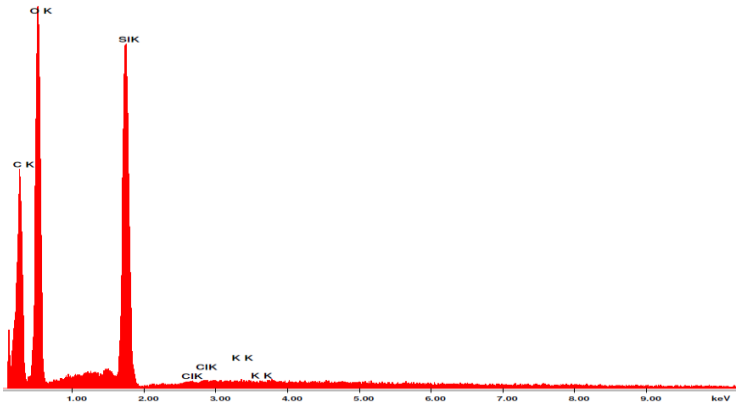

Figure 5.6 Cross-section of unaffected TPS with X-ray Mapping

5.4 Thermal Pane Fragments

The separated thermal pane fragment from Window 7 was first studied using photography and a digital microscope to detect any macroscopic features pertaining to distinguishing a charred layer, fracture initiation, and propagation. Figure 5.7 shows the top and bottom surfaces of the glass fragment where a gray charred layer is present on all sides except on the area that is attached to the window. The char layer also contains smaller light deposits on the top and bottom surfaces as pointed out in Figure 5.7b and d. The top view of the glass contains several indentations with the charred layer still adhered. The side views of the glass fragment appear to have evidence of fracture when viewed under a digital microscope (Figure 5.8). The fracture features are similar to Wallner lines exhibited by glass fracture [41] [42] and appear to travel in the directions shown. The fractured sides do not contain any deposits, they were only present at the bottom and top areas. Because a char layer was present identical to the work by Olivas et. al, the fragment will require a chemical analysis to determine the chemical species of the deposits and how they relate to the observed deposits on the carrier panel tiles.

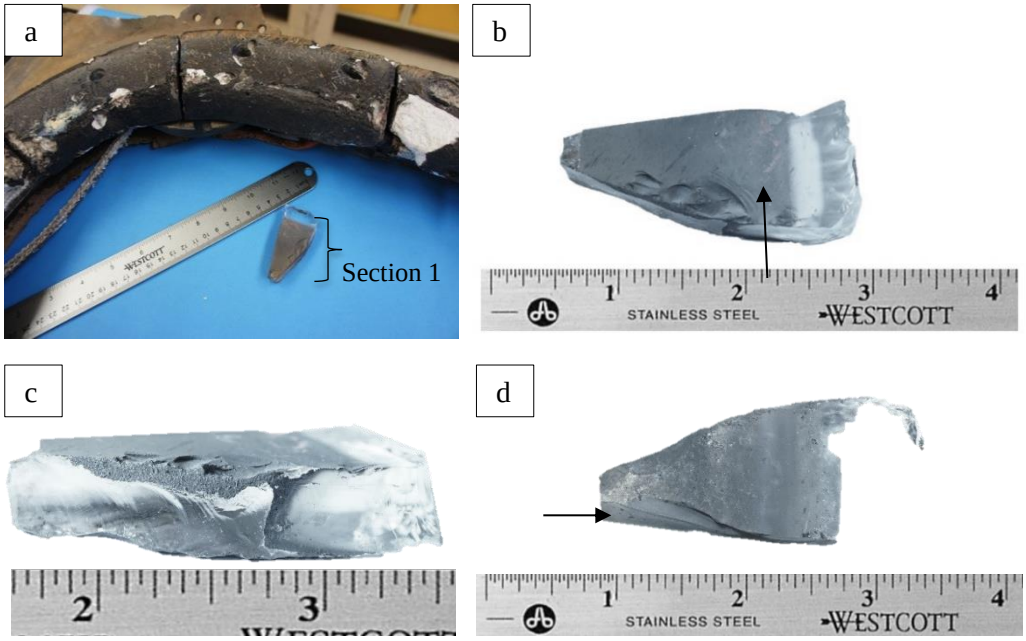

Figure 5.7 As-received thermal pane fragment shown on a. The top (b) and bottom (d) surfaces of the glass are shown along with one side showing the charred layer on the surface (c).

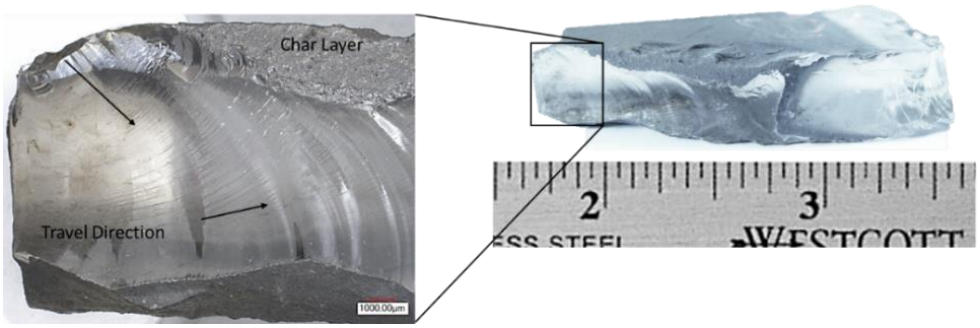

Figure 5.8 Digital image obtained from the side view shoeing travel direction of Wallner lines [41].

Before performing the chemical analysis of the char layer, another sample was used to test out sample preparation method and chemical analysis. The sample that was chosen was a scrap thermal pane sample belonging to Window 8 from *Columbia* and exhibited identical size and geometry. The test sample also contained a gray charred layer which was first scrapped off with a laboratory spatula for SEM/EDS analysis. The sample was mounted in a two-part epoxy mount under vacuum and was ground (80-1200 SiC grit) until a cross-section was obtained. The sample was polished with alumina suspension from 1 micron, 0.3 micron, and 0.05 micron. Two SEM cross-sections of the glass are shown in Figure 5.9 and

were observed using an FEI Quanta 400 field emission SEM. A deposit layer as indicated by the white arrow was concentrated in one location of the glass and contained porosity. Next, the removed charred particles were observed with a Hitachi S-4800 Field Emission SEM shown in Figure 5.10 and all particles were irregularly shaped with various particle sizes. The EDS spot spectra of several particles identified similar elements and the most prominent peaks are titanium oxide, silicon, and aluminum. Other constituents were also recognized and the results are comparable to the metallic elements obtained from Olivas et al., 2010. The same procedure was used when studying the Window 7 thermal pane glass fragments.

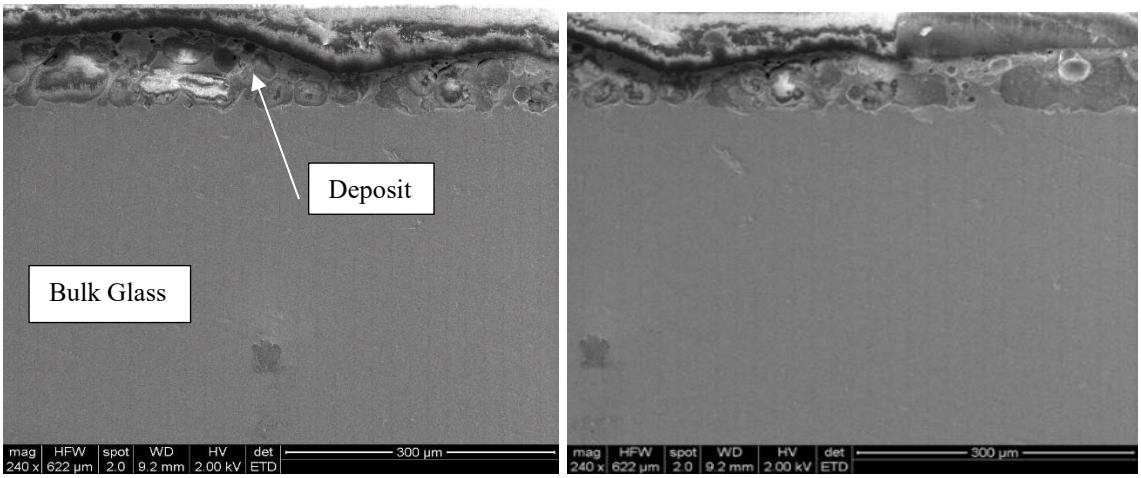

Figure 5.9 SEM images of the cross-section of the test glass sample from Window 8 with evidence of a deposit layer.

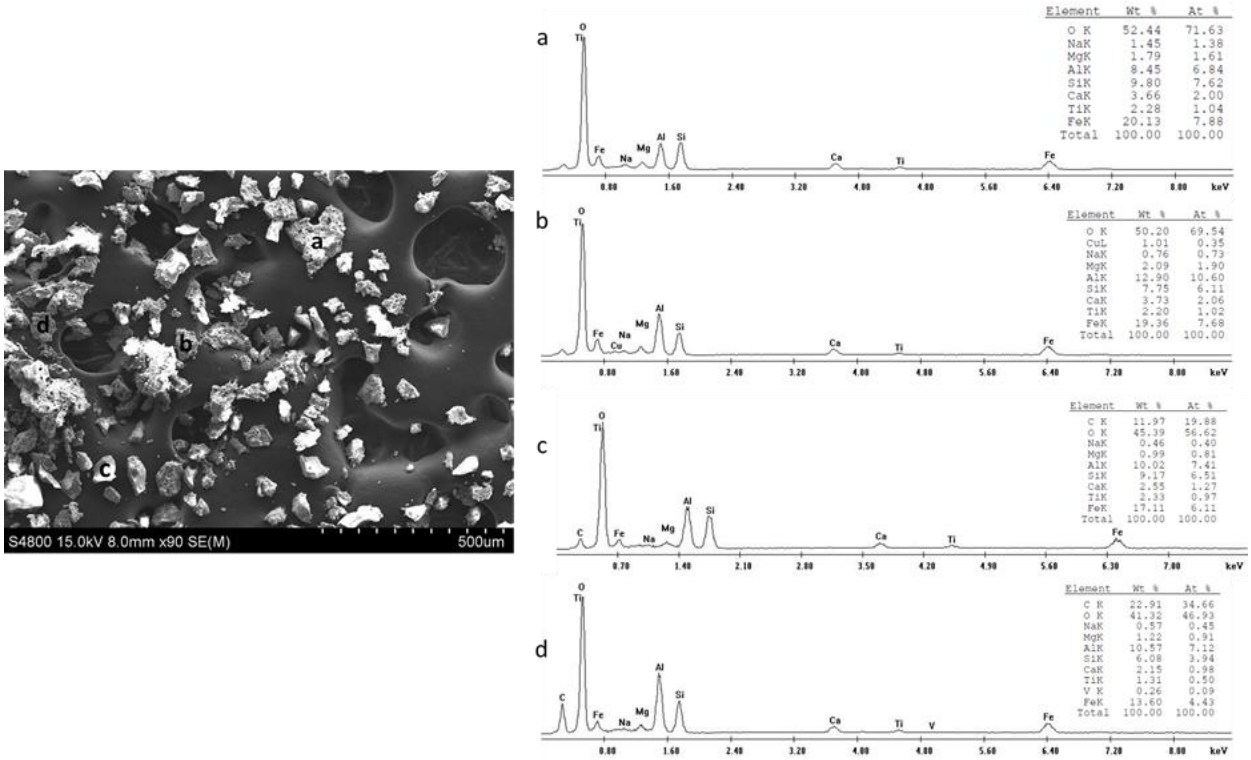

Figure 5.10 SEM image of the removed charred particles from the Window 8 test sample and several EDS spot spectras a through d of several particles.

Because smaller Window 7 thermal pane glass fragments were readily available and of proper specimen sizing for all equipment used, the sample was mounted and prepared identical to the Window 8 glass sample. The polished sample is shown on Figure 5.11a-d. The cross-section of the sample at a magnification of 100X demonstrates a deposited film on two sides of the sample. The bulk glass material is shown and the deposits are shown on Figure 5.11a. Observing the deposit at a higher magnification on Figure 5.11b, the deposit itself contains open pores and some areas are not adhered. Another deposit contained a dissimilar morphology with distinct phases as illustrated on Figure 5.11c and d. The deposit contained dark gray areas within a eutectic-like structure. It also contained evidence of spallation. The microstructure is shown in 11d with a light gray phase and a gray structure.

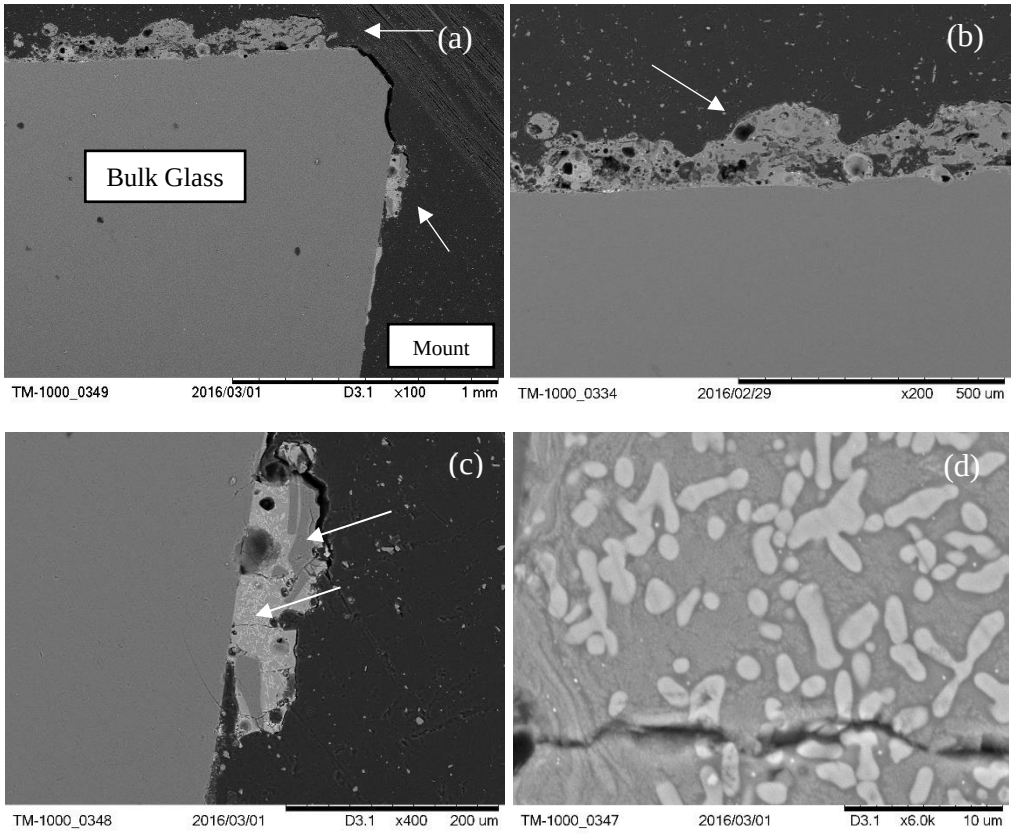

Figure 5.11 SEM image cross-sections of (a) the small Window 7 glass sample, (b) evidence of deposit, (c) a deposit with microstructure shown on (d).

EDS spot measurements were obtained to determine the chemical composition of these formed phases. Figure 5.12 shows four EDS spot readings for determining their chemical compositions. Spots a, b, and d were located within the light gray phase that contained between 59 to 63wt% of Ti. However, when analyzing the darker gray phase, it was a titanium oxide mixture with minor amounts of silicon, aluminum, calcium, and copper. When mapping the entire cross-section, the elements detected are also shown to be concentrated in certain areas. This is shown in Figure 5.13 along with the spectra. It is clear that the light gray phase contains a mixture of titanium, oxygen, and vanadium. However, the concentration of titanium is higher. The dark gray phase contains titanium oxide, silicon, and calcium. Two areas are shown not to be an oxide but aluminum particles as illustrated by the yellow color. Sodium was also present on the cross-section as well as copper. The carbon present was located in areas where

pores or cavities were present. These compositions present are comparable to the obtained particles from the Window 8 glass samples.

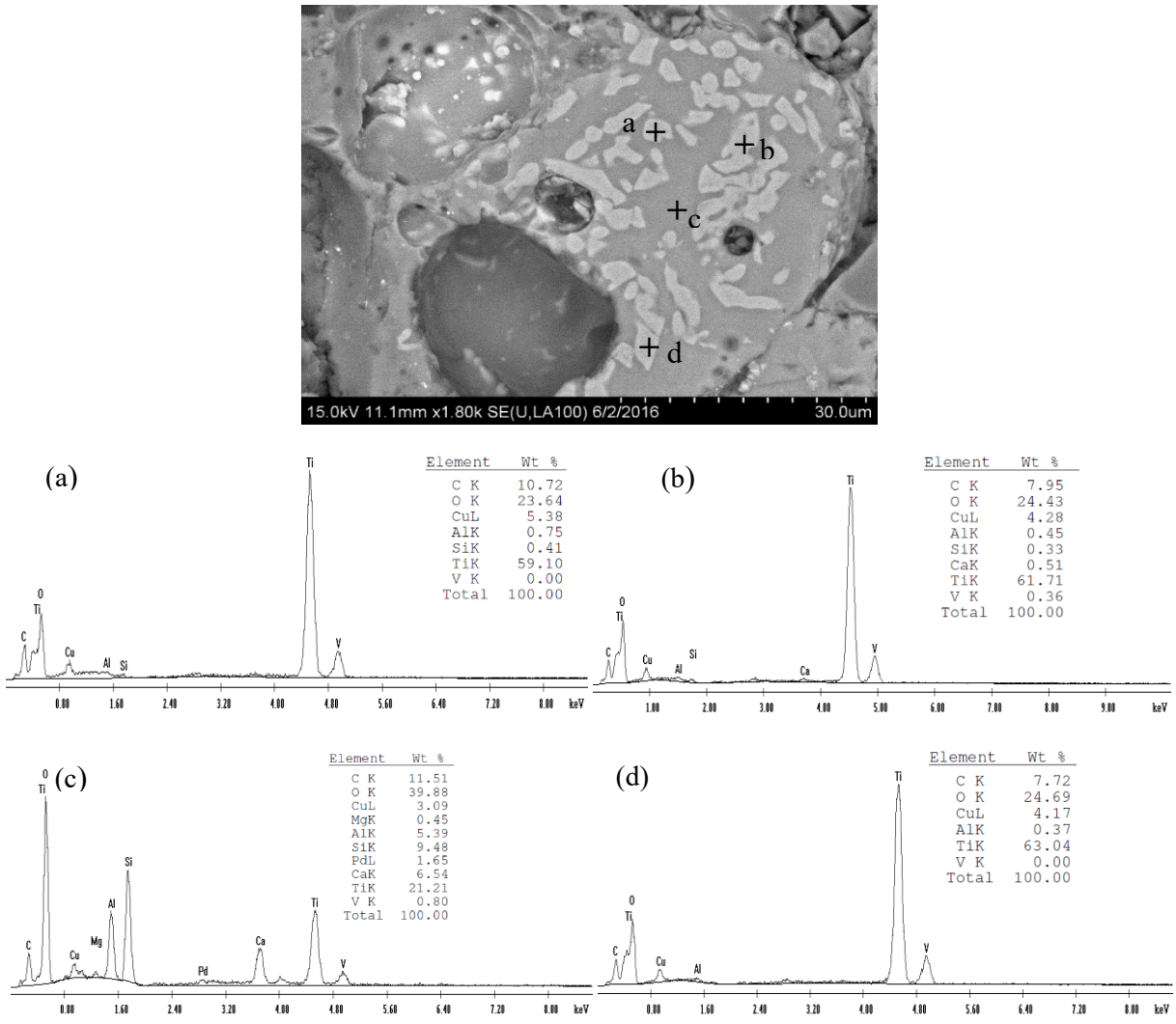

Figure 5.12 SEM micrograph of a deposit with EDS measurements of the light gray phase (a,b,d) and the dark phase (c).

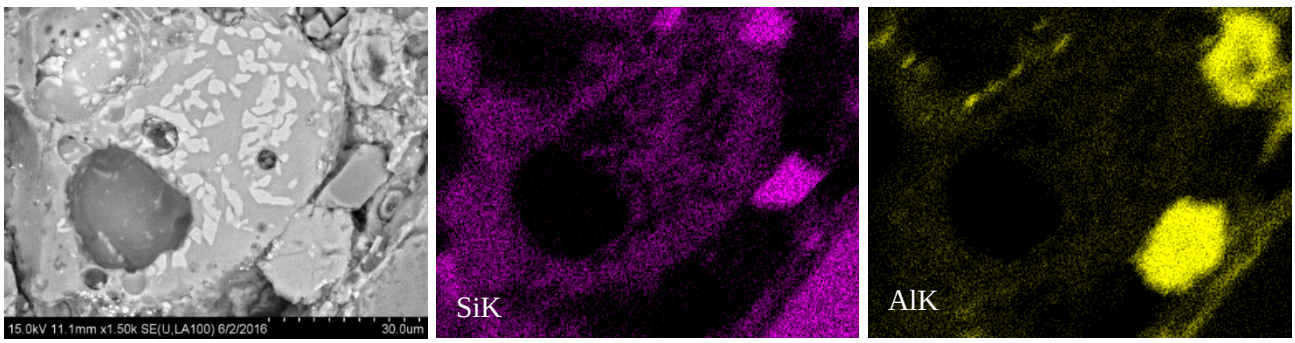

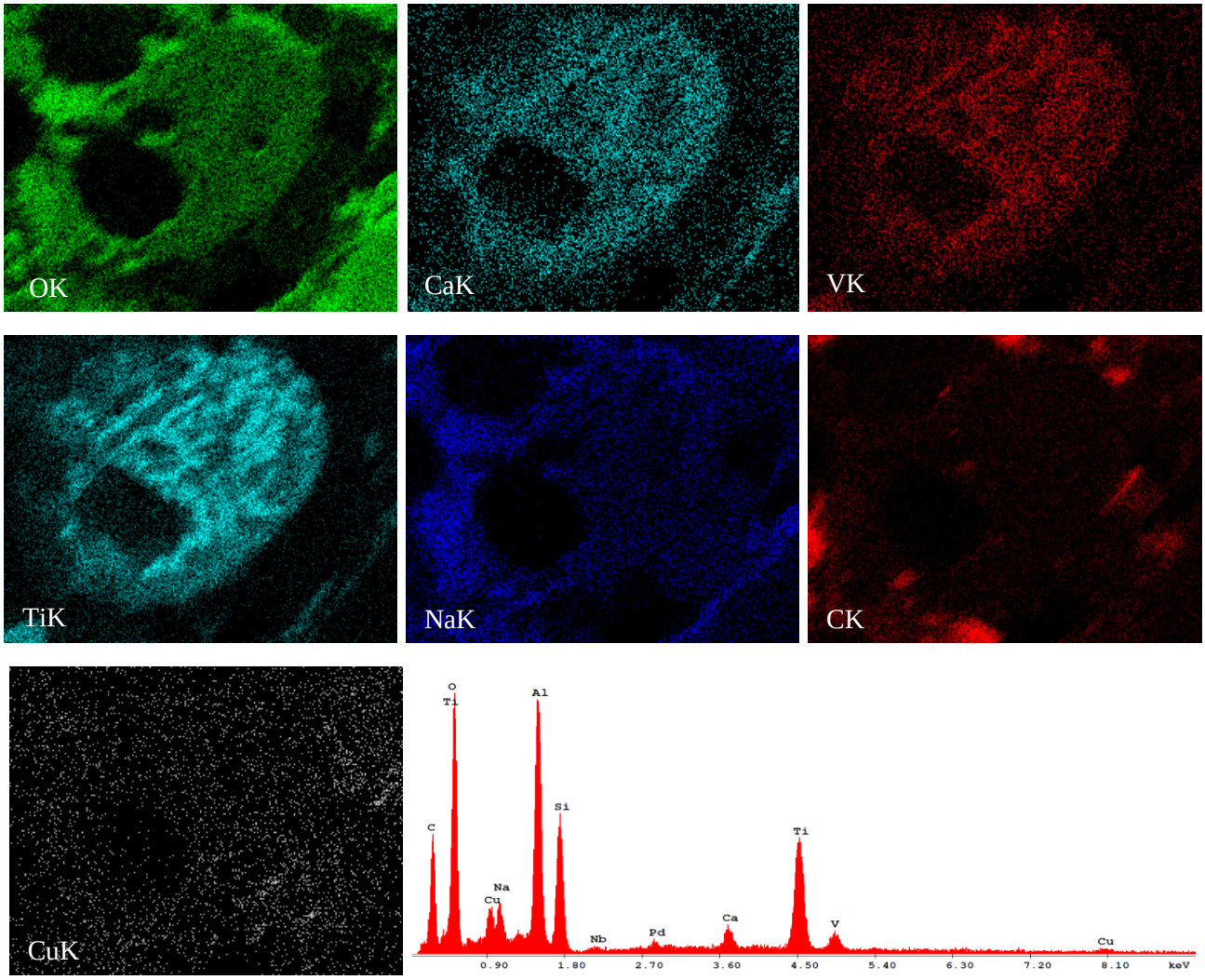

Figure 5.13 X-ray map and corresponding spectra of the deposit.

5.5 Window 8 TPS

Initially, the proper mounting media was undetermined and a test sample obtained as part of the debris loaned by the *Columbia* Research and Preservation Office, was used to select the proper mount. Also, the sample was studied to observe the morphology of the tile under SEM/EDS. A cross-section of carrier panel tile from Window 8 was previously mounted in an epoxy mount and the surface was ground from 800 to 1200 SiC grit paper. After the sample was cleaned and dried, the microstructure is shown in Figure 5.14 with an irregular TPS coating and silica base material. The coating of the tile sample was studied to reveal any existing deposits in relation to the Window 8 thermal pane charred layer and to

observe changes in the coating. The TPS coating exhibited heavy porosity and severe cavities present throughout the coating and between the interface. Figure 5.14 also provides several areas selected for EDS measurements, light gray areas (a and b), dark gray area in c, and d represents an area analyzed of the silica base material. Most of the areas were consistent with aluminum, oxygen, and silicon. The major difference is that the light gray area on the upper surface of the coating (a) contained titanium oxide (TiO) whereas the areas below did not.

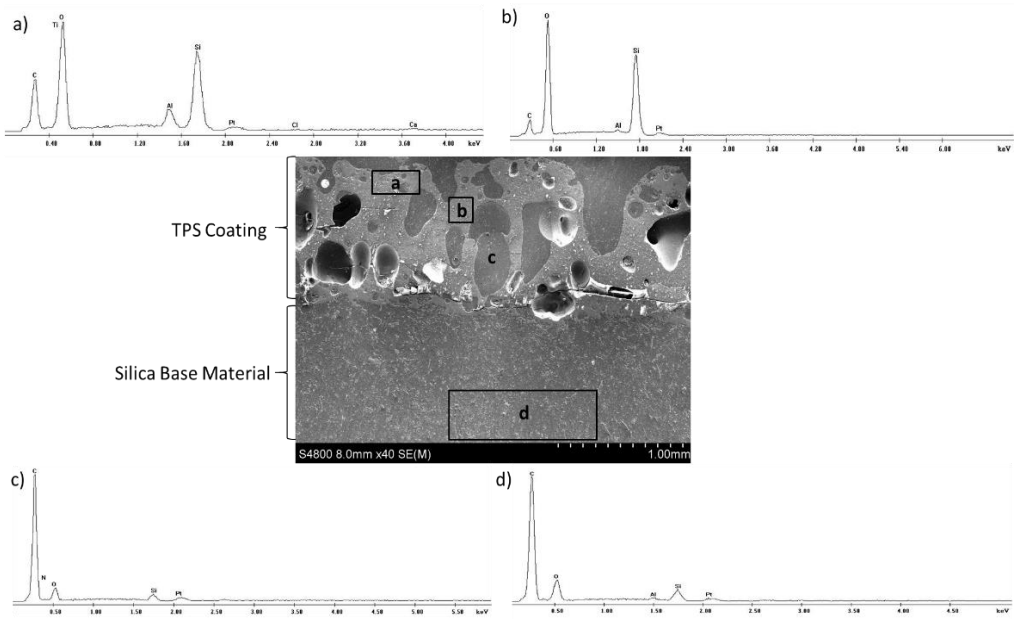

Figure 5. 14 A cross-section of the mounted TPS specimen along with selected areas for EDS measurements.

The TPS coating contained degradation given that the upper surface appeared to be highly disordered. An example of the damaged surface is shown in Figure 5.15 and Figure 5.16 along with EDS spot readings along the edges of a deep "valley" in the coating. Most of the locations also contained similar peaks of oxygen, silicon, aluminum, and traces of carbon. Readings closest to the concave area (2-6), all exhibited similar EDS peaks. The upper surfaces in spots 1, 7, and 8 contained other unique constituents such as titanium oxide (TiO) and smaller intensity peaks of sodium, magnesium, and calcium. Elemental titanium was also found in these three areas from 1.82wt% to 5.75wt% including traces of iron and vanadium.

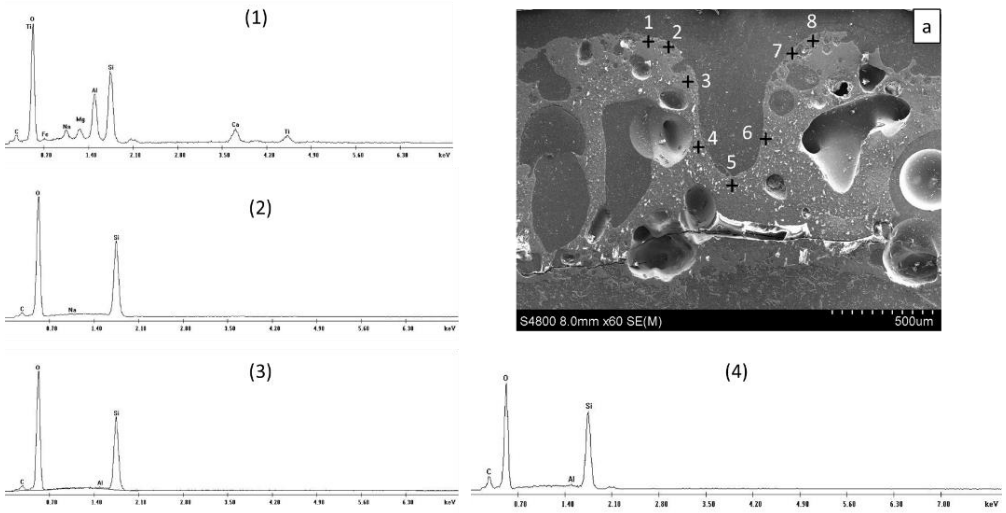

Figure 5.15 SEM image depicting the irregular upper surface of the TPS coating and EDS measurements of spots 1 through 4.

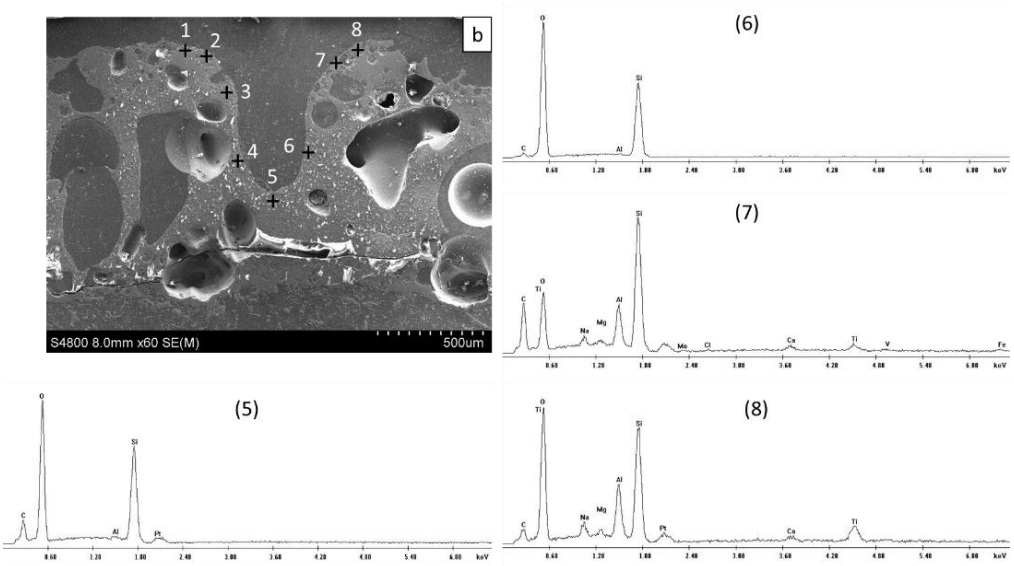

Figure 5.16 Completed EDS results for the remaining spots 5 through 6.

Changes in the compositional results were inspected by analyzing EDS line readings along four lines through the cross-section as shown in Figure 5.17. Line a represents the top edge of the TPS coating and lines b through c signify lower regions of the cross-section. The characteristic peaks detected on line a are similar to other spot readings taken at the top edge of the coating which correspond to carbon, titanium oxide, silicon, aluminum, magnesium, and platinum. On line b however, the titanium oxide is not present as well as magnesium. Just above the interface between the coating and the inner silica

material, the titanium oxide (TiO) was identified. The EDS line results of the silica correspond to the results obtained in Figure 5.14d. Another area showed a large presence of hollow cavities and porosity present on the TPS coating as seen in Figure 5.18. Several EDS readings were completed and were comparable to the previous spot measurements of the light gray and dark gray areas. The EDS analysis indicated peaks corresponding to titanium oxide (TiO) that were predominately concentrated on the upper surface of the TPS coating. Both spots in Figure 5.18 contained the same elements detected including elemental titanium and vanadium.

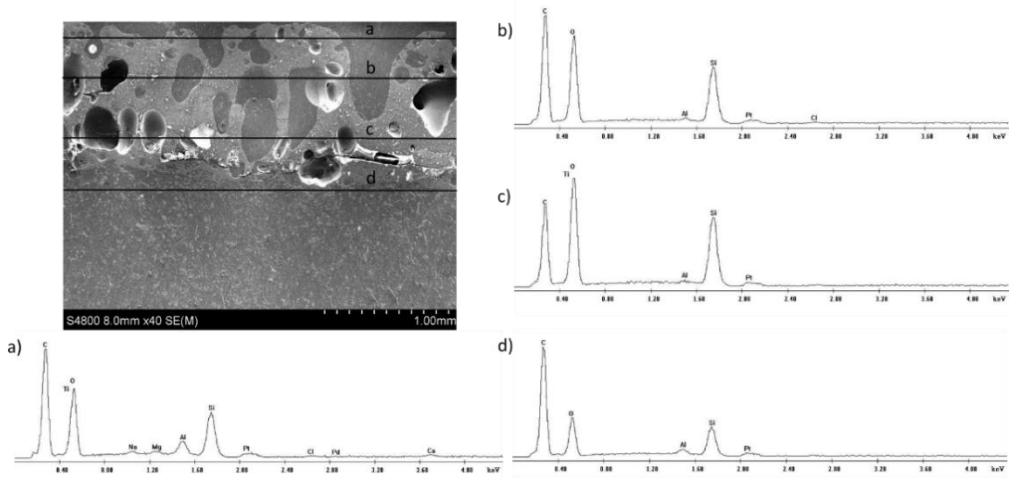

Figure 5.17 EDS results along lines shown in a through d to determine the change in compositional results throughout the coating.

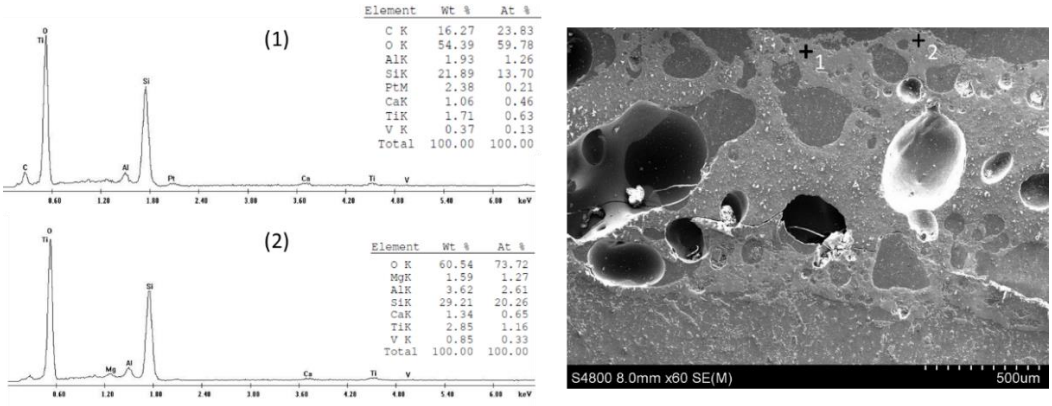

Figure 5.18 Additional spot readings with elemental percentages on the upper surface taken at another location of the TPS coating.

Examining the coating close to the distinctive lip of the carrier panel tile in Figure 5.19, showed hollow black pores and cavities. The spots analyzed on the upper surface (a-c) were consistent in the characteristic EDS peaks of titanium oxide and silicon. Area d on the coating consisted of mostly oxygen and silicon peaks. When comparing the EDS results of the upper surfaces of the Window 8 specimen to the surface XRF results of the carrier panel tiles from Window 7, the main elements of aluminum, silicon, and titanium were present.

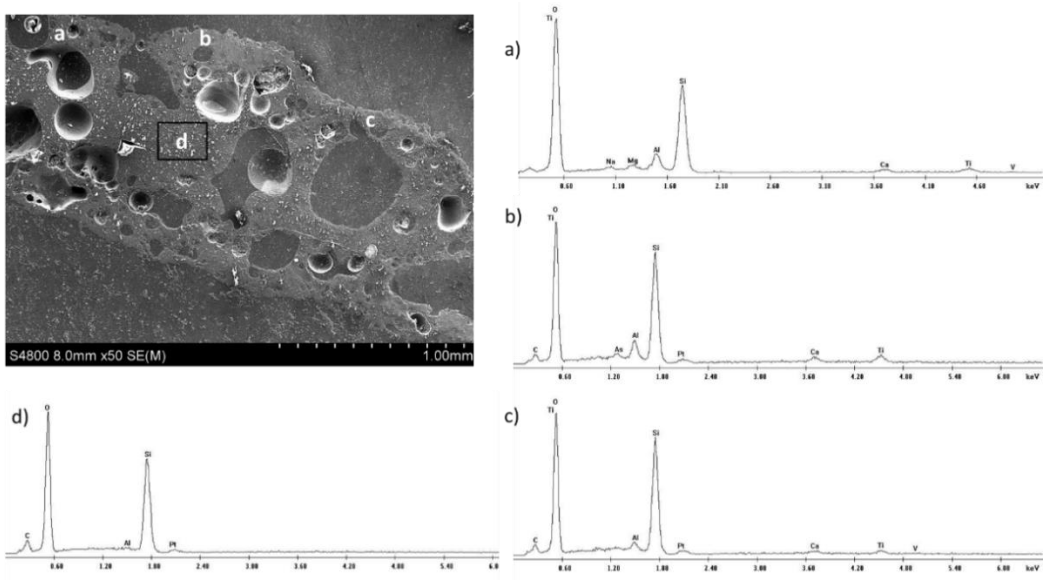

Figure 5.19. Microscopic image of the TPS coating near the carrier panel lip along with EDS spectrums of spots a-c and area d.

5.6 Summary

The carrier panel tiles are extremely brittle materials with a soft inner foam-like silica coating with the hard borosilicate coating. Samples for forensic characterization required the removal of small samples from the window component. A sectioning procedure was developed and tested to determine what tools would yield less damage of the surrounding tile material attached to the window. It was discovered that different sectioning saws will cut through the TPS. One carrier panel tile was safely removed from the window to prepare for sample removal and to determine if the tiles should be removed before sectioning.

Because several small samples were cut using the sectioning method, the carrier panels do not need to be removed from the window. This will also help in conserving the window component for future research.

The loaned carrier panel tile was also analyzed for being a control sample to compare with further data. The morphology of the tile cross-section was examined and exhibited an adhered uniform coating along the bulk silica cross-section. Characterization of the surface was collected as well as SEM/EDS analysis of the cross-section using the SEM microscopy. The elements at the surface consisted of silicon. XRD measurements were performed to identify unknown compounds of the surface that contained silicon oxides, carbon, and Zn. The presence of Zn may be attributed to a zinc based primer for protecting the structural interior of aircraft materials. X-ray maps were obtained to highlight the different phases in the image being scanned. The elements found typical for an unaffected tile include O, Si, K, Cl, and C.

A sample obtained from the loaned debris was examined to identify the elemental compositions and experiment with sample preparation. A thermal pane glass sample used was obtained from the overhead Window 8 and the coating was analyzed through SEM. The removed particles from the opaque glass contained TiO, Al, Si, and Fe. Furthermore, the cross-section of the mounted glass included an adhered and porous deposit. Elemental maps produced on the Window 7 small glass shard, demonstrated a titanium rich spherical phase surrounded by a mixture of other elements. Another sample obtained from the other window was a mounted piece of carrier panel tile. Elemental compositions were explored by observing the TPS cross-section using SEM and EDS analysis. TiO, Si, and Al were present only at the coating cross-sections with a larger presence of TiO at the upper surfaces of the tile. Because there was a common trend in elements determined by XRF of Window 7 and the Window 8 test samples, characterizing the deposits found must be performed to confirm results and determine if layering is present.

Chapter 6: Results and Discussion

6.1 Sectioning Results

Moreover, secondary sectioning was performed on the samples to conform to equipment size requirements. Sample 1 was sectioned into three smaller samples as shown in Figure 6.1 with samples 1.1, 1.2, and 1.3. This image also shows sample 1.1 sectioned into two separate samples to facilitate examination. Sample 2 was sectioned to separate the lip area of the tile into samples 2.1 and 2.2.1 shown in Figure 6.2. Sample 2.1 was sectioned once more into Samples 2.1.1A and 2.1.1B to access the transverse edge of the tile. This transverse edge (2.1.1B) did not contain any colored surface discolorations. The rest of the samples obtained from sample 2.1 include 2.1.2, 2.1.3, and 2.1.4. Figure 6.3 contains the samples from the aft tile with secondary sectioning. Sample 3 was sectioned into samples 3.1 and 3.2 where 3.1 was sectioned one more time to obtain samples 3.1A and 3.1B. Two final samples were also cut from Sample 4 as shown in Figure 6.3. Supplementary tile specimens were obtained for the investigation in the case where the samples need additional analyses. Additionally, exemplar tiles belonging to the loaned carrier panel were sectioned for comparing characterization results.

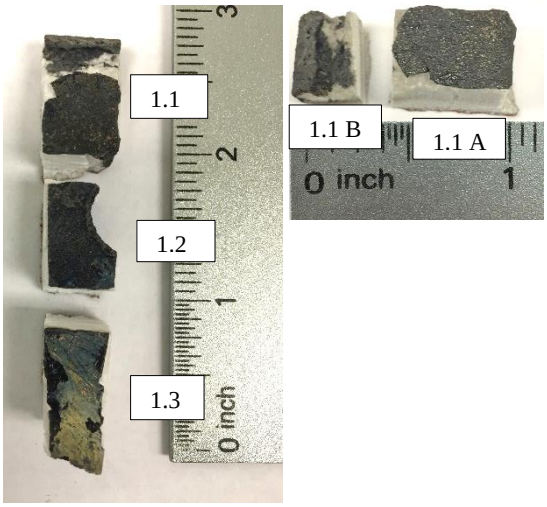

Figure 6.1 Sample 1 from the forward port side carrier panel required additional sectioning to obtain samples shown. Sample 1.1 was also sectioned into two parts.

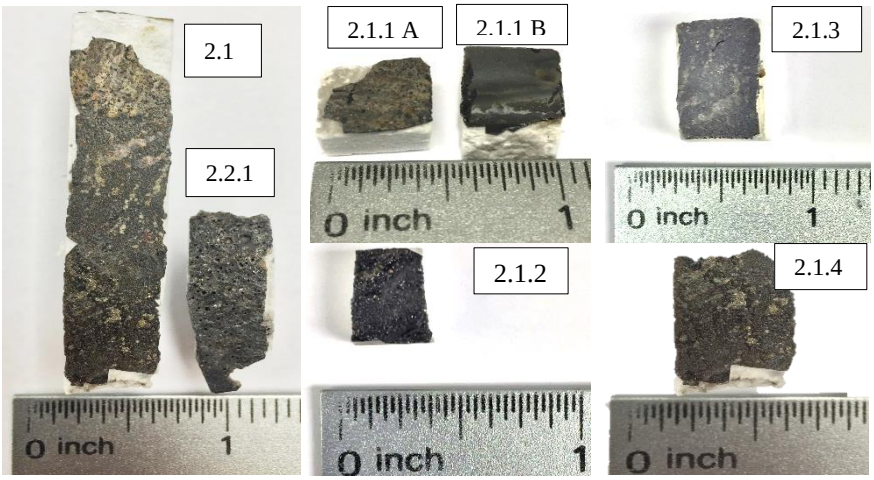

Figure 6.2 Sample 2 was extracted from the forward starboard side carrier panel tile with additional sectioning to obtain five smaller samples.

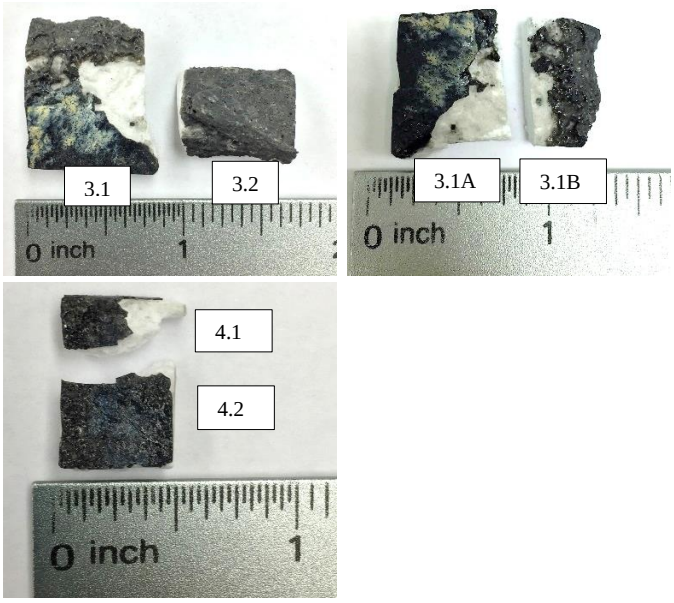

Figure 6.3 Sample 3 and 4 were both obtained from the aft tile where sample 3.1 required secondary sectioning. Sample four consists of two separate samples.

6.2 Scanning Electron Microscopy Analysis

After concluding that all surfaces of the carrier panel tiles from Window 7 contained several elemental species, the SEM was used to confirm the presence of such compositions. The SEM was used to examine surface and cross-section morphology of the samples collected after secondary sectioning. The use of EDS was also performed to determine the elemental composition of selected areas, individual points, and mapping a distribution of an image.

6.2.1 Forward Port Side Carrier Panel Tile

The list of samples located on the forward portside of Window 7 include: Sample 1.1A, Sample 1.1B, 1.2 and 1.3. Each sample was analyzed at the surface and cross-section.

6.2.1.1 Surface Analysis

The morphology of the TPS samples was first examined for indications of deposits or effects resulting from the re-entry plasma. From the visual inspection, sample 1.1A and 1.1B contained few visible deposits. Only a faint metallic and yellow discolorations were present. When observing sample 1.1A under the SEM, several unique surface details were observed. Figure 6.4 shows four areas along the sample with marked surface features. The sample contained a rough surface with elevated areas of the coating as indicated on Figure 6.4a. There were other smaller spherical deposits comparable to blistering and are pointed out in Figure 6.4a. Cracks at the coating surface and small pores were frequently present. Signs of deposits on the coating are shown in Figure 6.4c where several distinct and bright areas were present. This image also shows larger surface cavities. Additional deposits were present as white particulates on Figure 6.4d. It was clear that the surface of this sample contained evidence of deposits at the surface.

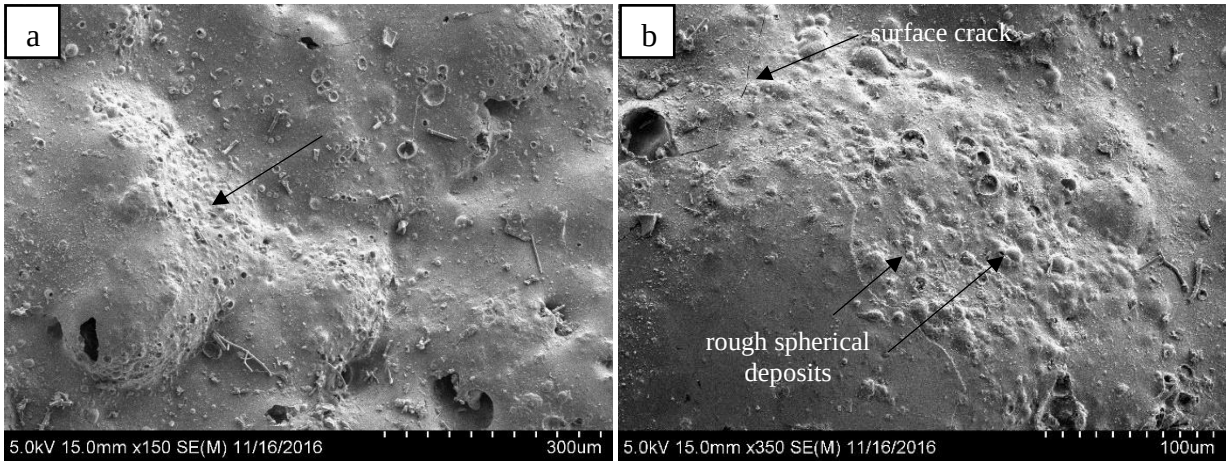

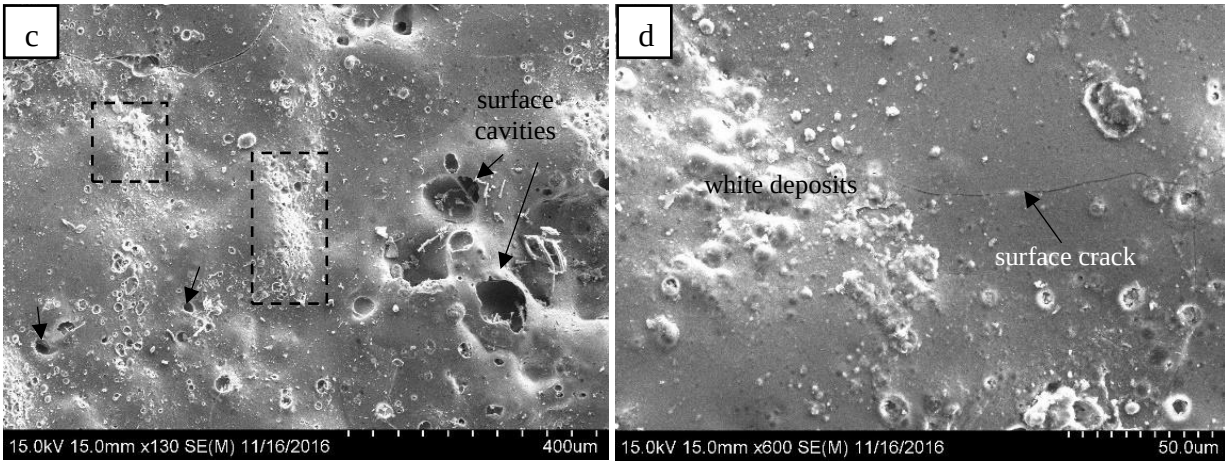

Figure 6.4 Surface characteristics of sample 1.1A at surfaces a-d.

Two areas were chosen to reveal elemental compositions and verify the results obtained by XRF. Figure 6.5a shows an EDS spot reading of a dark area with no apparent deposition. The results show that the surface contains Si and Al only. However, an area with a white deposit is shown on Figure 6.5b to contain major elements of Si and Cu. Minor elements consisted of Al, Ti, and Ni. Additional EDS spot measurements are presented in Figure 6.6 where a dark spot number 1 is shown to contain TiO_2, Al_2O_3, and SiO_2 major concentrations. Spot 2 on Figure 6.6a was measured on the white deposits were shown to be abundant in Al, O, and Si. The white deposits also contained copper and iron as shown.

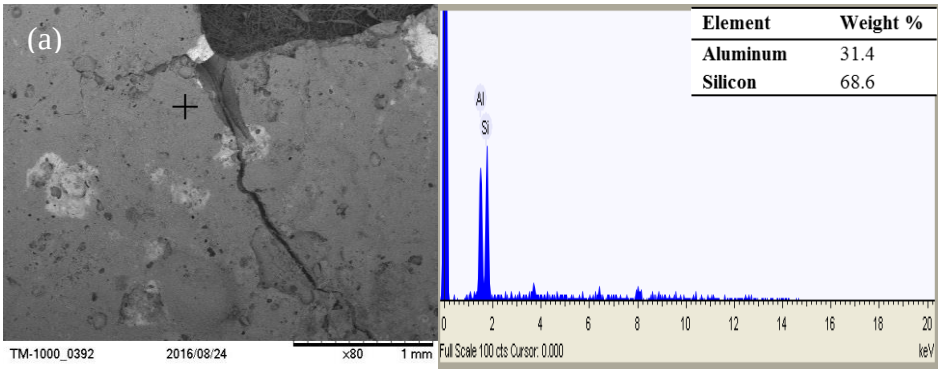

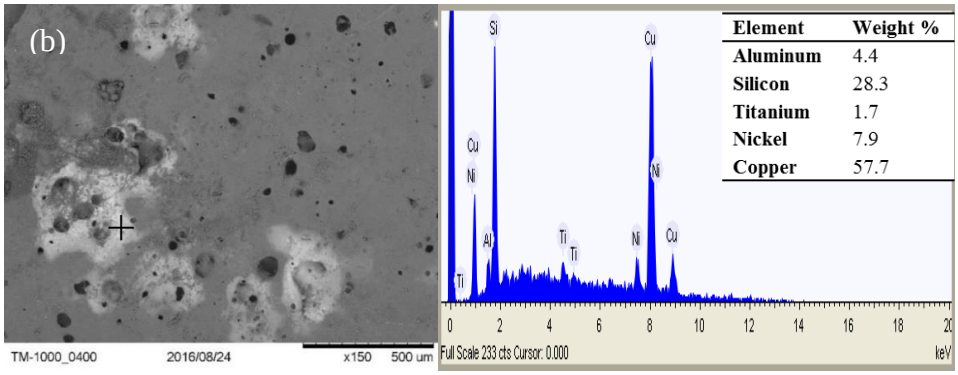

Figure 6.5 Two EDS spot measurements of a dark gray area in (a) and a white deposit in (b).

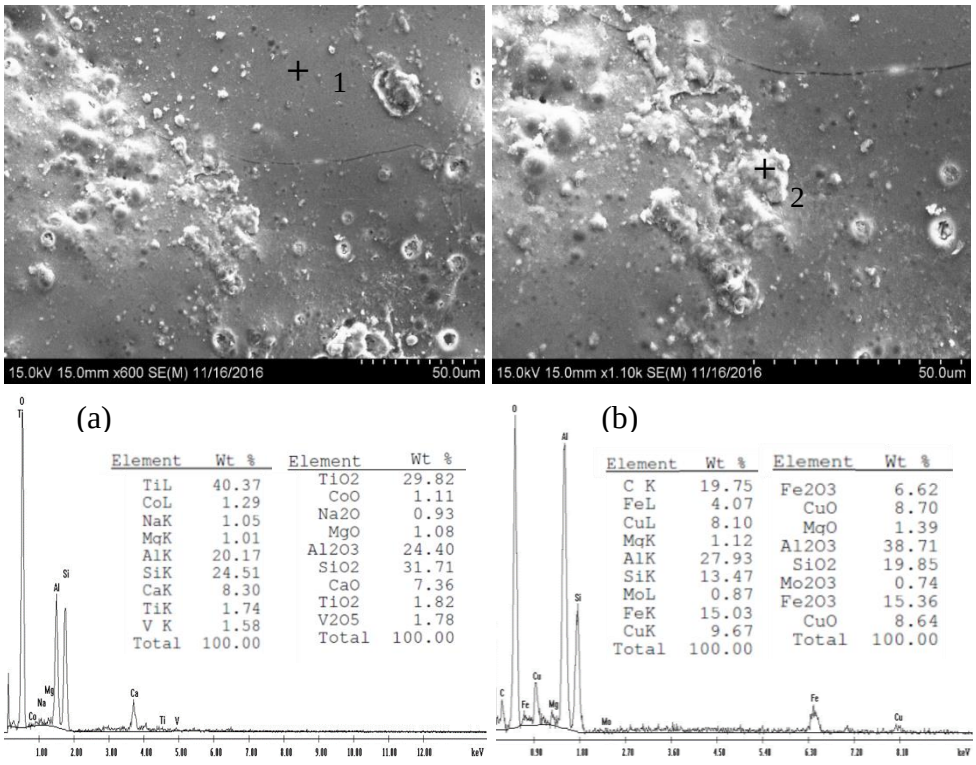

Figure 6.6 EDS measurements of (a) spot 1 and (b) spot 2 with individual element compositions and oxide compositions.

The next sample that was studied was sample 1.1B which was originally attached to sample 1.1A. The surface is presented in Figure 6.7, which was highly irregular. The surface is no longer flat and had several cracks that branched out as shown in the figure. The surface also may have contained deposits as the surface had a rough and jagged texture. When analyzing the surface through EDS, the largest weight percentage of an element detected was aluminum. This is shown on the image in Figure 6.8 that contains the EDS results within areas a and b. Both areas analyzed also contained major elements of oxygen. Other

features observed on the surface of the sample, in which small areas of the coating appeared to be individually fragmented and found to be aluminum oxides (Figure 6.9). The EDS results of one of these cracked pieces were consistent with major element aluminum with 63.62 wt%.

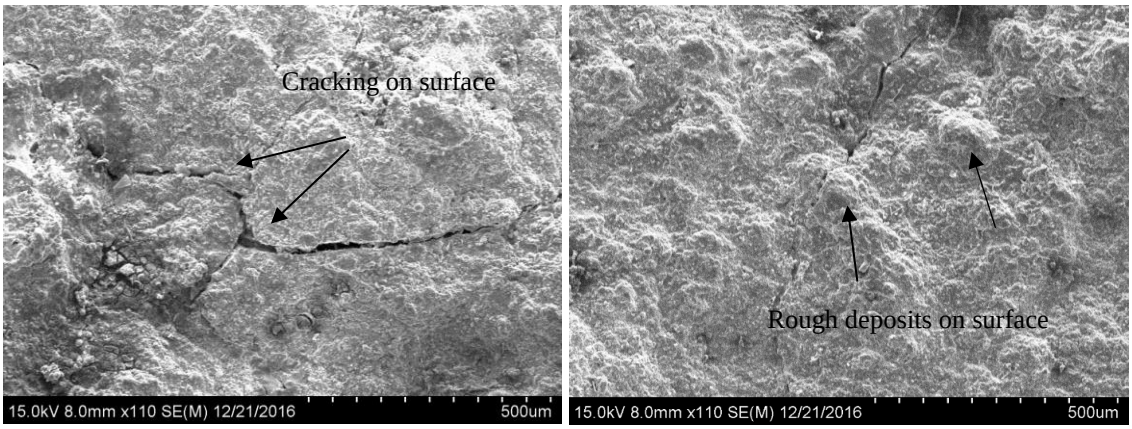

Figure 6.7 Surface condition of sample 1.1B

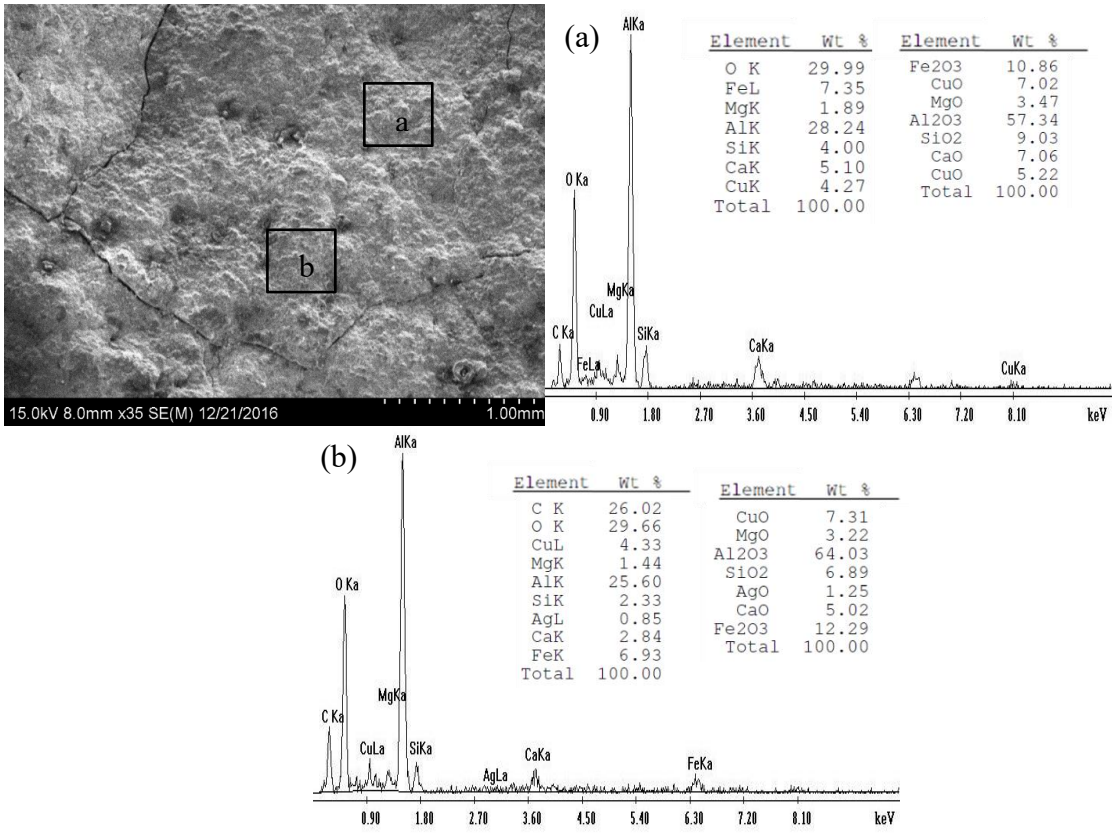

Figure 6.8 Two areas analyzed at (a) and (b) with EDS data showing similar compositional results.

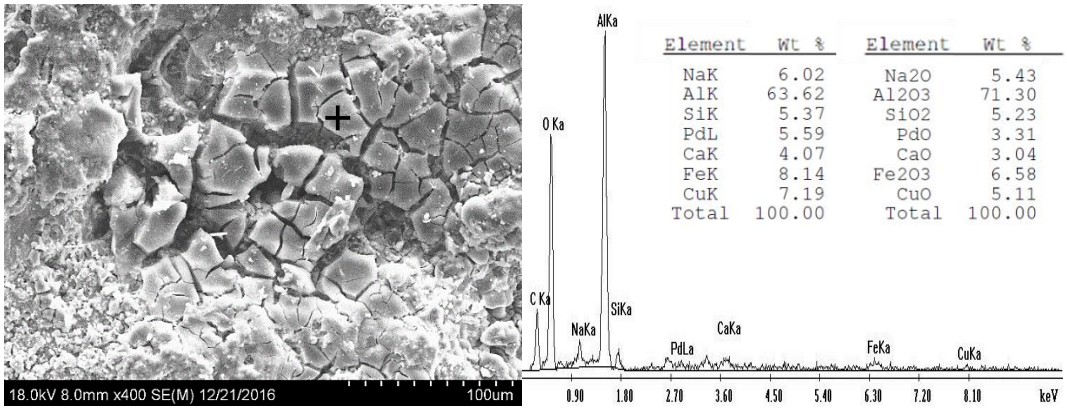

Figure 6.9 The micrograph shows an area on the surface of 1.1B with aluminum oxide fragments analyzed through EDS.

Moreover, the next sample that was examined was sample 1.2 that did not have such a rough texture compared to the previous specimens. Figure 6.10 shows the as-received surface that was generally flat with some changes in contrast and several indentations or pores at the surface There were also several white spherical spots observed as well as small areas of white deposits. These features are demonstrated by the black arrows. EDS analysis was also performed on the surface of this sample as it did not contain a thick and irregular surface. Figure 6.11a shows a boxed area at a bright contrast with the major compositions of 42.62 wt% O and 21.84%Ti. The following minor elements included 11.90 wt% C, 7.48 wt% Si, and 4.36 wt% Al. Gold was detected as the sample was sputter coated with an Au/Pd target and often times, it is detected with EDS. When obtaining oxides calculated through the EDS software, the major oxides were TiO_2, SiO_2, and Al_2O_3.

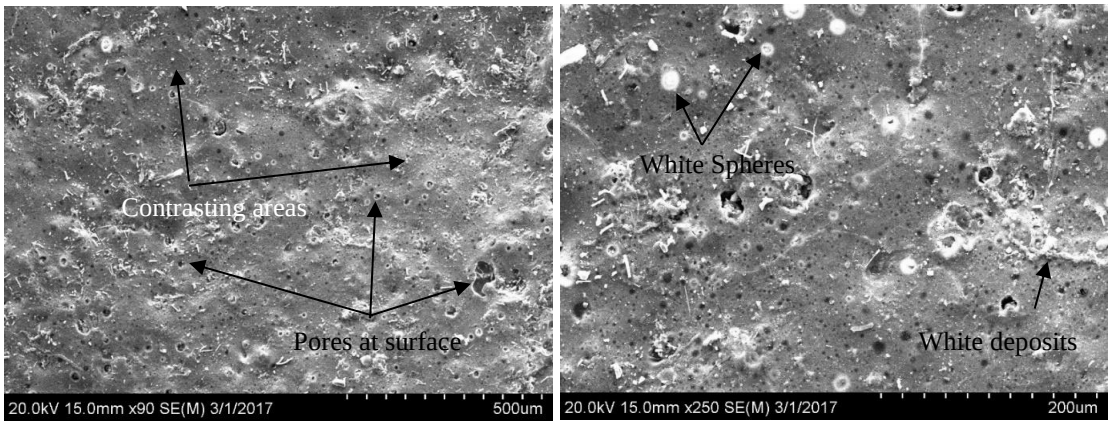

Figure 6.10 Surface of as-is condition of sample 1.2 with several features pointed out.

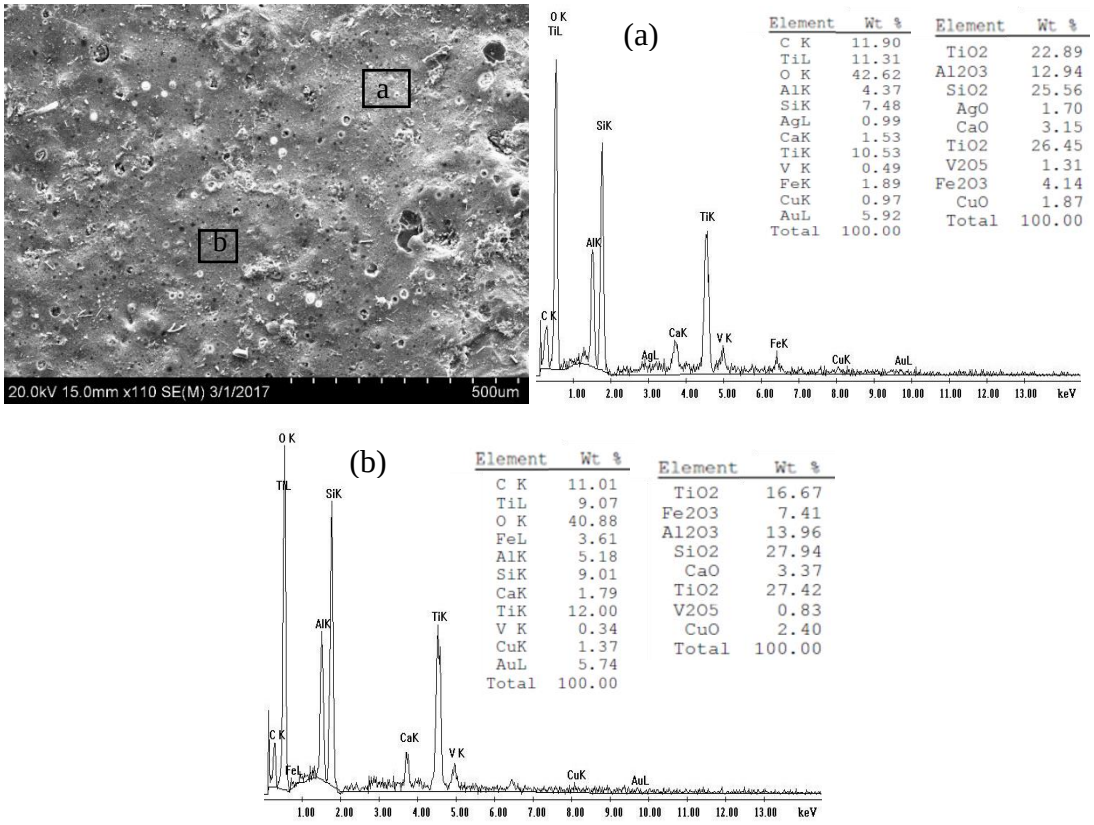

Figure 6.11 EDS area measurements of darker area (a) and a lighter area (b) with compositional results for sample 1.2.

Moreover, Sample 1.3 was the TPS piece that contained the brightest yellow and blue deposits. These areas were analyzed to determine the composition of these deposits. The appearance of the as-received surface is shown in Figure 6.12. Similarly, to the other TPS samples, surface cracks were present on most of the coating. A deposit was observed on the surface as shown in the figure which may be representative of the metallic splats seen in Figure 4.5. Several small surface indentations were also recorded which are located by the white arrows. EDS results obtained from the metallic splat on Figure 6.13 reveal that it is enriched in aluminum (25.67 wt%), oxygen (32.43 wt%), and carbon (36.14 wt%). In contrast, spot b was measured at an area where no deposit was present and it was rich in titanium oxide with 59.11 wt% O and 10.34 wt% Ti. Other elements detected include 13.03wt% Si and 7.31 wt% Al.

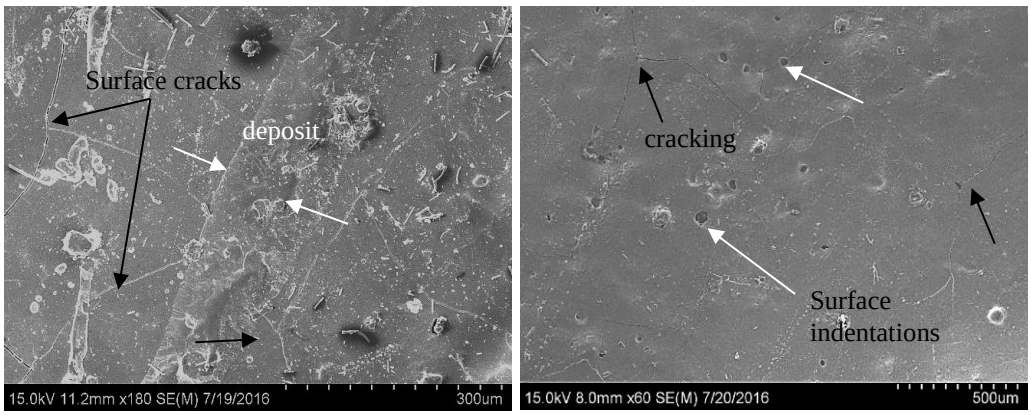

Figure 6.12 Surface of sample 1.3 with the characteristics shown.

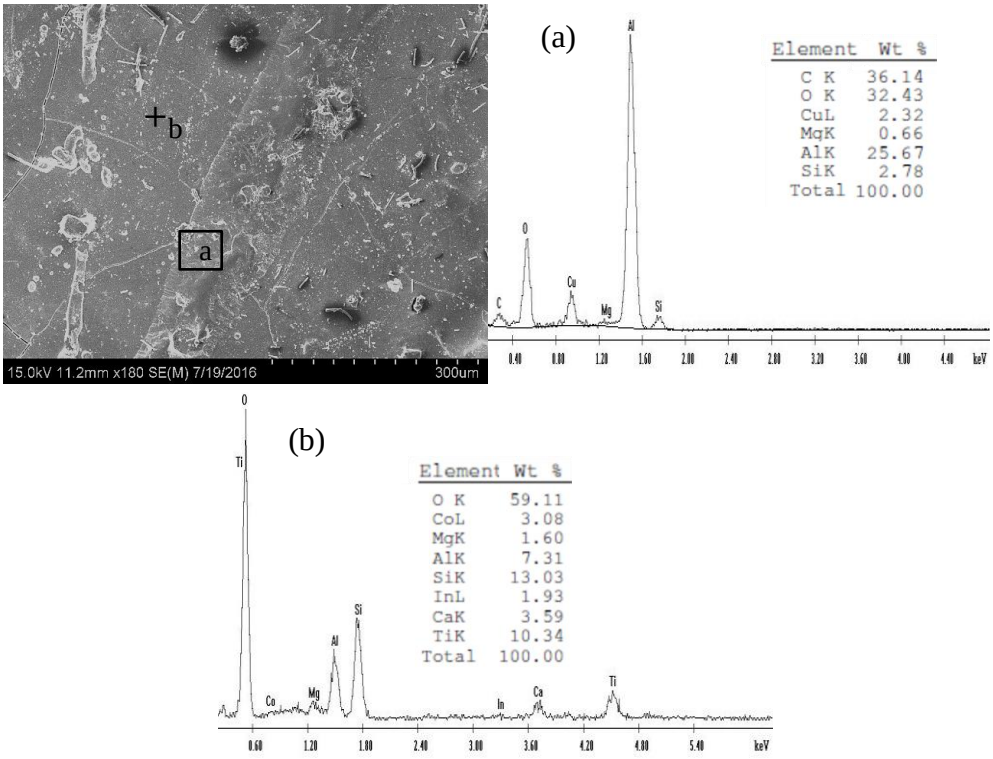

Figure 6.13 Area EDS measurement (a) and spot measurement (b).

6.2.1.2 Cross-sectional Analysis

The sample cross-sections were examined to find evidence of deposits that were present in the TPS coating or base material. Images of the first sample 1.1A at the cross-section are shown on Figure 6.14 a-d. The location of the TPS coating is shown directly adhered to the silica base material on Figure 6.14a. Several of the silica fibers were obscured by the hard epoxy mount. Several cavities and pores with a

variety of sizes were predominately present in areas closest to the surface of the TPS. Figure 6.14b shows additional cavities at the surface and the interface between the coating and silica fibers contained small cavities. The cross-section also shows two distinct layers where a difference in contrast can be distinguished. These two areas are pointed out in Figure 6.14c. It was clear that the surface of the coating was irregular and evident on Figure 6.14d. Throughout the sample observation, the coating thickness did not remain constant but irregular. Within the coating, a light gray phase close to the upper edge was present. One edge of the sample is shown on Figure 6.15 and contained severe damage within the coating. The texture of the coating was altered when compared to the upper surfaces (Figure 6.14) with removed areas of the coating (indicated by black arrows).

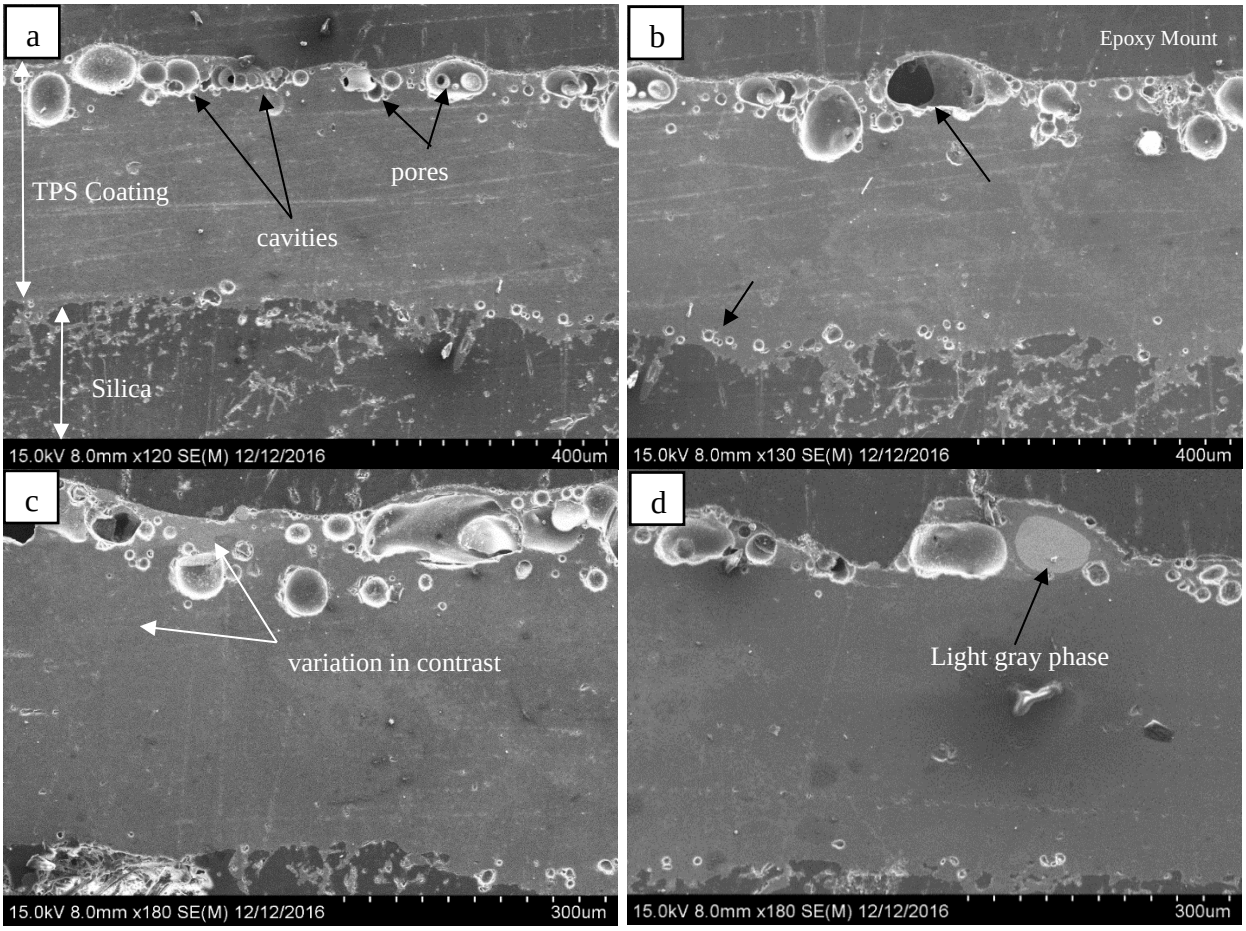

Figure 6.14 Cross-sections of sample 1.1.A detailing various residual characteristics.

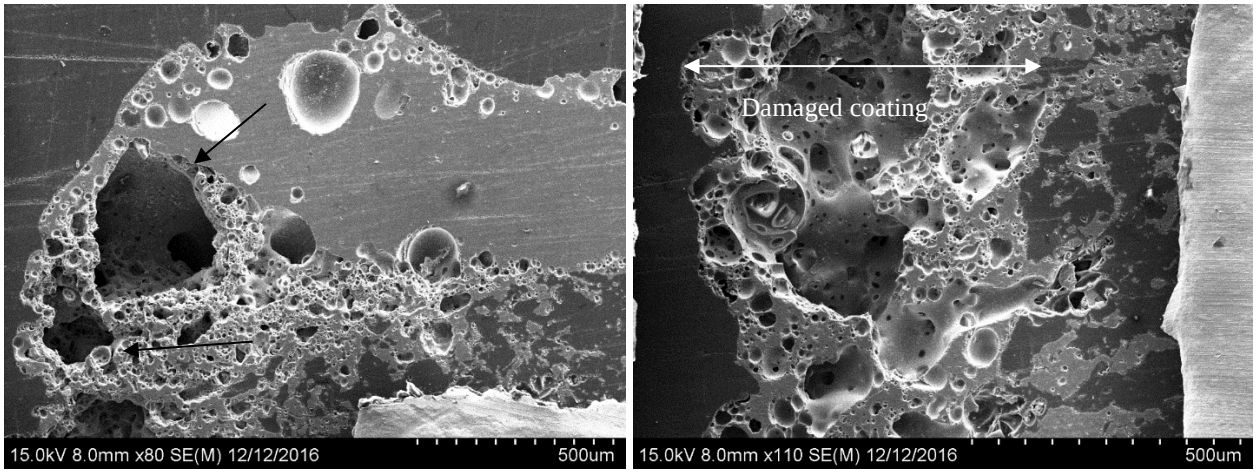

Figure 6.15 Outer edge of sample 1.1A with severe damage at the coating.

Next, EDS analysis was performed to discover if any deposits were embedded in the cross-section. The coating was first analyzed in an area located in Figure 6.16a where area EDS results show that it was rich in Si and O. However, all areas at the top edge of the coating contained additional elements or oxides. This is shown in Figure 6.16b where the results of the top edge consisted of TiO_2 and SiO_2. Copper was also frequently present as a minor oxide, CuO, and an aluminum oxide Al_2O_3.

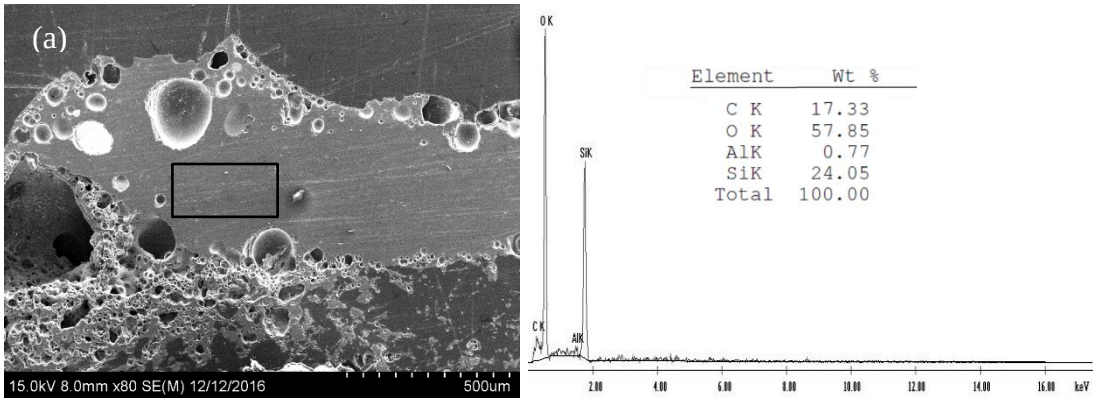

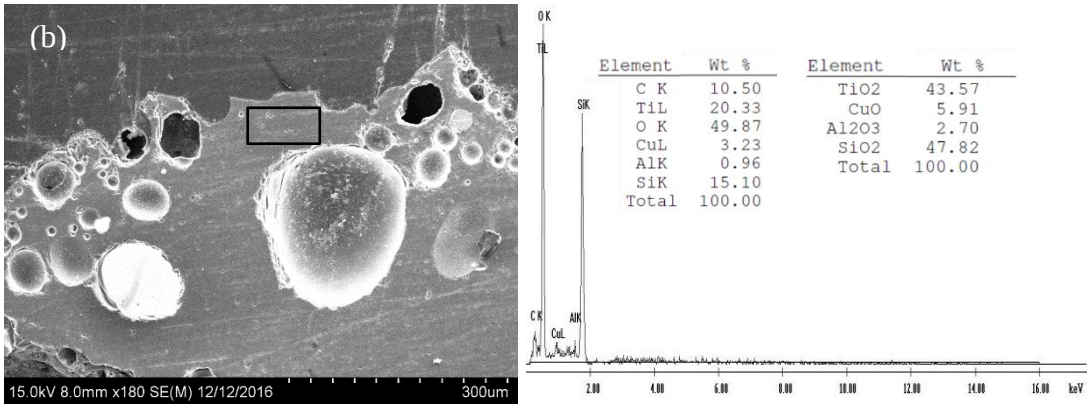

Figure 6.16 Two areas (a) and (b) analyzed through EDS.

The light gray particles that were present in the coating were analyzed and two particles are shown in Figure 6.17. The first area was located at the upper edge of the coating at a higher magnification, at a light gray phase. Through EDS, the light gray spherical particle was Cu-rich as shown in the spectra. A second larger particle is also shown except it contains an additional minor element of Ni mixed with major element Cu. Several of these particles were observed in the upper areas of the coating.

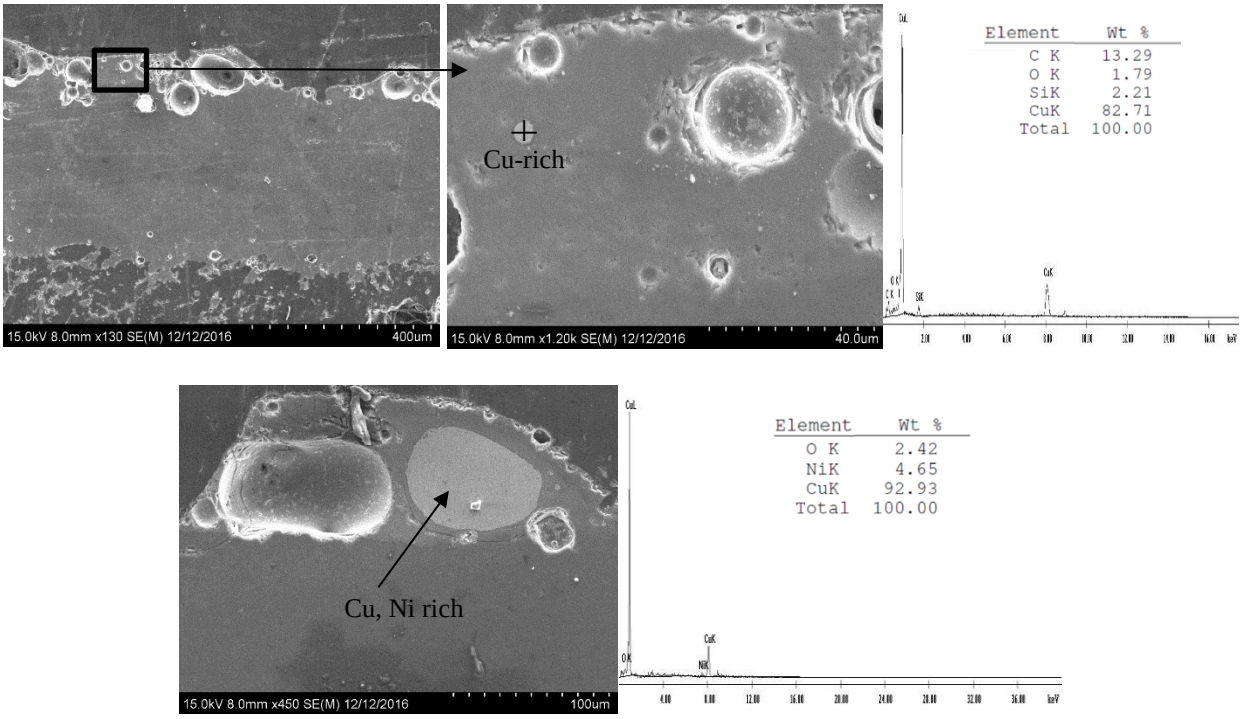

Figure 6.17 The uppermost area of two cross-sections with spot EDS spectras of two light gray spots.

Next, the edge of Sample 1.1A was evaluated since the coating contained the most damage. Two areas and one spot at the coating were studied and shown in Figure 6.18. Area 1 is located close to the edge of the sample and was found to contain O, Si, and Ti. These correspond to SiO_2 and TiO_2 oxides. Other minor elements found were aluminum and copper. Area 3 was located in an area away from the edge of the coating and its spectra shows the same major oxides of SiO_2 and TiO_2. Additional minor oxides of Fe_2O_3, CuO, Al_2O_3, and V_2O_5 were present. Much further from the edge of the coating in spot 2 was rich in O, Si, and C. Copper was a minor element present at this area.

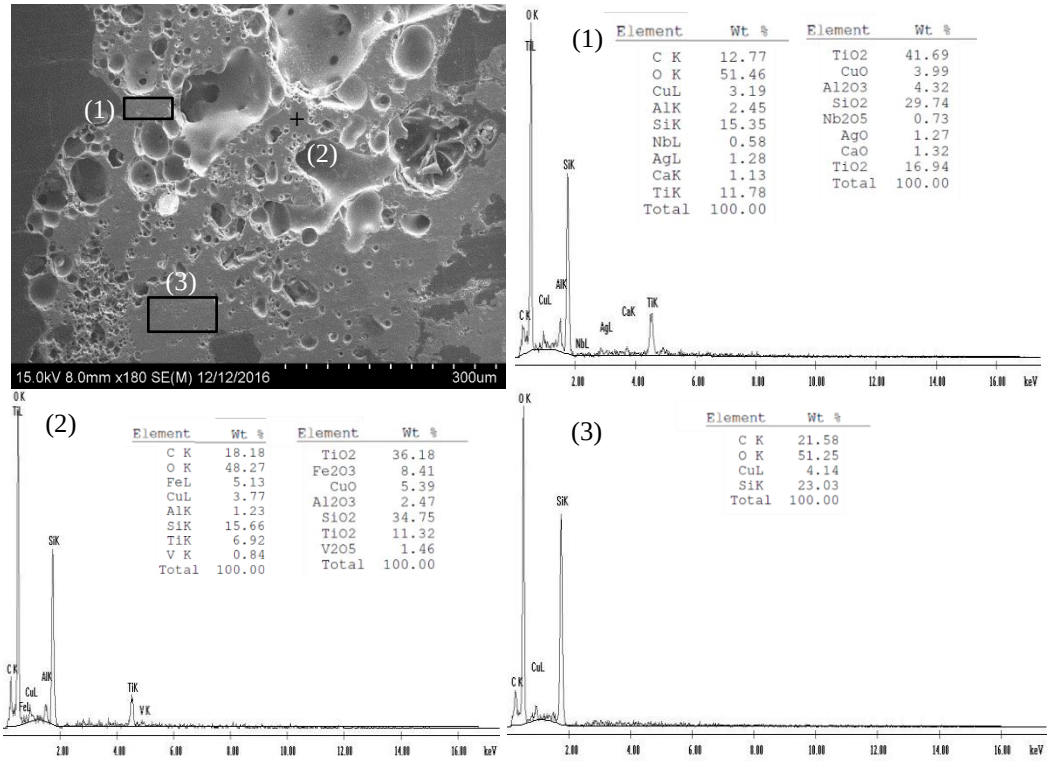

Figure 6.18 Outer edge of the sample with area reading (1), spot reading (2) and an area on (3).

Because there were clear indications of the aforementioned constant elements and oxides existing well below the TPS coating, EDS area X-ray elemental maps were generated from an image obtained from SEM. The intensities of the color and distribution are related to the concentration and the distribution of each element detected. The positions of the specific elements of a cross-section of the TPS coating are shown in Figure 6.19. The elements present at the entire surface analyzed are oxygen and silicon. The image measured also contained a lighter contrasted phase and it is clear from the X-ray maps that this area

was rich in Al, Ti, and Ca. Aluminum was concentrated on this lighter phase and dispersed throughout the cross-section. The calcium and titanium were mostly prevalent at the light gray layer. Iron was also present and located in one area near the cavities of the coating. Vanadium and copper were dispersed throughout the cross-section. The location of the carbon detected was due to the plastic mount of the sample and the deep porosity of the coating.

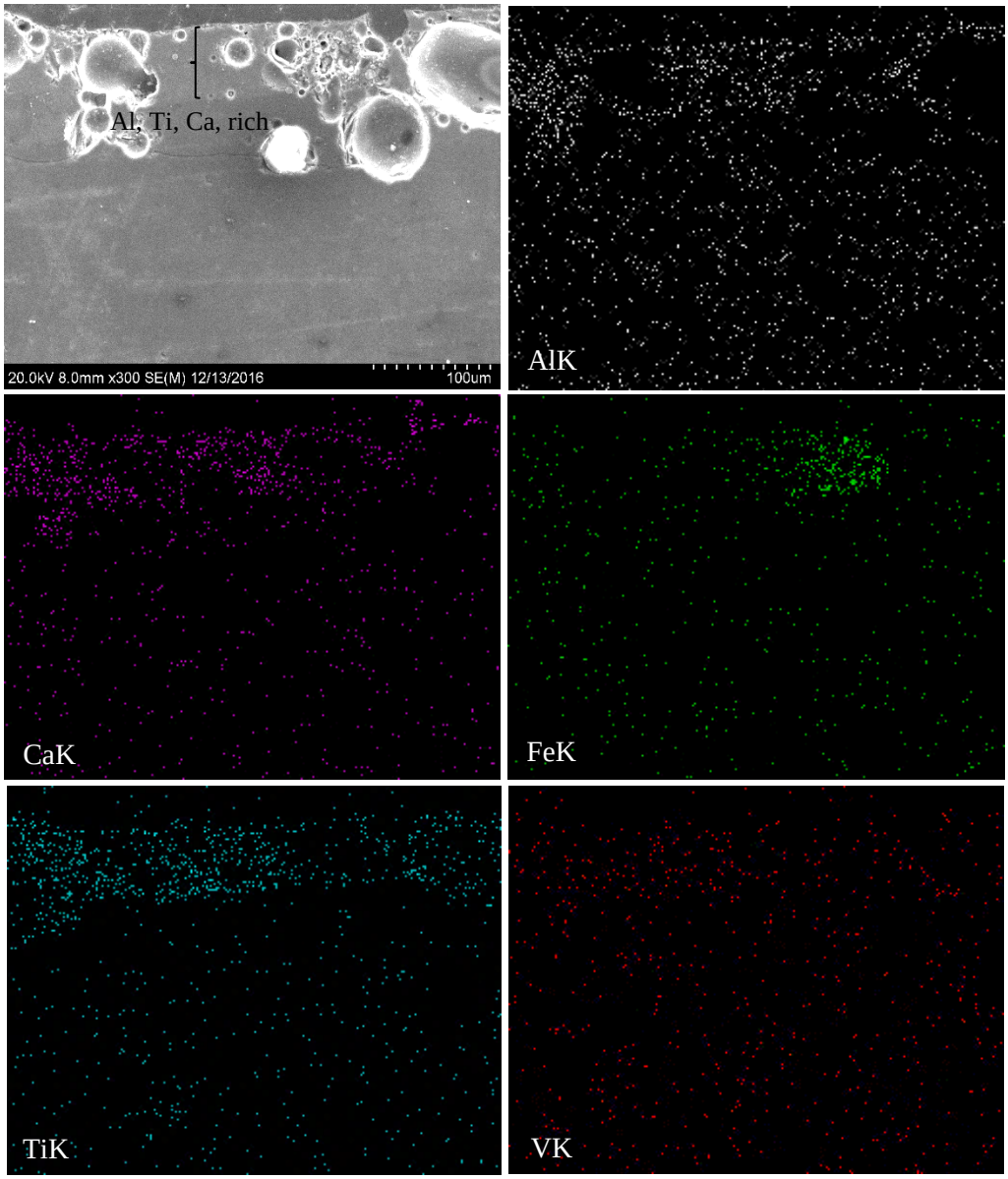

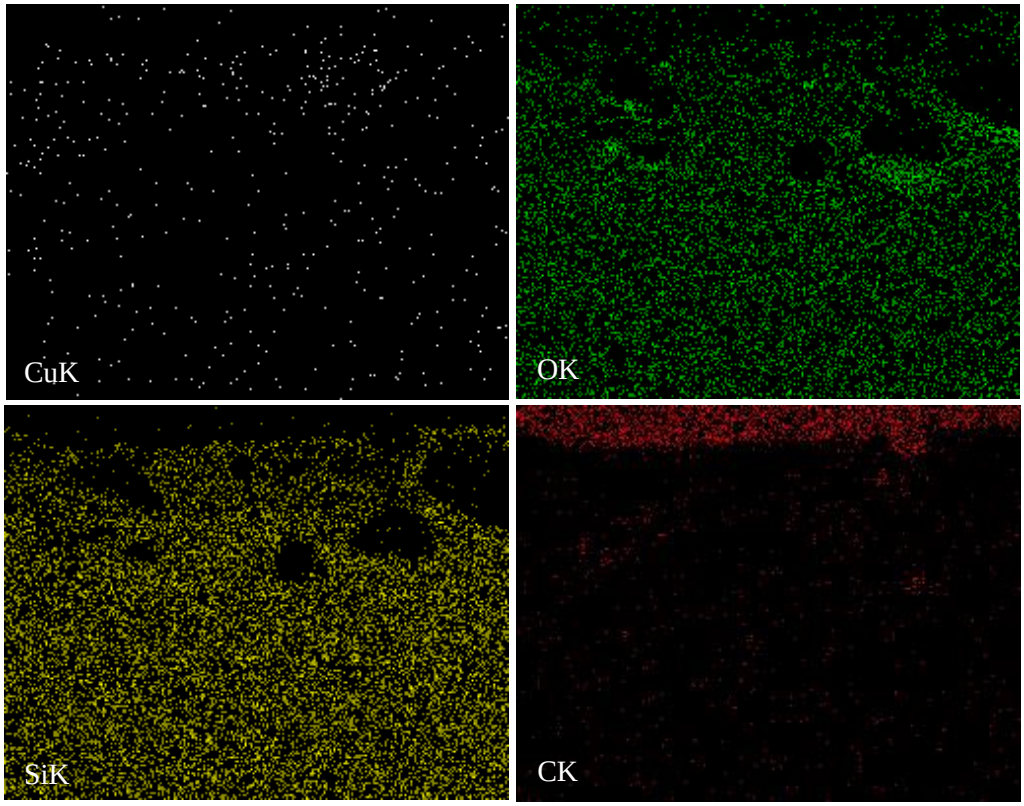

Figure 6. 19 X-ray maps of one cross-section of sample 1.1.A.

A second area was also analyzed through X-ray mapping at a location closer to the top edge of the coating. This area previously contained TiO_2 and SiO_2 and developed a light gray spherical phase. The X-ray maps are shown in Figure 6.20 where similar elements were detected and include Al, O, Ti, Si, Fe, Cu, Ni, V, and C. The difference between the area shown in Figure 6.19 was that calcium was the only element not detected. The common elements present throughout the coating were silicon and oxygen. The presence of oxygen shows that there are oxides present on this cross-section. The aluminum detected was concentrated at one edge of the surface and diminished through the coating. Iron contained a similar characteristic and was also shown to be located on the same edge of the coating. The map demonstrates that titanium formed at most of this area of sample 1.1A. Similarly, vanadium formed along where titanium is located. A light gray particle was present on the cross-section where it is confirmed to be comprised of copper and nickel highlighted by their maps.

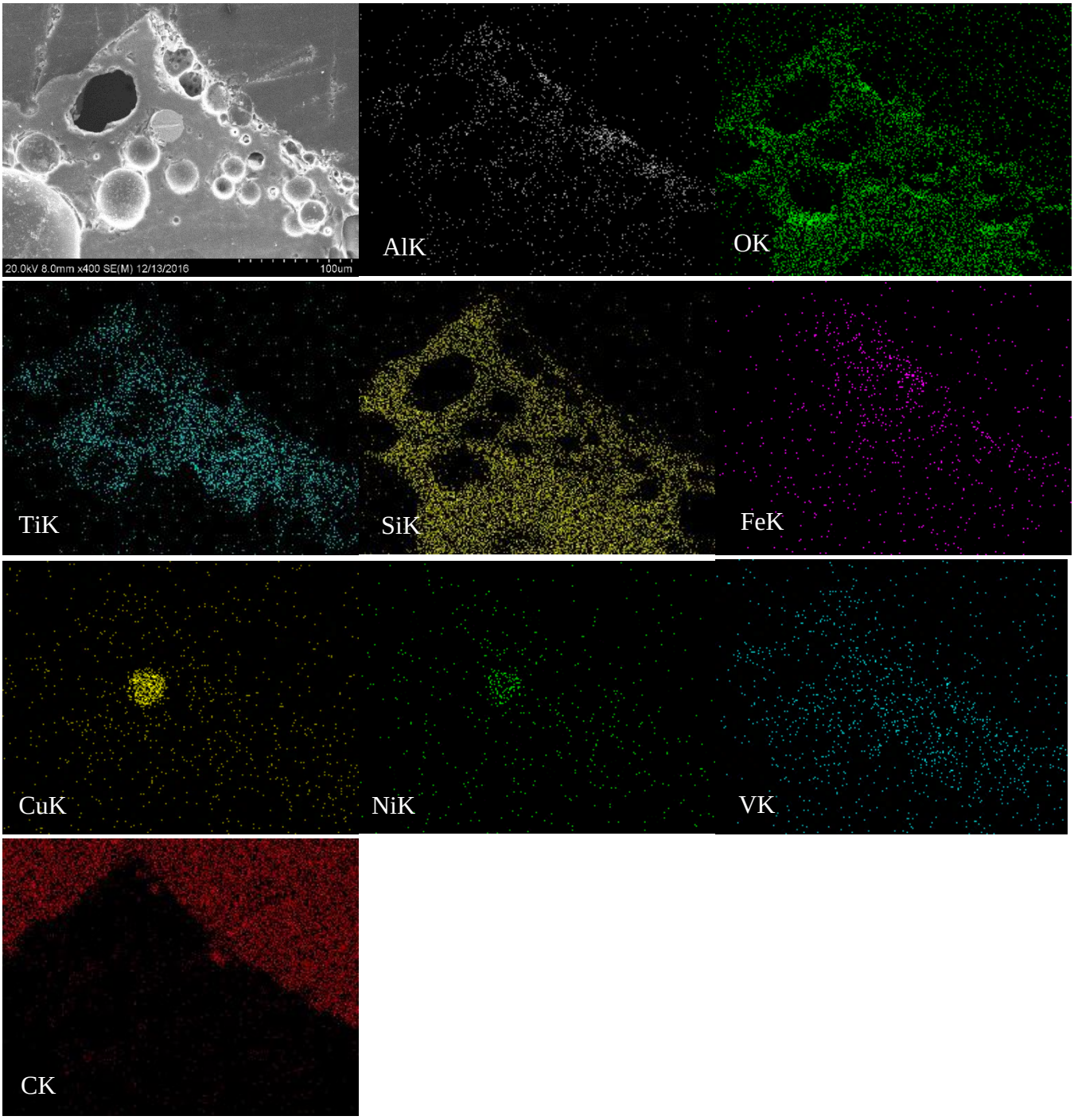

Figure 6.20 X-ray maps of sample 1.1A on the upper edge of the coating.

The following sample that was examined at the cross-section was sample 1.1B which was previously attached to sample 1.1A. Four microstructures, a through d, show several areas of the sample in Figure 6.21. The coating of the sample is exhibited by the black arrows in Figure 6.21a and b. The coating of this sample ranges from 50 to 55µm and is smaller in width when compared to sample 1.1A.

Also present in the coating are a few open pores within the coating and several areas of the silica fibers were not fully encapsulated by the mounting material. The exposed silica fibers are noticeable in Figure 6.21c and d. Image d also shows open pores and cavities along the interface of the coating and base material. On the coating, several light areas were also distinguished. The micrograph shown in Figure 6.22 shows two areas that were studied with EDS. Area a was located near the surface of the sample, while area b was located well below the interface at the bulk material. The difference in both areas was that near the surface, silicon and oxygen were the largest weight percentages obtained of 24.58 wt% and 52.31 wt%, respectfully. This corresponds to having a SiO_2 composition of 56.39 wt%. Whereas, the area below the interface contained 44.13 wt% Al, 22.0 wt% O, and 10.52 wt% Ti.

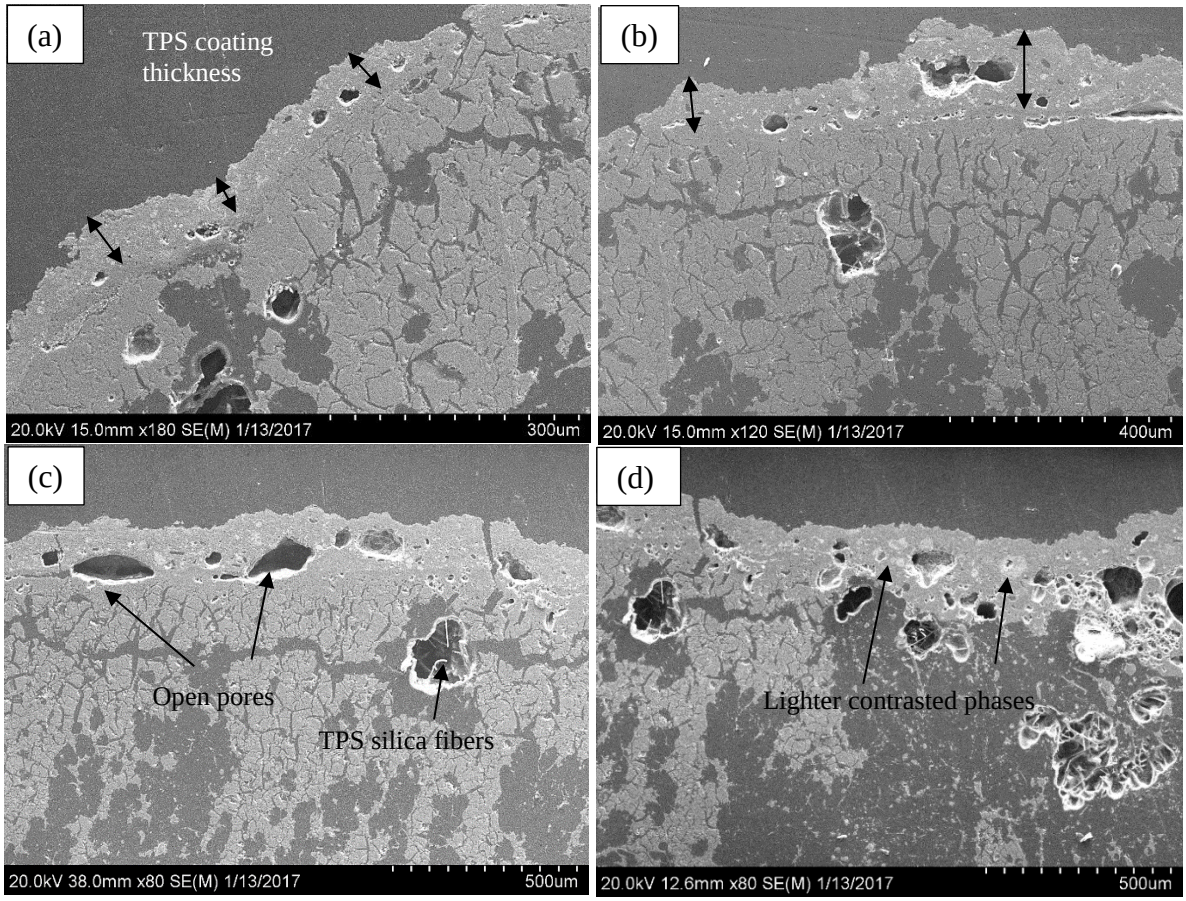

Figure 6.21 Four microstructures depicting different areas a-d of sample 1.1B.

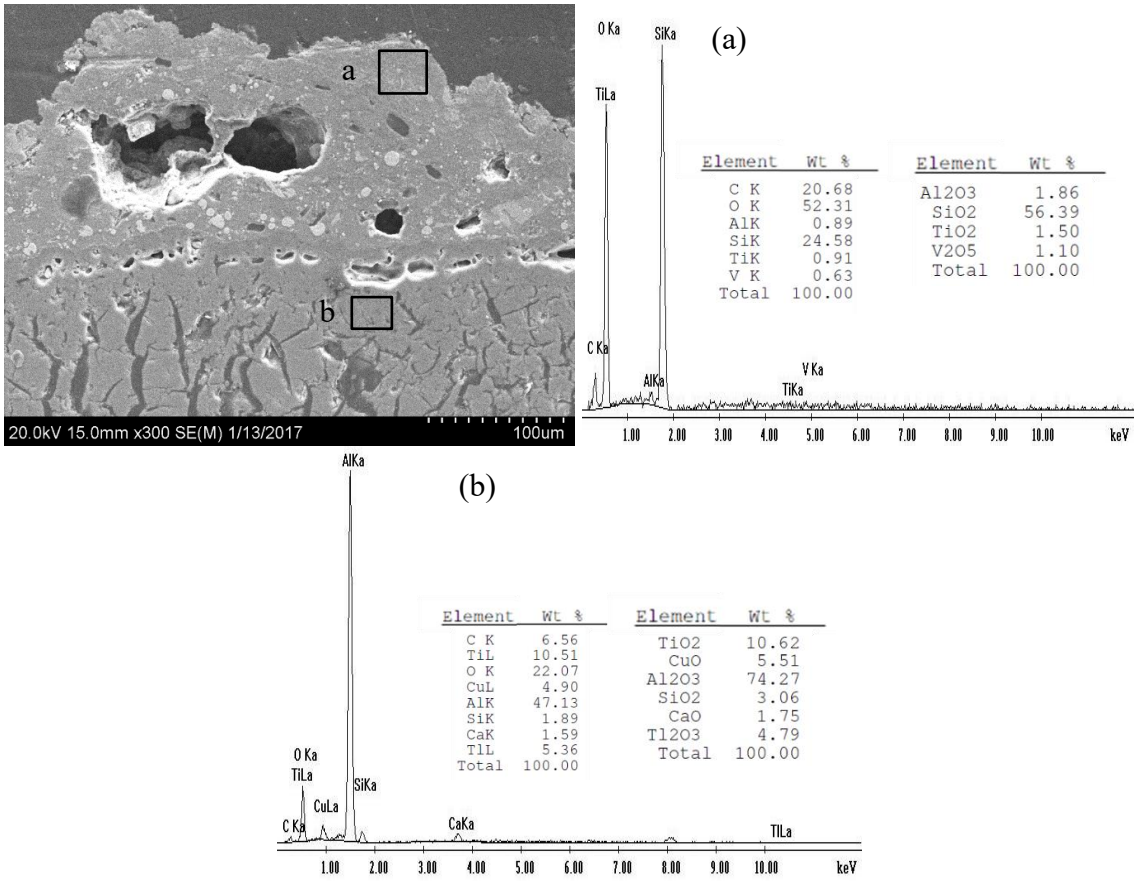

Figure 6.22 Two EDS readings at (a) and (b).

A second area was studied where one side of the sample sloped downwards and the SEM image is presented in Figure 6.23. EDS was performed at the coating and base material where the coating at this location contained 44.32wt%Al whereas at the base material contained mostly silicon and oxygen. It is evident that different locations on this sample contain dissimilar formed deposits. In order to better determine the location of the phases present, X-ray maps were generated for a cross-section shown in Figure 6.24. The elemental maps show that the light gray phases are concentrated with aluminum, iron titanium, and copper. Oxygen and silicon appear to make up most of the sample analyzed. Calcium was only present it the coating of sample 1.1B. The vanadium as shown in red was finely distributed mostly within the coating.

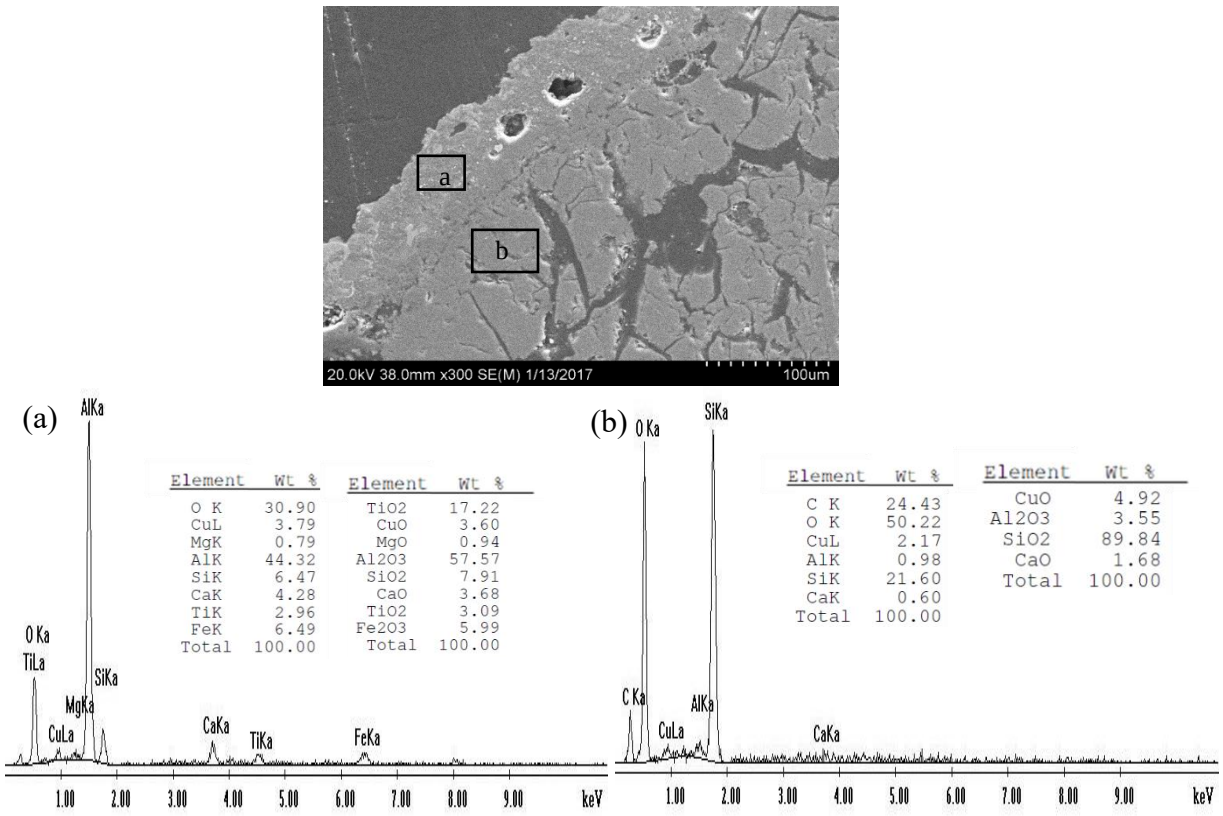

Figure 6.23 A second micrograph showing the difference in elements detected of the coating (a) and the base material (b).

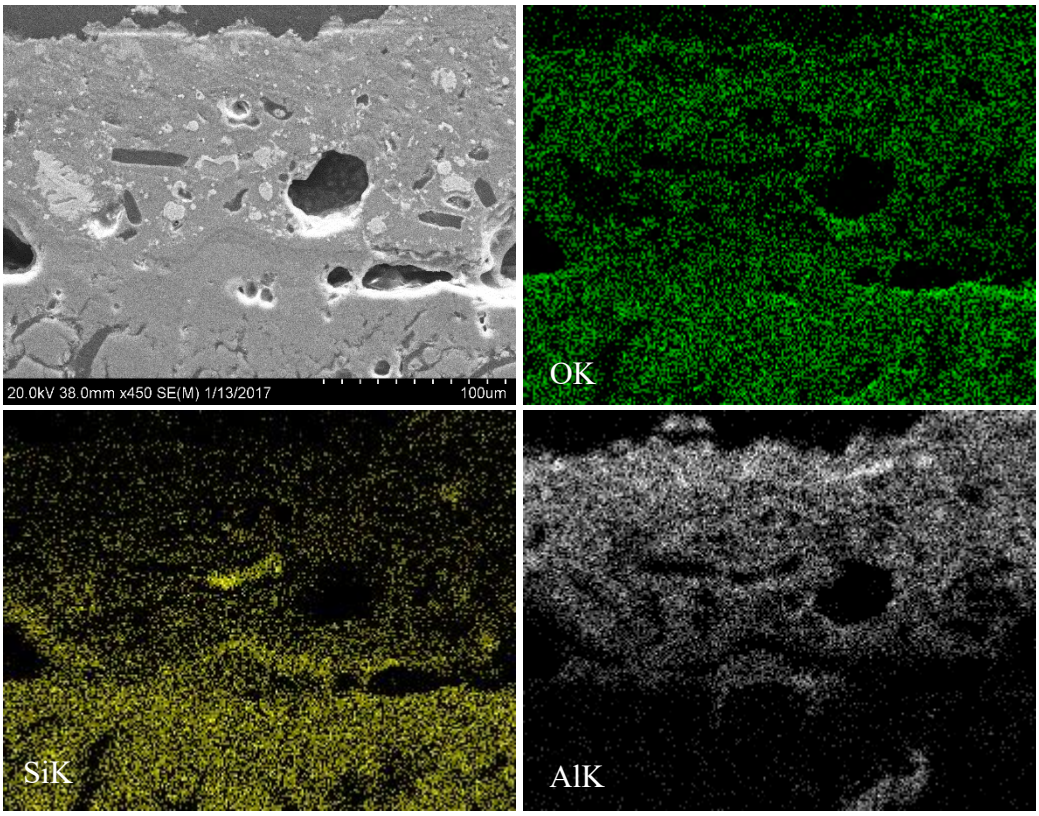

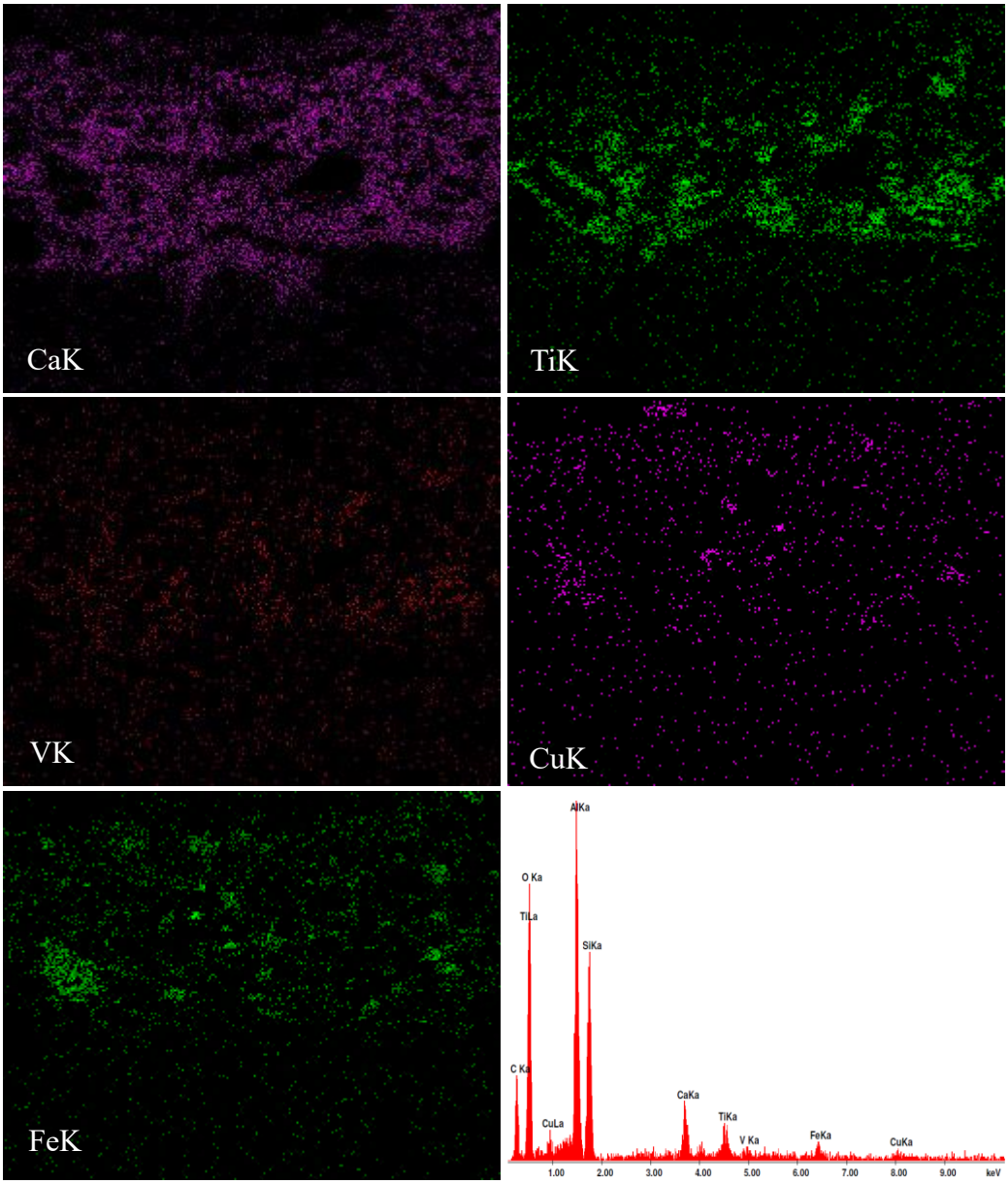

Figure 6.24 The presence of light phases analyzed through elemental mapping.

Because the maps show a mixture of elements within the light gray phases in the coating, an SEM image was obtained at one of these phase locations. Figure 6.25 demonstrates the morphology of the phase that seems to contain a darker gray and light gray contrast. Smaller specks of light gray particles can also be identified. When analyzing a spot through EDS, the phase was consistent with the elemental maps with 41.51 wt% Al, 30.30 wt% Fe, and 14.20 wt% Si. No oxygen was found in these areas, which show that it is a metallic phase mixture. Another microstructure shows that the light gray phase mixture was also

located near the interface between the coating and bulk material. The micrograph in Figure 6.26 shows these Al, Si, Ti, Fe, and Cu phases also exist at the interface as illustrated by the X-ray maps.

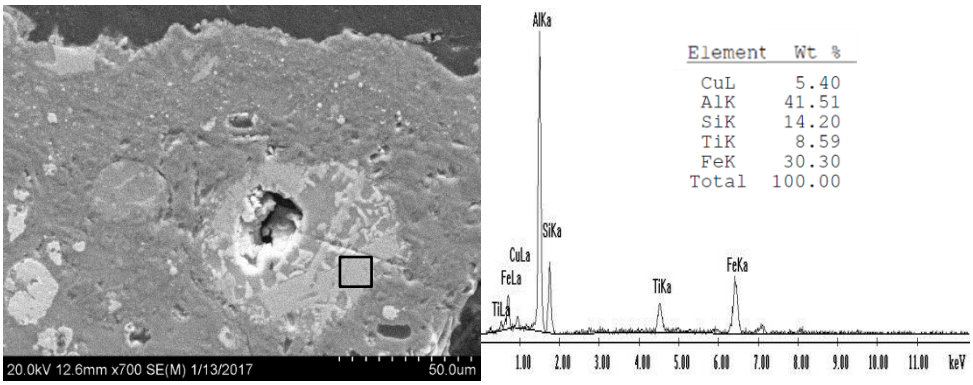

Figure 6.25 A light gray area analyzed with the EDS composition shown.

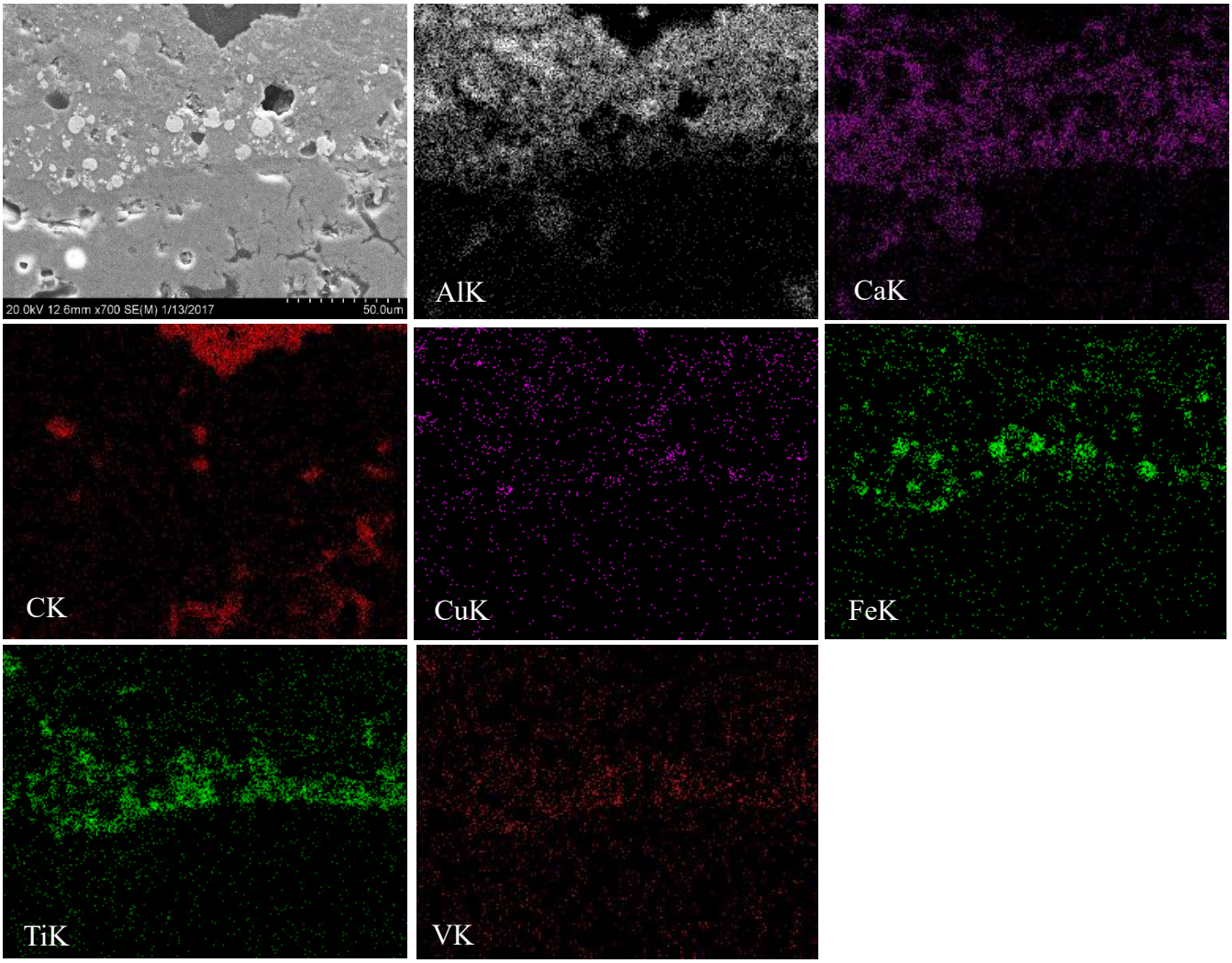

Figure 6.26 X-ray map distribution of sample 1.1B with a phase mixture at the interface.

Sample 1.2 was then evaluated to determine the existence of deposits as the surface did not contain a thick coating. However, similar elements were detected. Figure 6.27 shows the microstructures of the sample with several characteristics pointed out. On Figure 6.27a, cavities are present near the surface of the TPS and the thickness of the coating remains constant. Figure 6.27b shows cracks emanating from the surface that branch through the coating. Some light gray phases can be discerned especially on Figure 6.27c and d. Several spherical phases were developed along with fracture areas of the surface. The arrow on image d shows a distinct light layer.

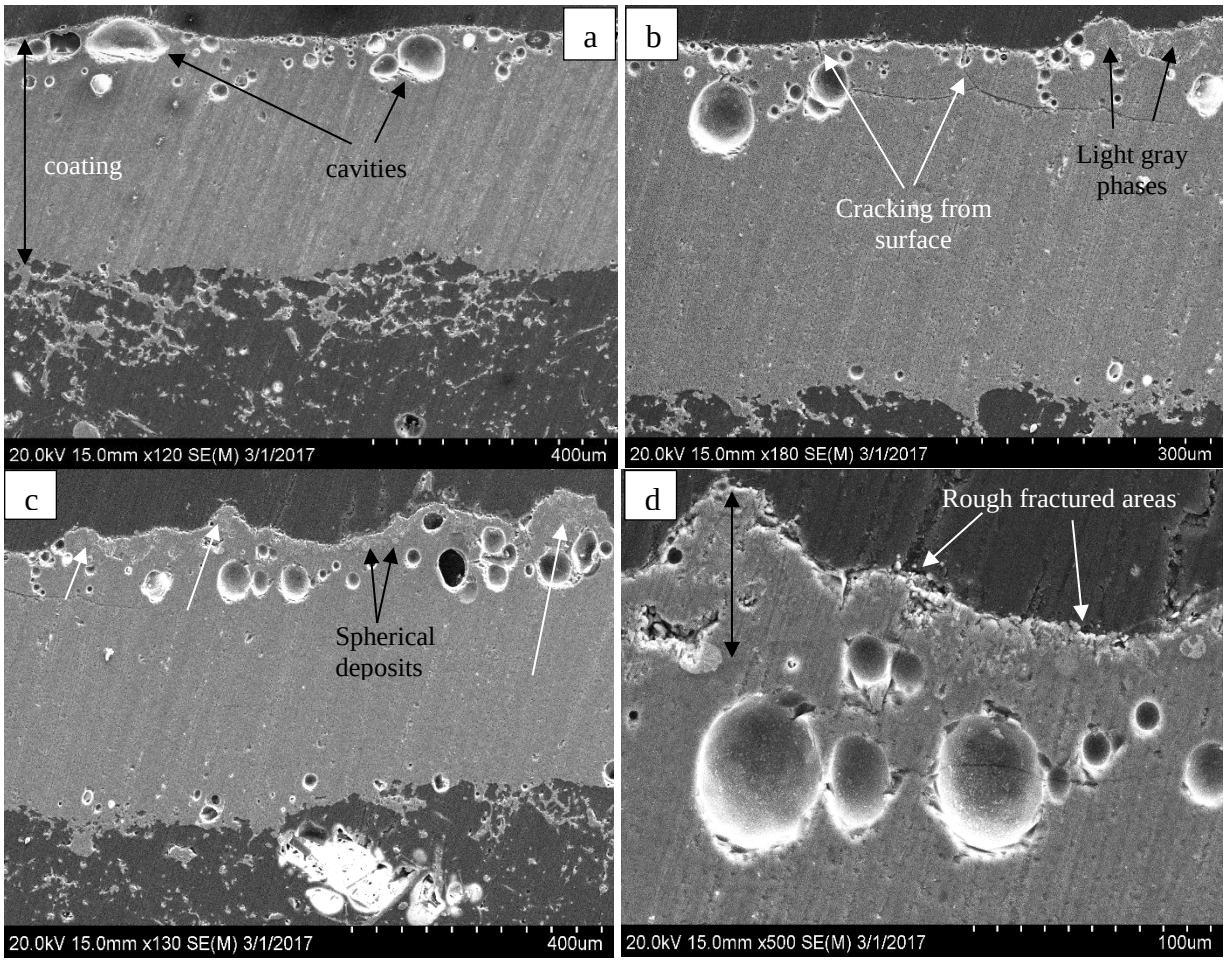

Figure 6.27 Cross-sections a-d of sample 1.2.

As a result of evidence of light phases, EDS spot measurements were obtained near the coating of the sample. Figure 6.28 shows three spot evaluations to represent a location of a gray layer on spot a, a light gray spherical phase b, and a dark gray area c. Spot a contained prominent peaks of titanium oxide,

aluminum, silicon, calcium, and titanium. Spot b did not contain any oxygen but was a combination of 48.35 wt% Ti, 17.91 wt% Si, 11.09 wt% Fe, and 3.21 wt% Cu. Spot c however, was comprised of 57.36wt% O and 24.10wt%Si. Because the light gray phases were abundant in titanium, X-ray maps were collected on the microstructure shown in Figure 6.29. The light gray dispersed phases are emphasized in the titanium map. Within the titanium phases, other small phases of copper and vanadium were also highlighted on the element map. Oxygen and silicon were also present on the entire cross section, however, an aluminum layer surrounded the Ti and Cu phases. The titanium suggests that it was deposited before the aluminum layer. The calcium map shows it was mostly located in the aluminum layer.

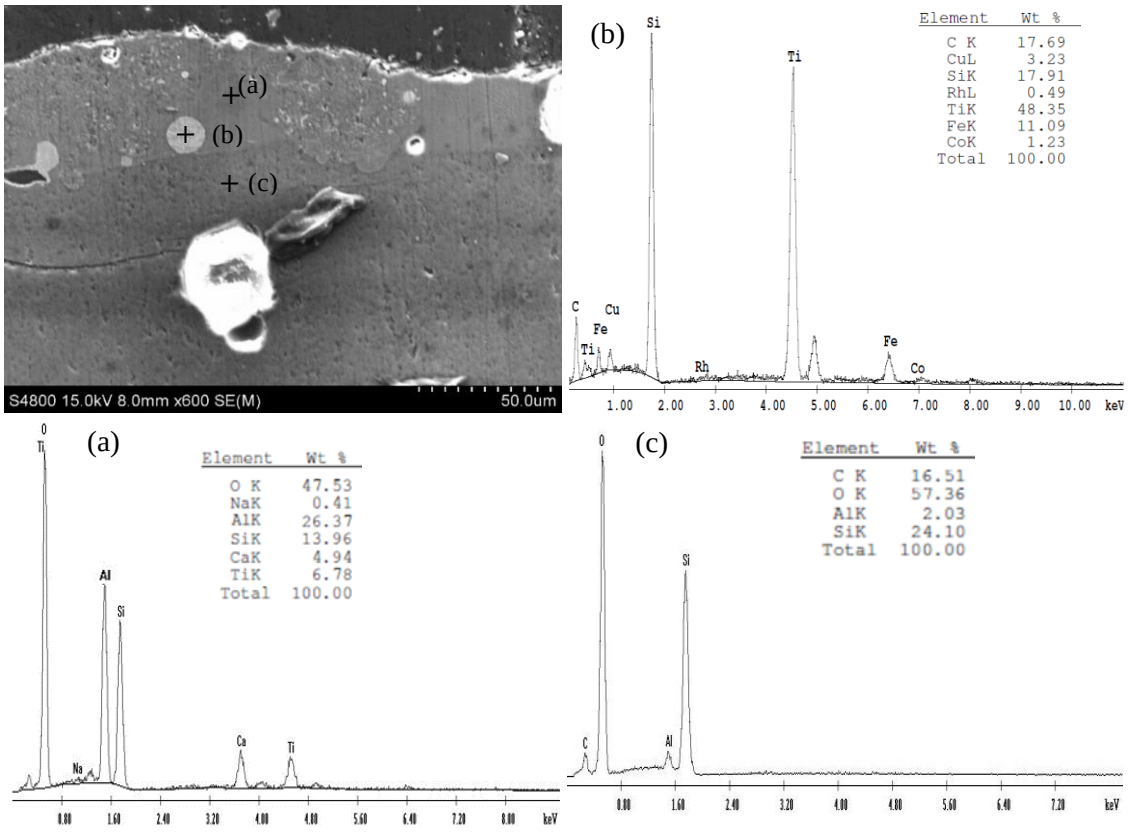

Figure 6.28 Spot EDS measurements of a gray area (a), spherical phase (b), and a darker area on (c).

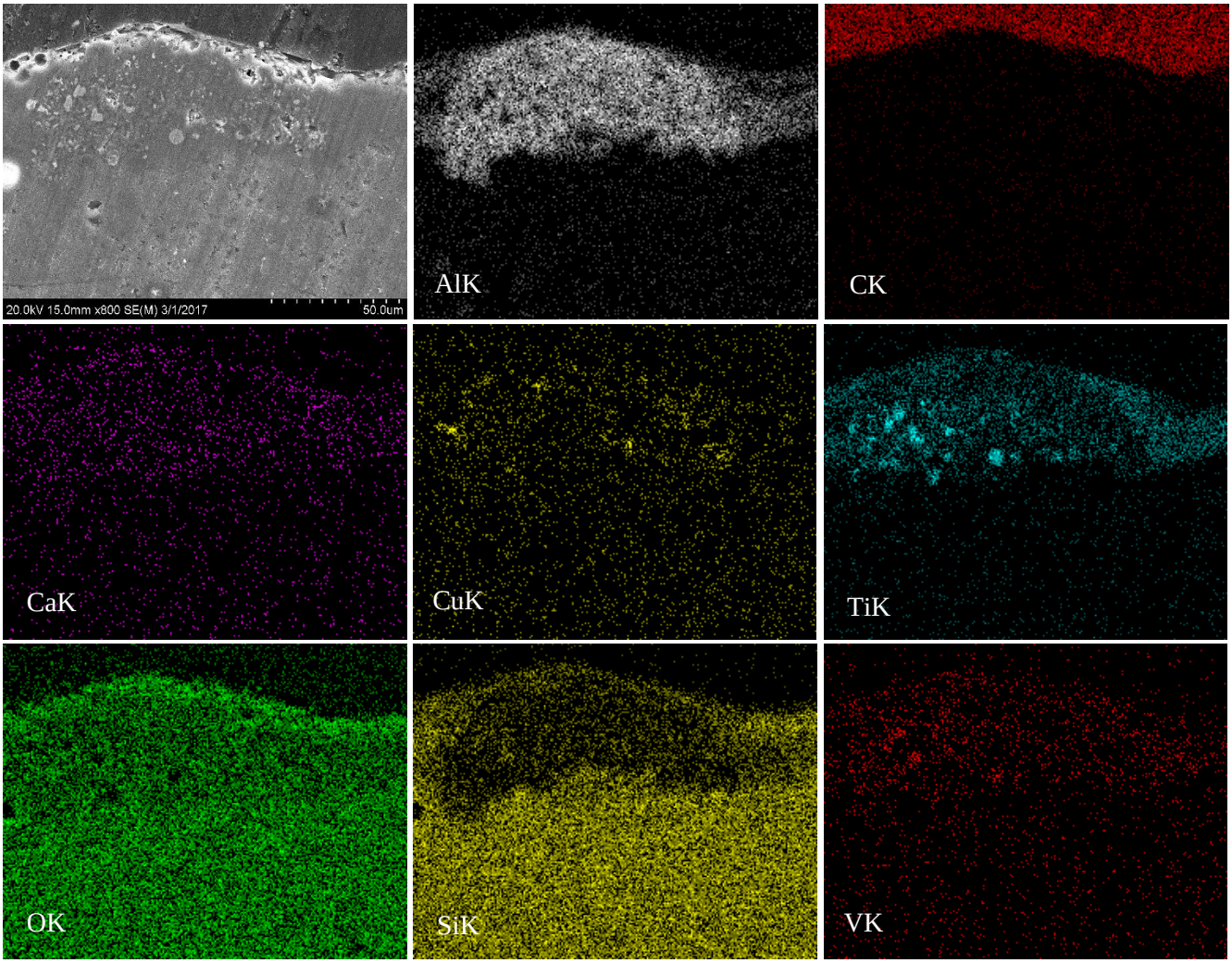

Figure 6.29 X-ray map of an area close to the upper edge of sample 1.2 that contained light gray phases.

As sample 1.3 contained metallic splats rich in aluminum, the cross-section was evaluated for deposits and microstructural features. Figure 6.30a and b show a light gray deposit layer that was present on the surface of the sample. Several hollow areas and cavities were present near the coating as well as cracks that initiated at the surface. Within the light gray coating, a certain texture was observed along with a bright spherical phase shown on Figure 6.30c. Another area in the sample contained a large deposit formation with a light gray coloring as illustrated on figure 6.30d. At higher magnifications of the deposit revealed the morphology shown on Figure 6.31a through d. Several areas of the deposit contained a dendritic-like structure at higher magnifications. The morphology consisted with tree-like formations, indicative of secondary and tertiary dendritic arms, with branching in certain directions.

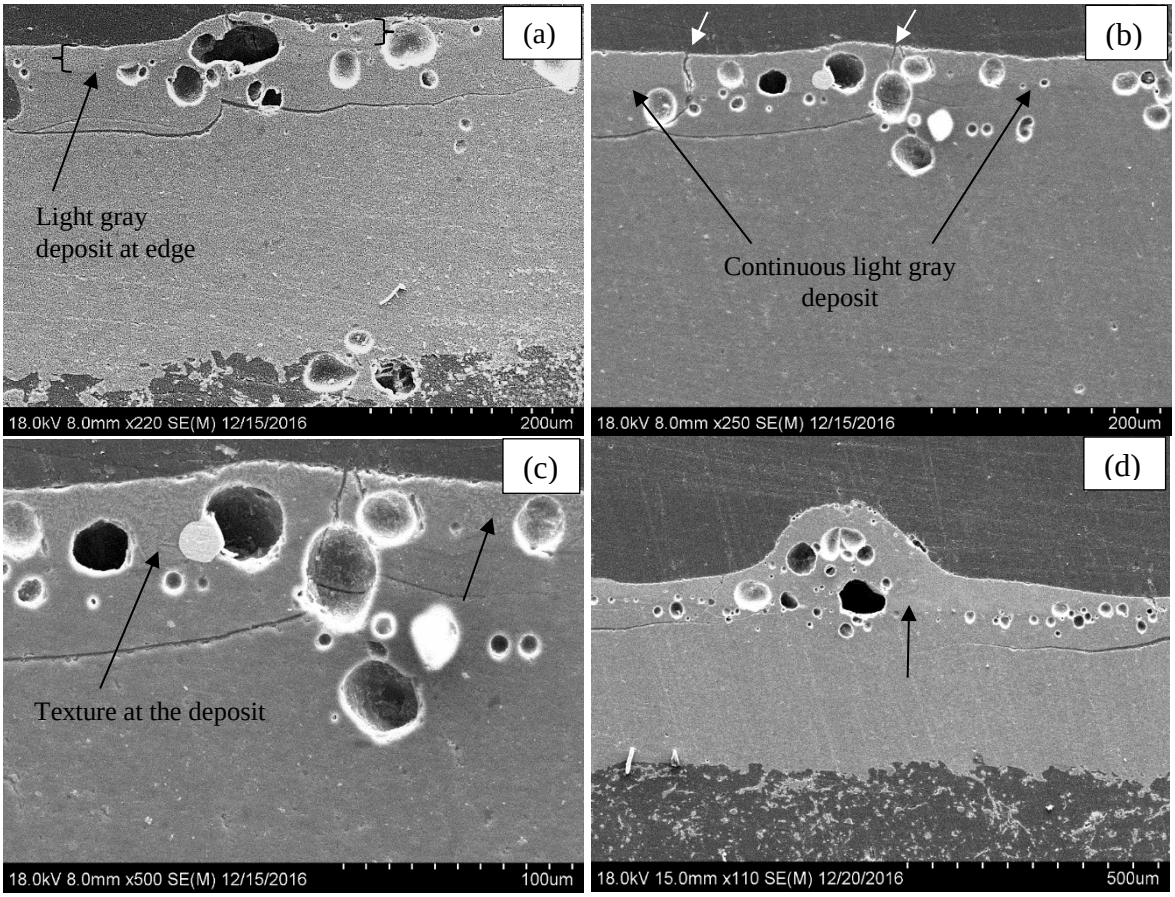

Figure 6.30 Sample 1.3 cross-sections (a) and (b) are shown with a continuous light gray deposit. Area (c) shows the deposit line with texturing and area (d) shows a large deposit formation.

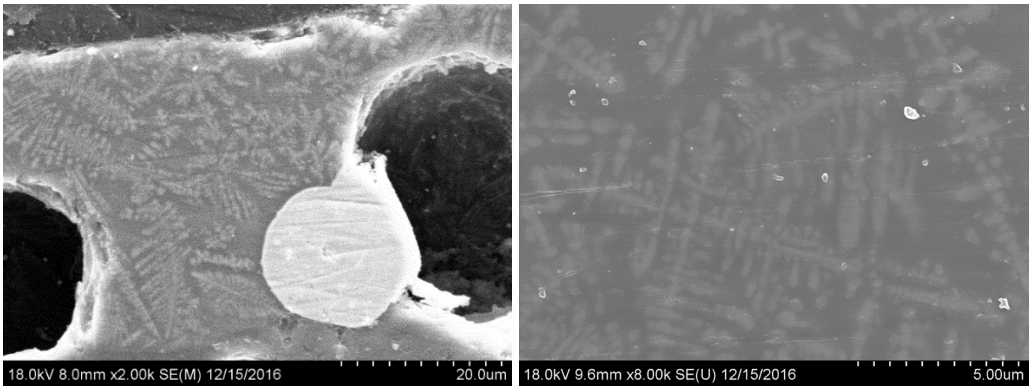

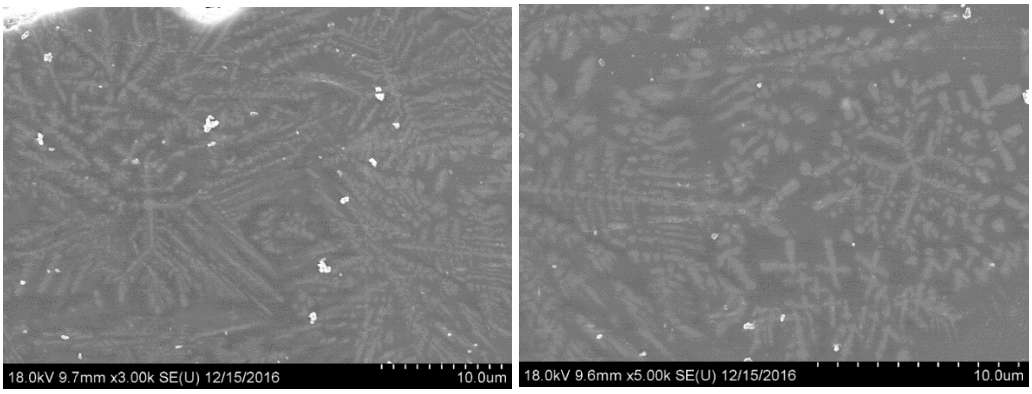

Figure 6.31 Four images showing areas of the deposit line near the surface with a dendritic-like structure.

Elemental analysis was next completed and Figure 6.32a shows an area analyzed near the interface of sample 1.3. The main elements detected were 28.85 wt% Si and 57.35 wt% O. The minor elements included 8.26 wt% C, 4.01 wt% Cu, and 1.5 3wt% Al. Conversely, the previously discussed unique features in the microstructure were analyzed and presented in Figure 6.32b. Several major elements were identified and included 38.60 wt% Ni, 27.38 wt% Co, and 19.45 wt% Fe. These compositions were not previously present in the samples studied. After that, the dendritic region was investigated with EDS. Figure 6.33 presents two spot evaluations with a light gray dendrite at spot 1 and a surrounding dark gray phase spot 2. There is a major difference in these two phases in which the light dendrites contained an average of 38.76 wt% Ti and 38.26 wt% O. The minor elements at spot 1 constituted of 6.28 wt% Si, 5 wt% Al, 3.72 wt% Cu, and 2.18 wt% Ca. Spot 2 contained less titanium (16.86 wt%) and 35.13 wt% O. The minor elements were similar with compositions of 9.16 wt% Cu, 9.14 wt% Si, 4.09 wt% Ca, 3.50 wt% Fe, and 9.45 wt% Au.

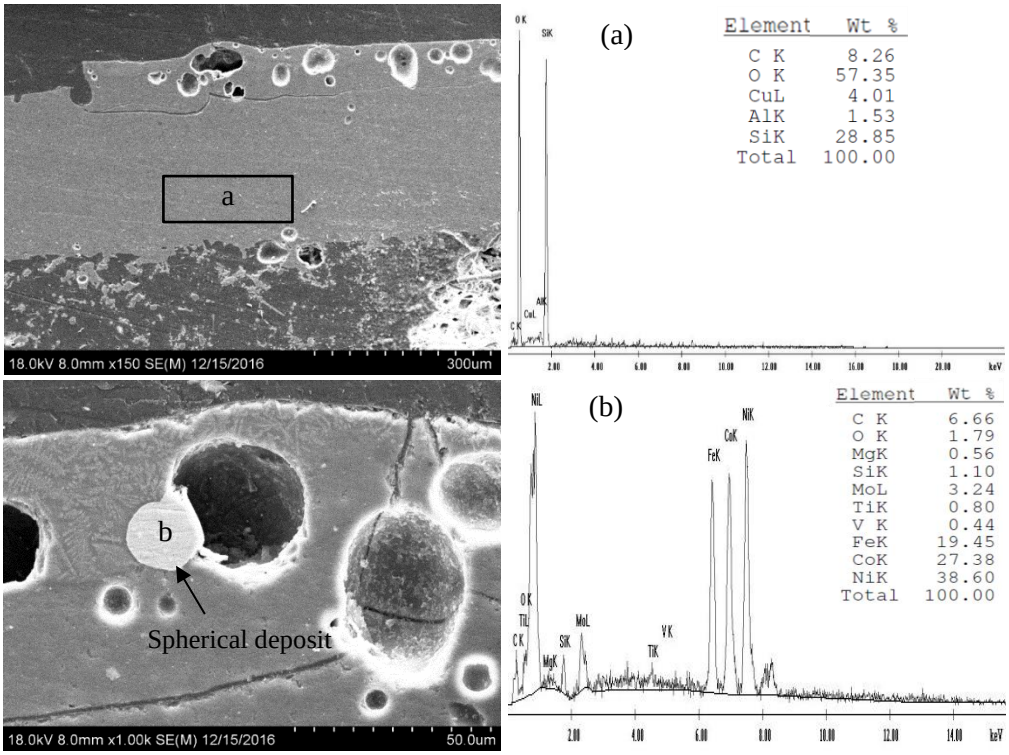

Figure 6.32 EDS area analysis deep within the TPS coating cross-section (a) and a bright deposit (b).

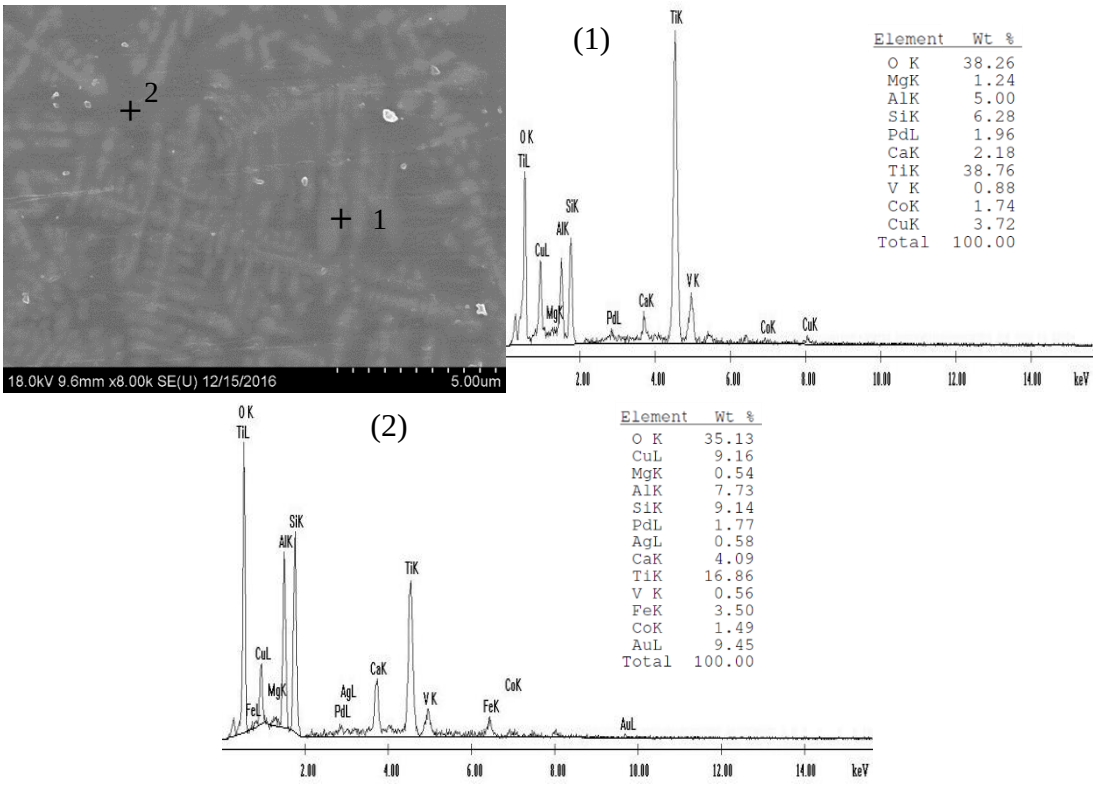

Figure 6.33 Spot EDS evaluations of an area of the coating with dendrites.

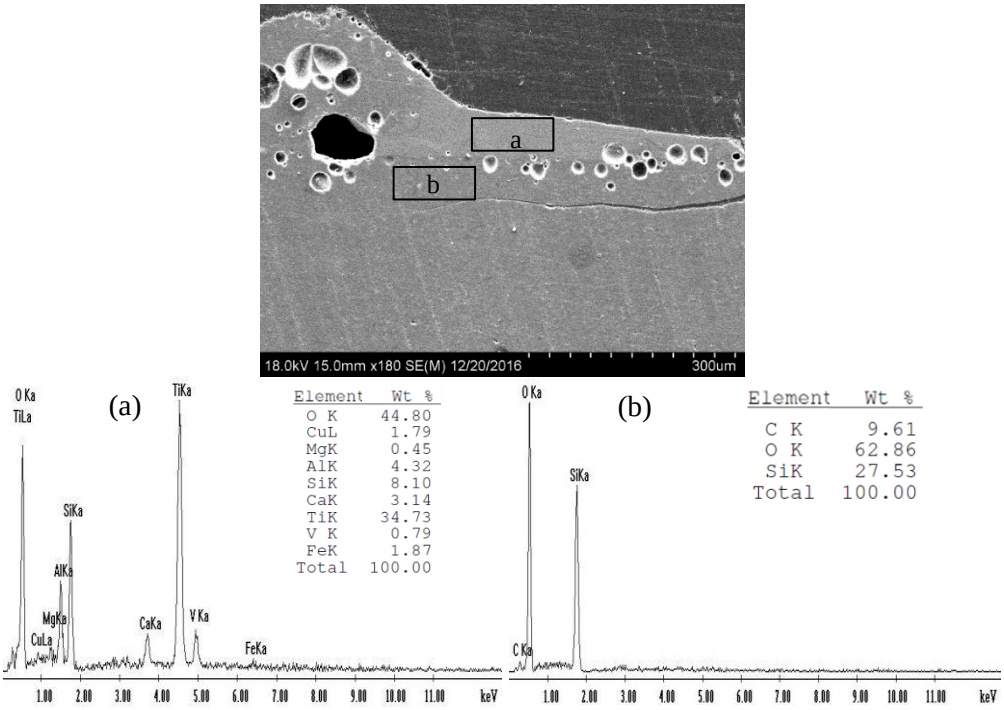

Figure 6. 34 EDS area assessment of the deposit (a) and below the deposit (b).

The deposited layer near the largely formed deposit was also inspected to determine where the composition changes. Figure 6.34 distinguishes the light gray deposit on a and a darker area following the interface on b. The dark area does not have most of the elements identified on the top layer. Area a contained 44.80 wt% O, 34.73 wt% Ti, 8.10 wt% Si, 4.32 wt% Al, and 3.14 wt% Ca. The only compositions present on area b were 62.86 wt% O, 27.53 wt% Si, and 9.61 wt% C. To determine what phases deposited first, a set of individual X-ray maps were performed to highlight the phase distribution. In the set of element maps shown in Figure 6.35, the light gray deposit shows high aluminum, calcium, titanium, oxygen, and vanadium. In this area after all, is richest in titanium as shown. The dendritic area was analyzed next to reveal the phases at the dendrite grains. Figure 6.36 shows a micrograph used to develop individual maps where the black arrows show the extension of the dendrites. The microstructure changes after this area. The majority of the dendritic area contained titanium, silicon, oxygen, and

vanadium. It was observed on the maps that the areas with no dendrites are high in aluminum and calcium. Nickel was a minor element and dispersed through the microstructure.

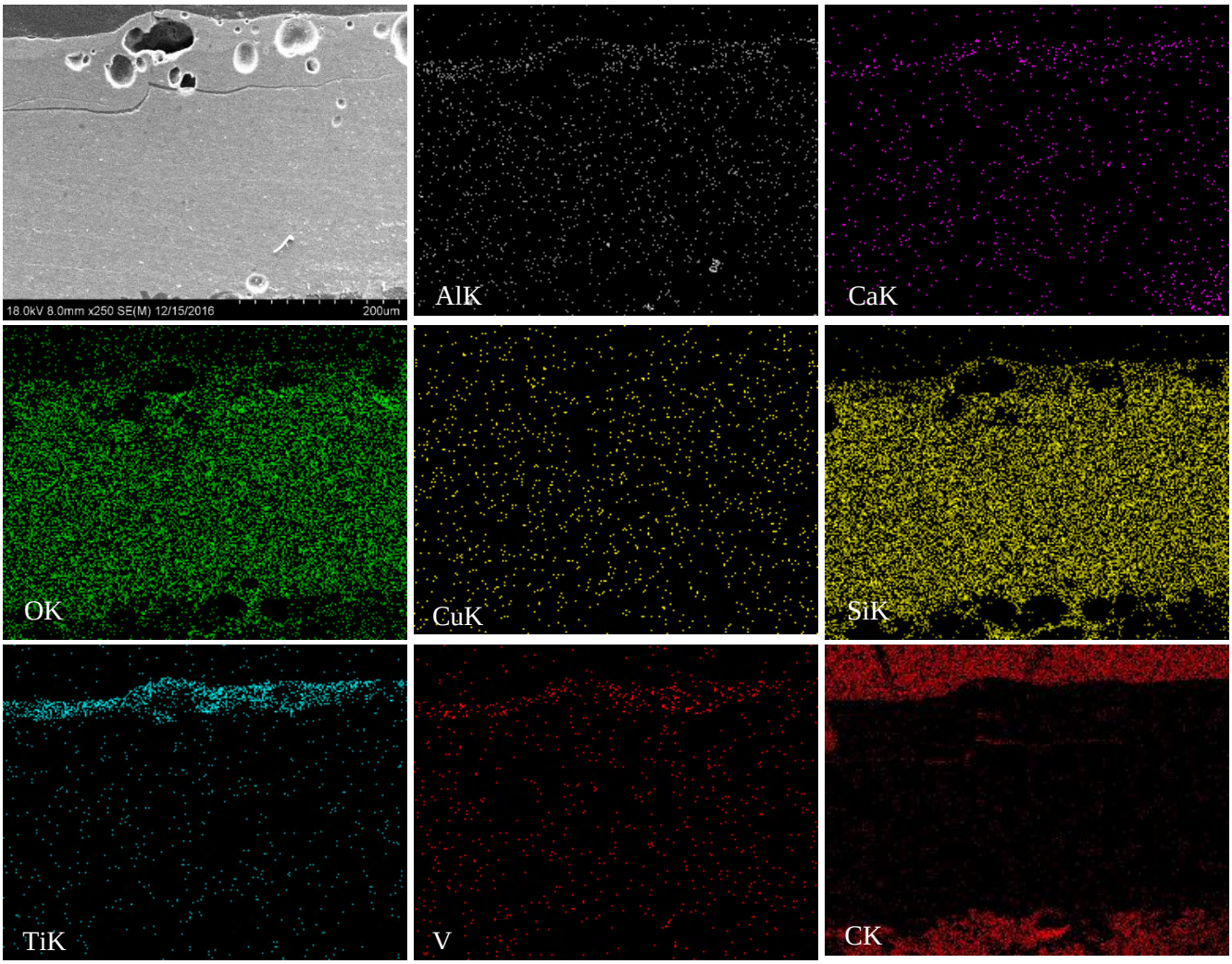

Figure 6.35 X-ray maps of an overall cross-section of sample 1.3.

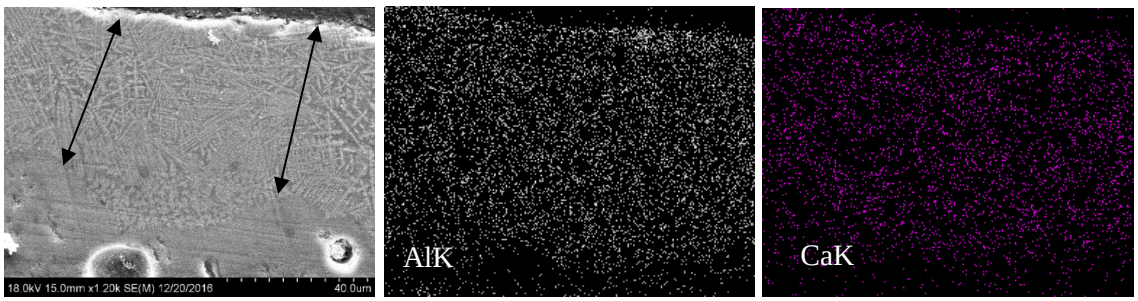

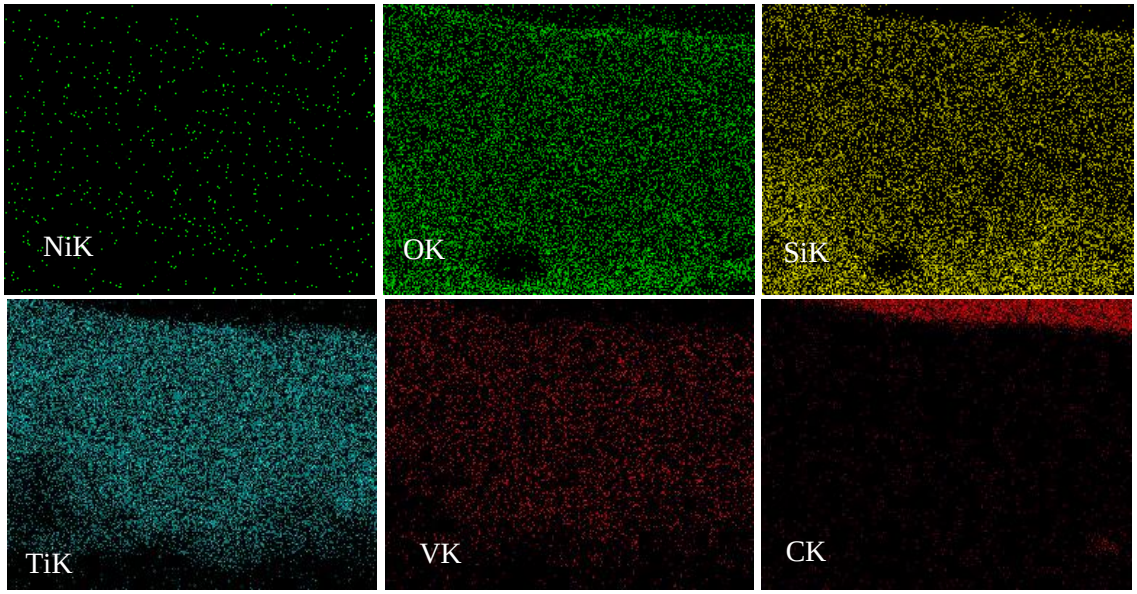

Figure 6.36 X-ray maps of the dendritic area of sample 1.3.

6.2.2 Forward Starboard Side Carrier Panel Tile

The list of samples located on the forward starboard side of Window 7 include: Sample 2.1A, Sample 2.1B, 2.1.2, 2.1.3, and 2.1.4. Each sample was studied at the surface and within the cross-section for deposits.

6.2.2.1 Surface Analysis

The morphologies of the samples extracted from the forward starboard carrier panel tile were studied to determine if there were traces of shuttle materials on the TPS. The samples obtained from the secondary sections of sample 2.1 were all examined as a colored deposit was found concentrated on one side of the TPS. The visual inspection also indicated metallic depositions of titanium, aluminum, iron, copper, and silicon were present.

Surface features of sample 2.1.1A were examined and presented in Figure 6.37. The morphology of the surface contained areas where a light deposit was applied. Some dark areas as shown in the image were exposed areas of the black TPS coating. Thinly shaped deposits were present along with indentations, cracks, and pores. When acquiring elemental information on the surface, all locations measured contained

similar compositions. Figure 6.38 shows the recurring composition of the surface that consists of 56.95 wt% O, 15.20 wt% Si, 13.68 wt% Ca, 4.31 wt% Cu, 4.18 wt% Ti, and 3.33 wt% Al. Other minor elements detected included 1.56 wt% Na and 0.80 wt% V.

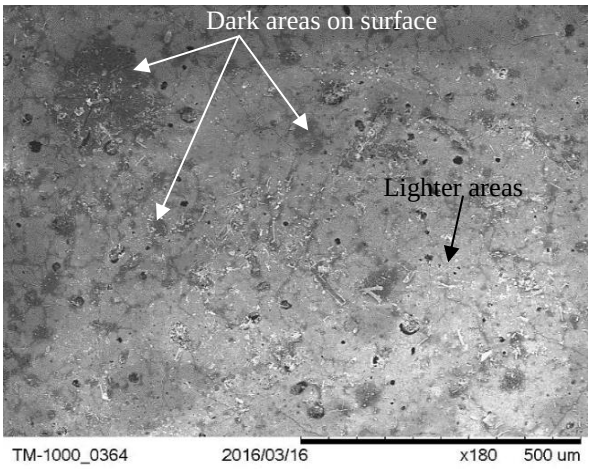

Figure 6.37 Surface SEM of sample 2.1.1A with dark spots and lighter areas.

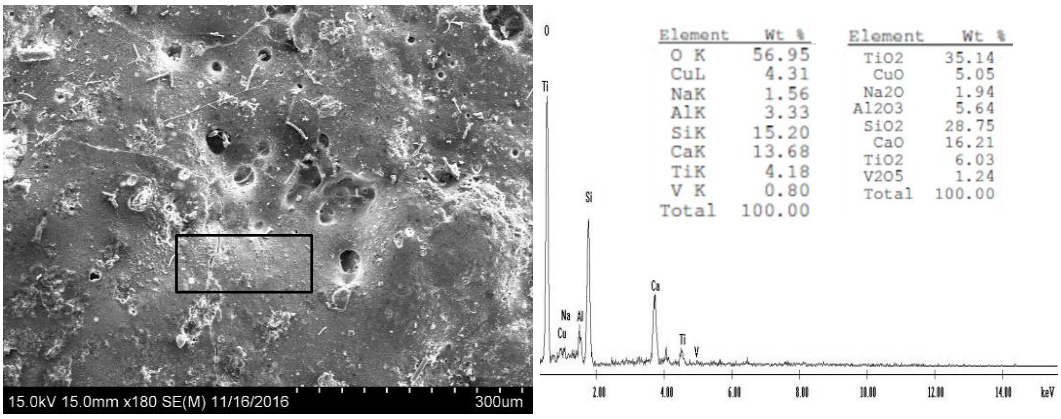

Figure 6.38 Surface SEM analysis and EDS results of sample 2.1.1A.

The next sample analyzed was the sample sectioned perpendicular to the top surface of the TPS. Sample 2.1.1B was originally attached to sample 2.1.1A but it's vertical edge. The surface of the sample contained visible white discoloration during NDE. Under SEM, a light deposit was recognized and at a higher magnification, the surface appeared to contain grain-like particles (Figure 6.39). The marked areas show the positions of where EDS spot measurements were taken. Figure 6.40 displays the corresponding EDS results of two measurements in the light deposit and an area without the deposit. Spots b and c

confirm that the light deposit contained a high weight percentage of Zn, O, and C. The oxides present were shown to be mostly ZnO, TiO_2, and SiO_2. In this sample dissimilar to all previous sample, the trace elements were Al, Ca, V, Cr, and Ni. Spot c contained a high amount of Zn followed by O, C, and Ti. The amount of Zn was higher than that of spots a and b. The measured oxides also included ZnO, SiO_2, and TiO_2.The source of the Zn would have been the zinc based chromate used to protect the aluminum substructure of the orbiter [2]. Another possible source of Zn would be derived from any 7000 series Al-Zn alloys within the substructure.

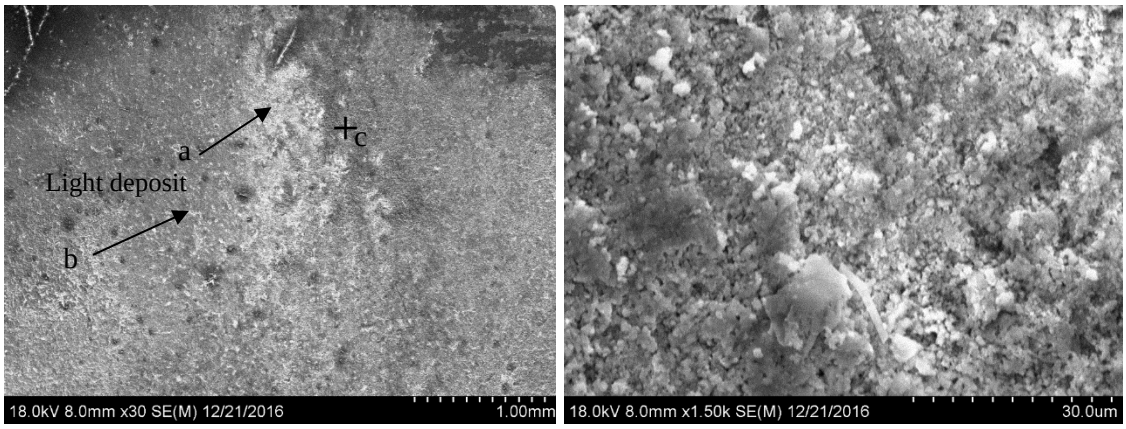

Figure 6.39 Surface of sample 2.1.1B at 30X and 1,500X. Image also shows areas where EDS measurements were obtained.

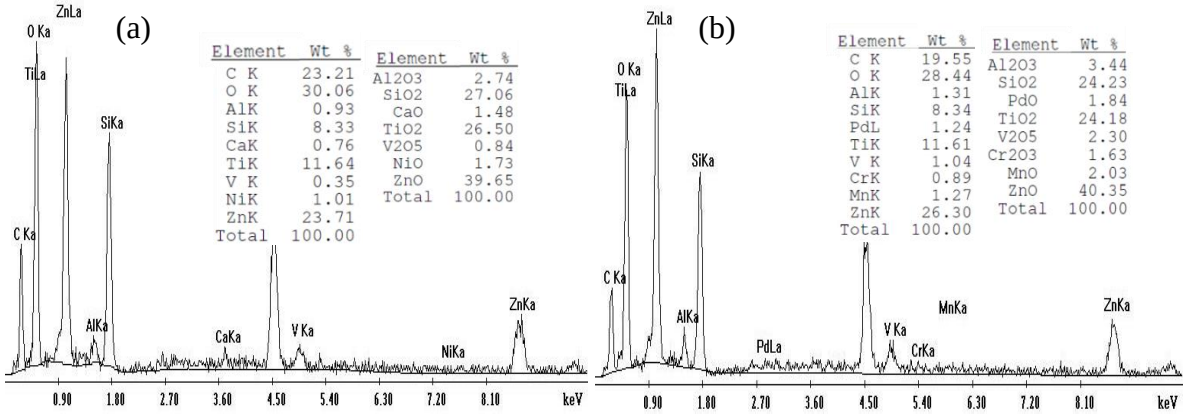

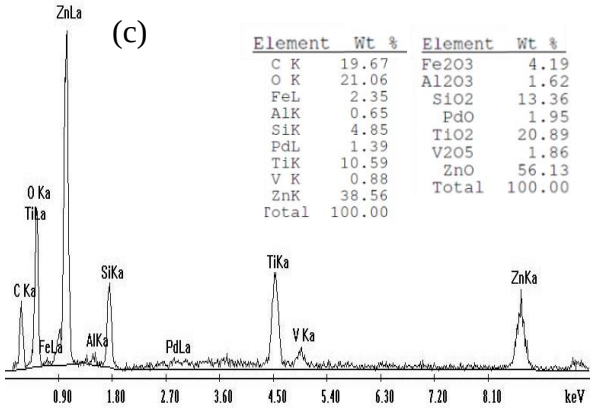

Figure 6.40 Corresponding EDS spot measurements of locations a-c.

The adjacent samples 2.1.2 and 2.1.3 contained similar deposits during NDE, as the bright yellow discolorations began to diminish in these locations. The surface of sample 2.1.2 was preserved for XPS surface analysis. The surface morphology of sample 2.1.3 was identical to that of sample 2.1.1A. The surface contained a variety of white deposits and darker areas. Pores that penetrated through the coating were also observed along with small indentations. Surface cracks were also present. The EDS analysis was also comparable in white a light deposit on Figure 6.41a contained major peaks of TiO_2, Si, Al, and Ca. A darker area with no visible deposit (Figure 6.41b) also consisted of similar compositions except without the trace elements of Fe, Na, V, Cr, Mn, and Co.

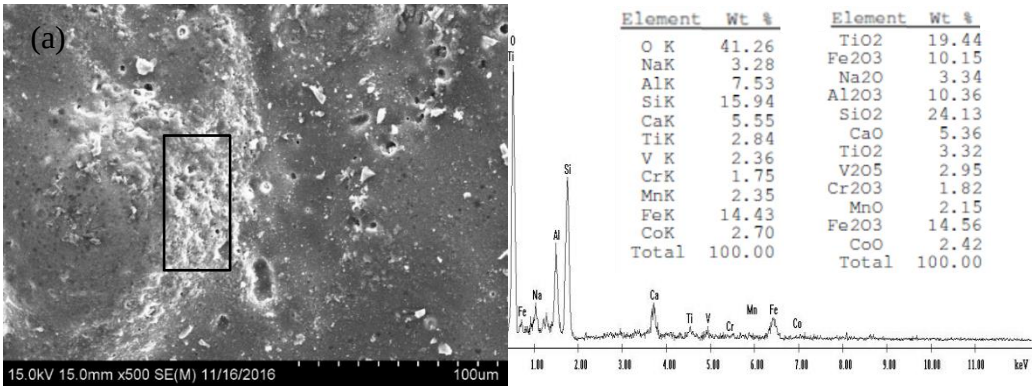

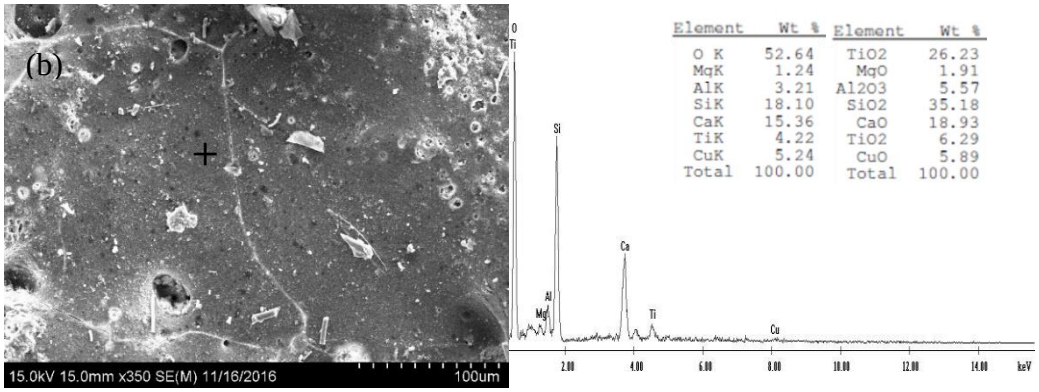

Figure 6.41 EDS results obtained on the white area (a) and dark area (b) of sample 2.1.3.

The sample that was close to the inner side of the tiles was sample 2.1.4 and had small metallic deposits with yellow discolorations. The surface was uneven and had an irregular texture when compared to the previous samples. No flat areas were obtained and some difference in contrast was also observed. Figure 6.42 shows the morphology of the overall surface of sample 2.1.4. Image b also demonstrates small white impacts on the surface. Differences in the surface elemental composition results were recorded and displayed on Figure 6.43a and b. The identification of elements in the first area showed that the major amounts were 59.57 wt% O, 18.35 wt% Si, and 16.18 wt% Ca. Al, Mg, and Mn were present in minor amounts. The oxide results show major oxides of SiO_2 and CaO. A second area b contained elevated titanium oxide. The major amounts of Si and Ca were similar to area a. Minor elements were present that include Cu, Al, Fe, V, and Mn.

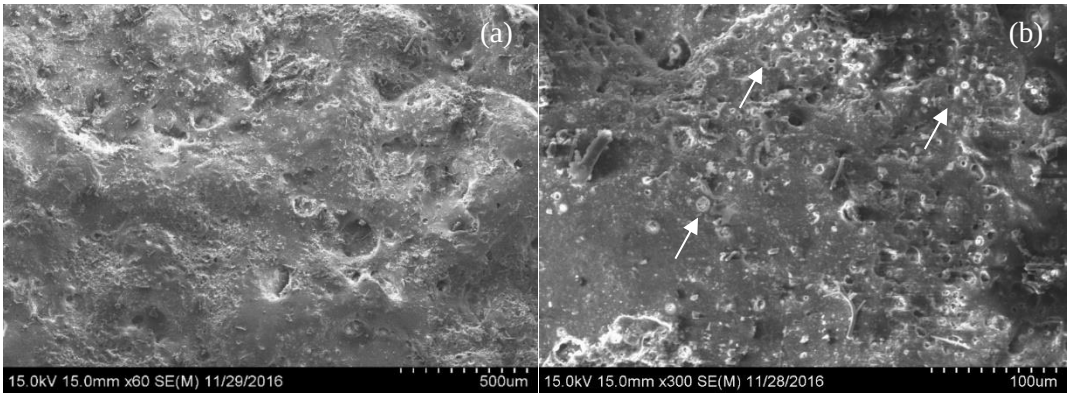

Figure 6.42 Sample 2.1.4 surface SEM image (a) shows the surface with a rough uneven texture and at a higher magnification, image (b) shows small white impacts on surface.

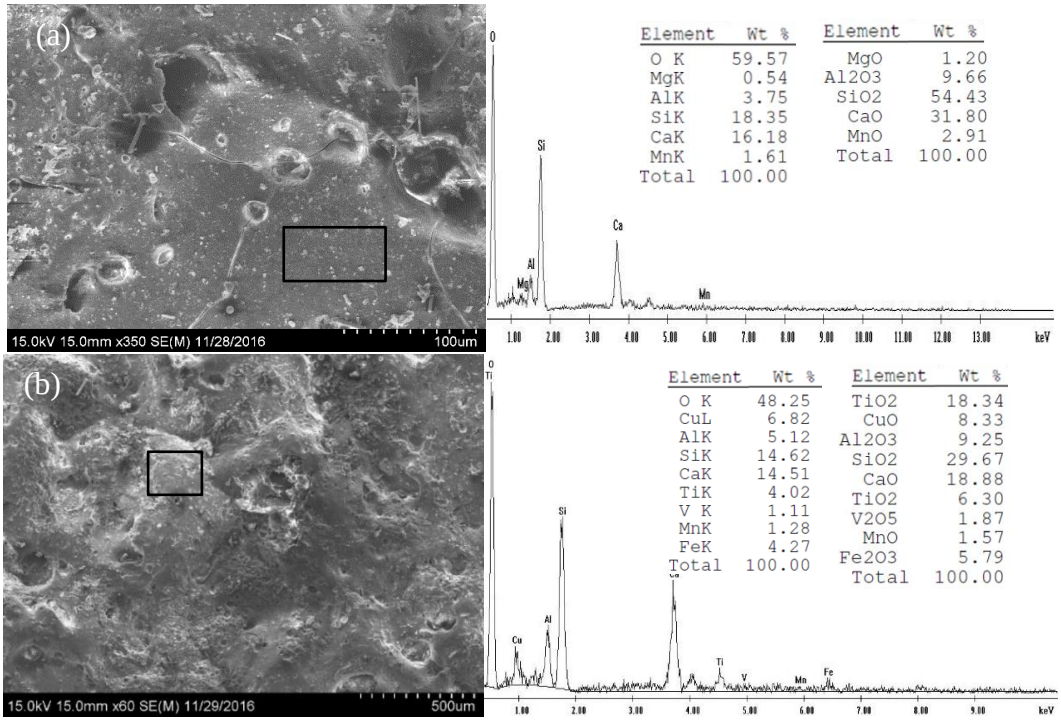

Figure 6.43 EDS results of two areas (a) and (b).

6.2.2.2 Cross-sectional Analysis

The sample cross-sections were studied to determine if oxides formed within the TPS coating of the samples similar to the forward port side samples. Figure 6.44 shows the typical SEM image of sample 2.1.1A with various features in the coating. In general, the coating contained a damaged surface with cracking shown on Figure 6.44a that is concentrated on the surface. Image b demonstrates a lot of cavities and open pores. A few smaller pores were also present near the coating to silica interface. A deposit layer can also be distinguished as shown in image c and d. The layer appears to be tightly adhered to the TPS coating and an interface was observed on image d. This layer is also more prominent in this sample than the previous TPS from the forward port tiles.

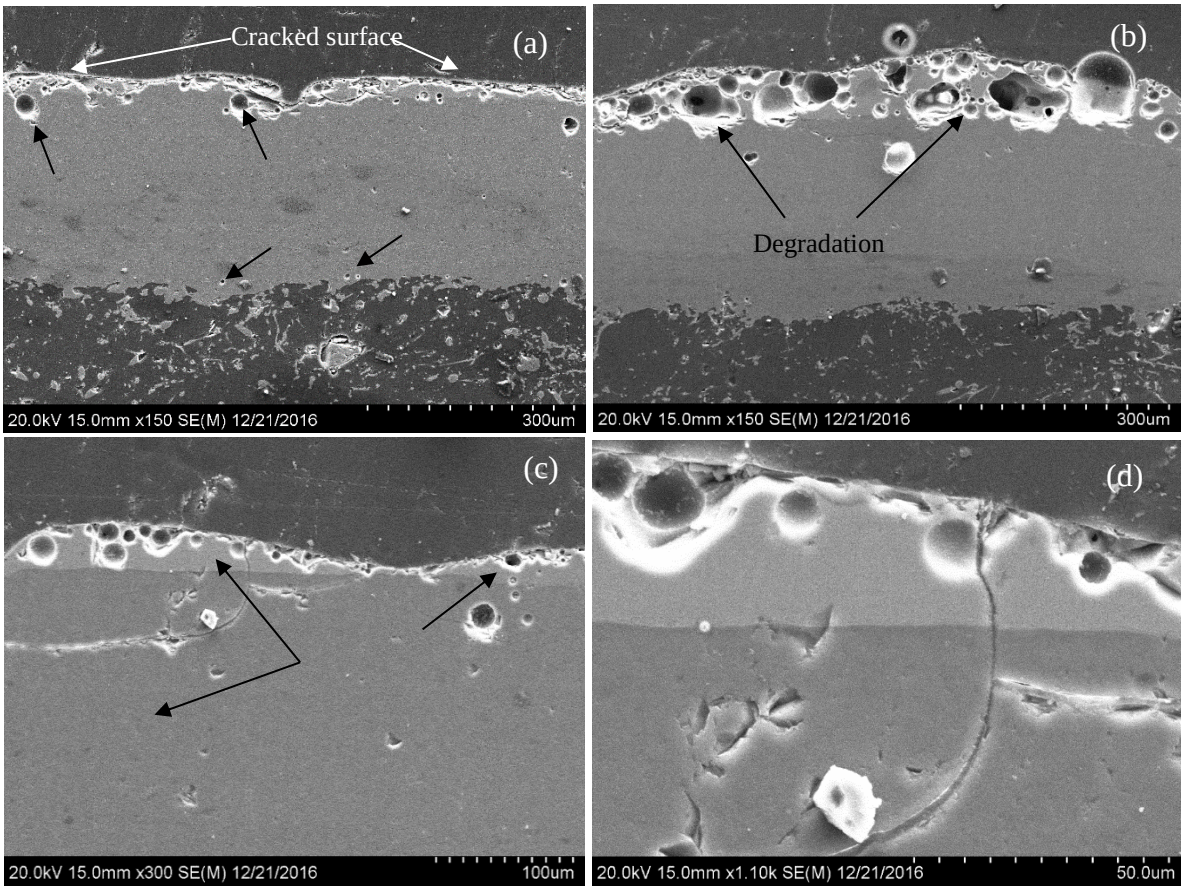

Figure 6.44 Several cross-sections of sample 2.1.1A. Images a and b show the entire cross-section with degradation at the surface. Images c and d show a difference in contrast from the top layer.

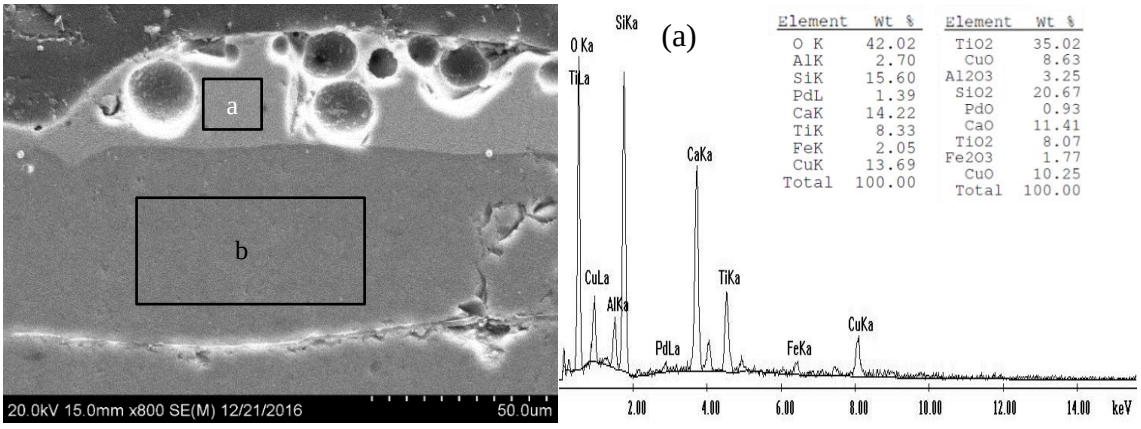

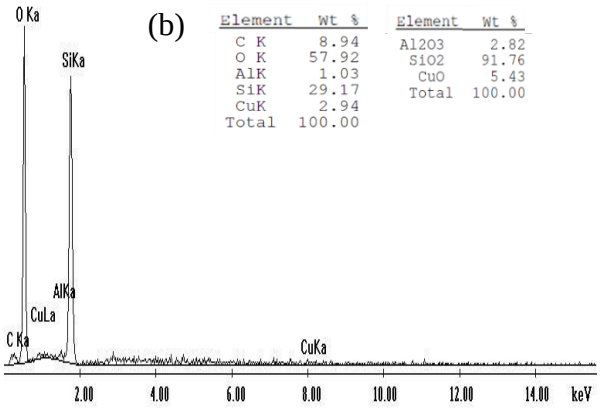

Figure 6.45 EDS results of an area on the light gray layer (a) and darker layer (b).

Elemental composition was collected to determine if the present layer contained identical composition to the layer seen on the previous TPS samples. Figure 6.45 shows the elemental identification of the layer on a and at a location separate from the deposit on b. The deposit contained major characteristic peaks of titanium oxide with 42.02 wt% O and 8.33 wt% Ti. Other major peaks correspond to 15.60 wt% Si, 14.22 wt% Ca, and 13.69 wt% Cu. The second area b shows a change in the composition where it is comprised of 57.92 wt% O and 29.17w t% Si. The amount of copper decreases to 2.94 wt% and no calcium, iron, and titanium was present. Another area at near the edge of the coating was also analyzed and is presented in Figure 6.46. The measured spot shows similar compositions to Figure 6.45a except for an increase in titanium was present (16.42 wt%). EDS mapping confirms that the layer is a mixture of aluminum, titanium, oxygen, copper, and silicon. The SEM image along with the individual elemental maps are displayed on Figure 6.47. The distribution of aluminum shows that it was also present well below the deposited layer. Although the microstructure contained aluminum maps from the micrograph on Figure 6.45 the maps show no aluminum present on Figure 6.48 since the weight percentage was low. The deposited layer in this area was composed of calcium, copper, oxygen, silicon, and titanium. The elemental compositions of the deposited layer vary when analyzing different areas of the sample.

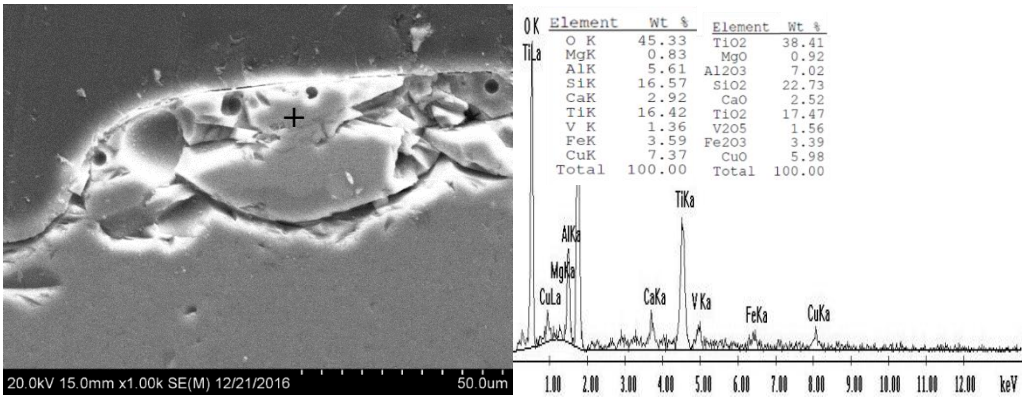

Figure 6.46 Micrograph at 1000X with spot EDS results.

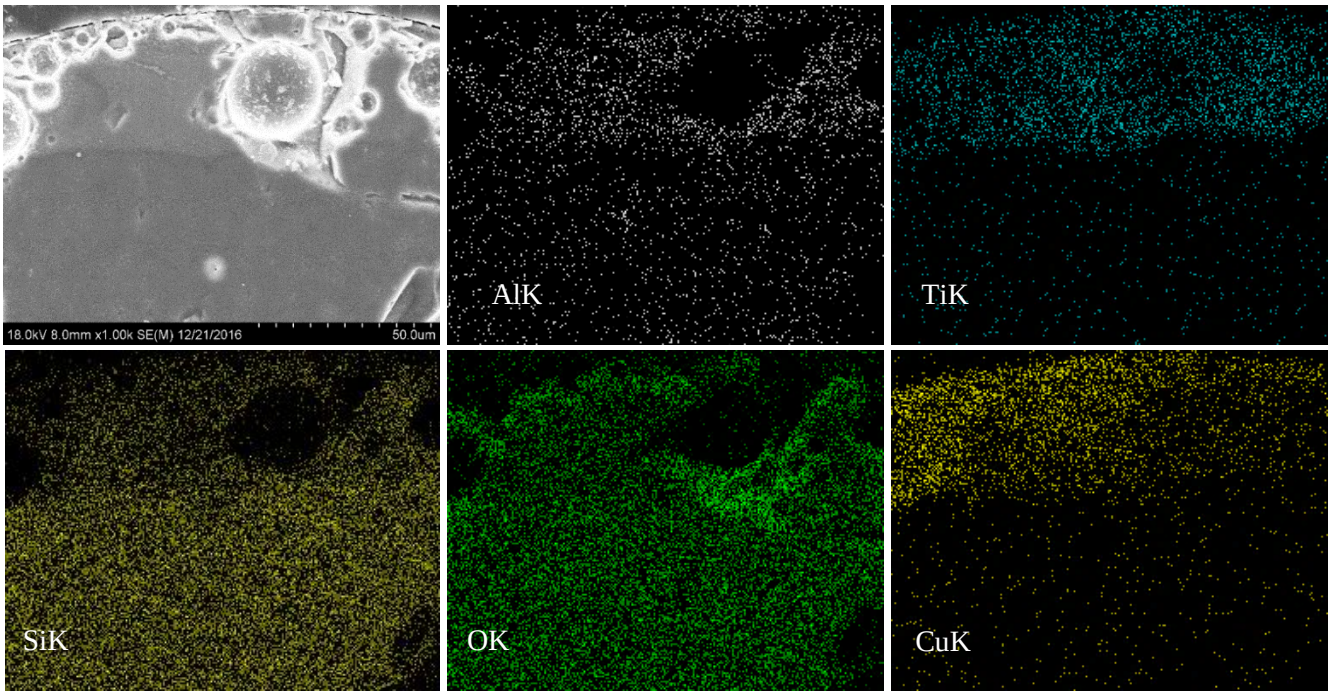

Figure 6. 47 X-ray maps collected from the micrograph shown of sample 2.1.1A.

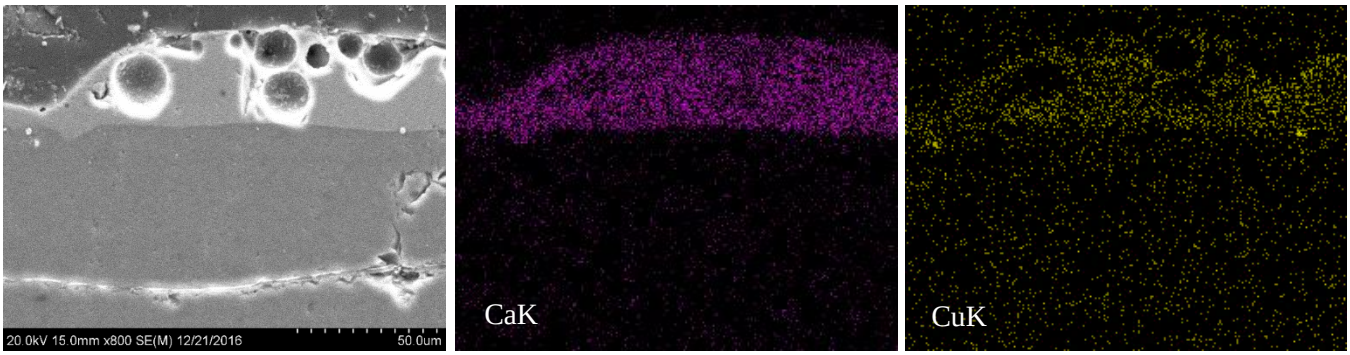

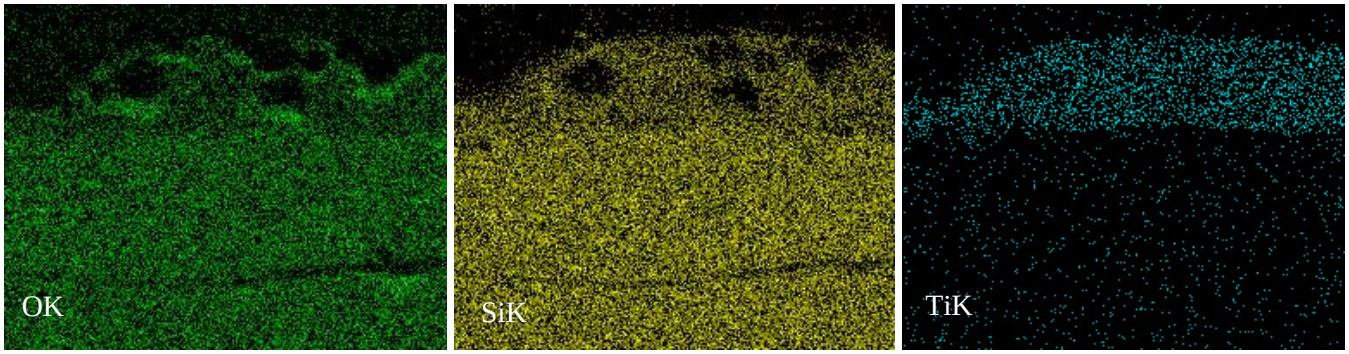

Figure 6. 48 X-ray maps collected from the micrograph shown with the addition of Ca.

Seeing that the connected sample 2.1.1B involved high amounts of zinc at the surface, the cross-section was also studied. The entire sample was consistent in coating thickness and adhered to the silica fibers as shown in Figure 6.49. Unlike the previous samples, areas near the surface or interface did not contain any pores or cavities. No frequent cracks were present and small indentations were present as a result of polishing. A light deposit layer or white spherical deposits were not observed in this sample. To determine if any deposits were present, an elemental composition was obtained along two large areas on Figure 6.50 a and b. Both areas show identical elements present of Si, O, Cu, and Al. The zinc present at the surface of the sample did not penetrate through the cross-section. When examining the X-ray maps, they show that aluminum was first deposited near the coating-to-silica interface. The evidence is shown in Figure 6.51 along with silicon and oxygen maps. Carbon was present at areas of the mounting material.

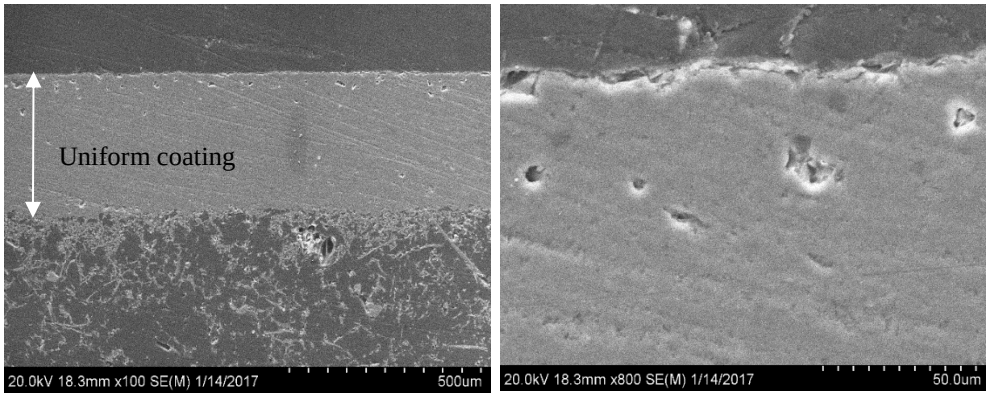

Figure 6. 49 Cross-sections of sample 2.1.1B with no surface degradation.

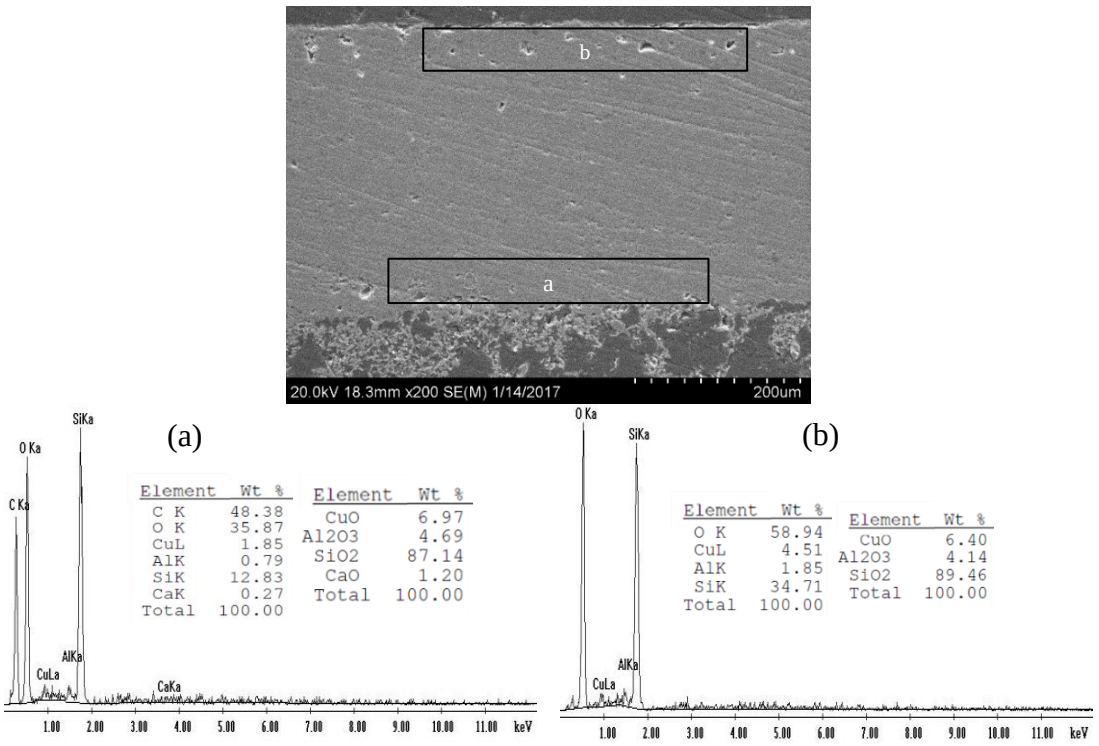

Figure 6.50 Two locations near the interface (a) and surface (b) for EDS.

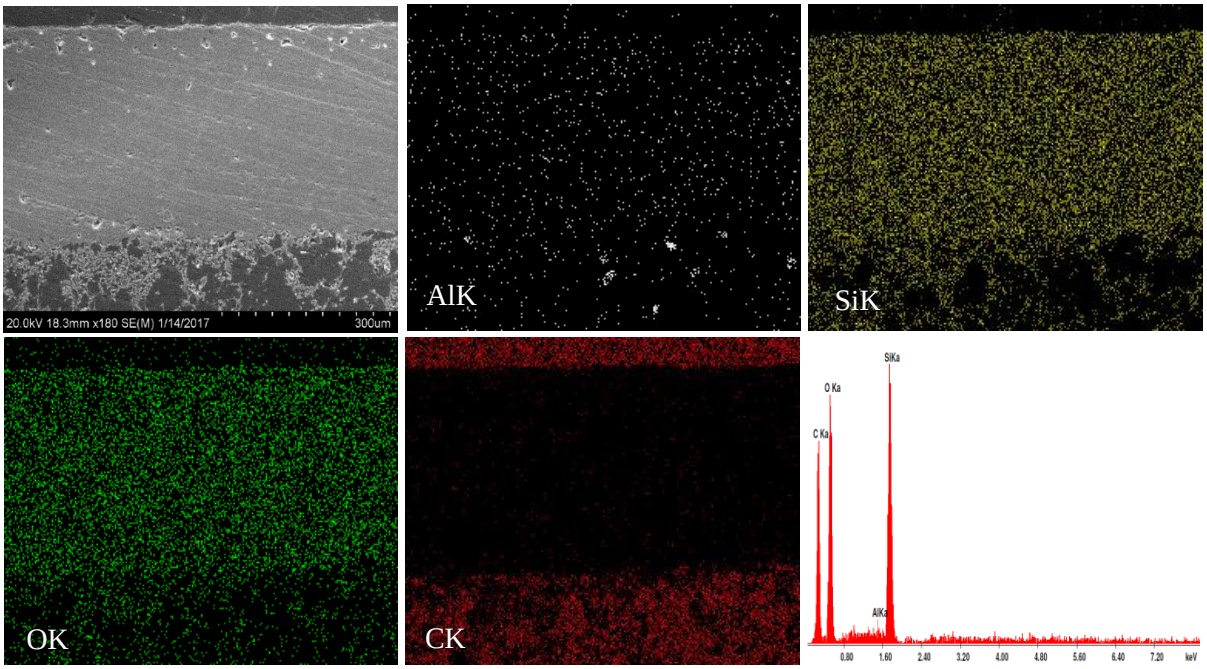

Figure 6.51 Elemental maps and spectra obtained over the image shown.

The following sample 2.1.3 did contain evidence of deposits and surface damage. Figure 6.52 shows these features where image a shows cracks emanating from the surface to the coating and damaged

areas illustrated by the black arrows. A faint deposit layer was also present. Image b shows cavities on the surface edge and in the coating. Image c and d highlight the deposit line at areas close to the surface along with more damage. EDS analysis of the coating was performed and contained 64.79 wt% O, 26.12 wt% Si, 3.29 wt% Co, and 5.80 wt% C. However, Figure 6.53 shows that the composition changes when analyzing the layered deposit. An area measured at the deposit contained amounts of 48.16wt% TiO_2, 18.90 wt% Si, 13.54 wt% Ca, 3.65 wt% Cu, 2.03 wt% Al and 1.40 wt% V. The X-ray maps support the compositional changes at the coating and are displayed in Figure 6.54. The coating shows a mixture of the elements determined by the previous EDS area measurement. The maps show more titanium deposited than aluminum, calcium, and vanadium.

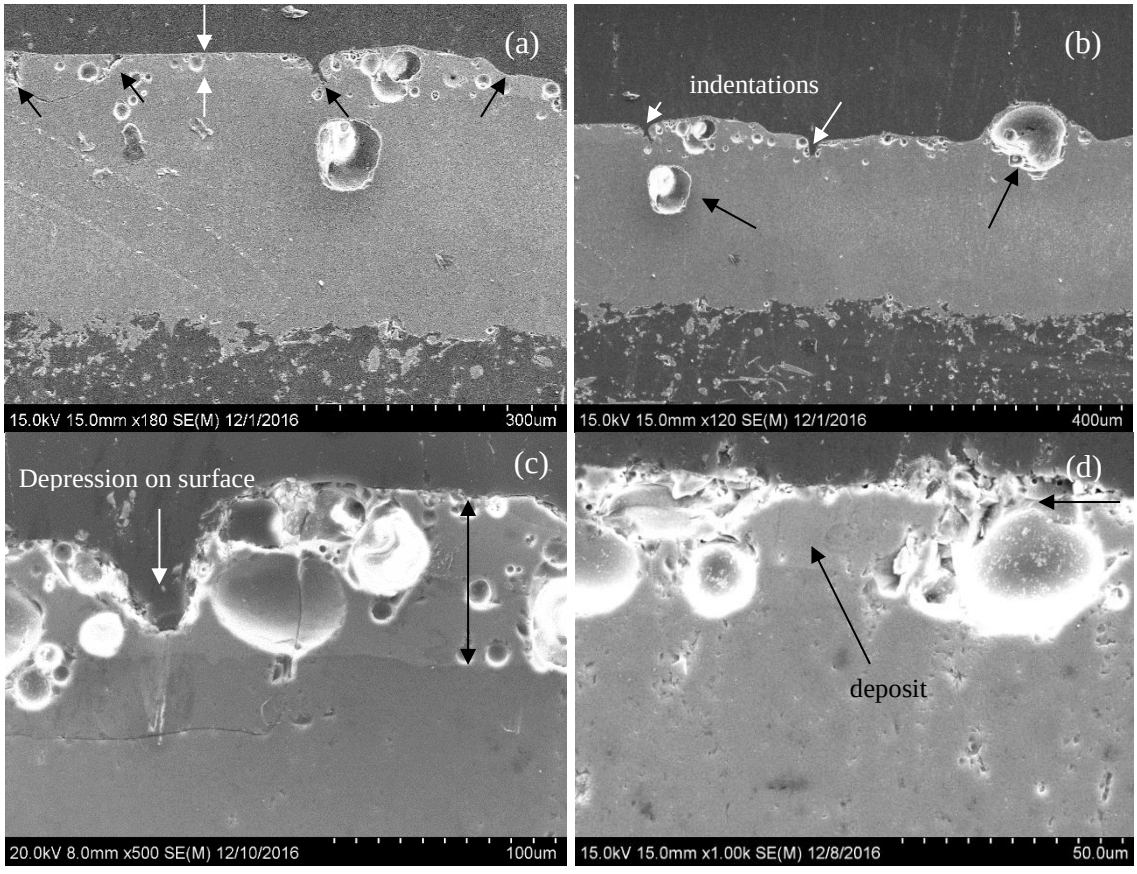

Figure 6.52 Cross-sections of sample 2.1.3 where (a) shows a possible deposit line and surface cracks. Image b shows surface indentations and large cavities near the surface and in the cross-section. Images (c) and (d) show additional damages and evidence of a deposit layer.

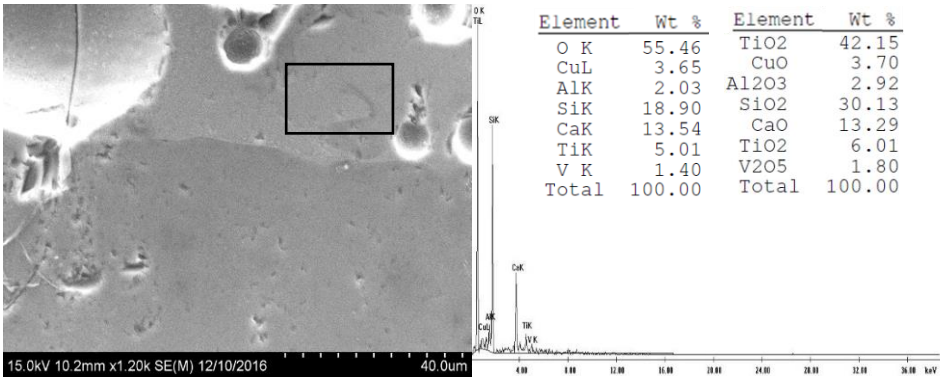

Figure 6.53 The analyzed deposit layer with EDS results.

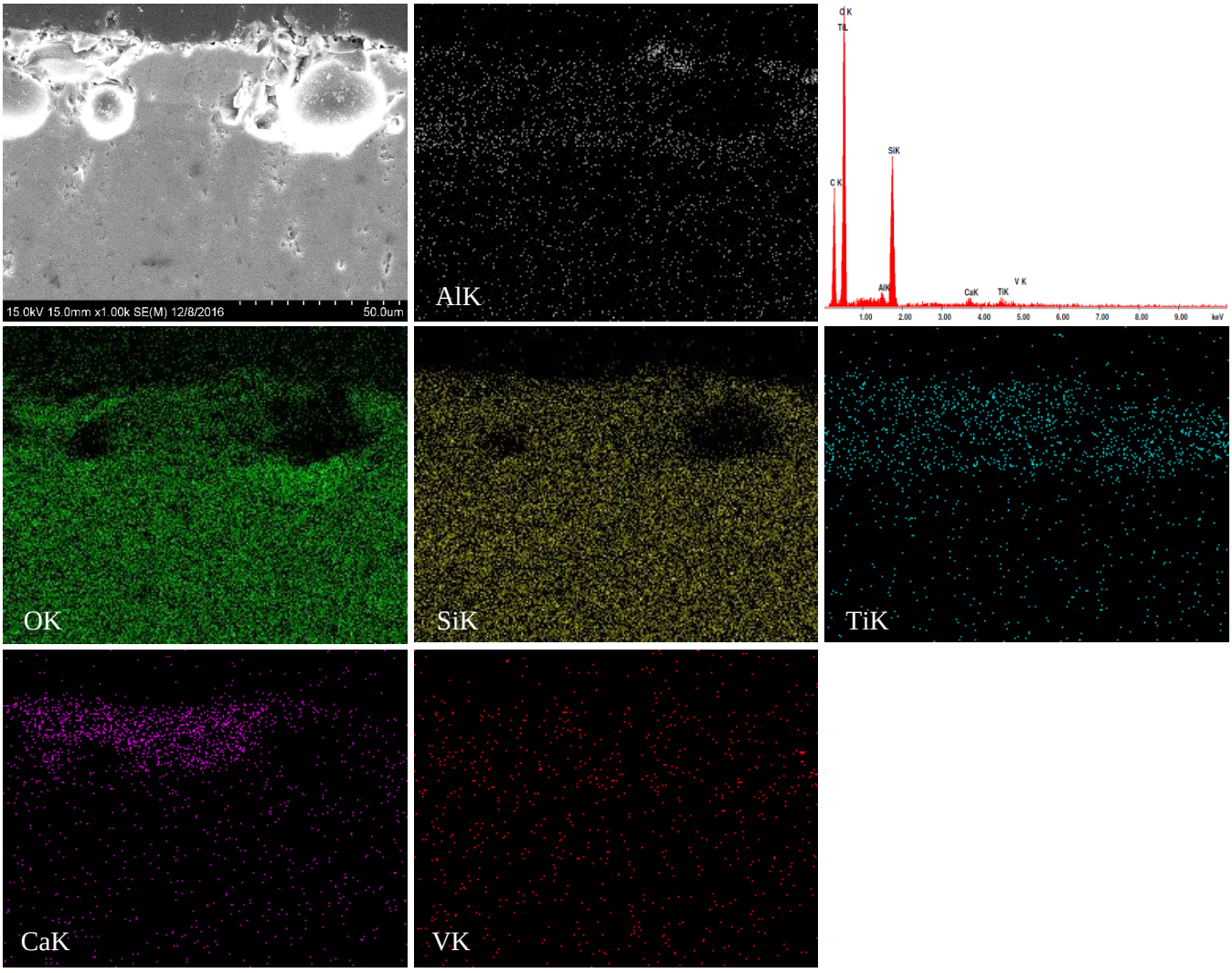

Figure 6.54 X-ray maps of the cross-section shown at 1000X.

Sample 2.1.4 was further analyzed at the cross-section as variations in surface compositions were present. Figure 6.55a and show how the upper area of the surface was severely affected. Elongated hollow areas were frequently formed (Figure 6.55a) thus causing cracks to propagate through the coating as shown on Figure 6.55b. The surface of the TPS in this sample contained several depressions on the surface. Image c exhibited a deposited layer within the porous area. A white spherical-like phase was also present within the deposited layer as pointed out by the black arrow in Figure 6.55c. EDS results of different locations on the micrograph are given in Figure 6.56. Areas a and b show a compositional change where Ti was present as an oxide on area b at the deposited layer. Ca was also only present on the deposited layer. Area a contained the major oxide of 90.77 wt% SiO_2. The white spherical phase was a mixture of 81.34 wt% Fe and 14.05 wt% Cu. Several minor elements of Si, Ca, Ti, V, and Ni was also detected.

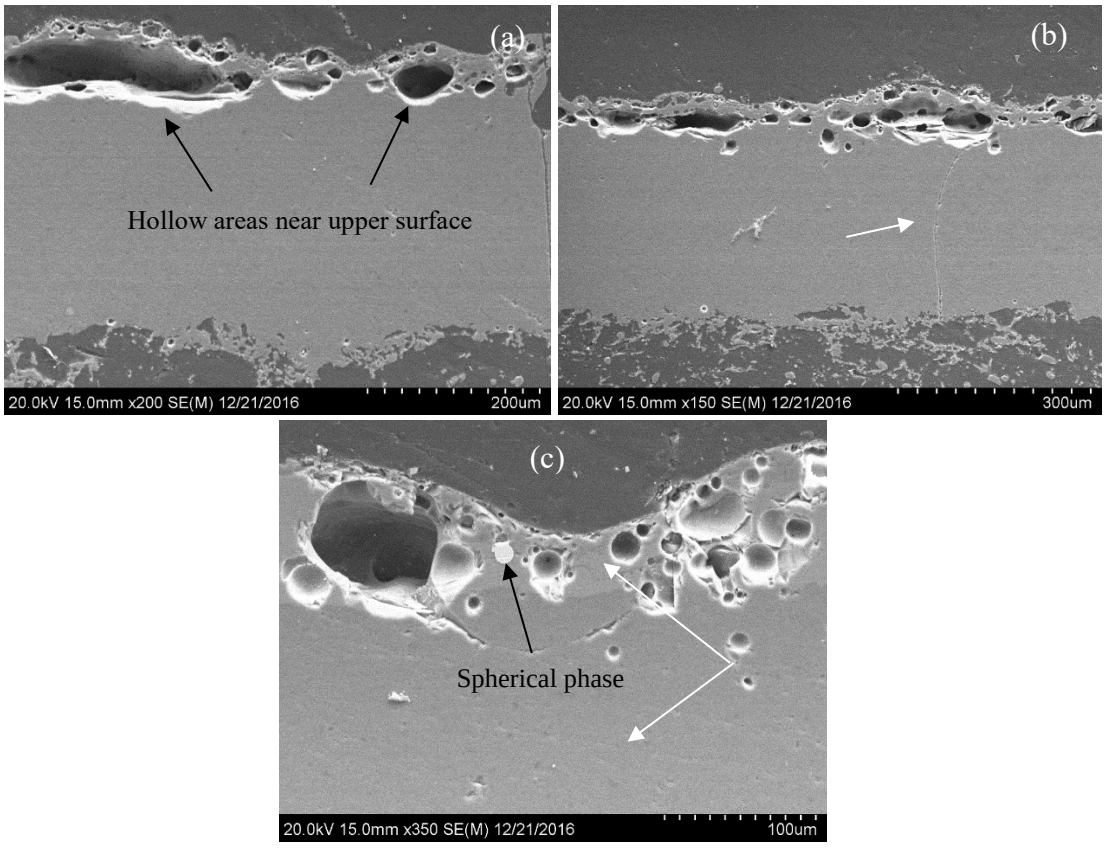

Figure 6.55 Three cross-sectional areas exhibiting severe degradation with porosity and cavities (sample 2.1.4). Image (c) shows a possible deposition layer and a spherical white phase.

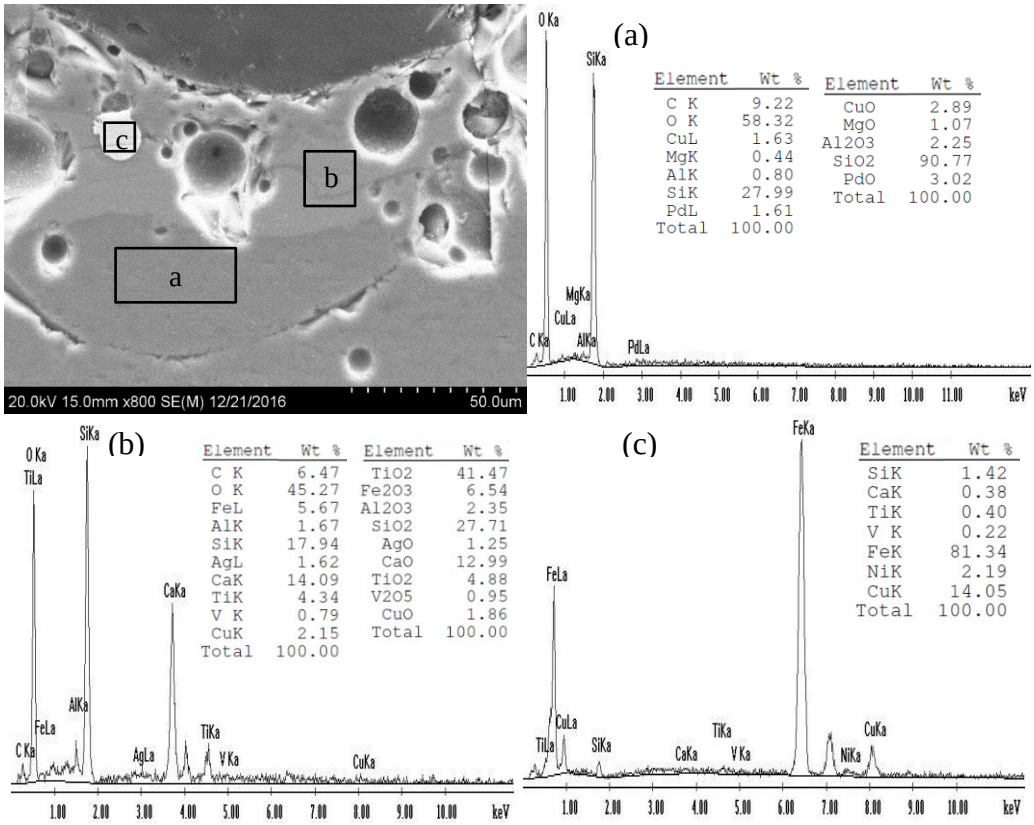

Figure 6.56 Three areas for EDS measurements at the deposit line (a), below the deposit line (b), and the spherical phase (c).

Sample 2.1.4 also contained changes in the composition of the deposited layer and is shown in Figure 6.57. The layer was not as clear as the areas previously analyzed, and spherical cavities masked the entire layer. The corresponding composition of the area analyzed was composed of several elemental species. The layer contained primarily TiO_2, Si, Ca, Ti, and Cu peaks. The minor and trace elements included C, Al, V, and Fe. When compared to the deposited layer in Figure 6.56b, the layer contained higher percentages of Ti and Cu. Figure 6.58 shows additional maps with no Al in the cross-section, but with a greater presence of Fe. The maps also indicated that Ti, Ca, Fe, O, and Si constructed the deposited layer. The Fe present did not appear in white phases as illustrated by the elemental map but was dispersed throughout the deposited layer. In contrast, X-ray maps of the previous microstructure analyzed (Figure 6.55) are given on Figure 6.59. The deposited layer shows that it was formed with Al, Ca, O, Si, and Ti. The Al present was concentrated on the top border of the surface and at the beginning of the deposit

formation. Titanium and calcium were both located at the deposit-to-tile interface. Vanadium was dispersed through the sample and the white phase was consistent with Fe.

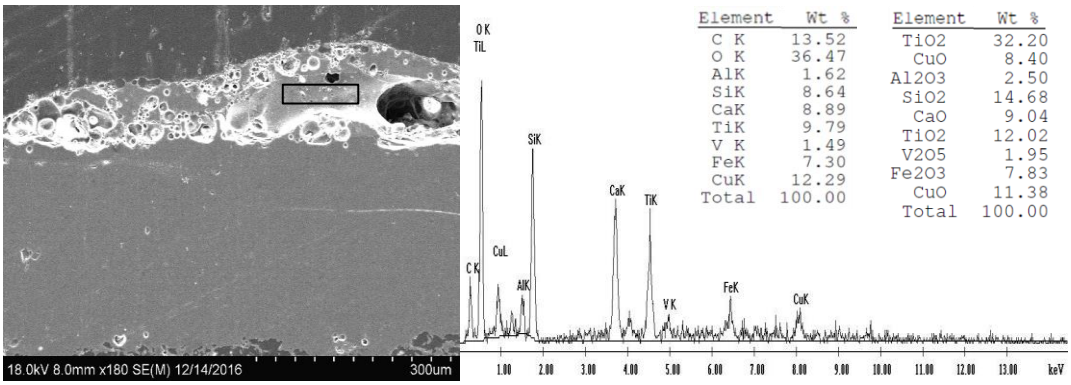

Figure 6.57 Area analyzed at the upper edge of the cross-section near the degradation.

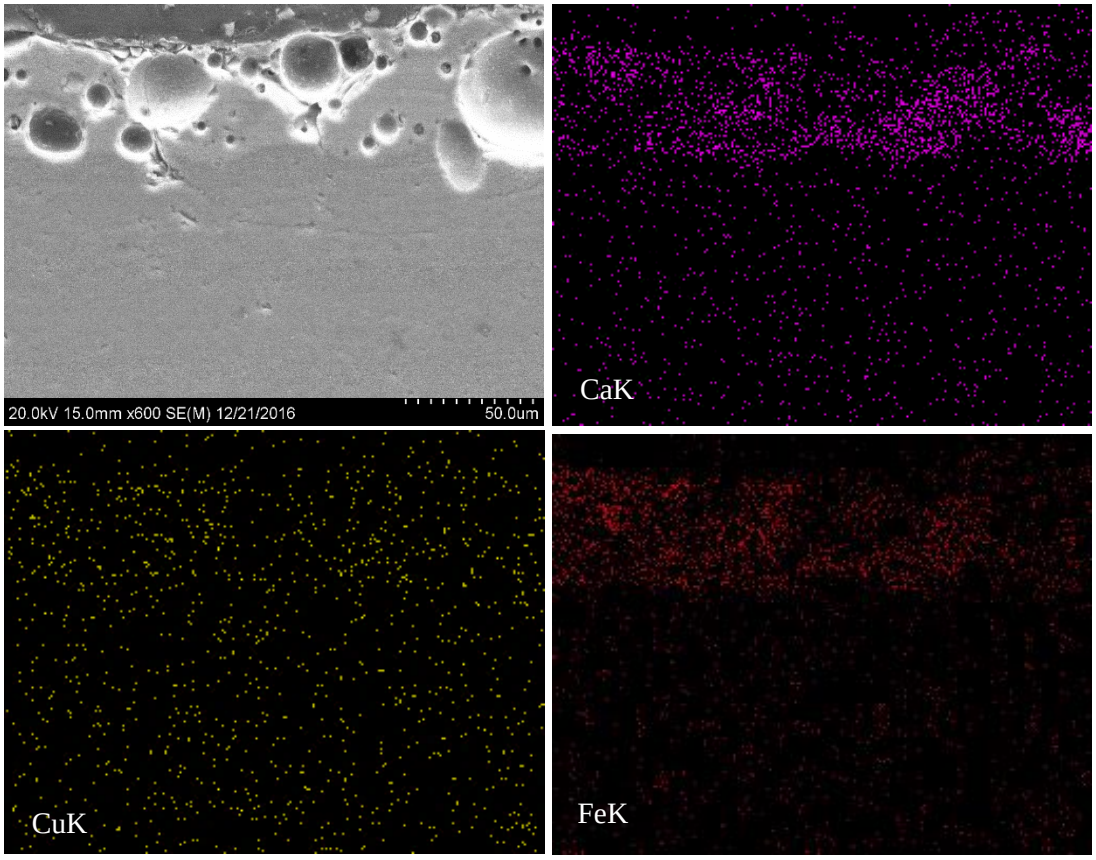

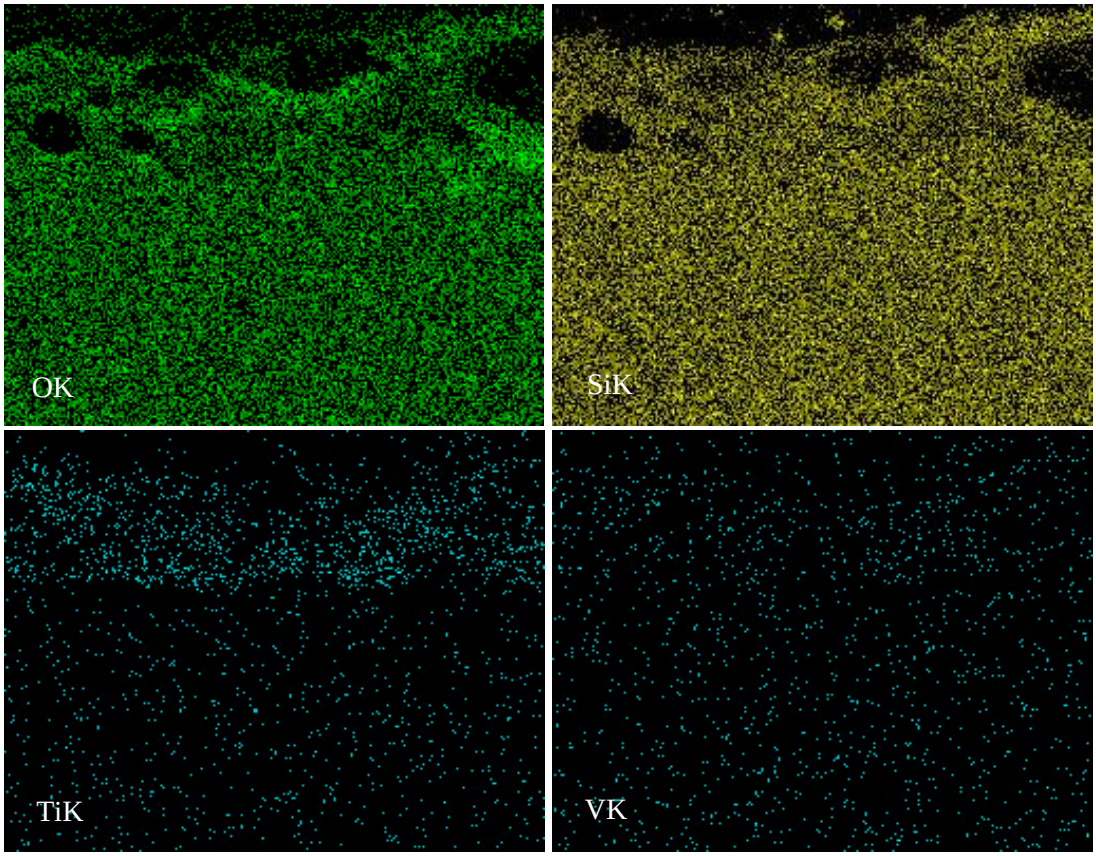

Figure 6.58 X-ray maps at 600X illustrating the distributed elements detected.

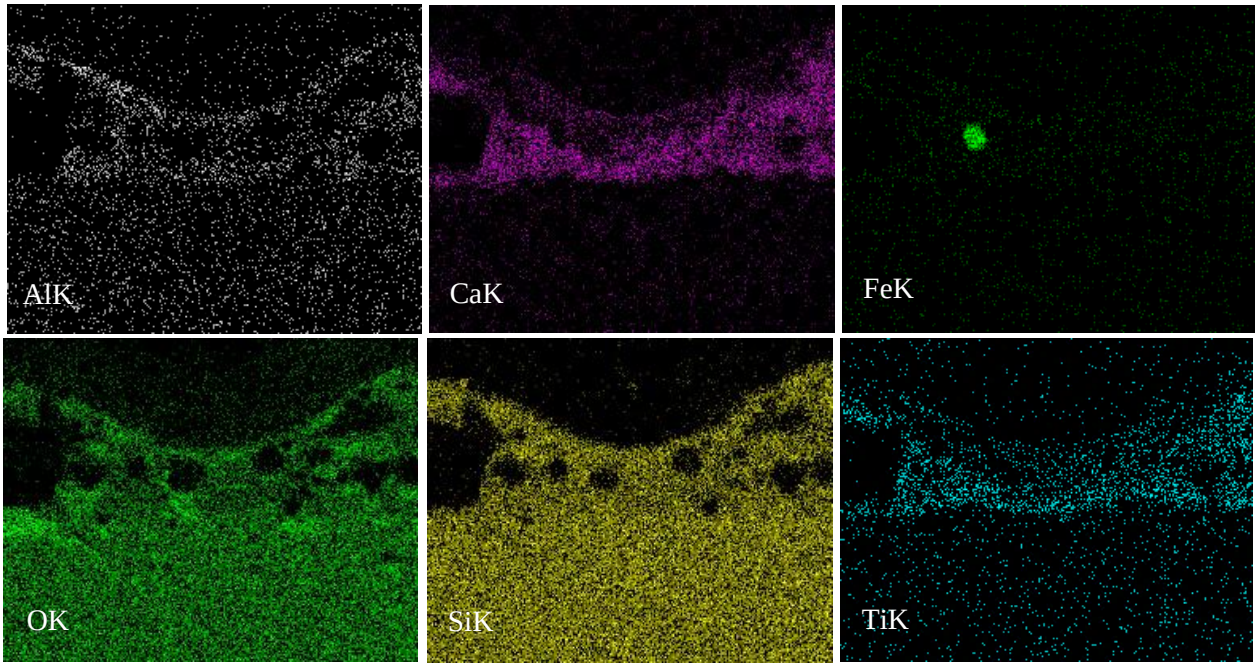

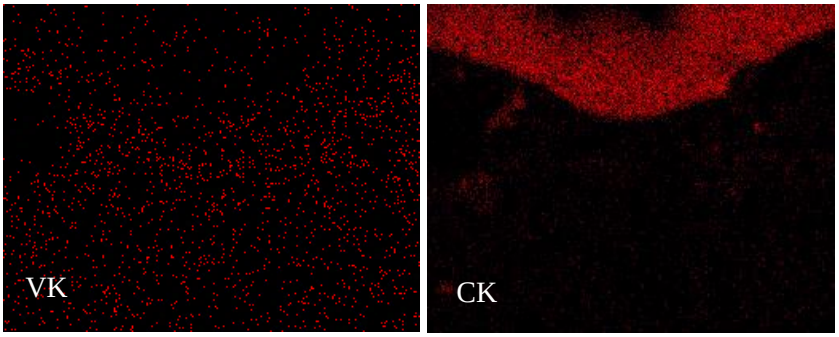

Figure 6.59 X-ray maps of the upper edge of sample 2.1.4.

6.2.3 Aft Tile

The samples sectioned from the aft tile of Window 7 included: Sample 3.1A, 3.1B, 3.2, 4.1, and 4.2. All samples were analyzed at the surface and cross-section. The aft tile contained the most damage to the TPS coating and was located near the payload bay door latch roller.

6.2.3.1 Surface Analysis

SEM surface analysis results of sample 3.1A and 3.1B are shown in Figure 6.60. Image a represents sample 3.1A which had similar surface features to sample 3.1B. Both samples sustained large amounts of porosity and small impacts to the surface. Bright surface deposits were also observed in both samples (Figure 6.60a and b) and more indications of surface degradation are shown in image c. Elemental compositions of the surfaces of both samples are provided in Figure 6.61. Spots 1 and 2 were measured on sample 3.1A, in which both contained equivalent compositions of Ti, O, Al, Si, Ca, and Mg. Spot 3 and 4 from sample 3.1B show comparable results with primary peaks of Ti, O, Si, and Al. Overall, both samples show identical deposits.

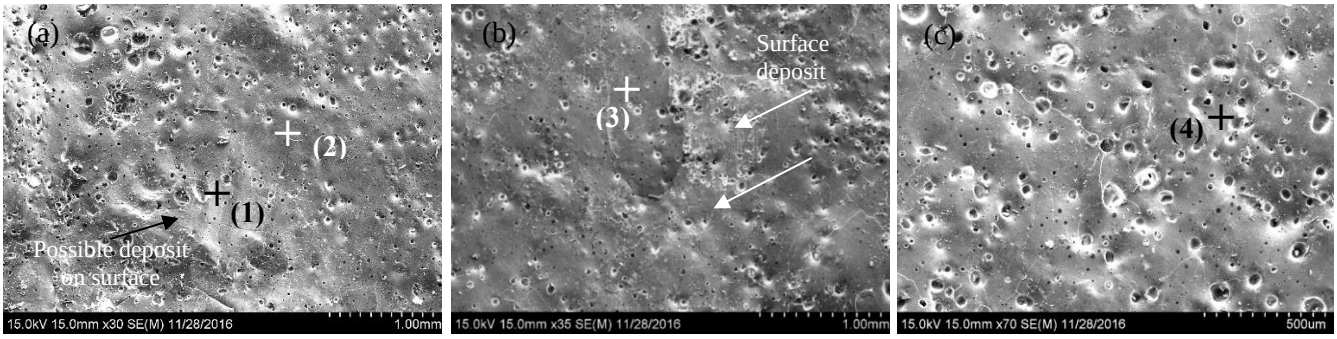

Figure 6.60 Surfaces of (a) sample 3.1A and 3.1B (b and c). EDS readings were measured at spots 1 and 2 for sample 3.1A. Spot 3 and 4 for sample 3.1B.

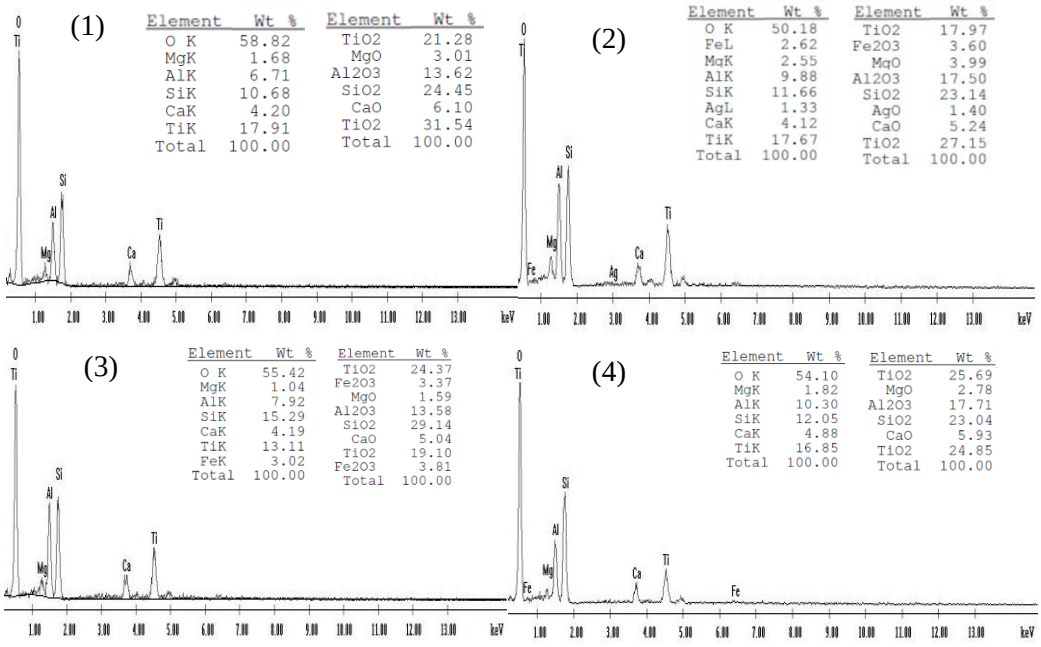

Figure 6.61 Corresponding spot results 1-4 of sample 3.1A (1 and 2) and 3.1B (3 and 4).

The adjacent sample analyzed was sample 3.2 which was located at the inner side of the carrier panel tile. This sample contained the maximal damage at the coating with visible pores. The damage of the surface is demonstrated on Figure 6.62 with a coarse and irregular surface. Possible anomalous white deposits were observed. In contrast to the previous samples (3.1A and 3.1B), changes in elemental compositions appeared. Aluminum and oxygen were the most prominent elements measured on Figure 6.63a and b. Titanium oxide was still present except aluminum surpassed in weight percentage of area a.

The minor elements included Mg, Si, and Ca. Area b was analyzed at a different location which shows major peaks of Al and O.

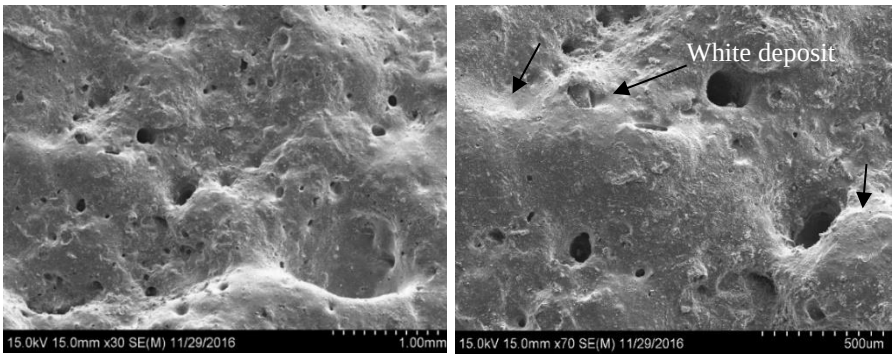

Figure 6.62 Images depicting the uneven surface of sample 3.2

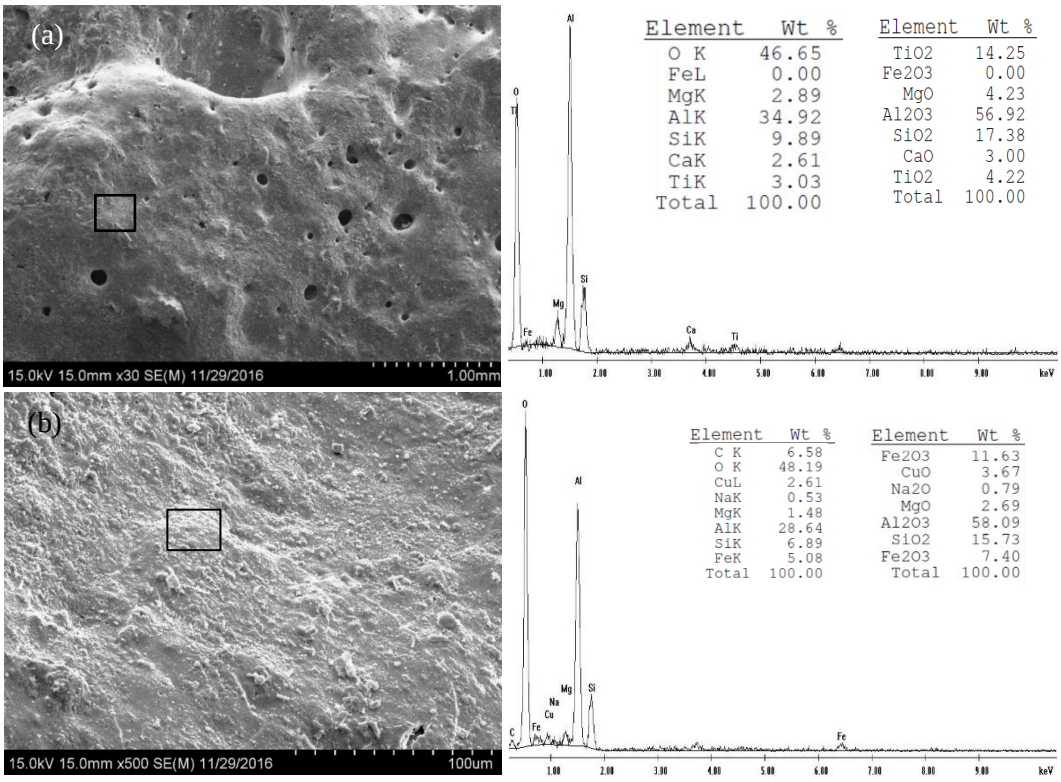

Figure 6.63 Area EDS analysis of (a) and (b).

The second set of samples were also retrieved from the aft tile located near the outer surface of the tile to identify the elemental species. Sample 4.1 consisted of two sides of the coating as it was located at the edge of the tile. Figure 6.64a and b demonstrates the damaged surface of sample 4.1. The nature of the coating suggests deterioration as large indentations were present (image a). The coating also contained

dark and light contrasts as demonstrated on Figure 6.64b. The surface of Sample 4.2 (Figure 6.64c and d) also contained similar surface characteristics with dark or light areas. It was assumed that the dark areas are the black TPS coating and the light areas are surface deposits.

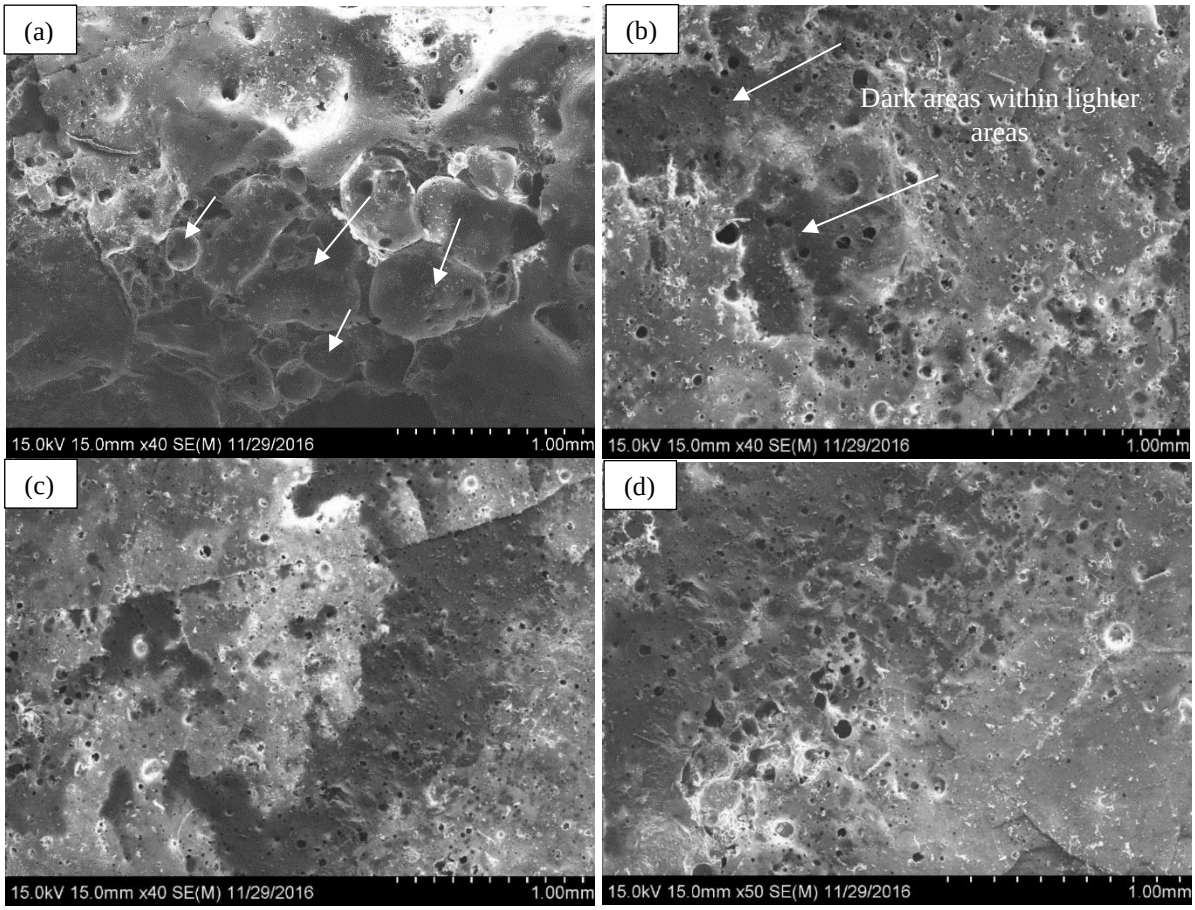

Figure 6.64. Sample 4.1 surface images (a) and (b). Sample 4.2 surface (c) and (d) with similar features.

The identification of the surface discolorations present on sample 4.1 and sample 4.2 are shown in Figure 6.65. Most of the surface chemistry of sample 4.1 was consistent with the spectra shown on image a. The major peaks were comprised of 55.36wt% O, 12.49wt% Si, 11.47wt% Ti, 8.53wt% Ca, and 7.38wt% Al with minor elements of V and Fe. Sample 4.2 contained resembling compositions on Figure 6.65b with the exception of Zn and Mg minor elements. When compared to samples 3.1A and 3.1B, all samples contained similar surface deposits and discolorations at the surfaces. Sample 3.2 however, contained aluminum as the primary element deposited.

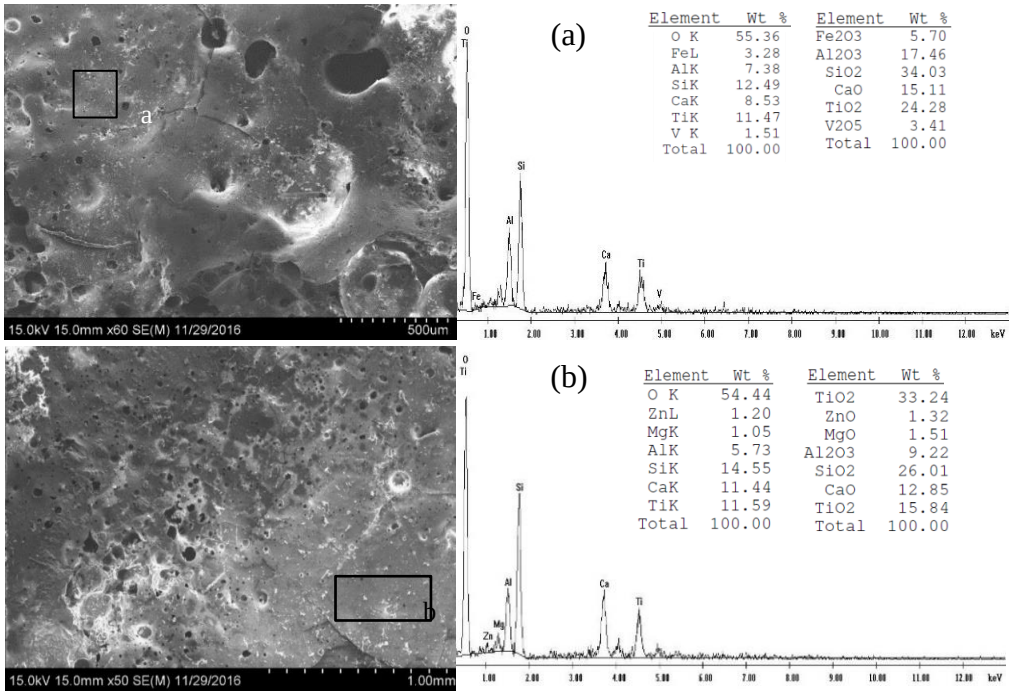

Figure 6.65 EDS results of area (a) of sample 4.1 and area b of sample 4.2.

6.2.3.2 Cross-sectional Analysis

The areas beneath the TPS coating were explored as all previous specimens contained a deposited layer. Severe damages at the coating were present on sample 3.1A (Figure 6.66a-b). Lots of cracks originated at the surface and extended down through the coating (image a). Plenty cavities were concentrated at the topmost surface (image b) and a deposited layer can be observed on image c. Defined microstructural phases began to form at the deposited layer on Figure 6.67a when observed at high magnifications. The boxed area in this micrograph represents image b which contained texturing. Thorough images of the microstructural features are provided on Figure 6.67 c and d. These images were obtained from image b at higher magnifications of 5000X and 4000X. Changes in the morphology of the microstructure are shown in image c. First, a grain-like shaped texture was observed in the area indicated by the white arrows. Thin needle-like grains take up most of the cross-section however, small dendritic structures begin to form as demonstrated on Figure 6.67c. These phases appear to begin the process of growing dendritic arms or solidification. Spherical grains are also present below this area. Another area

of the coating (Figure 6.67d) also contained similar microstructure arrangement. The top most area contained the lath-like texture followed by grain-like areas. Next, the small branch development of dendrite formation was also found and large circular phases were present.

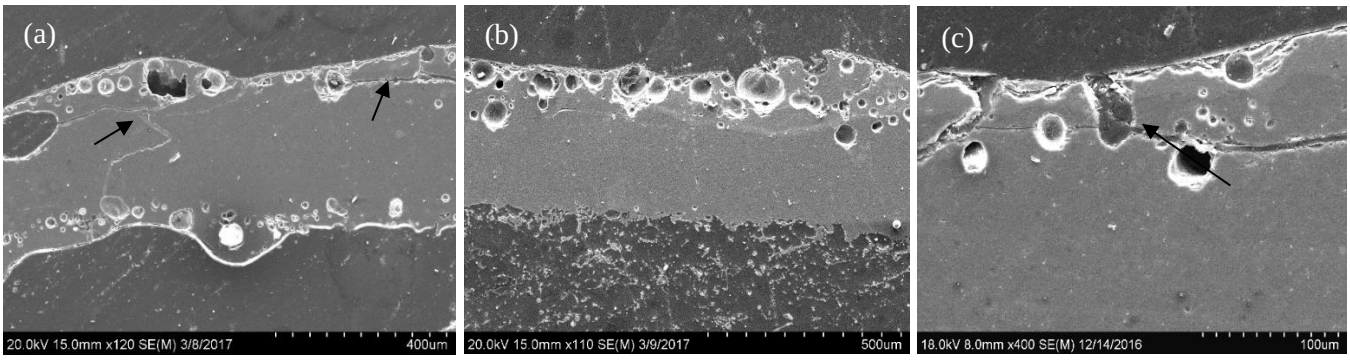

Figure 6.66 Cross-sectional images of sample 3.1A. Image (a) shows continuous open pores and cavities, (b) illustrates increasing cavities, and (c) shows a light gray layer.

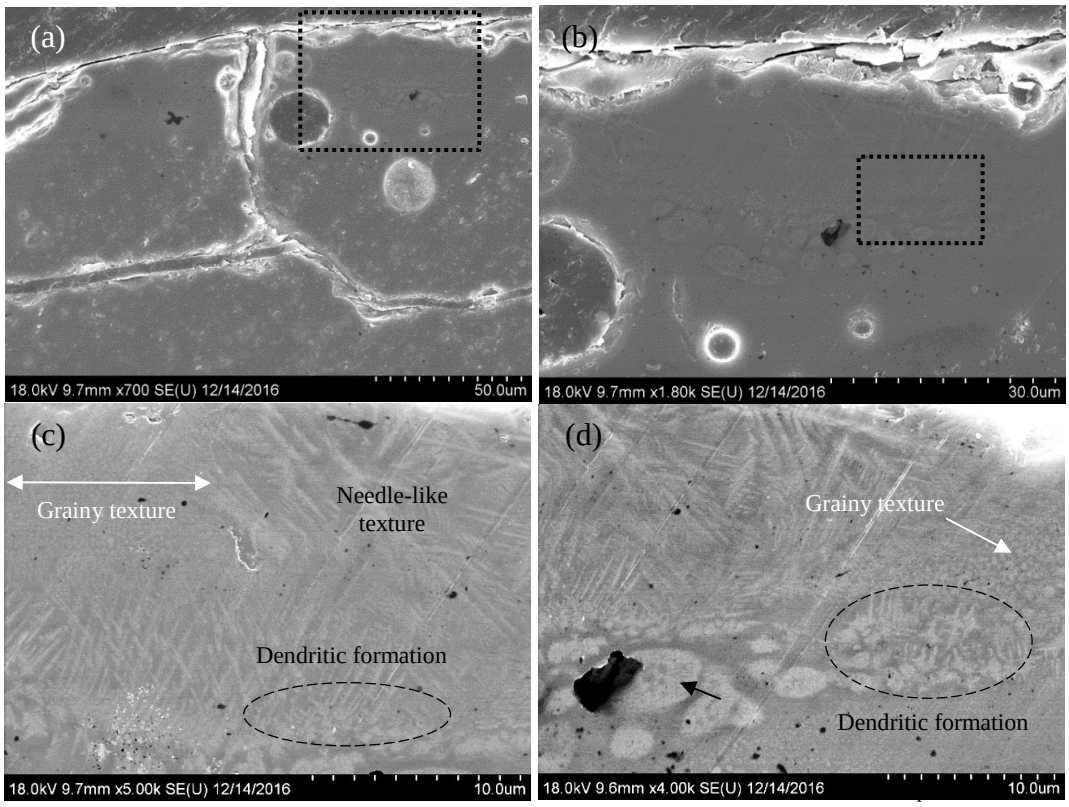

Figure 6.67 Several cross-sections are shown near the upper surface of the sample. Image (a) shows the coating at 700X where the black box represents where image (b) was obtained. Texturing in these areas are shown in images (c) and (d).

EDS measurements were collected at the light gray needle-like phase (1) and dark gray phase (2) and the results are shown on Figure 6.68. The compositions show that the needle-like phase consists of 37.16 wt% Ti, 37.69 wt% O, 10.55 wt% Si, 5.23 wt% Al, 3.72 wt% Ca, and 4.25 wt% Cu with trace amounts of Mg and V. The dark areas (spot 2) contain less Ti weight percent and detected additional elements. The primary elements were 23.55 wt% Ti, 38.92 wt% O, 12.70 wt% Si, and 5.60 wt% Al, respectively.

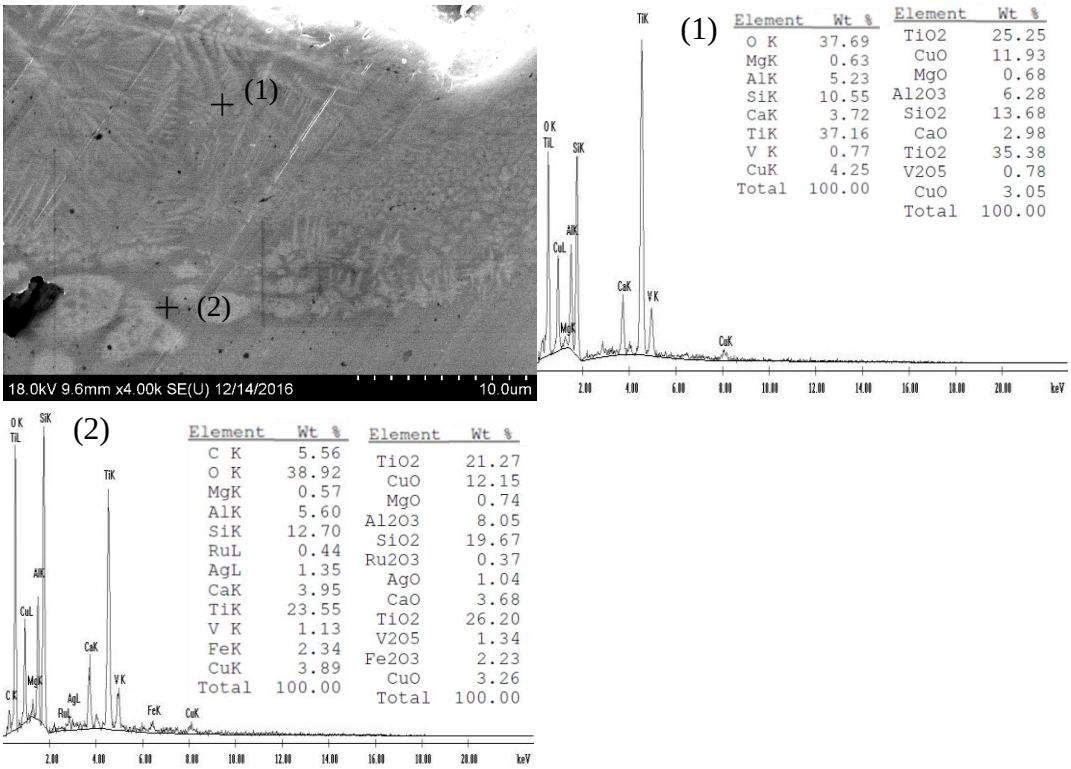

Figure 6.68 EDS spot measurements representing a light phase (1) and dark phase (2).

X-ray maps (Figure 6.69) were developed to examine the cross-section from Figure 6.67a with arrows indicating the start of the deposited layer. The maps show that aluminum was deposited but its concentration was higher near the top surface of the sample and decreases through the cross-section. A distinct interface was clear and shows a large concentration of titanium. The beginning of the titanium deposit is illustrated by the white arrows. Vanadium, silicon, oxygen, and calcium also make up the deposited layer. The silicon map shows a decrease in weight percentage. Iron was present as a trace

element and lightly scattered through the microstructure. Carbon was still present at the cracks in the coating, cavity, and mounting material. The second map at a lower magnification of 200X revealed areas of aluminum at the tile-to-silica interface as shown in Figure 6.70. Titanium was more pronounced in the coating area than any other element detected and was even present in the cavities. The deposited layer in this area does show a large presence of iron and is also dispersed through the coating. Again, oxygen and silicon also show up in the coating.

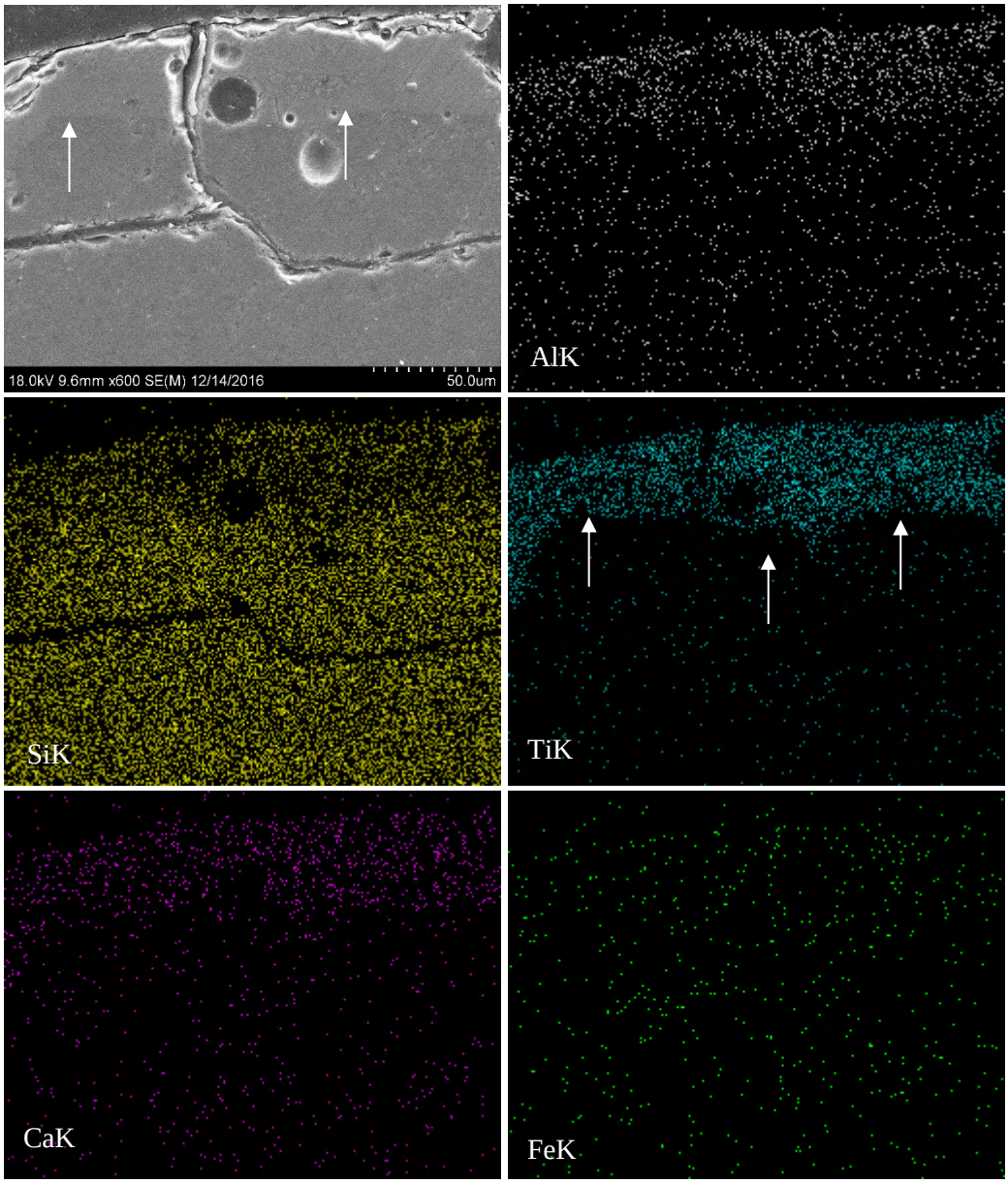

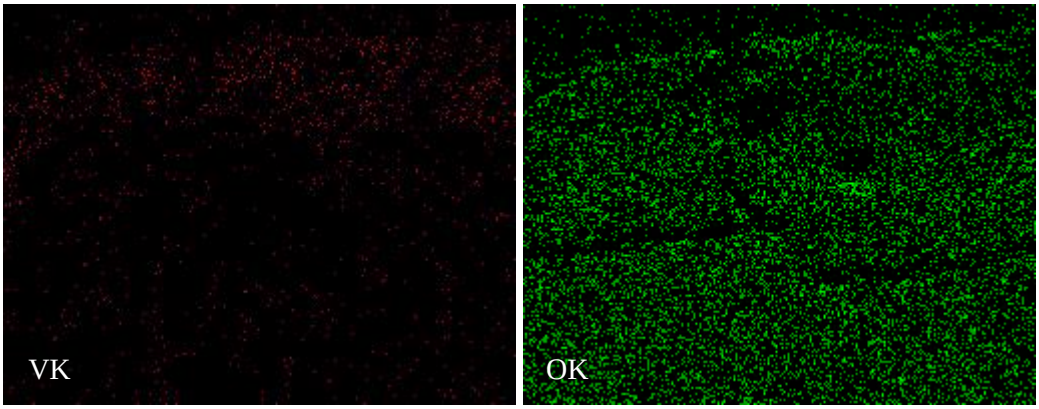

Figure 6.69 X-ray maps at the cross-section of sample 3.1A sample shown.

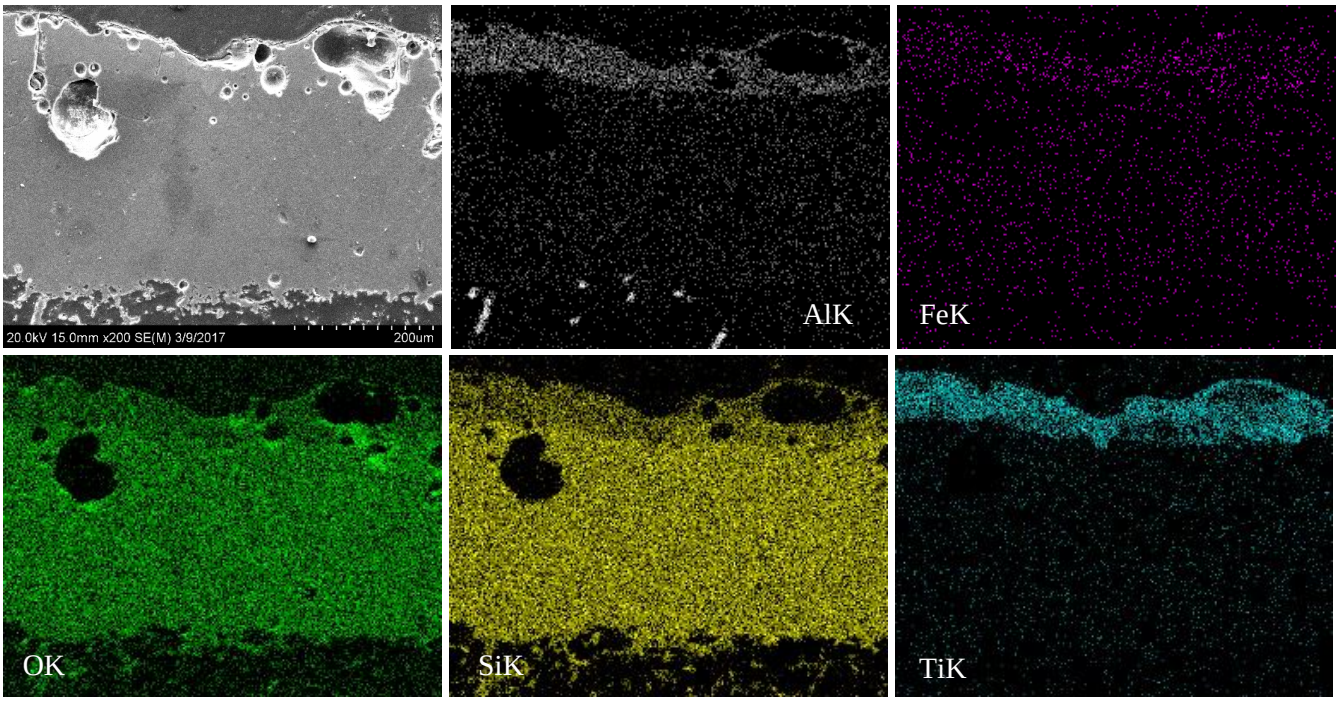

Figure 6.70 A cross-section showing the coating and base material with X-ray maps.

Further examination of sample 3.1.1B revealed missing areas of the coating with varying thicknesses. These features can be seen in Figure 6.71 a-c and the sample contained the greatest damage to the coating out of all samples analyzed. Image c shows that the surface sustained enough heat that diminished the entire thickness of the tiles and almost reached the inner silica. A prominent area of the coating contained differences in EDS composition results. Unlike the previous samples, this sample did

not have a definite deposit layer. As a result of this, EDS analysis was performed in different areas of the cross-section. Spots a and b from Figure 6.72 had similar major elements except for trace elements and Ti. No titanium was found on spot a only on spot b. Additional acquisition of elements present at the two areas analyzed (Figure 6.73 a and b), were found to be rich in Ti. The presence of these elements was surprising as no clear accumulation of a deposited layer was observed.

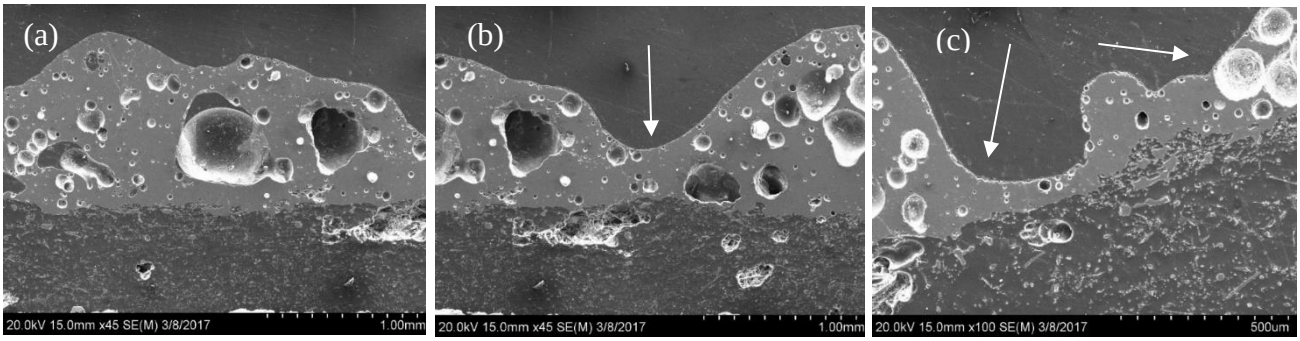

Figure 6.71 The cross-sections of sample 3.1.1B detailing the changes in coating depth.

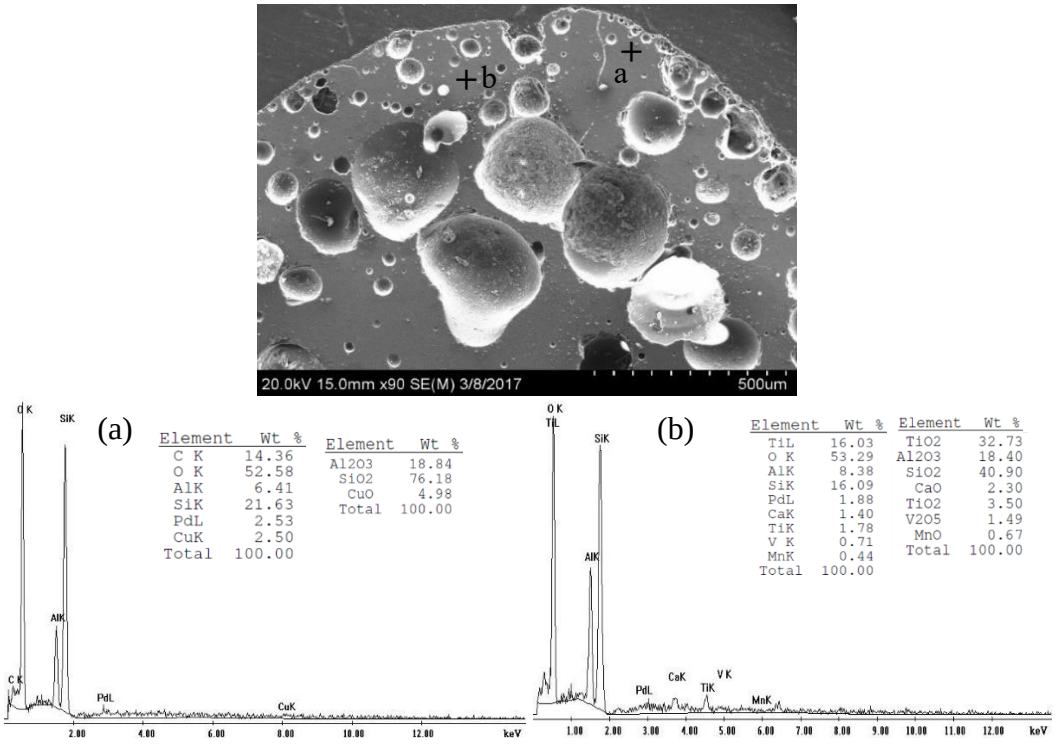

Figure 6.72 EDS spot measurements at the highest point of the coating.

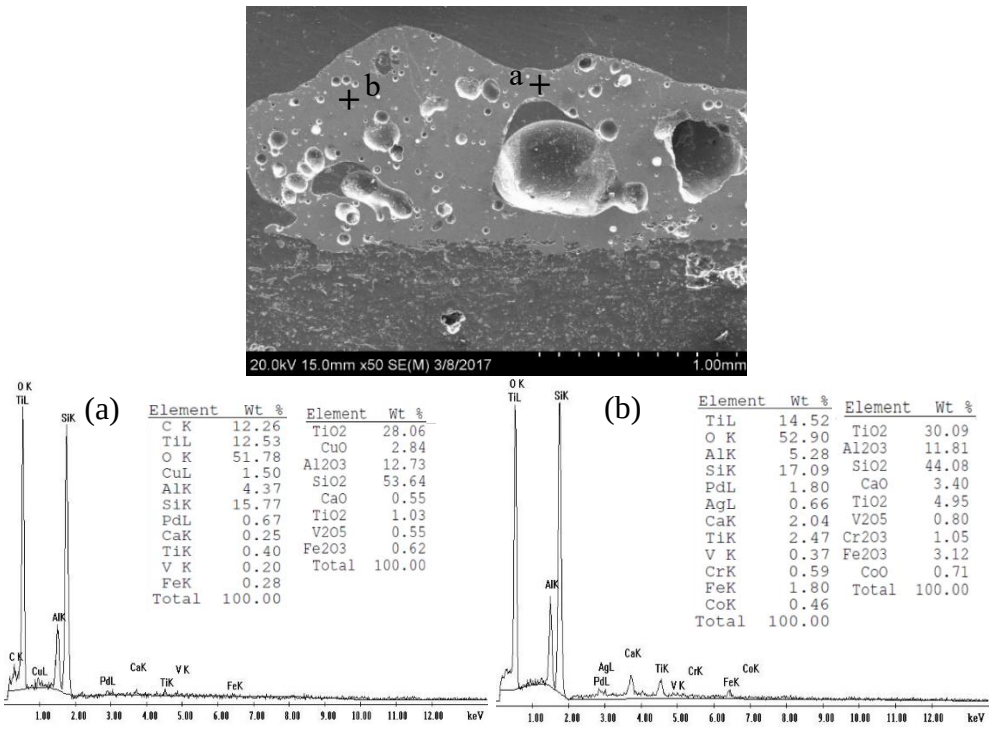

Figure 6.73 Spot readings (a) and (b) revealing similar compositions.

In addition to point analysis, the variations in the composition of the sample are provided in Figure 6.74 and Figure 6.75. Although no evidence of a bright layer was observed, the elemental species previously identified were deposited on the sample. Deposits existed beyond the TPS surface and spanning down to the silica fibers (Figure 6.74) with elements of aluminum, oxygen, silicon, titanium, and vanadium. Aluminum accumulated first as several areas of the silica were highlighted. Bright areas near the top surface of the coating contained aluminum. The coating contained oxygen which was distributed throughout its thickness while elemental titanium, along with calcium, were the last deposits to accumulate. The distribution of vanadium was also concentrated on the TPS coating. No copper deposits were present. A large number of spherical cavities on the coating were surrounded by the deposits and appear to be consistent with carbon and copper. Further analysis of the protruding residual coating was found to contain aluminum, iron, titanium, silicon, and oxygen. The collected maps are shown in Figure 6.75. Small unique areas of aluminum were also present beyond the coating. The cavities on the coating

did not contain any of these deposits only carbon. The assortment of these elements was unique as no defined changes in microstructure was observed.

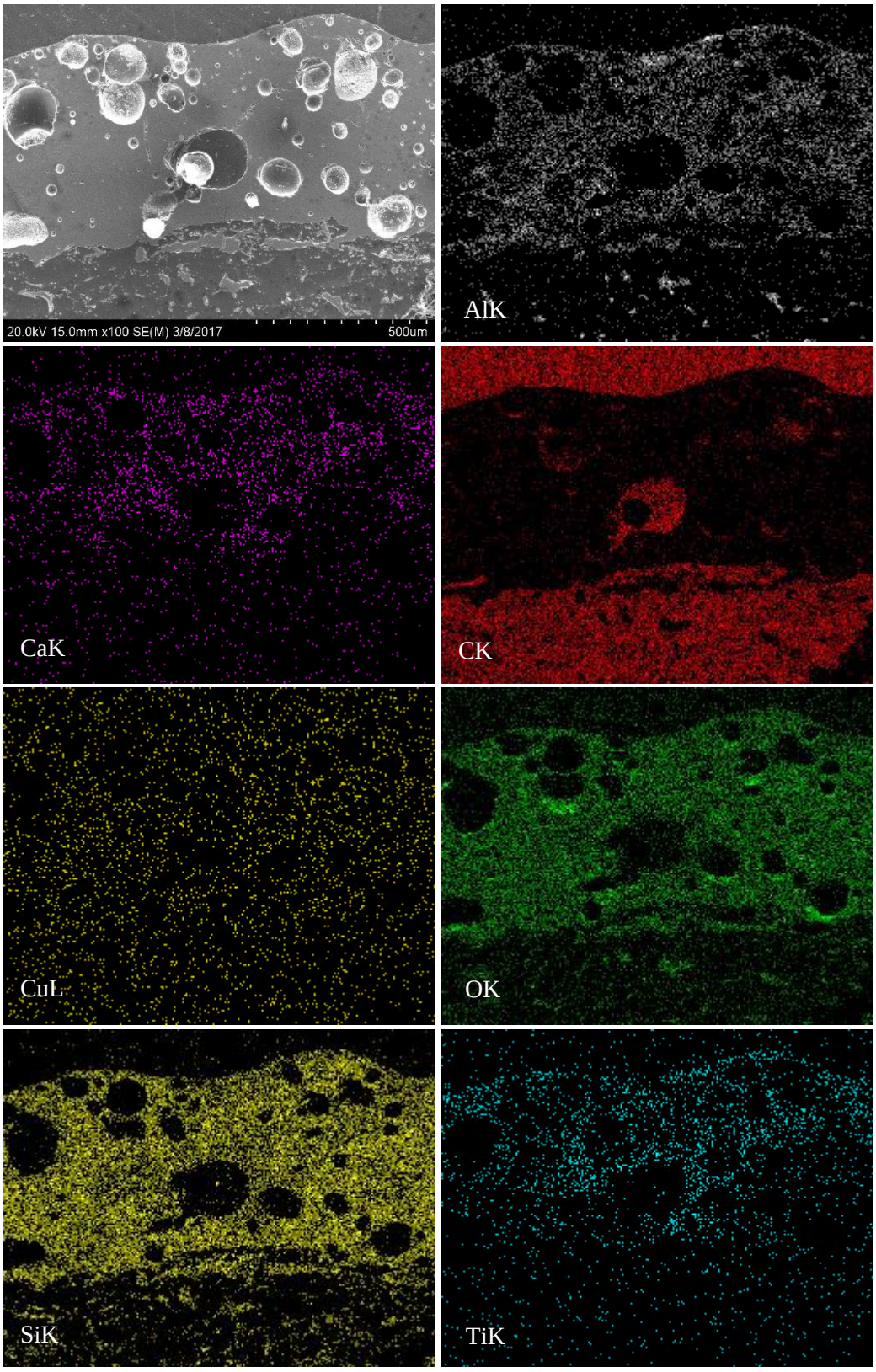

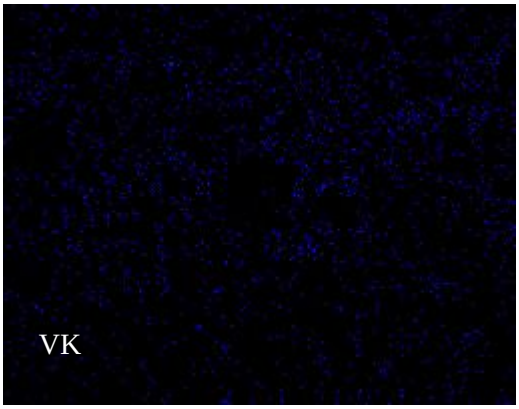

Figure 6.74 X-ray map of the cross-section of sample 3.1B.

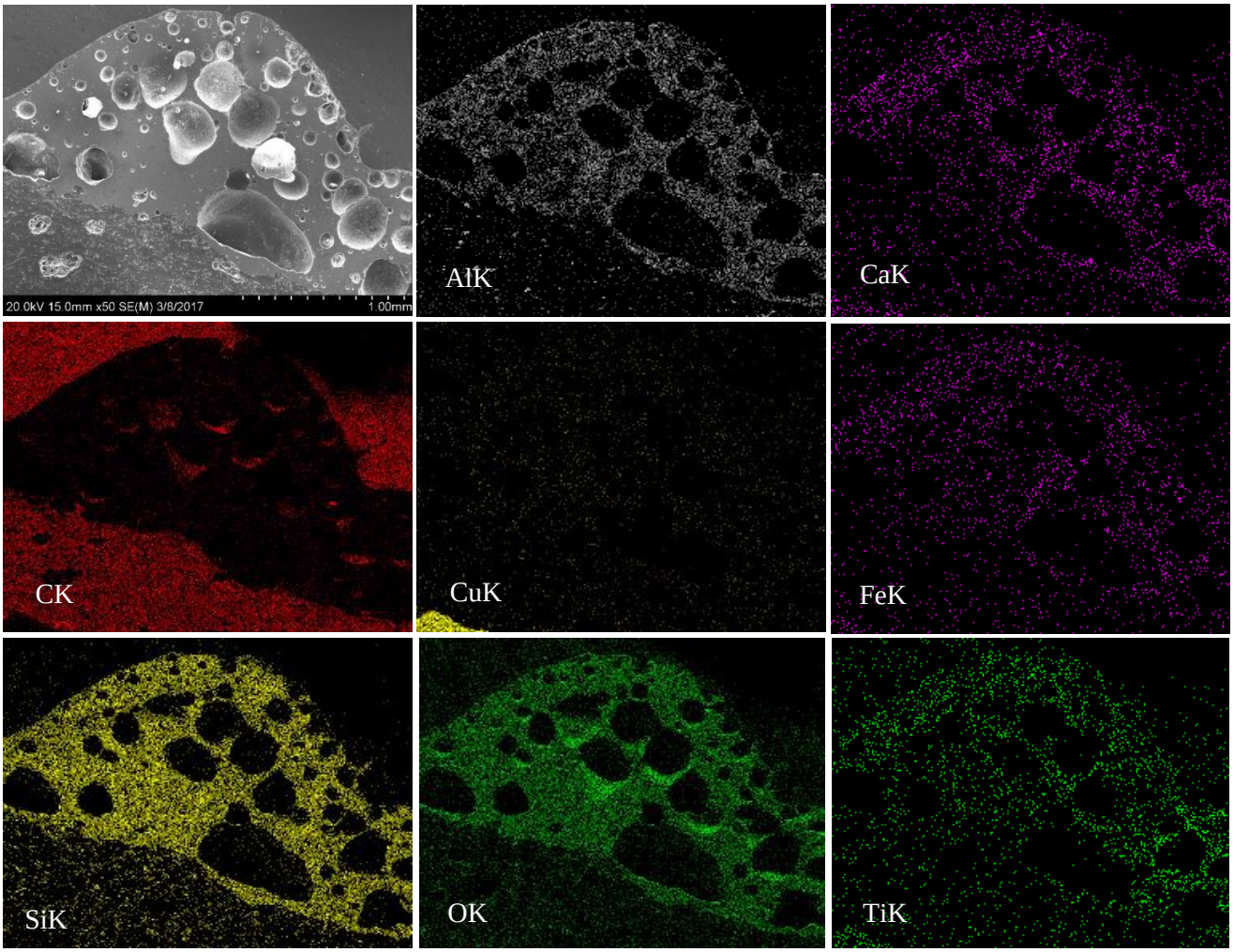

Figure 6.75 Remaining high point of the TPS coating and resultant elemental maps.

Next, sample 3.2 located at the inner lip geometry of the tiles exhibited enlarged cavities and a receding coating. The cavities on Figure 6.76a, nearly engulf the entirety of coating. Several areas appeared to show missing coating material as shown by the white arrows. Another area shows elongated cavities mostly present near the coating-to-tile interface (Figure 6.76b). Large hollow pores begin to appear and are distinguished by the white arrows in figure 6.76c. The deteriorated coating is illustrated on image d and found to contain missing coating material, cavities, and hollow pores. Unlike the previous samples, a deposited layer was formed and the EDS spectrum is shown on Figure 6.77a. The quantification of deposit layer a resulted in Ti, O, Al, Si, Ca, and Fe major peaks. Area b however, contained Si and O peaks. However, EDS also revealed that the compositions were not constant. For instance, an area close to the top surface of the coating (Figure 6.77c) contained primary peaks of Si and TiO_2. The elements that were deposited on this sample were not evenly deposited. It is possible that changes in plasma flow directions during re-entry may have caused the alterations in elemental weight percentage distribution.

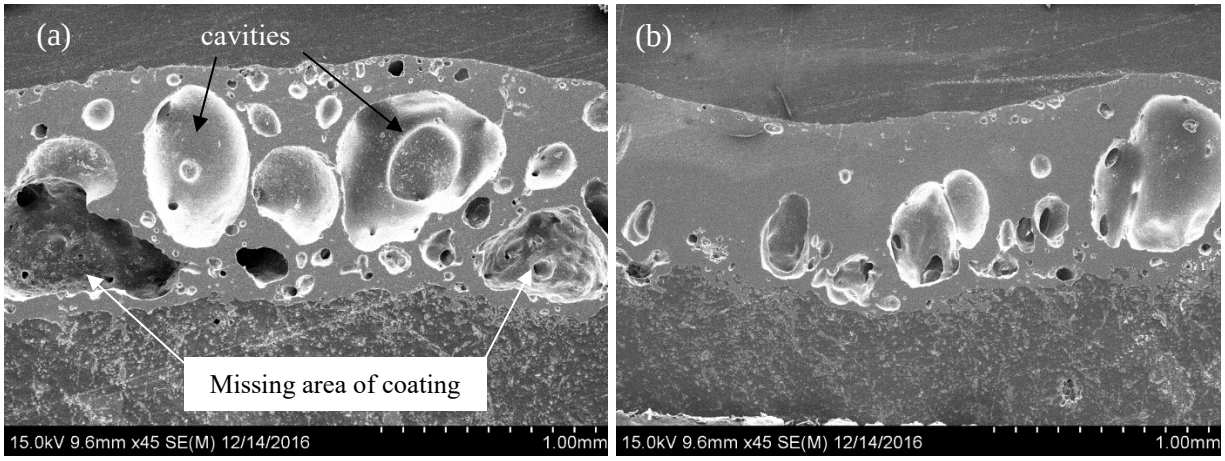

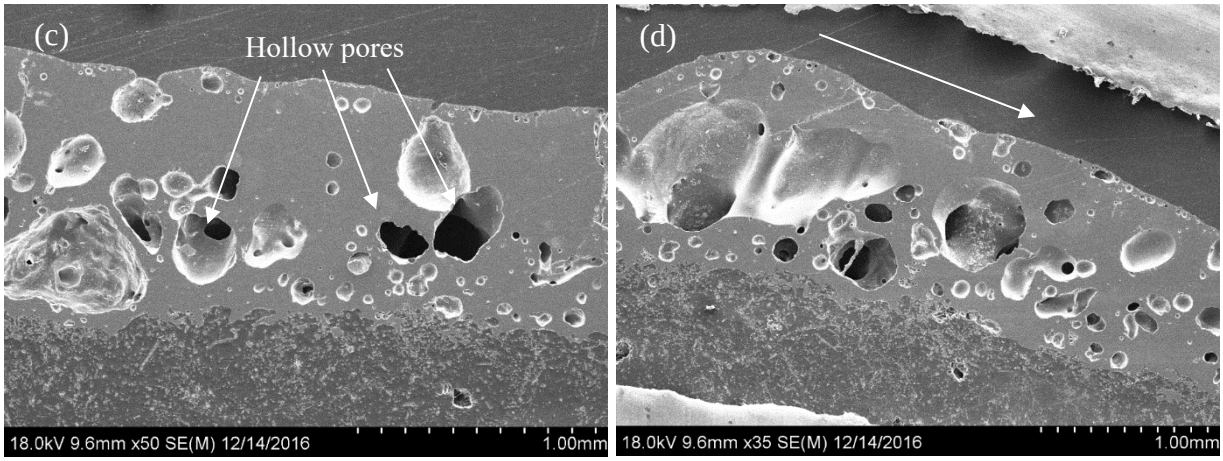

Figure 6.76 Images of sample 3.2 showing the large number and sizing of cavity damage in (a), the cavities and pores also are present near the interface on (b), deep pores are shown on (c), and a decrease in coating is shown on (d).

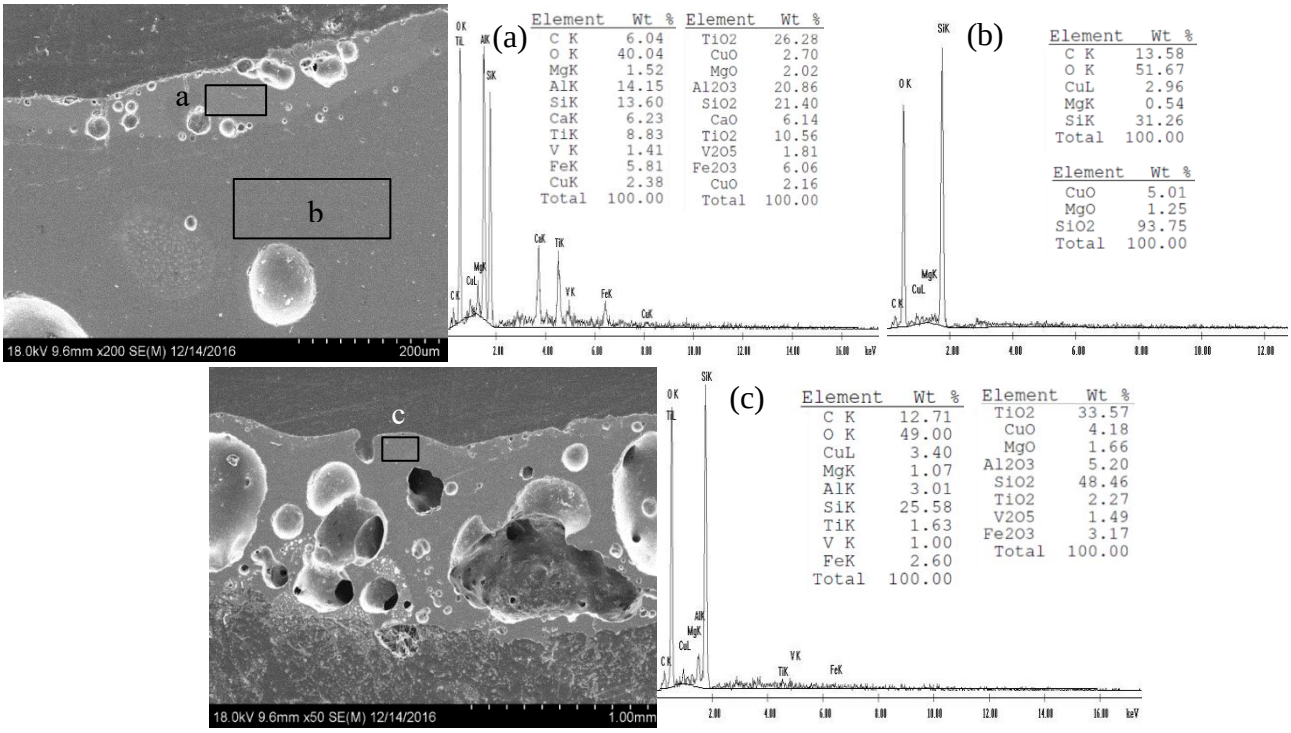

Figure 6.77 EDS spectra of two areas (a) and (b) on the micrograph shown. Area (c) was analyzed at a different location.

To distinguish how the depositions differed at this sample, individual X-ray maps are provided in Figure 6.78. Aluminum was first deposited as it was concentrated below the coating in addition to a thin deposit at the surface. The thin deposit was confirmed to be a mixture of Ca, Ti, O, and Si. The vanadium

deposit was not as concentrated as the other deposits. Some carbon was found to be located in the cavities. However, the hollow pores located above the silica interface did not show to contain any deposit. The next area that was mapped was the micrograph in Figure 6.79 which had missing areas of the coating. The distribution of aluminum was also located at the interface and top surface of the coating. Minimal evidence of titanium was deposited whereas vanadium was uniquely present in the coating. The brightness of the vanadium map shows that it contained a greater concentration than titanium. Calcium did not settle on the cross-section. Similar to the previous area, copper was distributed throughout the coating. Silicon and oxygen were the primary elements concentrated on the coating. Minimal areas with carbon were concentrated near the coating-to-tile interface.

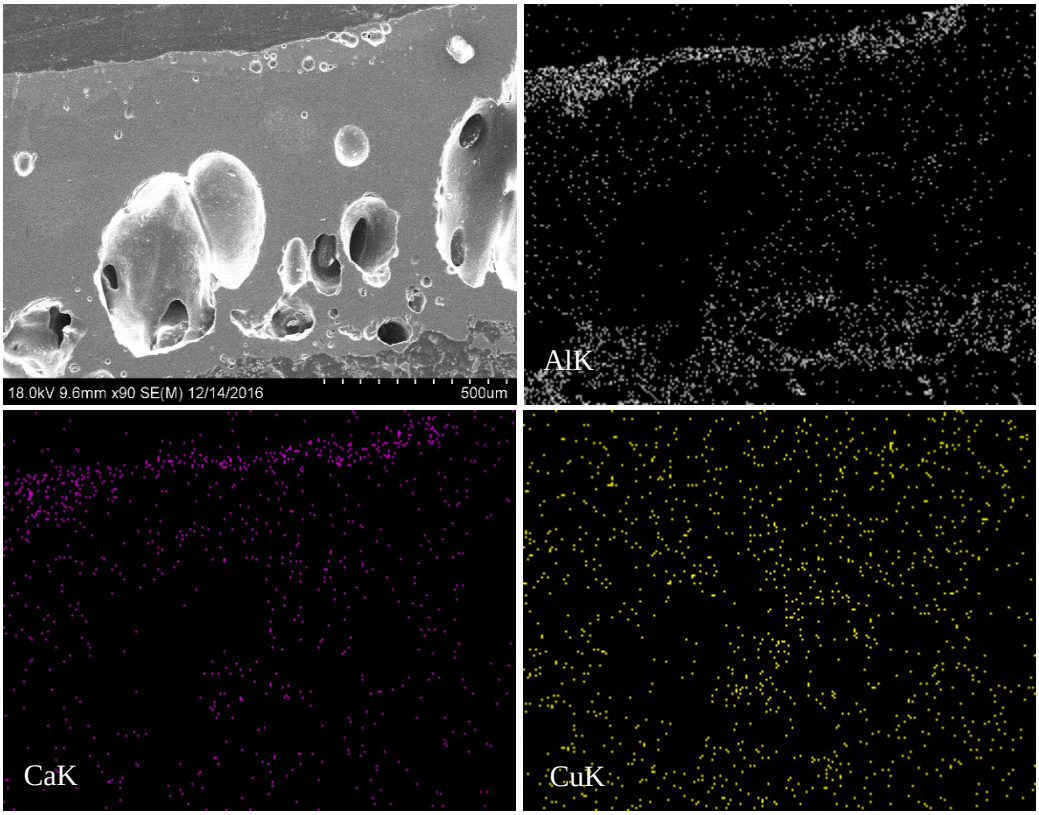

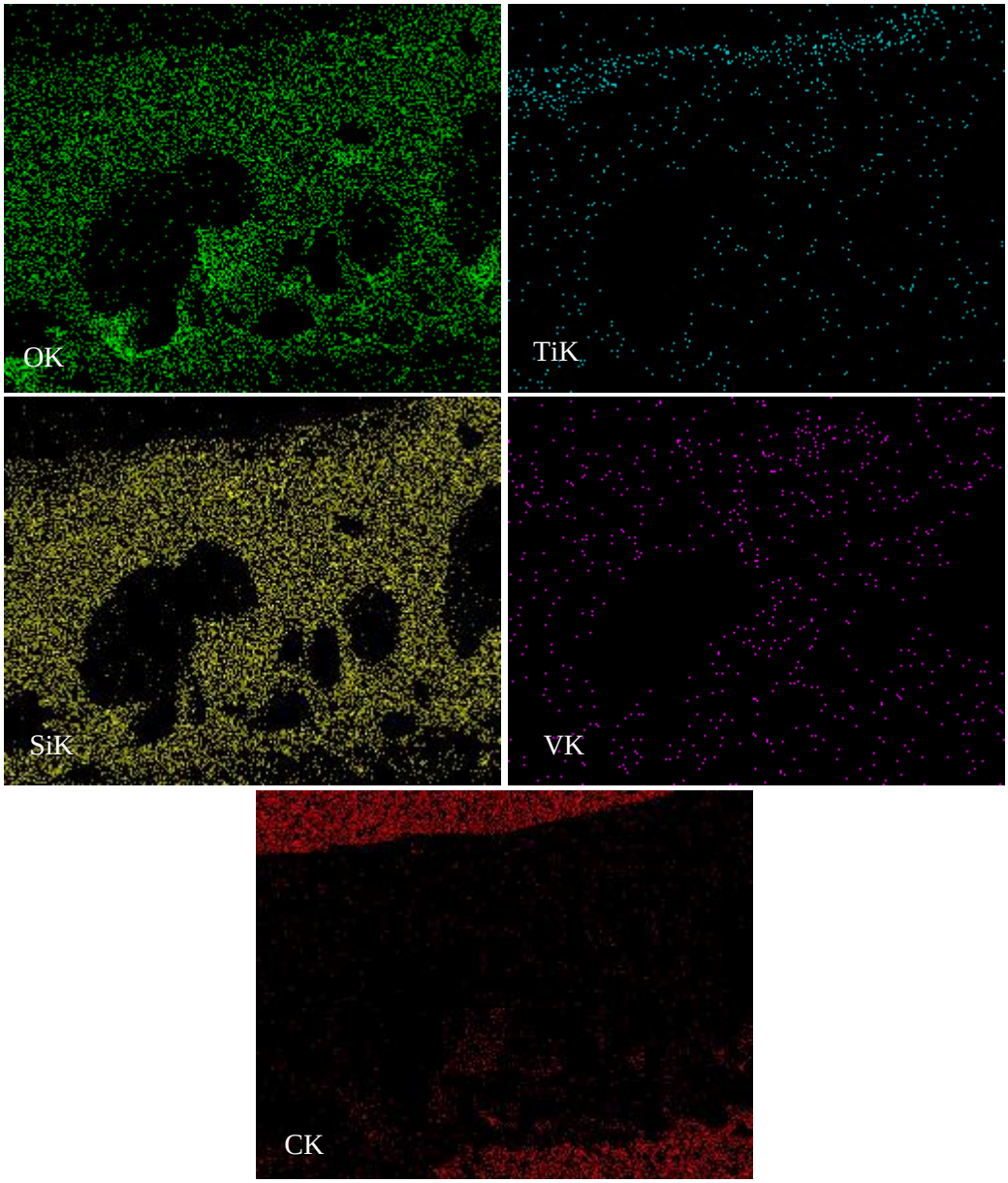

Figure 6.78 X-ray maps of sample 3.2.

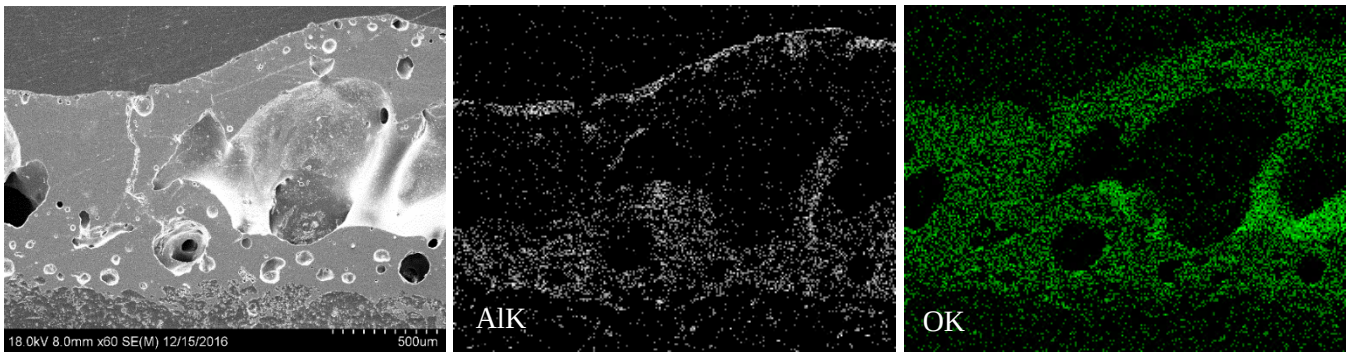

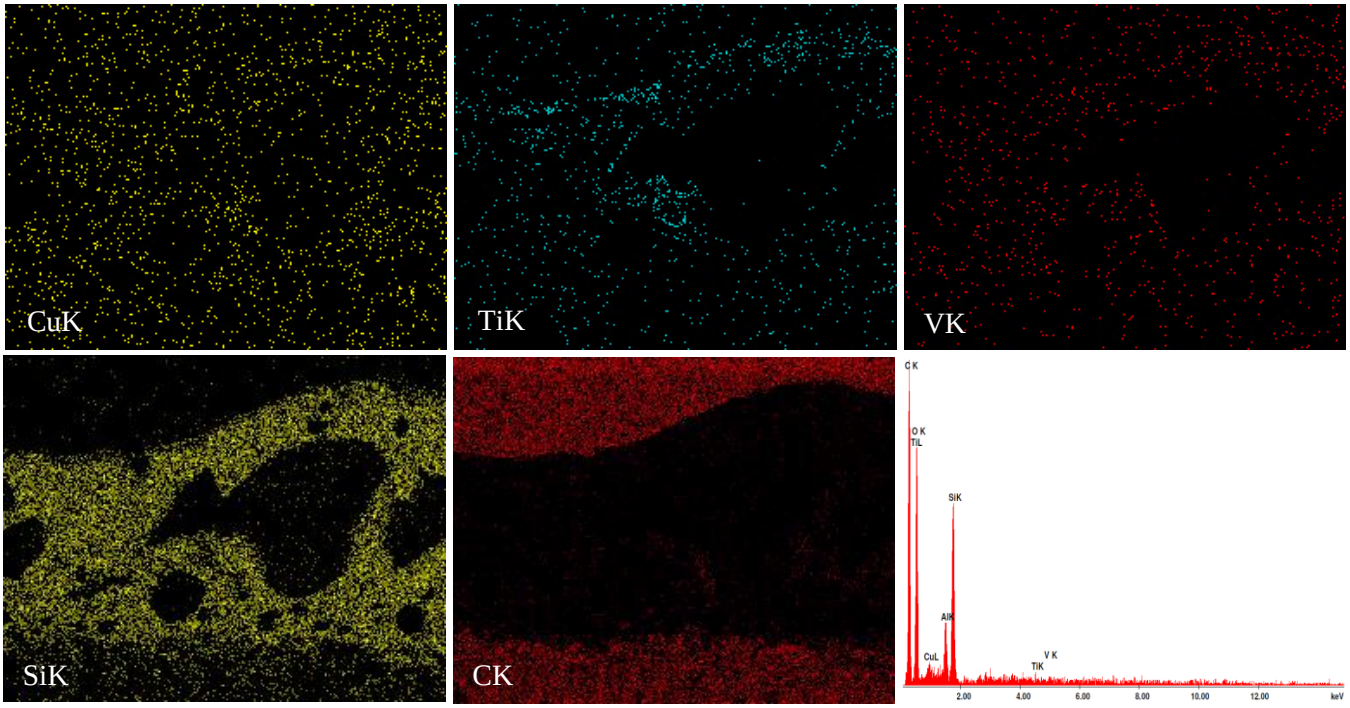

Figure 6.79 X-ray map of an additional cross-section.

Sample 4.2 contained a vertical and horizontal TPS coating and the microstructures are shown in Figure 6.80 a through d. Image a shows the vertical side of the tile with segments of deposit on the surface pointed out with the white arrows. The deposit was not fully adhered to the coating. Further across the sample on image b, a light gray layer was formed and contained small cavities. The rest of the sample circular cavities and hollow pores near the upper surface of the coating (image c). A uniform deposited layer at the surface is shown with spherical cavities (image d). A lateral crack was found on the coating and appeared to originate from the surface of the TPS. The deposited layer found on the vertical side of the sample contained a fragmented and solid texture. Differences in compositions of this deposit were observed and the results are presented in Figure 6.81. EDS area analysis was measured at areas 1 and 2 while point analysis of spot 3 was obtained. The deposit at the outer edges (areas 1 and 2) contained major elements of Al, O, Si, and Ca. Additional minor elements of V and Fe were detected on area 2. These two areas were not deposited uniformly as they appeared to settle in pieces. The area analyzed at point 3

contained a different texture as the deposit had the appearance of granulated particles. This area did not contain any Al except it contained C, O, Ca, Si, Cu, and Fe.

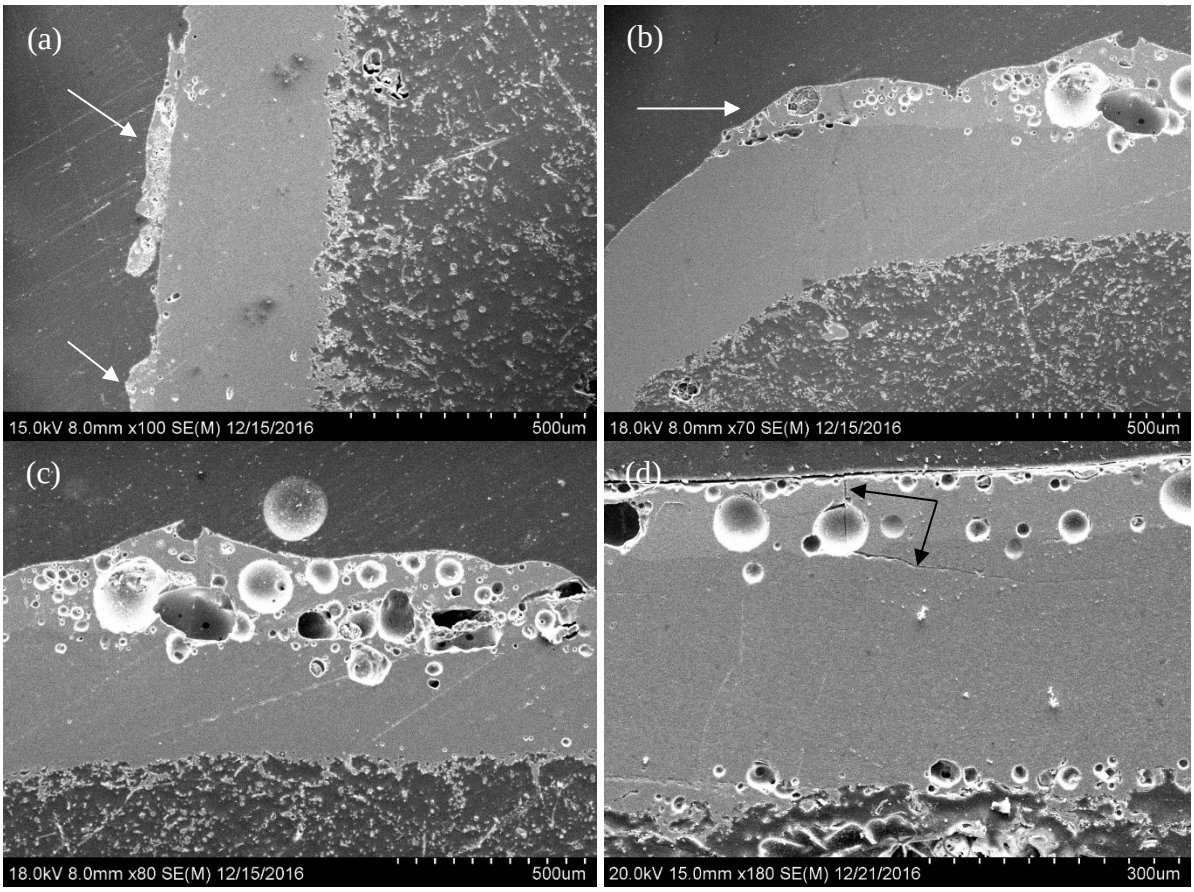

Figure 6.80 Cross-sectional images of sample 4.1 where (a) is taken at the left vertical side of the sample leading to the top surface on (b). Area (c) shows degradation concentrated at the upper surface the coating. Image (d) shows a deposit line with cracking.

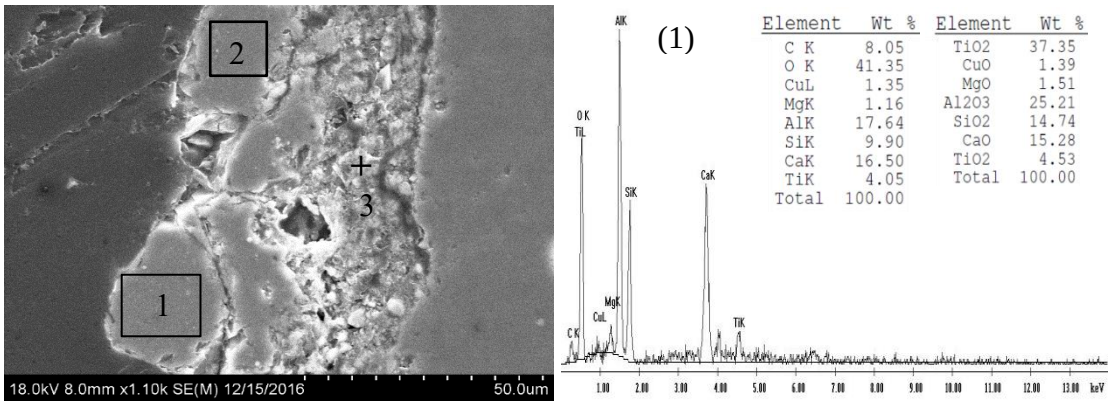

Element	Wt %	Element	Wt %
C K	8.05	TiO2	37.35
O K	41.35	CuO	1.39
CuL	1.35	MgO	1.51
MgK	1.16	Al2O3	25.21
AlK	17.64	SiO2	14.74
SiK	9.90	CaO	15.28
CaK	16.50	TiO2	4.53
TiK	4.05	Total	100.00
Total	100.00		

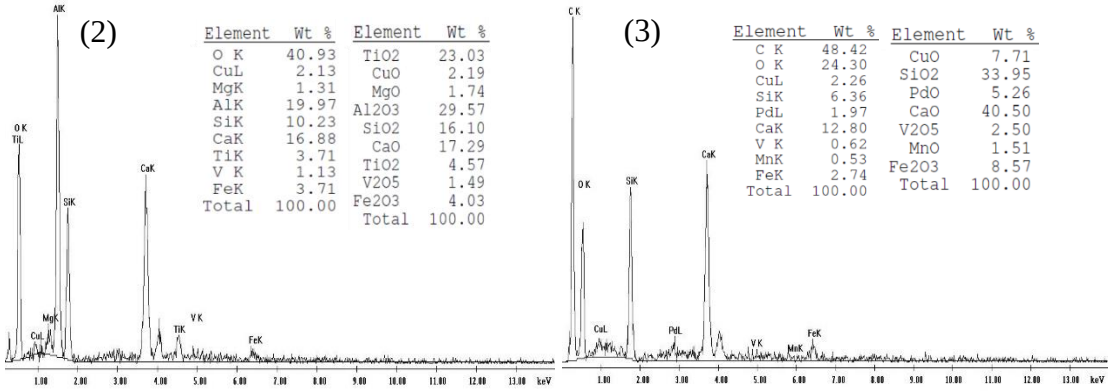

Figure 6.81 EDS area readings (1) and (2) along with spot reading (3) on the edge deposit areas.

The coating at the horizontal area was not found to contain texture changes. The deposit was adhered and contained spherical cavities. The recurring composition of the deposited layer is shown in Figure 6.82. The primary elements were 45.91wt%O, 17.66wt% Si, 17.16wt% Ca, 6.80wt% Ti, and 7.65wt% Al. The deposit contained less weight percentage of Al than the deposited layer found at the vertical side. Other areas of the deposited layer at the vertical end were analyzed through EDS mapping.

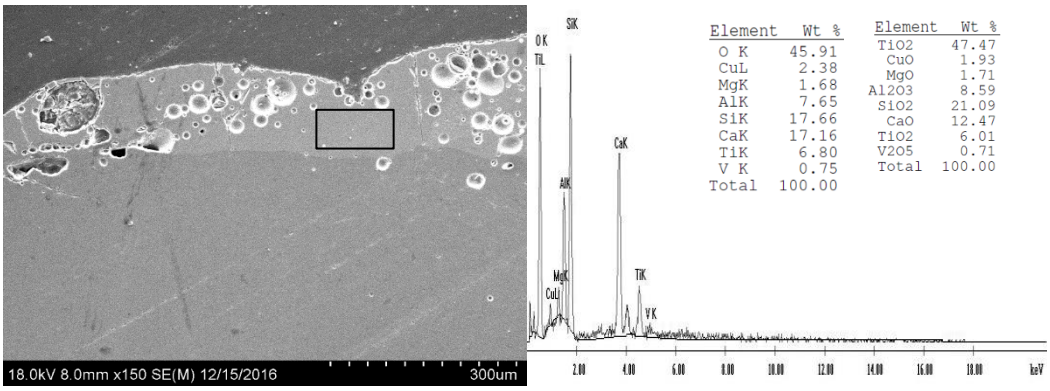

Figure 6.82 Area EDS results of the coating at the horizontal location.

The X-ray maps of a fully-adhered light gray deposit layer at the vertical side are provided in Figure 6.83. The maps show that the layer was a mixture of Al, Ca, O, and Si. Remarkably, the relative concentration of titanium occurs beyond the deposited layer. Titanium was mostly deposited on the coating width. Aluminum also appeared at areas near the silica fibers. This is also true for the maps obtained from the micrograph on Figure 6.84.

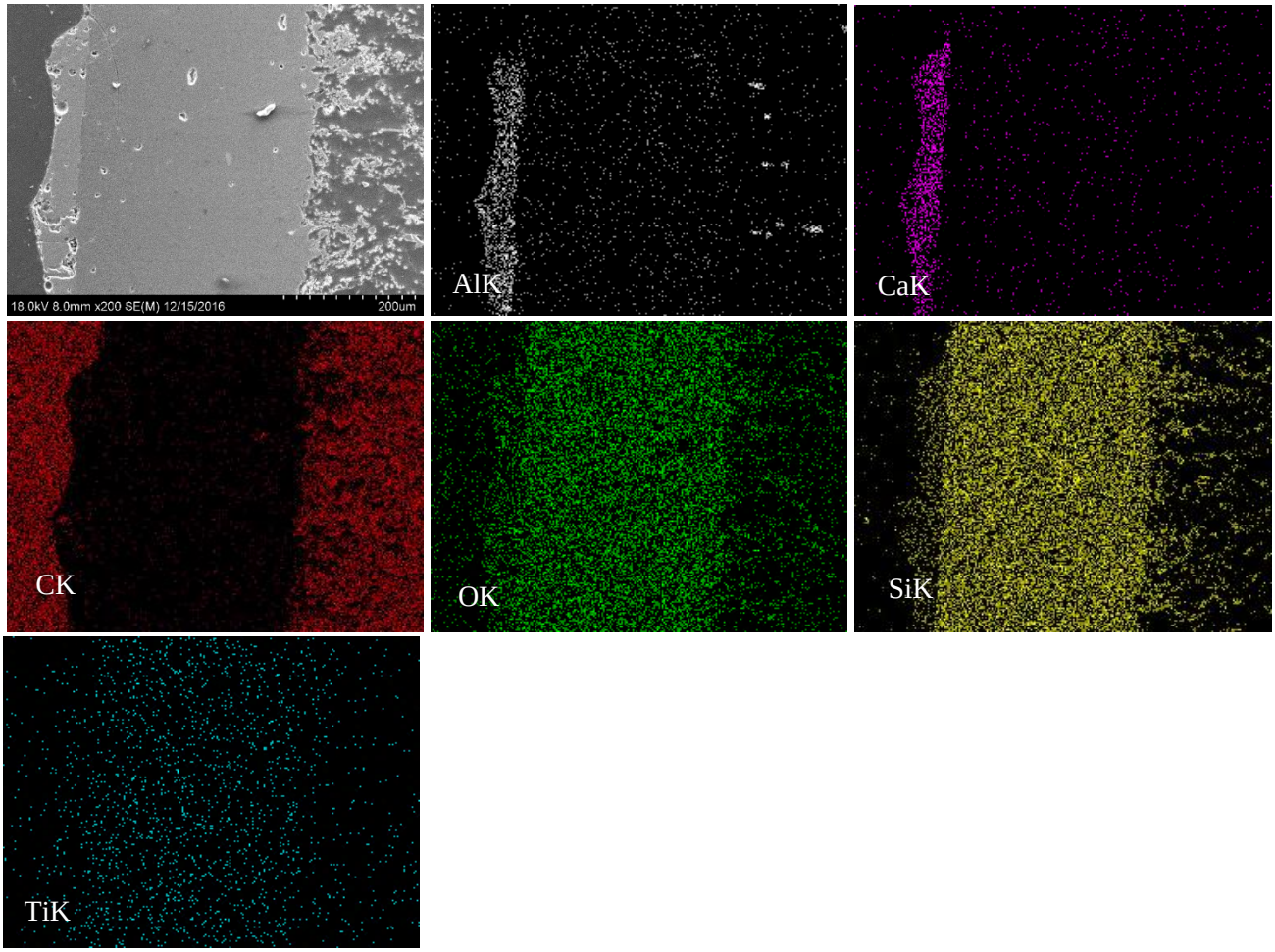

Figure 6.83 X-ray maps of the vertical side of sample 4.1.

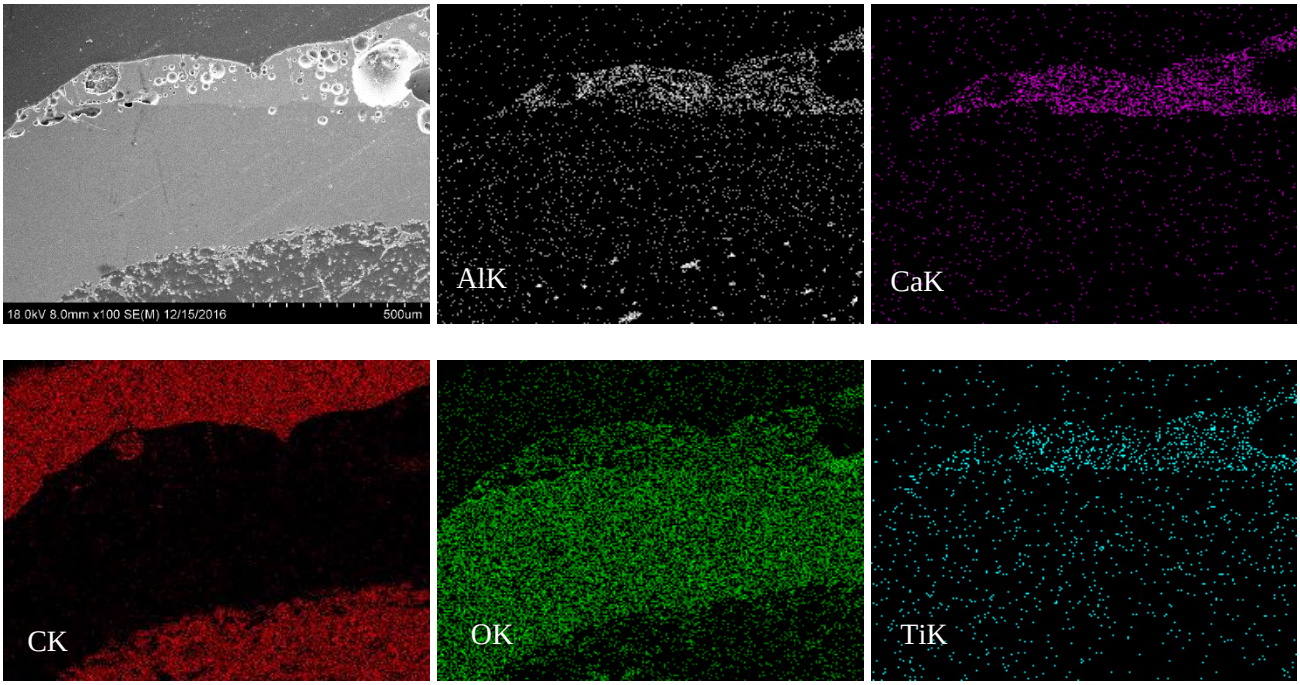

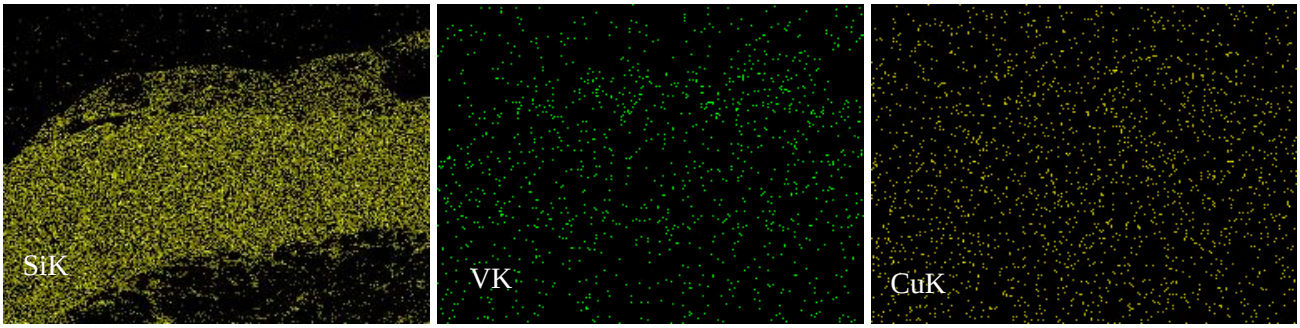

Figure 6.84 Additional X-ray maps of sample 4.1.

The morphology of sample 4.2 is shown on Figure 6.85a through c. The cross-section in image a contained a variety of pores that were concentrated at the top surface of the sample. The deposited layer is evident on image b and its thickness also varied as illustrated by image c. The differences in compositional results are presented in Figure 6.86. Area a contained 55.26wt% O, 26.65wt% Si, and 14wt% C. Whereas area b contained 44.35 wt% O, 13.84 wt% Si, 13.36 wt% Al, 6.47 wt% Ti, 6 wt% Ca, and 5.22 wt% Mg. The distribution of these elements on the sample contained aluminum near the coating-to-tile interface. Figures 6.87 and 6.88 both confirm this as well as the elements that make up the deposited layer. In both cases, the deposited layer consisted of aluminum, calcium, silicon, oxygen, and titanium. The layer also was comprised of magnesium and vanadium as illustrated in Figure 6.88. Also, dispersed iron was present on Figure 6.87 only. The spherical cavities present at the deposited layer (Figure 6.87) contained oxygen and titanium. This was also evident on the second map on Figure 6.88.

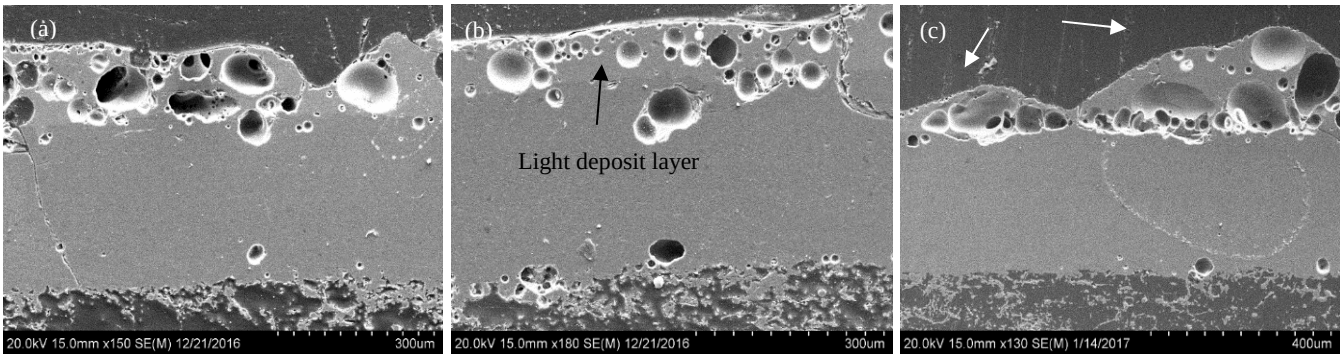

Figure 6.85 Cross-sectional areas a-c of sample 4.2.

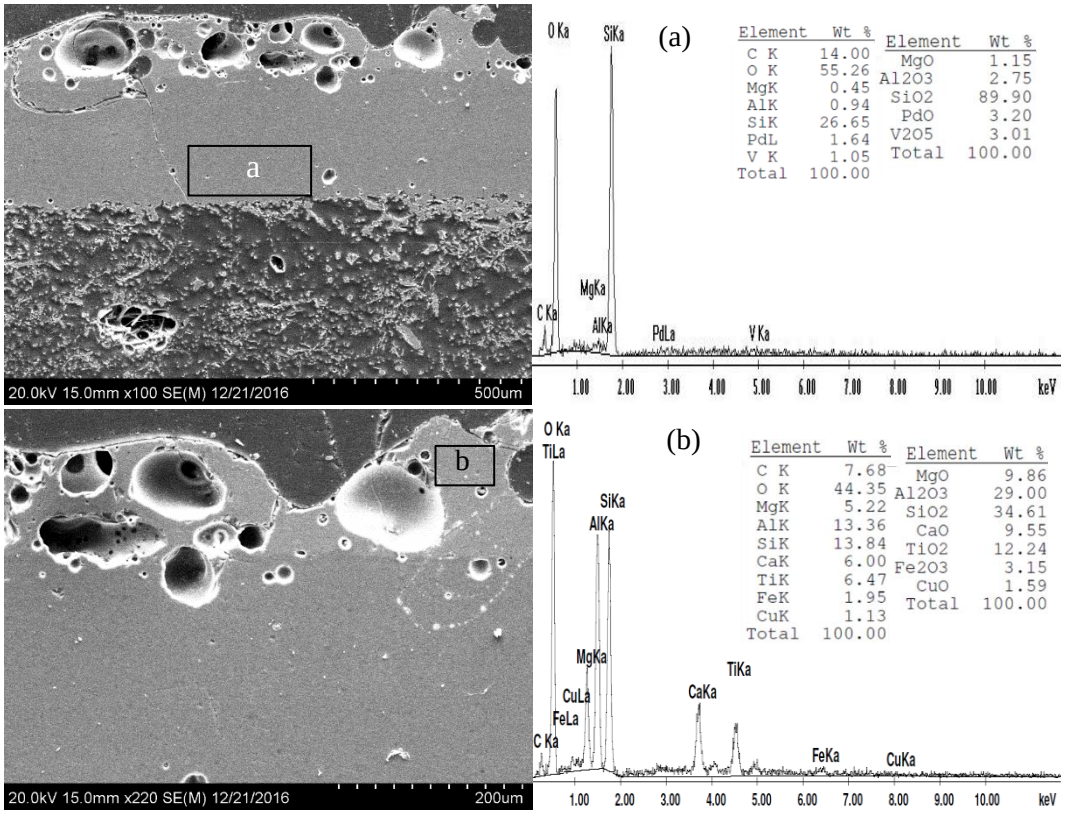

Figure 6.86 Contrasting EDS area measurements (a) and (b).

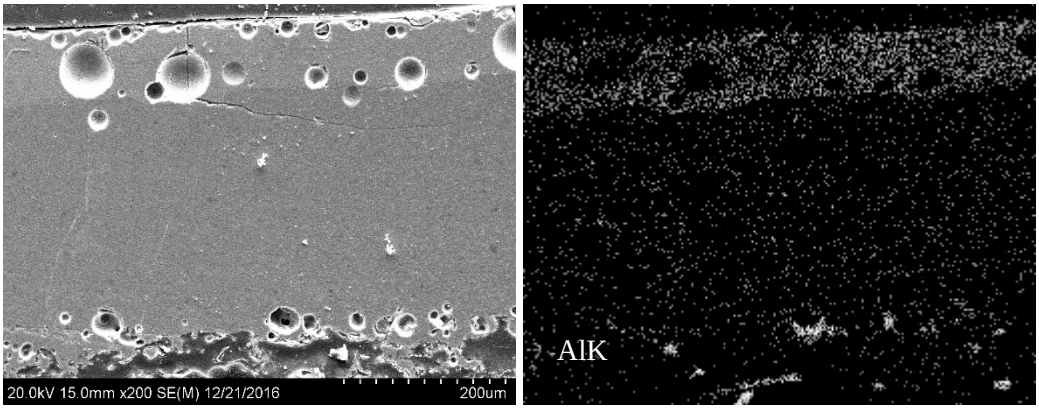

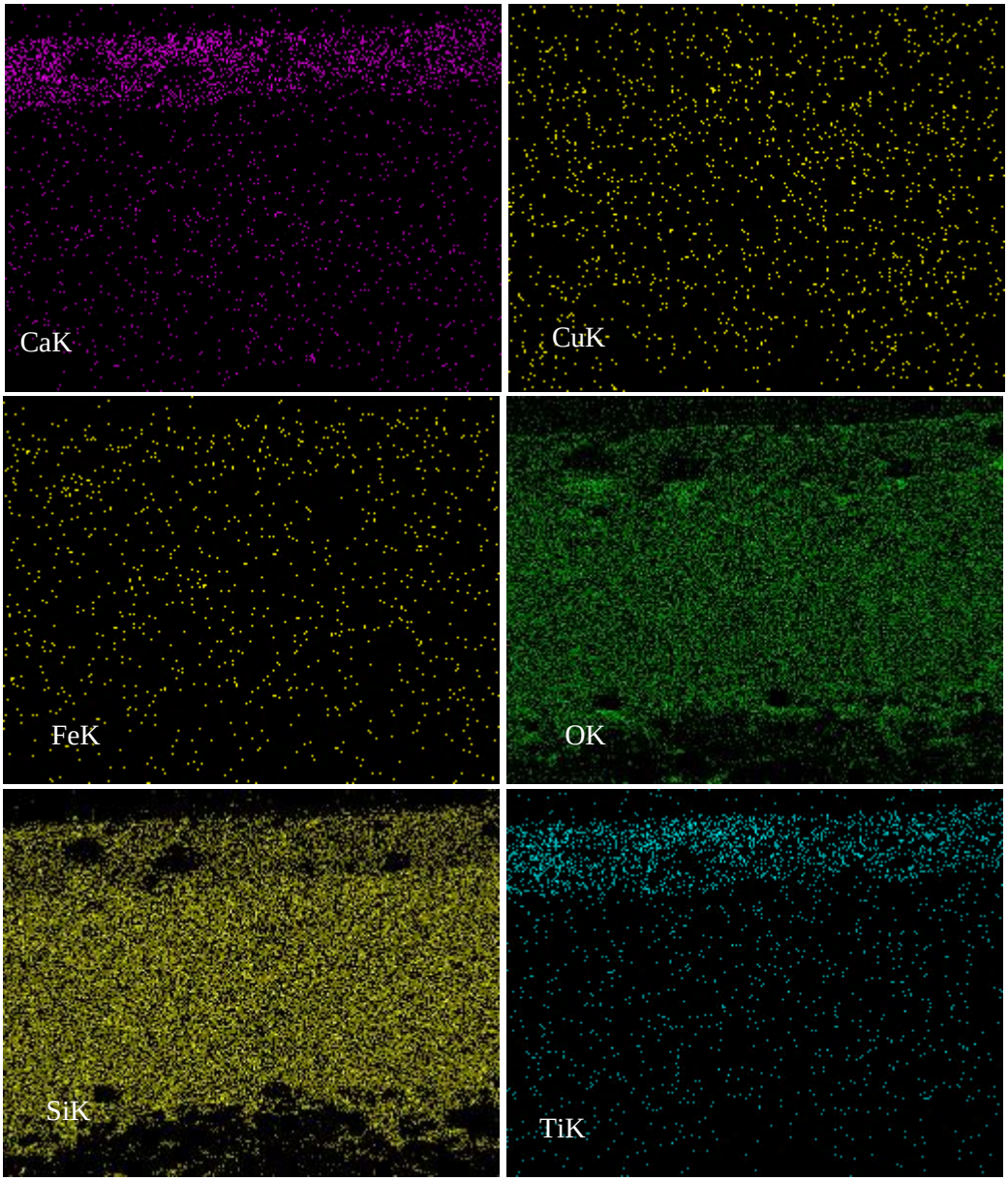

Figure 6.87 Element maps of sample 4.2.

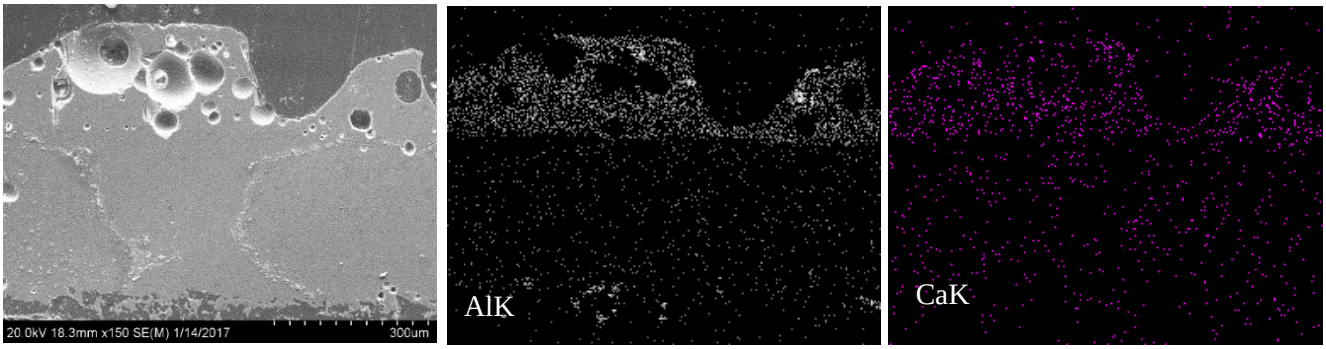

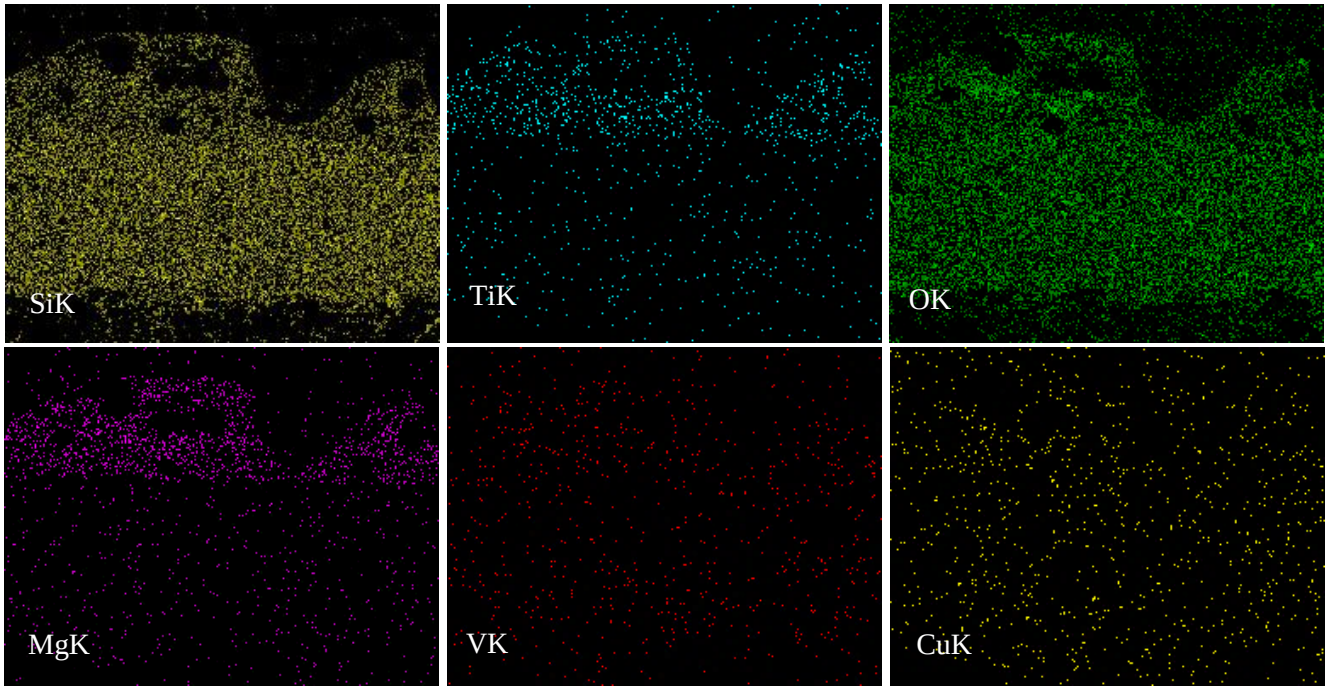

Figure 6.88 Maps obtained showing deposits at the uneven coating.

6.2.4 Thermal Pane Glass Fragment

The glass fragment obtained was section 2 near the forward side of the window and was easily removed from the frame. The glass fragment was mounted in the two-part epoxy mount and ground at the cross-section to reveal the materials that deposited. Not enough powder was obtained for XRD analysis therefore, EDS analysis was performed on the cross-section.

6.2.4.1 Cross-sectional Analysis

After standard sample preparation, the as-received microstructure of the glass sample is provided in Figure 6.89 a through d. The glass cross-section in Figure 6.89a and b demonstrates small areas with cracking at the top surface of the glass. These small fractures were consistently present throughout the sample. Evidence of possible deposits was observed such as Figure 6.89c that contained granulated-like deposits at the surface. More deposits accumulated on the surface at different thicknesses as illustrated by Figure 6.89d. The large deposit contained various hollow pores and spherical cavities similar to the deposits present on the tile specimens.

EDS confirmed that the deposits were a combination of different elements. Several examples are demonstrated in Figure 6.90 in which two areas and a spot analysis were measured. The majority of the deposits contained high weight percentages of aluminum. The first area (Figure 6.90a) was comprised of 51.71 wt% O, 23.42 wt% Al, 9.50 wt% Si, 11.33 wt% Ti, 2.63 wt% Cu and 1.02 wt% Ca. Si and O were the main elements detected when measuring an area below the edge of sample (b). Spot c was verified to contain the primary elements of 48.35 wt% O, 25.82 wt% Al, and 11.34 wt% Ti.

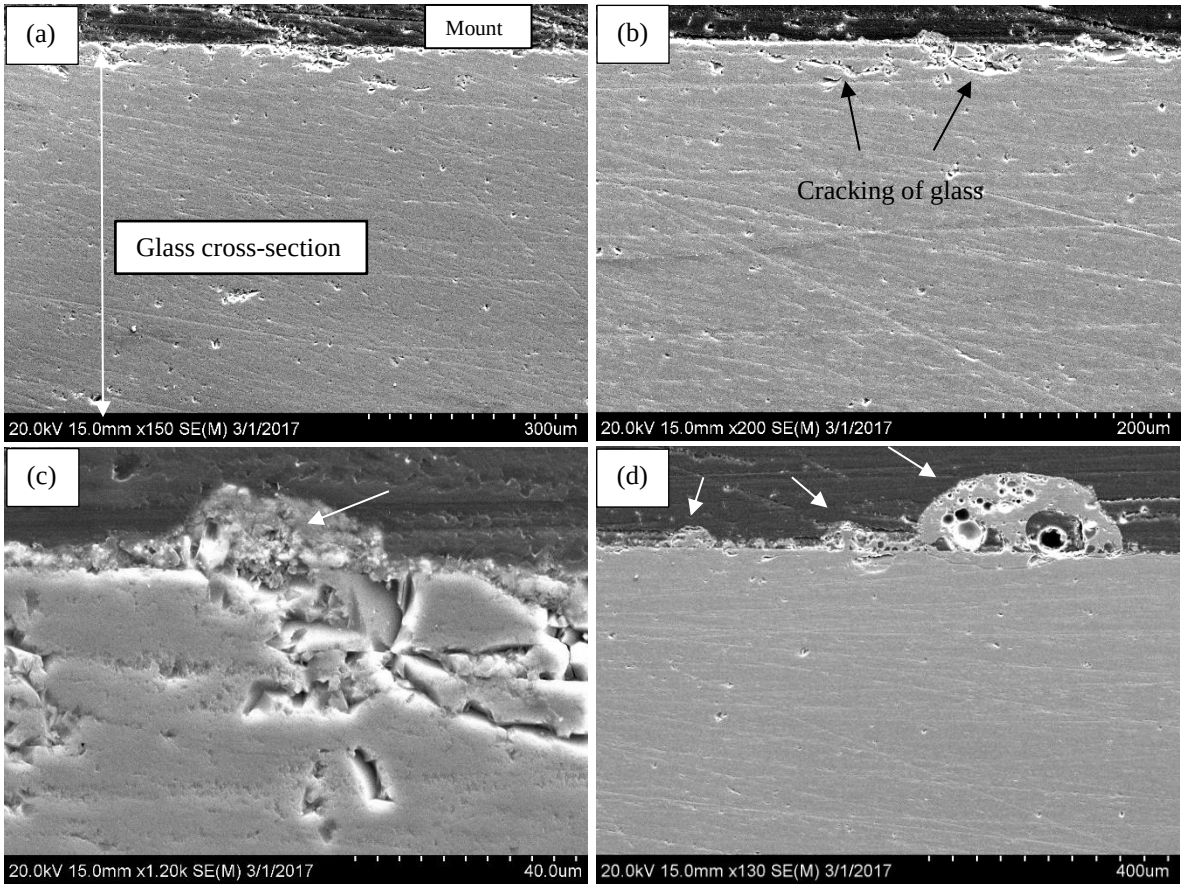

Figure 6.89 Mounted glass shard and polished at the cross-section. SEM images a through d show several features seen at the surface.

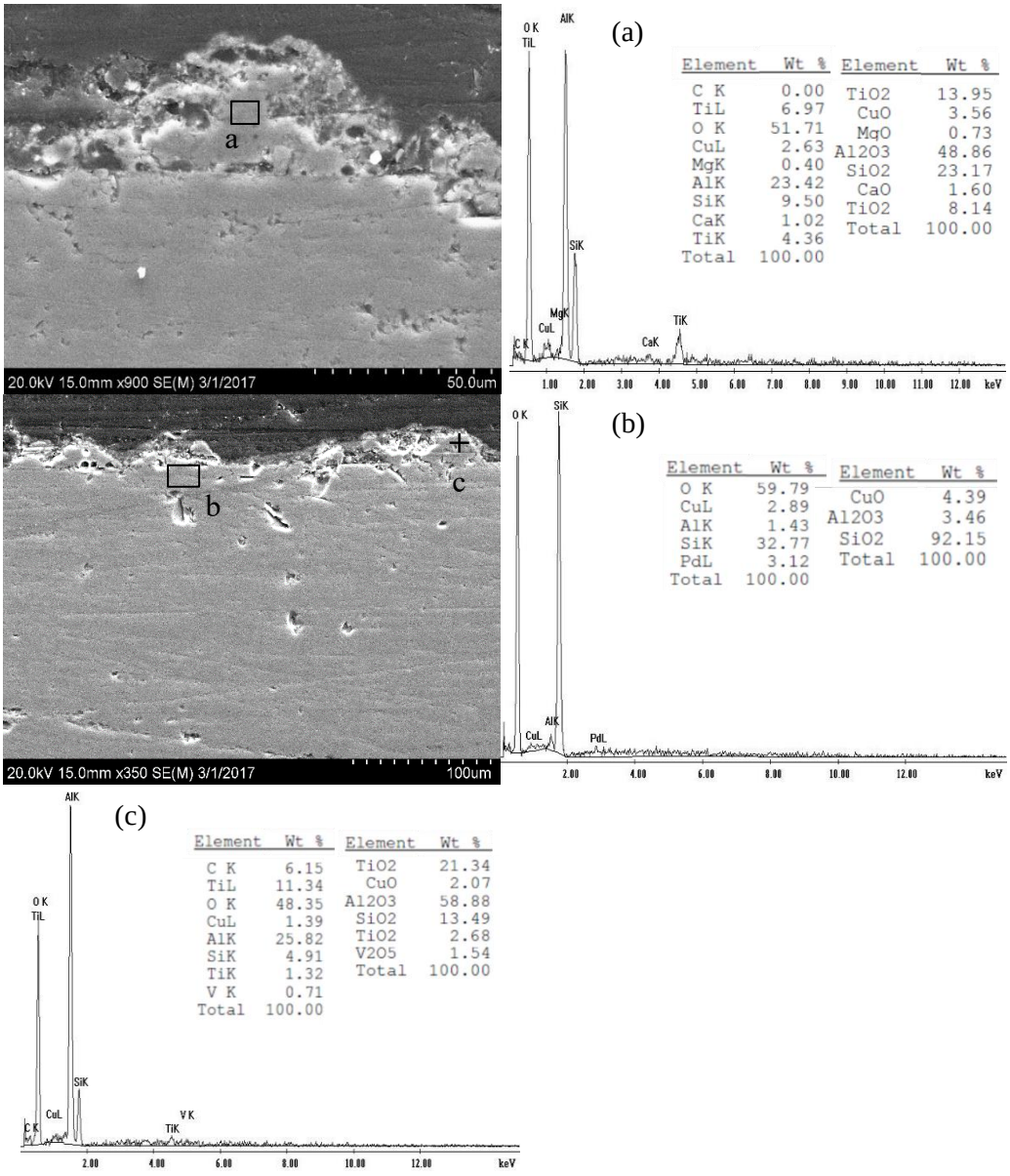

Figure 6.90 EDS area measurements (a), (b), and point (c).

Additional EDS measurements were obtained to distinguish the chemistry of the solid versus the oxide-type morphologies of the deposit. Solid areas a and b in Figure 6.91 show that area b represents the chemistry of the glass with no deposit. The results from point a show that it was rich in aluminum oxide (44.5 wt% O and 29.96 wt% Al). The dark grainy area on c contained 25.03 wt% Al, 21.65 wt% O, and 11.21 wt% Ti. X-ray mapping was used to decipher the distribution of the spot and area EDS readings. Individual maps obtained from the micrograph on Figure 6.92 highlight the irregular deposit layer.

Aluminum, oxygen, silicon, titanium, and some carbon construct the layer. A larger weight percentage of aluminum was applied to the surface of the glass as the brightness of the element map is directly related to the weight percent of the element present. Oxygen was also present in a high weight percentage. The relative amount of titanium was low however, it appeared to collect directly on the surface along with aluminum and oxygen. Vanadium was also randomly dispersed through the cross-section.

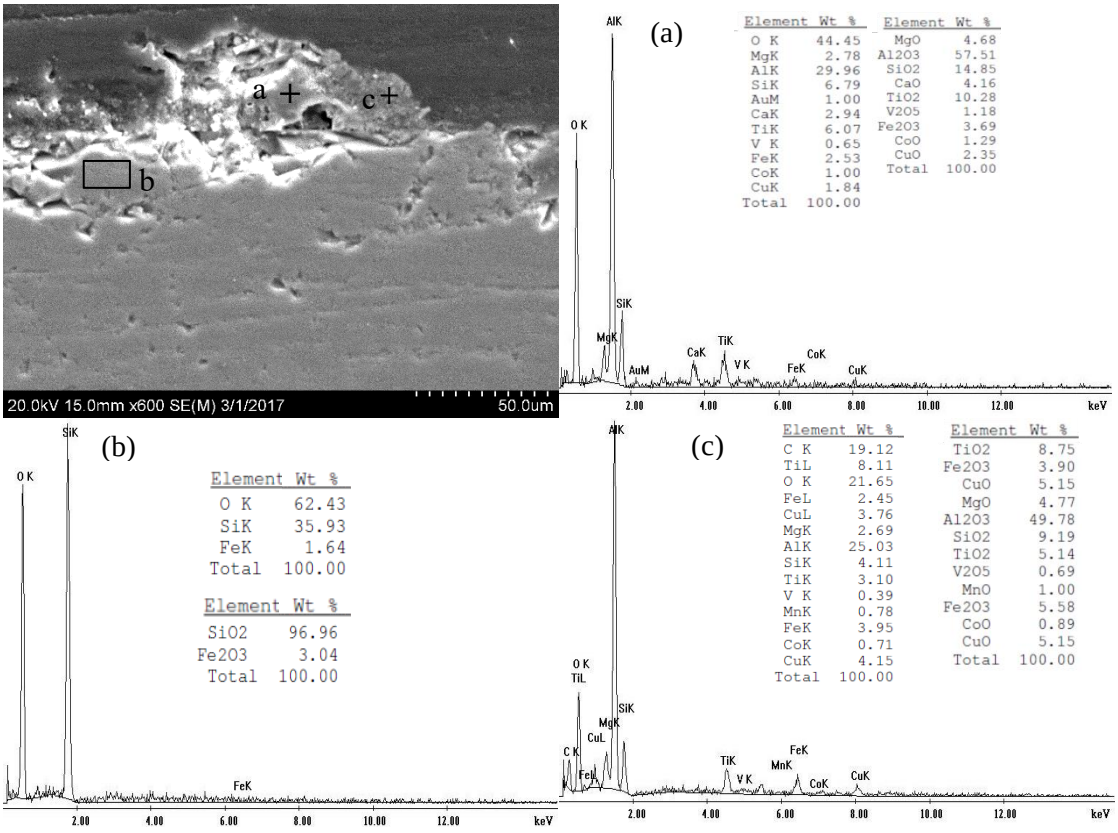

Figure 6.91 SEM micrograph with EDS of (a) deposit, (b) bulk material, and (c) an additional deposit.

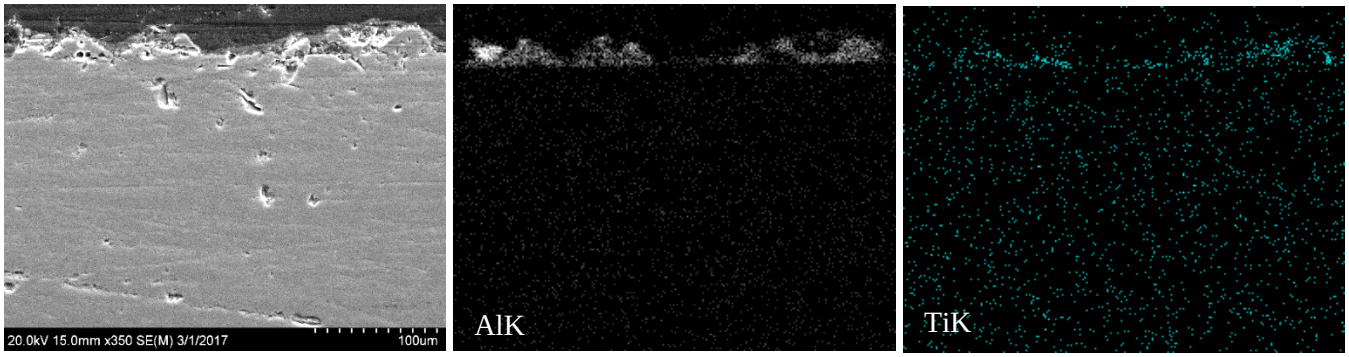

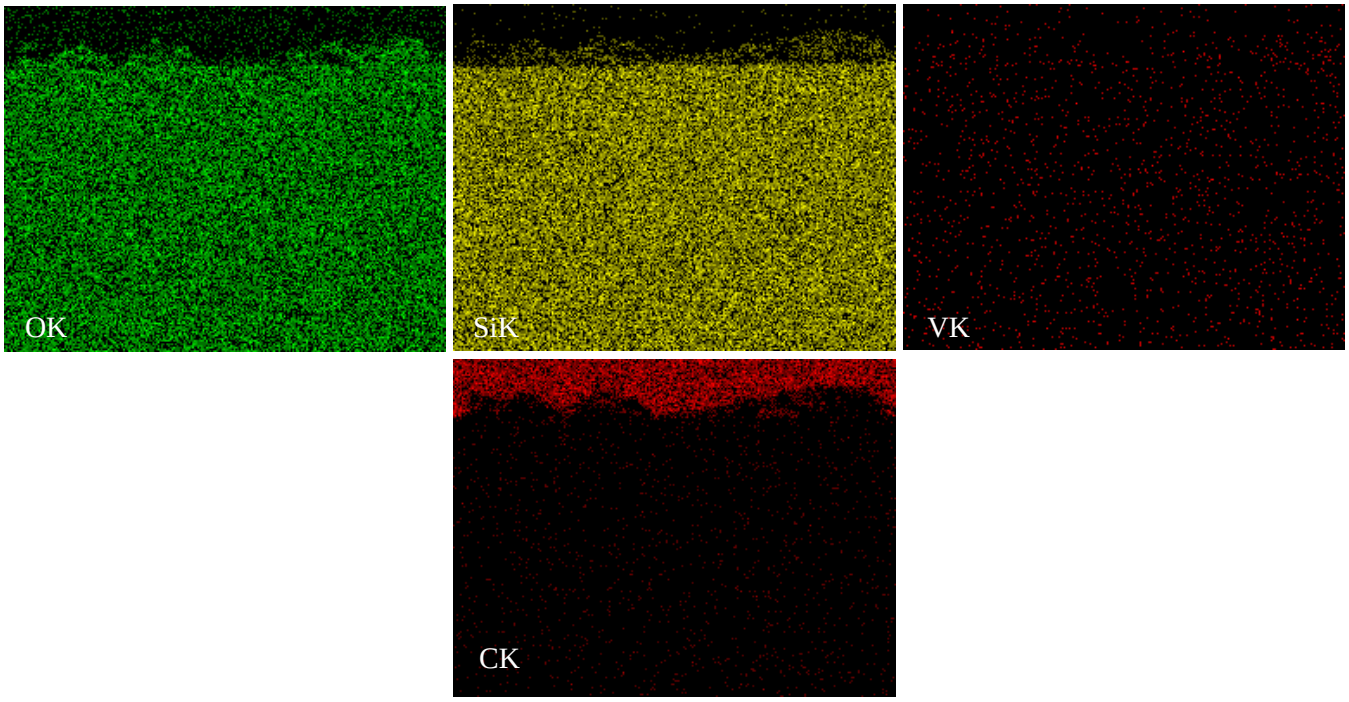

Figure 6.92 X-ray map of the micrograph shown.

The largest compacted deposit remnant was mapped to characterize the elements present. The elements collected at the surface of the glass were comprised of aluminum, calcium, iron, oxygen, titanium, silicon, and vanadium (Figure 6.93). No clear distinction between different phases in the deposit were present. The deposit in this area contained iron whereas the previous thin deposit (Figure 6.92) did not have any iron present. The spherical cavities on the deposit contained calcium, titanium, and vanadium. The carbon map shows that it was concentrated in the dark areas near the upper surface. Additional deposit residues were also analyzed through X-ray mapping and shown in Figure 6.94. Both areas consisted of a light gray phase surrounded by a darker phase. Figure 6.94a marks the elements present at the locations shown. Most of the light gray phase was a mixture of Al, Ca, O, Si, Ti, and V. Whereas the darker surrounding phase was comprised of Al, O, and C. Some areas of the deposit were not tightly adhered to the glass substrate and small darker areas with high carbon were present. Smaller particles of predominately Ti or Al were applied near the top surface. A smaller deposit was shown to be a mixture of Al, O, and Si. Figure 6.94b also contained a similar deposit with the darker phases consisting

of Al, O, C, and the addition of Si. The more solid deposit contained similar chemistry of the previous deposit except without vanadium. Several light gray spherical particles were rich in Ti as pointed out by the two black arrows. An aluminum particle was observed at the higher point of the deposit. The dark areas where the deposit is not fully attached consisted of carbon. The deposits on the glass contained Al and Si particles that were able to be distinguished in a matrix of Al, O, Si, and Ti.

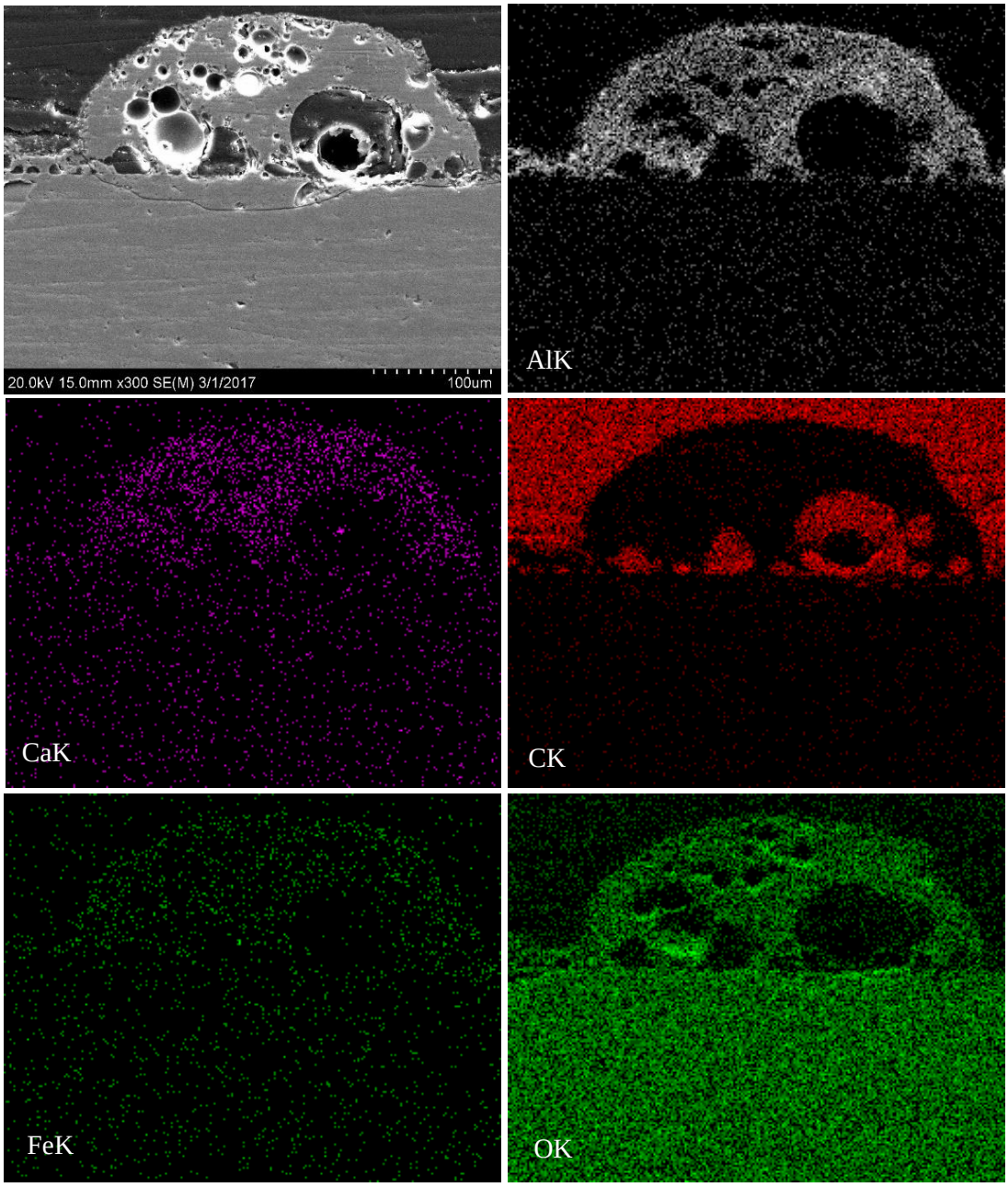

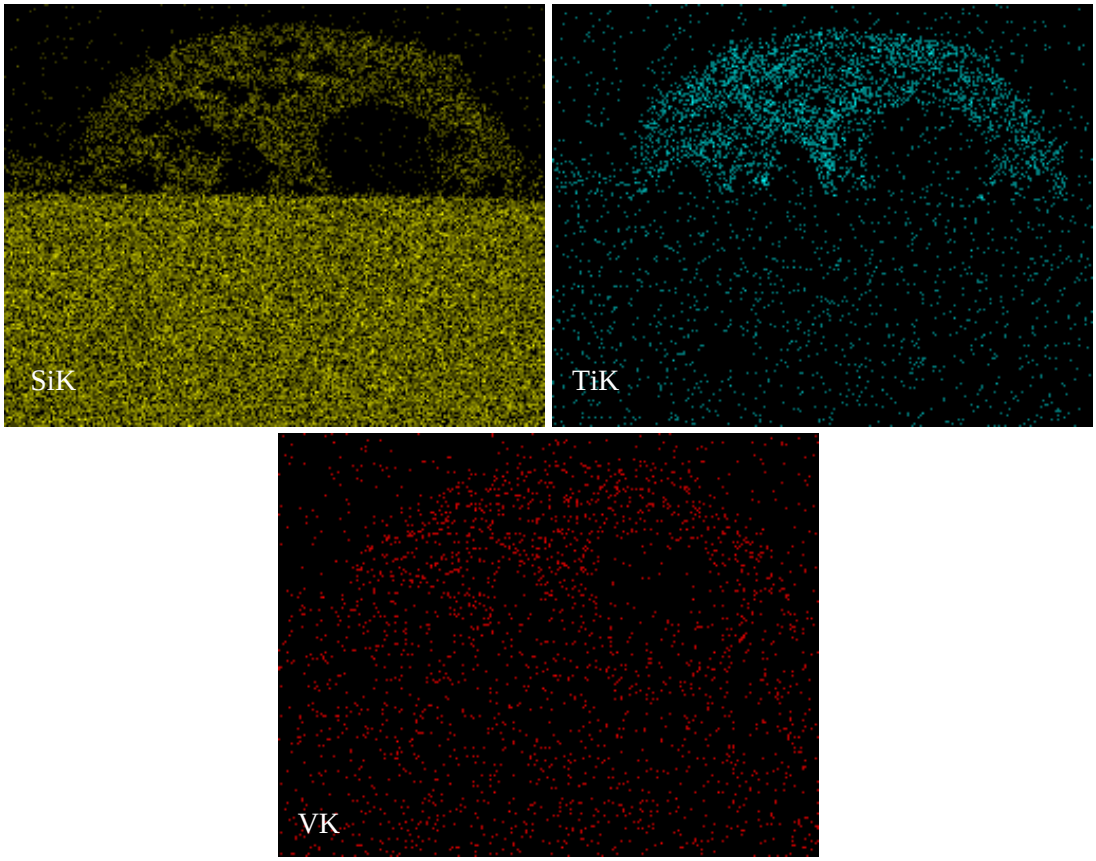

Figure 6.93 X-ray maps of the large deposit.

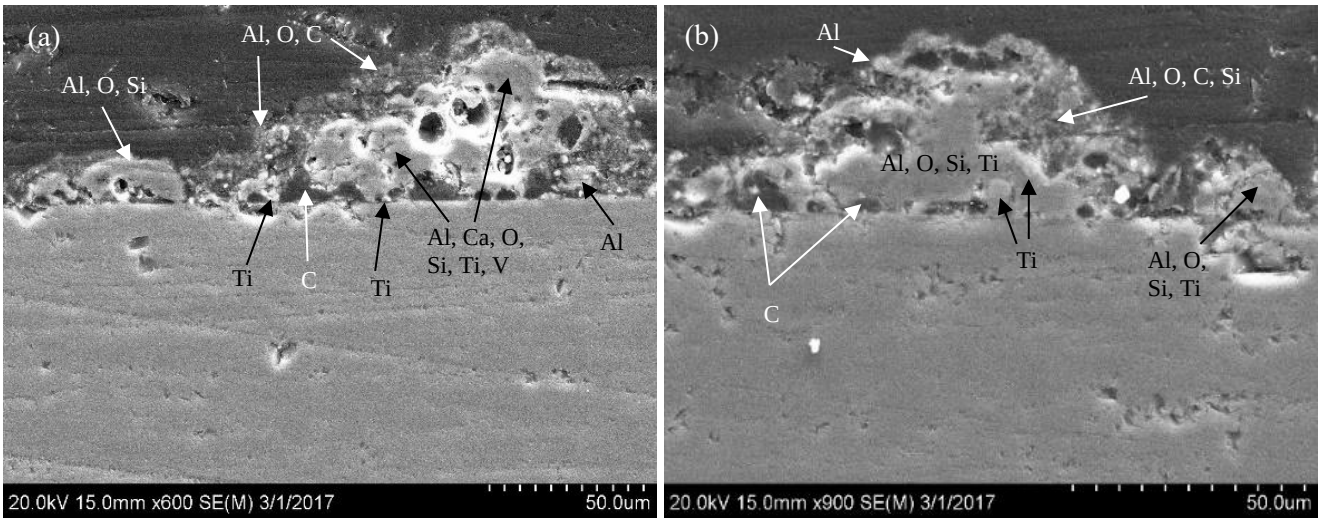

Figure 6.94 Two micrographs (a) and (b) illustrating the elements of the deposit.

6.3 X-Ray Diffraction

The next characterization method used to identify and confirm the chemical composition of the deposits was X-ray diffraction. All tile samples were used for the analysis and were measured at the surface using the aforementioned test parameters. XRD was also a non-destructive procedure which did not require additional sectioning and can be conducted under ambient conditions. The only requirement was that the surface to be analyzed must be a flat surface and the material must be crystalline. Therefore, several sectioned tile samples such as the curved areas on the inner lip side of the samples were not analyzed. The measurement consists of a spot analysis at any location desired and the depth resolution depends on the material and the X-ray incidence angle. Several measurements were conducted on one sample therefore, only a few XRD results will be discussed. Several samples sectioned from sample 1, sample 2, sample 3, and sample 4 contained identical XRD results hence, only the differences will be presented.

6.3.1 Forward Port Carrier Panel Tile

The tile samples obtained from the forward port side carrier panel consisted of four samples (1.1A, 1.1B, 1.2, and 1.3) where each sample was analyzed by XRD. Samples 1.1A and 1.2 contained similar XRD results as both surfaces contained similar characteristics. Sample 1.1B did not contain any flat surfaces for an accurate reading. Figure 6.95a represents the spectra obtained with phase identification including the location of where the measurement was conducted. The composition of these two samples was consistent with TiO_2 and Al. The EDS analysis of these two samples showed predominately aluminum and titanium oxide peaks which show the accuracy of XRD. XRD confirmed that the type of oxide present was the rutile form of TiO_2. This compound was frequently detected in most samples analyzed. However, the minor and trace elements of Si, Ca, Cu, or Fe was not detected. Most of the minor elements were present beneath the TPS surface. The next sample analyzed contained additional distinct phases present when the spot reading was placed at the colored deposit shown on Figure 6.95b. Besides TiO_2 and Al, Si

and $AlTi_2$ (aluminum-titanate) were detected. This sample contained visible metallic streaks and EDS experiments show that it contained mostly 25.67 wt% Al and 32.43 wt% O. The surrounding areas of the metallic deposit were high in titanium oxide. The formation of an aluminum-titanium compound may be a result of these mixtures especially since both elements were found at the cross-sections of the sample. These results demonstrate the changes in compounds on different locations of the tile surfaces.

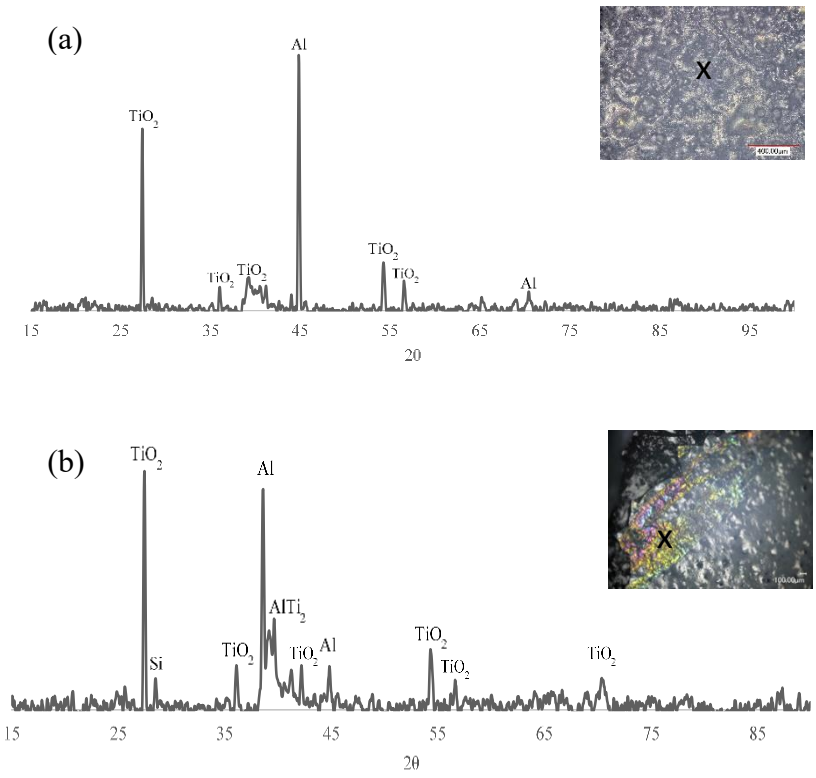

Figure 6.95 XRD spectra (a) representing similar samples 1.1A and 1.2 measured at the location shown. Spectra (b) was measured at sample 1.3 in the spot shown.

6.3.2 Forward Starboard Carrier Panel Tile

The following samples obtained from the forward starboard side comprised of five samples; 2.1.1A, 2.1.1B, 2.1.2, 2.1.3, and 2.1.4. The entire sample contained visible discolorations that diminished towards the inner side of the tiles. When analyzing all samples through XRD, several noticeable changes were observed. Sample 2.1.1A contained the majority of yellow discolorations with EDS measuring 56.95 wt% O, 15.20 wt% Si, 13.68 wt% Ca, and 4.18 wt% Ti. The corresponding XRD results on Figure 6.96a

show silicon oxide in cristobalite form (SiO_2), titanium oxide in rutile form (TiO_2), aluminum oxide (Al_2O_3), and silicon carbide (SiC). Subsequently, the yellow discoloration was only concentrated on the outer areas of the TPS coating and the discoloration diminishes. Samples 2.1.3 and 2.1.4 possessed similar surface characteristics of dim discolorations. The compositions found on these samples and the location of where the reading was measured is shown on Figure 6.96b. The compounds include SiO_2, Al_2O_3, TiO_2, $CaTiO_3$ (perovskite form), and SiC. This spectrum directly upholds the results obtained from EDS with similar elements detected. Next, the sample at the inner side of the tile was evaluated as the sample was long enough to provide a flat and stable surface. Originally through EDS, the sample contained titanium oxide, aluminum, silicon, and calcium major peaks. The compounds present on Figure 6.96c on the corresponding image consisted of TiO_2, Ti (hexagonal), and Al peaks. The results show that the XRD measurements varied when the surface condition was changed. All XRD measurements confirmed the type of the deposits on the tile surfaces consisted of titanium oxide, silicon oxide, aluminum oxide, silicon carbide, elemental Ti, Al, and calcium titanate.

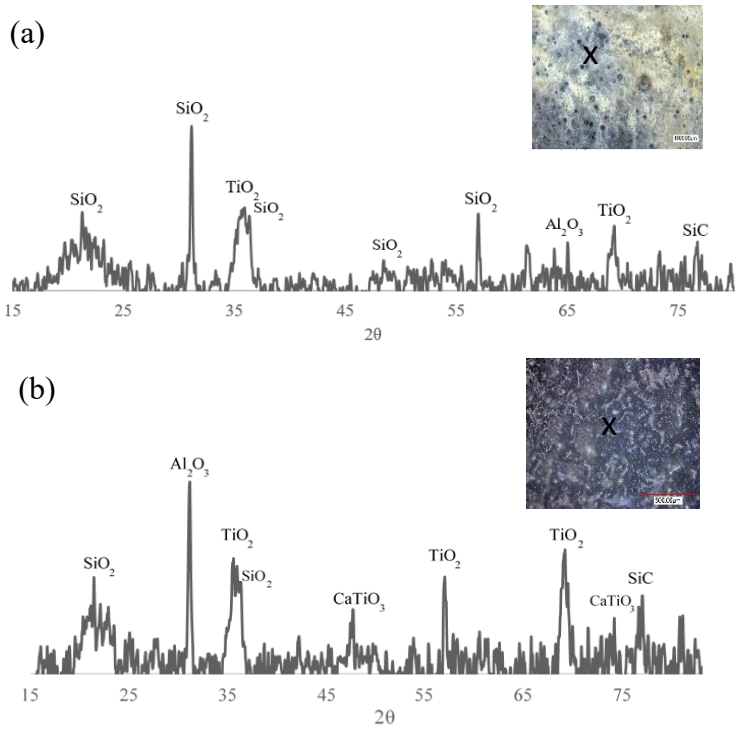

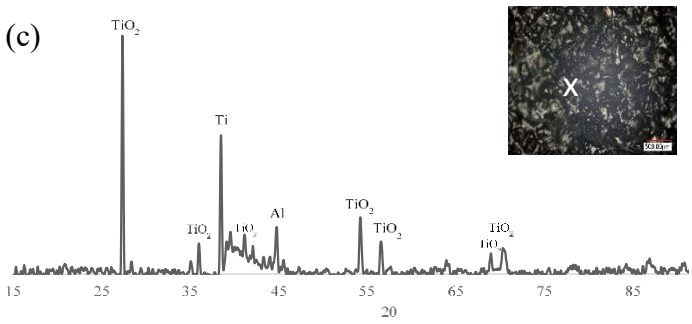

Figure 6.96 XRD spectras of (a) yellow discolorations from sample 2.1.1A, (b) represents the rest of the samples with minimal discolorations, (c) was the inner tile sample 2.2.1.

6.3.3 Aft Tile

Two samples were collected from the aft tile and the visual inspection showed that they contained similar discolorations and higher degradation of the coating. Samples 3.1A and 3.1B contained coinciding XRD results and the spectra for sample 3.1A was interpreted due to the surface conditions. The spectrum is given on Figure 6.97a where SiO_2, TiO_2, and intermetallic $AlTi_3$ were existent on the point shown. EDS at this location also detected 58.82wt% O, 17.91wt% Ti, 10.68wt% Si, and 6.71wt% Al. These results are plausible as the XRD determined these deposits to be oxides and mixtures of other elements (such as $AlTi_3$). The following sample did not have any visible bright discolorations but a few dark blue areas as provided by Figure 6.97b. It is evident that this area contained more diverse compounds. The type of phases present is different from this area. The oxides present in this area were $Al_6Si_2O_{13}$ (mullite) and $CaTiO_3$. Titanium and carbon were also detected as well as an aluminum silicon titanium compound $AlSi_3Ti_2$. These results coincide with the EDS results found at the surfaces which involved 34.92wt% Al, 46.65wt% O, 9.89wt% Si, 2.62wt%Ca, and 3.03wt%Ti. Additional EDS measurements show that the surfaces of sample 3.2 were rich in aluminum and titanium oxide. The final sample obtained from a different location from the aft tile contained dark areas with light deposits under SEM observation. When analyzed with EDS, samples 4.1 and 4.2 held the same elemental compositions. The majority of the surface was high in titanium oxide, silicon, aluminum, and calcium. The spot evaluated for XRD is shown on Figure 6.97c along with its spectrum. The spectrum shows no aluminum oxides but titanium, silicon, and

a calcium iron titanium oxide. An aluminum titanium intermetallic was also present. When XRD is used in conjunction with EDS, results are able to support the oxides and compounds present on the tile surfaces.

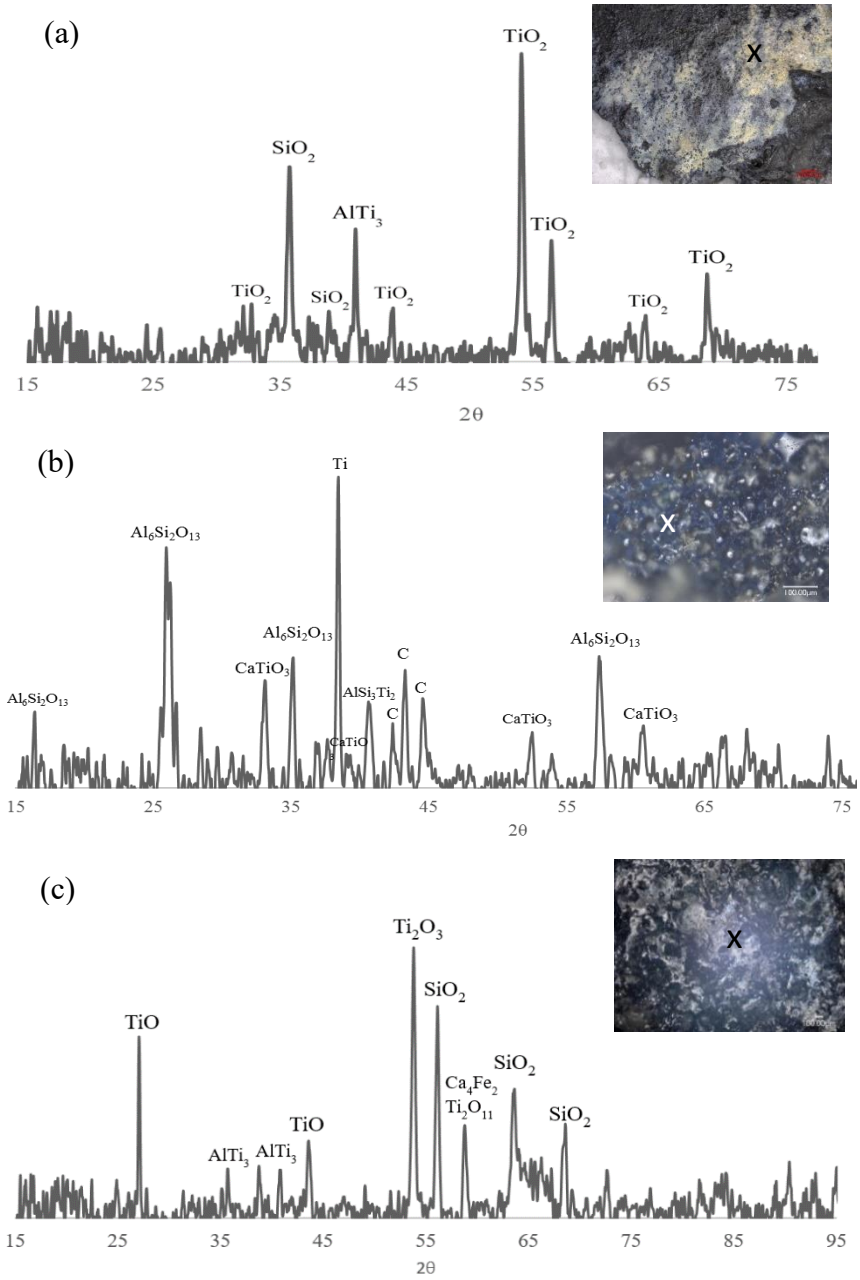

Figure 6.97 XRD spectra of sample 3 (a and b), and sample 4 (c).

6.4 X-Ray Photoelectron Spectroscopy (XPS)

Supplementary samples were sectioned from the forward port side sample 1 for XPS analysis. One sample with minimal surface discolorations is discussed in this section. The spectrum obtained from the sample is shown in Figure 6.98 where intensity versus binding energy is plotted. The elemental identities of this sample confirm that the TPS samples contained similar elements present when compared to EDS and XRD results.

The binding energies found in the sample at the surface by XPS spectroscopy results are related to the electronic orbital structure of titanium (Ti^{+4}), oxygen (O^{-2}), calcium (Ca^{+2}), carbon (C^{+4}) and silicon (Si^{+4}). The binding energies at 555.2 eV, 52.1 and 25.8 eV may be ascribed to titanium (Ti^{22}) 2s-orbital, 3s-orbital, and 3p-orbital, respectively. The binding energy (BE) of 532.1 eV signal is ascribed to oxygen (O^{8}) 1s-orbital. The binding energy at 348.1 eV is related to calcium (Ca^{20}) 2p-orbital. The carbon 1s-orbital signal was found at 285 eV. The binding energy signals at 103.1 eV and 154.2ev are ascribed to silicon (Si^{+4}) 2p-orbital and 2s-orbital, respectively. It is worth mentioning that signal at 25 eV is linked to Ti (3p-orbital)-O (2s-orbital) and signal at 51 eV is linked to O_2/Ti (3s-orbital)/Mo (2p-orbital) as suggested by Corneille et al. [43]. The results obtained are comparable to EDS results from the forward port sample.

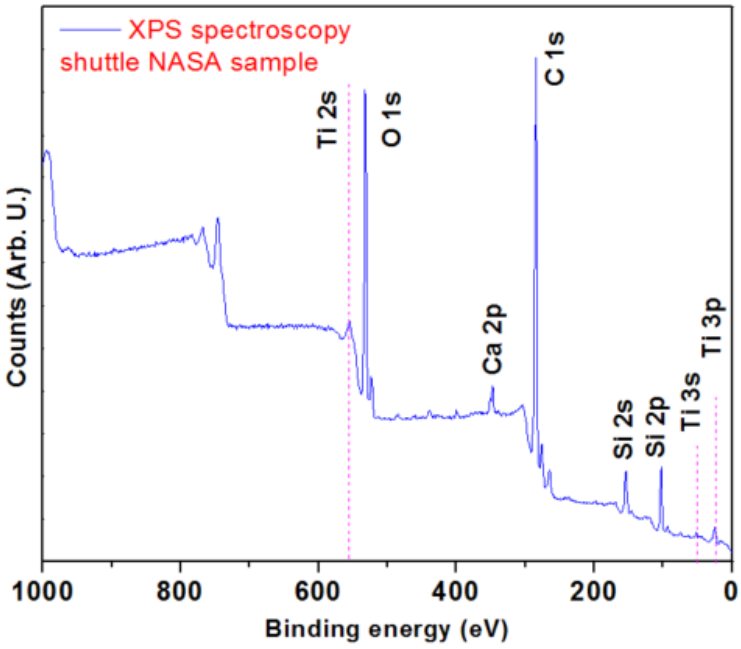

Figure 6.98 XPS spectra of the additional forward port side sample.

6.5 Summary

The beginning of this chapter described the secondary sectioning results as larger samples could not conform to equipment size requirements. Sample 1 was obtained from the forward port side carrier panel and sectioned into smaller samples of sample 1.1, 1.2, and 1.3. The samples from 1.1 in turn, were sectioned again to obtain sample 1.1A, 1.1B, 1.2 and 1.3. The samples obtained from the forward starboard tile were originally obtained from sample 2. The resultant samples from secondary sectioning were 2.1.1A, 2.1.1B, 2.1.2, 2.1.3, 2.1.4, and 2.2.1. Samples from the aft tile were obtained at different locations. Sample 3 consisted of 3.1A and 3.1B from secondary sectioning. Samples 4.1 and 4.2 were also sectioned. Each sample was further analyzed.

The characterization results were divided into three main sections of the forward port side carrier panel results, forward starboard tile results, and the aft tile results. Surface analysis was first presented using SEM and EDS spot and area readings of the surface. The forward port side tile specimens from sample 1 were all examined. All specimens contained several anomalous features that were thoroughly discussed and analyzed through EDS. Afterwards, cross-sectional analysis was performed where the

morphology of the tiles was reviewed. Area and point EDS measurements were obtained to find traces of other materials within the TPS samples. It was determined that the elements present on the surface were also present at the cross-sections. Several elements detected through EDS were constant throughout all samples. X-ray mapping was obtained to distinguish the elemental distribution of the detected elements. This helped determine how the materials were deposited. In the same way, the forward starboard tile samples (secondary sections from sample 2) were studied at the surface and cross-section. The surface morphologies were similar to those of the previous carrier panel tiles. However, some differences in compositions were observed. The cross-sectional analysis determined degradation present and a distinct deposit layer was present. Elemental maps were used to characterize the locations of the phases present. Finally, the samples obtained from the aft tile (sample 3 and sample 4) were also examined for unique surface features and surface chemistry. The aft tile samples confirmed the existence of a deposit beneath the TPS surface. Both samples contained identical compositions of the surface. The cross-sectional analysis reveals alternating phase morphologies such as sample 3.1A. The deposited layer in this sample contained a dendritic-like structure rich in titanium surrounded by a darker phase with a mixture of several elements.

The next sample examined was the thermal pane glass fragment (section 2) that was located near the forward port carrier panel. The detached glass was mounted and prepared identically to the tile samples. Surface EDS was not performed as removed particles from one area were removed for the preliminary analysis. These results are discussed in Chapter 5. The glass sample was viewed under SEM to identify any deposits present at the surface. It was verified that thin, grainy, and solid deposits were present. Their chemistry also relates to the deposits found in the TPS samples. Elemental maps were produced of several areas which confirmed the chemistry of the accumulated deposits.

The next section described the XRD results of all tile sample surfaces for identifying the compositions of the deposits. This surface analysis technique detected several intermetallic compounds,

oxides, and elements present in all samples. The first spectra obtained were from the forward port samples where changes of the phases were discovered. The forward starboard tile that consisted of the top surface of the tile and the inner lip side of the tile. These samples also contained differences in the composition present. The alternating surface deposits on sample 2 showed different surface chemistry. The aft tile samples 3 and 4 also contained various oxides and intermetallic samples. This was particularly due to the visible surface conditions. The XRD results also confirmed the surface EDS results and proved to be an accurate way of determining the compounds present. In addition to XRD and EDS, the surface chemistry of several samples in their as-received state was achieved by XPS. The surface sensitive technique measured Ti, O, Si, Ca, and C. This method was essential as XPS electrons originate from the first few monolayers of a material.

Chapter 7: Conclusion

7.1 Material Degradation and Thermal Consequences

The first part of this investigation attempted to examine the material degradation and thermal consequences of the materials analyzed of the starboard obiter Window 7. Although the history of each carrier panel tile or windshield Window 7 is unknown, it is impossible to determine their original state or if the tiles were replaced. However, several conclusions may be drawn. A non-destructive analysis of visual inspection, photographic documentation, 3D modeling, and surface elemental analysis was performed. Exemplar tiles were used for a comparison of data and it was assumed that the tiles did not contain any distinct features or damage. The window was obtained in the as-received condition, while the component's history was unidentified. After the accident however, researchers found three distinct oxide and metallic deposits [24] [19] [44]. Having the knowledge of these deposit formations, led to the investigation of the window TPS.

Several conclusions may be made on the degradation of the materials even if the component's history is unidentified. The TPS may fail easily when any stress is applied due to their extreme brittle property. Fractures and dents were anticipated as the component eventually collided with the ground. The carrier panel tiles were also compromised by the evidence of erosion which created a variety of porosity on the carrier panels (Figure 4.4 and Figure 4.7). The only damage to the thermal pane glass windshields appeared to be fractures of the glass. Next, it was determined that the surviving carrier panel tiles contained evidence of localized thermal damage. This is supported by the highly directional slumping observed [1] [10] [9] [44] on the tiles. This research has distinguished the behavior of TPS slumping. The slumping was a result of hot plasma traveling over the tile surfaces causing the coating to melt and deform along the flow direction and exposing the inner silica bulk fibers. The TPS should have remained intact as they were able to withstand high temperatures. This investigation also determined that overheating of the tiles caused slumping and there is a risk of a breach occurring as the coating may completely melt and cause

the inner silica to also melt (as in the case of the forward port side carrier panel). The temperature reached appears to be a lot higher than the protection provided by the black tiles (between 1,200F and 2,500F [5] [10] [9]). The results also showed scratches and dents, which were common occurrences in the past [10] [9] [5]. However, these common damages may have occurred before the accident. Areas of erosion were observed and the coating appeared to be extremely glassy (Figure 4.4) suggesting melting of the borosilicate glass coating. Areas of porosity especially on the inner lip sides of the tiles caused small open cavities. These small openings may have been precursors to the slumping phenomenon. If the window was exposed to high heat for a longer time, the TPS may have melted away. Future TPS requirements consisting of similar shuttle TPS systems, should be carefully examined for any damage as these materials can be affected by extreme conditions. Slumping was evident on all carrier panels and the flow appeared to travel from the aft to forward direction. Anomalous features of surface discolorations were discovered with molten metallic streaks. Elemental analysis was performed to answer initial questions of the identities of the discolorations present. Several elements were detected with the majority being aluminum, silicon, and titanium. The weight percentages of these elements only changed when measuring the discolorations. Usually, larger weight percentages of titanium were present only at the discolorations. The fractured thermal pane glass also contained evidence of a char layer [19] [24] with a variety of elements present as confirmed by the XRF results.

Moreover, the shuttle experienced thermal effects from the Earth's atmosphere as a result of the hypersonic velocity and friction from the atmosphere. The temperature of the flow is so high that the chemical bonds of the diatomic molecules of air are broken. Plasma is created when these molecules break apart. As the shuttle began to disintegrate while re-entering Earth's atmosphere, shuttle debris began to shed as described in the *Columbia* Accident Investigation Board. As heat entered through the shuttle, the once protected materials were exposed to high temperatures. The aerodynamic effects of materials used in the orbiter may have melted and caused deposits on the surfaces of various components. It is known

that the forebody (crew module) rotated as it broke apart from the vehicle [44]. This dynamic rotation may have caused materials to deposit in different directions such as the ones deposited on the tiles. The deposit formations on the carrier panel tiles and thermal pane glass show that metals used in the space shuttle were compromised thermally. Temperatures well above 3,000°F (1,648°C) were generated as the shuttle disintegrated and thereby affecting materials near the window.

7.2 Characterization of Deposits

Selected areas for samples were obtained from each carrier panel based on the XRF results. The tile samples were analyzed through several characterization techniques. The first set of samples were extracted from the forward port side carrier panel tile. The morphologies of the samples contained various features of an uneven and irregular coating surface when compared to the surface of the unaffected tile sample. Evidence of spherical deposits of once molten material containing high cavities was found on sample surfaces. A large presence of cracks originating from the upper surface of the tiles and other artifacts were observed. One sample (1.1B) had increased surface irregularity. The entire surface of the sample was not consistent with a flat uniform morphology. However, sample 1.2 and 1.3 had also retained a flat surface. Several oxides and elements were confirmed by surface EDS in major, minor, and trace amounts. The primary compositions found on the samples included titanium, oxygen, silicon, aluminum, calcium, and copper. Titanium, oxygen, and aluminum were the frequent major elements present on these surfaces. Further cross-sectional analysis was executed to examine the morphology and determine if these materials exist beneath the TPS surface. The tiles contained a large presence of spherical cavities and irregular pores that were mostly concentrated at the upper surface of the coating. They may have generated from extreme heating as small holes were pronounced during the visual inspection. These minuscule pores may have provided a path for the hot plasma to flow in and produce the pores or cavities. The microstructures regularly contained distinct light gray deposits with other phases nucleated within the deposits. A few of these smaller phases were found to be rich in copper, nickel, aluminum, titanium,

vanadium, or iron. The deposited layer was a mixture of titanium, oxygen, aluminum, silicon, and calcium. The order and location in which these materials deposited were revealed through individual X-ray maps. Most puzzling, sample 1.1A, had titanium deposited before aluminum and contained higher weight percentages than aluminum. The rest of the samples showed that several of these materials may have been deposited at the same time. Sample 1.3 had a change in the microstructure where dendrites with secondary branching formed. This can be explained through the process of solidification which associates the transformation of molten metal into a solid state [45]. This process depends on the alloy or pure element. Cooling of the molten metal causes crystals to grow as needles of solid metal [46]. Secondary branches or tertiary branches may occur on the primary crystal. They are formed when a small nucleus grows during undercooling and a perturbation of the interface forms ahead of the surrounding surface. The cells grow in specified crystallographic directions that depend on the metal's crystal structure. These dendrite crystals (Figure 6.33) were titanium rich and surrounded by a mixture of titanium oxide, silicon, aluminum, copper, and calcium.

The following set of samples analyzed were from the forward starboard side carrier panel. Their surface morphologies and chemistries were similar to those of the port side tiles. Their cross-sections confirmed the frequent light gray deposit layer with a chemistry that involved titanium, oxygen, silicon, calcium, aluminum, copper, and iron. Areas well below the upper surface of the TPS coating were consistent with silicon oxide. X-ray mapping also indicated that these materials deposited on the coating surface. Several samples had varied compositions where aluminum was not present at certain locations (sample 2.1.1A and 2.1.4). Spherical phases appeared within the deposited layer and were predominantly iron. The results of the aft tile specimens showed light surface deposits and dark areas of the coating. The aft tile had more surface degradation with highly uneven surfaces when analyzed through the SEM. A large presence of aluminum was encountered on sample 3.2. The rest of the EDS surface results from samples 3 and 4 contained titanium, oxygen, silicon, aluminum, calcium and traces of vanadium or iron.

Phases were formed within the microstructure of sample 3.1A with acicular grains and spherical features (Figure 6.67). Several of these acicular features contained the formation of branches similar to sample 1.3. Similarly, the dendritic phase was predominately titanium. Moreover, a deposited layer was once again present in the cross-sections of the samples (3 and 4). The elements that constructed this layer were identical to those found in the forward port and starboard tiles. However, aluminum particles were present at the upper surface of the coating and beneath it at the coating-to-silica interface (Figure 6.70). Iron also took part in composing the deposited layer whereas, in previous samples, it was present as few small spherical phases. The samples also had an alternating coating thickness and some areas almost reached the silica bulk fibers. Although one sample (3.1B) did not have an obvious deposit layer, deposits were still present well beneath the silica fibers (Figure 6.74 and Figure 6.75). Extremely large pores and cavities were present in the coating from samples 3.1A and 3.1B that made up the majority of the coating. Samples 4.1 and 4.2 also contained a deposited layer with aluminum being the only element to deposit on the bulk silica substrate.

The thermal pane glass was examined for identifying the opaque deposit present. The history of the thermal pane was also not provided thus it was assumed that any deposited materials did not exist before the accident occurred. The glass cross-section showed deposits formed at the surface with compositions of aluminum, titanium, silicon, and oxygen as the major amounts. Oxidized morphologies were found as well as intermetallic solid phases. The charred layer likely formed at high altitudes and temperatures and remained attached to the glass upon reaching the ground. Most of the char layer from the glass specimen contained small adhered deposits and were mostly composed of titanium oxide. This suggests that they were deposited prior to ground impact.

The generated XRD spectra from the surfaces of the TPS demonstrated the oxides present. When comparing the XRD spectra of the unaffected samples to the *Columbia* artifacts, the existence of various oxides and single elements were confirmed. The samples analyzed from the forward port carrier panels

contained TiO_2 and Al peaks. An intermetallic compound ($AlTi_2$) was present at the locations with visible metallic streaks. Changes in the phases were observed on the forward starboard carrier panel tiles in which SiO_2, TiO_2, Al_2O_3, and SiC compounds. These were found on the yellow and blue discolorations. The second area with less visible discolorations contained Al_2O_3, SiO_2, TiO_2, and $CaTiO_3$. XPS spectra of additional samples saved for this analysis provided the chemical states of the elements detected such as Ti, O, Ca, C, and Si. The sample obtained from the inner lip area, however, contained primarily TiO_2, Ti, and Al. The samples from the aft tile consisted of similar oxides. Except for additional oxides of $Al_6Si_2O_{13}$ and $Ca_4Fe_2Ti_2O_{11}$ were found. Other intermetallic compounds of $AlSi_2Ti_2$ and $AlTi_3$ also formed on the surface. These results verified the EDS results. A chemical environment resulting from extreme heating caused these materials to mix and accumulate on the surfaces and within cross-sections.

7.3 Materials Interactions

The reported temperature of the orbiter's external surface during re-entry reached up to 3,000°F (1,648°C) [5] [6]. The environment caused by the shuttle re-entering the atmosphere is such that a shock wave of dissociated air molecules (nitrogen and oxygen) collide with the surface of the shuttle and acquire very high heat energy [5] [47]. Oxygen and nitrogen molecules transfer heat to the shuttle by convection. Atoms recombine and form new molecules on the orbiter surfaces. When radiation and charged particles cause molecules to split, they often left by themselves as atomic oxygen. The reaction of oxidation of metals is very likely to occur. When materials are exposed to atomic oxygen, oxidation of their surfaces can occur and thus weaken components and alter their thermal characteristics [48]. Glass-type materials were chosen they rejected a majority of the chemical energy. When metals are exposed to high temperatures and an oxidizing gas, however, oxidation can occur by direct reaction with the gas. This creates an oxide layer or scale and the more exposure the material undergoes, the higher the oxidation rate [49]. Shuttle materials may have melted, oxidized, accumulated at exposed TPS and glass surfaces, and

penetrated beneath the tile coating. They may have penetrated by entering exposed pores on the coating surfaces. A final deposited layer was generated.

Because of the large weight percentage of Ti present, there are indications that Ti alloys may combust and oxidize under re-entry conditions [50] [51]. The dynamic motion of the shuttle caused the various changes in weight percent compositions of titanium. Other materials were also deposited as a result of the rotational motion or a flat spin. Translational and rotational accelerations may have caused the changes in weight percentages of the other materials detected. One possible source of titanium and its oxides may be the payload bay door latch rollers that are attached to the X_0582 bulkhead. Also, it is important to note that the bulkhead was not protected by TPS. The rollers are directly connected to the overhead windows of the crew module and are composed of an aluminum alloy, Ti-6Al-4V alloy, and an Inconel sleeve [44]. The Ti-6Al-4V alloy has a melting temperature of 3,000°F (1,649°C) which shows that temperatures above the melting point must have been reached. This requires a great deal of heat and it is evident on the door latch rollers, particularly the starboard side behind Window 7. The starboard roller contained evidence of erosion and melting. The melting temperatures of the known materials near the overhead windows [1] [50] were;

1. Inconel 718- 2,368°F (1298°C)
2. 2024 Aluminum Alloy- 1,082°F (583°C)
3. Ti-6Al-4V- 3,037°F (1,1669°C)

The presence of titanium oxides on all tile surfaces and cross-sections is perplexing as aluminum and Inconel alloys have lower melting temperatures than the titanium alloy. Thermal analysis was conducted as part of the *Columbia* Crew Survival Investigation Report on the rollers and they predicted that the hot gas flowed from aft to forward and caused these materials to accumulate [24] [44]. Additionally, the crew module also contained attachment fittings or x-links composed of Ti-6Al-4V alloys that were found to contain significant thermal damage [44] [51]. These components attached the crew module to the forward

fuselage and the midbody of the shuttle at four main attach points. One x-link contained severe mass loss, a melted the top flange, and a melted hole through the component. Further research shows that titanium alloys are highly reactive with oxygen and may ignite [51] [50]. Usually, because of their extremely high affinity for oxygen, beneficial oxide films are formed spontaneously and instantly when exposed to air [49]. Stable oxides consist of TiO_2 but may consist of mixture of other oxides such as Ti_2O_3, and TiO. The highly crystalline form of TiO_2 or rutile, is formed during high temperature oxidation of 600 to 800°C (1,110° to 1,470°F) [49]. Lower temperatures produce an amorphous form of TiO_2 or anatase. The rutile form of TiO_2 was consistently present on tile surfaces.

The forward fuselage of the crew module was constructed of 2024 aluminum skins, stringers, longerons, bulkheads, and frames [44]. The crew module was also constructed from welded 2219 aluminum panels and protected the forward fuselage. A thin oxide is formed when aluminum alloys are exposed to the atmosphere, which protects the material from further oxidation. However, this protective coating may be removed when exposed to certain conditions. The type of aluminum oxide frequently present on the tile specimens was the α- Al_2O_3 or corundum form. This type of oxide is a naturally passive film formed over aluminum surfaces [52] [49]. The 2000 series aluminum alloys contain copper as the main alloying element [49] [53]. The copper present at the TPS surfaces and deposit layer in the sample cross-sections may have originated from these aluminum alloys. Another possible source of copper was the vast electrical wiring system of the shuttle orbiter [6]. The large presence of silicon oxide is expected as the materials constructing the window were rich in silicon. The window frames were reinforced with silicone rubber, silicone seals, and an additional source of titanium. The deposited materials of iron and calcium could not be traced to their original source. The only known materials near the component were the aforementioned titanium, aluminum, and a large amount of silicon stemming from the tiles themselves.

7.4 Recommendations and Future Work

Although spacecraft today have new insulating material systems, this research attempted to examine how silica based TPS and thermal pane glass behave under unexpected conditions. Extreme temperatures are the largest threats to spacecraft. Further research consisting of simulating common aerospace materials in off-nominal conditions will provide important information for space safety. So many complex systems constructed the shuttle and it is important to minimize risks. In order to provide a complete risk assessment for future vehicles, additional aerospace materials must be examined as they may be precursors to accidents.

As previously mentioned, there are some sources of materials that were unidentified such as calcium, magnesium, and iron. Obtaining knowledge of all structural materials used in the vehicle may answer those questions, especially those surrounding the windows. It is essential to further understand the combustion and oxidation mechanisms of materials such as titanium alloys as they are common materials for high-temperature applications. Further investigation of the oxidation products may be beneficial.

The thermal protection system of the port side window was also available for research. Similar characterization studies may also be performed to find indications of deposits. As the orbiter windows were both recovered detached from each other, Window 8 may or may not have the deposits identified on Window 7. Additional characterization tools may be used such as Transmission Electron Microscopy (TEM) for obtaining additional chemistry of the deposit layers and verifying their thicknesses. TEM provides more details about internal properties of a material such as crystallization, morphology, and has much higher resolution than SEM. TEM is able to provide qualitative and quantitative elemental analysis of microstructural features as small as 30nm [40]. Thermogravimetric Analysis (TGA) [54] is an additional characterization tool that studies the mass of a material as a function of temperature or time. This analysis can be performed on a variety of debris and will show how heat affects the weight of a material. Information on weight loss, weight gain, due to decomposition and oxidation may be determined.

At last, the thermal pane glass could not provide enough powdered deposits for XRD to compare with the spectra of the tile surfaces. Powder XRD would yield results to compare with the spectra obtained from the tiles.

Spacecraft disasters may involve failures from management errors, design, safety errors, or material failures. Designers of the space shuttle *Columbia* did not expect the underlying materials to be exposed to the heat of re-entry. Re-entry is a critical part of spaceflight and risks of re-entry anomalies must be understood. Quality assurance becomes critical and one can never assume accidents won't occur. Stronger safety regulations must be put in place for future spaceflight missions. This forensic materials investigation provided a warning for future designers and operators of spacecraft. It is our moral duty to carefully investigate the causes of past accidents and how to prevent them.

References

[1] Columbia Accident Investigation Report (CAIB), vol. 1, NASA and the Government Printing Office Washington D.C., 2003.

[2] W. Hale, L. Helen, C. Gail and L. Kamlesh, Wings in Orbit: Scientific and Engineering Legacies of the Space Shuttle, NASA, 2011, pp. 182-199.

[3] T. L. and K. J.M., "Degradation behaviour of a composite material," *Journal of Materials Science,* vol. 33, pp. 3137-3143, 1998.

[4] B. Laub and E. Venkatapathy, "Thermal protection system technology and facility needs for demanding future planetary missions," *Planetary Probe Atmospheric Entry and Descent Trajectory Analysis and Science,* vol. 544, pp. 239-247, 2004.

[5] *NASA Facts Orbital Thermal Protection System,* NASA, FS-2004-09-014-KSC, 1997 (Rev. 2006), pp. , .

[6] "Shuttle Crew Operations Manual," United Space Alliance, 2004.

[7] J. Cleland and I. Francesco, "Thermal Protection System of the Space Shuttle," NASA, Office of Commercial Programs, 1989.

[8] D. Glass, "Ceramic matrix composite (CMC) thermal protection systems (TPS) and hot structures for hypersonic vehicles," in *15th AIAA International Space Planes and Hypersonic Systems and Technologies Conference*, 2008.

[9] R. L. Dotts, D. M. Curry and D. J. Tillian, "Orbiter Thermal Protection Systems," in *Space Shuttle Technical Conference, NASA CP-2342*, 1983.

[10] D. M. Curry, *Space shuttle orbiter thermal protection system design and flight experience,* NASA Technical Memorandum 104773, 1993, pp. 1-22.

[11] J. Hughes and D. McBride, "TPS is more than tiles," in *American Institute of Aeronautics and Astronautics, Thermophysics Conference, 18 th, Montreal, Canada*, 1983.

[12] M. P. Gordon, "Space Shuttle Orbiter Thermal Protection System Processing Assessment Final Report," TPS Orbiter Engineering Materials & Processes, 1995.

[13] J. Davis, Ed., ASM specialty handbook: heat-resistant materials, Materials Park, OH: ASM International, 1997, pp. 83-84.

[14] H. E. Goldstein, D. B. Leiser and V. Katvala, "Reaction cured glass and glass coatings". Patent 4,093,771, 6 June 1978.

[15] "NASA: Spaceflight," 2002. [Online]. Available: https://spaceflight.nasa.gov/shuttle/reference/shutref/orbiter/tps/frcitiles.html. [Accessed 3 January 2017].

[16] NASA, 20 August 2014. [Online]. Available: http://www.nasa.gov/content/engineers-and-technicians-install-protective-shell-on-nasa-s-orion-spacecraft.

[17] W. Ko, L. Gong and R. Quinn, "Hypothetical reentry thermostructural performance of space shuttle orbiter with missing or eroded thermal protection tiles," NASA/TM-2004-212850, 2004.

[18] J. Olivas, "Proposed Scope of Work," NASA, 2006.

[19] J. D. Olivas, P. Melroy, L. Schachel, L. Hulse, G. Morgan, T. Wallace, C. Zapata and S. McDanels, "OV-102 Thermal Pane Window Debris Analysis, part of Spacecraft Crew Survival Integration Investigation Report," NASA, SP-2008-565, 2008.

[20] K. S. Edelstein, "Orbital impacts and the Space Shuttle windshield," in *SPIE's 1995 Symposium on OE/Aerospace Sensing and Dual Use Photonics*, 1995.

[21] Y. Jiyun, Z. Jidong, G. Zizheng and P. Hewei, " Damage analysis for hypervelocity impact experiments on spaceship windows glass," *InEPJ Web of Conferences,* vol. 6, no. EDP Sciences, p. 39001, 2010.

[22] K. Bedingfield, R. D. Leach and M. B. Alexander, "Spacecraft system failures and anomalies attributed to the natural space environment," NASA Reference Publication 1390, 1996.

[23] R. P. Bernhard, E. L. Christiansen and J. C. J. L. Hyde, "Hypervelocity impact damage into space shuttle surfaces," *International journal of impact engineering,* vol. 17, no. 1, pp. 57-68, 1995.

[24] J. D. Olivas, M. C. Wright, D. M. C. R. Christoffersen and S. J. McDanels, "Crystallographic oxide phase identification of char deposits obtained from space shuttle Columbia window debris," *Acta Astronautica,* vol. 67, no. 5, pp. 553-560, 2010.

[25] A. Campece, M. Kinmonth, R. Chumakov and M. A. Deacon, "Failure Analysis of a Thermal Tile on hte Space Shuttle Columbia," *Journal of Failure Analysis and Prevention,* vol. 6, no. 1, pp. 55-60, 2006.

[26] D. B. Leiser, *Space shuttle thermal protection system,* vol. 83, American Ceramic Society Bulletin, 2004, pp. 44-47.

[27] D. E. Myers, C. J. Martin and M. L. Blosser, "Parametric weight comparison of advanced metallic, ceramic tile, and ceramic blanket thermal protection systems," NASA Technical Memorandum-210289, 2000.

[28] J. L. Shideler, N. H. Kelly, D. E. Avery, M. L. Blosser and H. M. Adelman, "Multiwall TPS- An Emerging Concept," in *AIAA Structural Dynamics Specialists Meeting*, Atlanta, 1981.

[29] M. L. Blosser, "Development of Metlalic Thermal Protection Systems for the Reusable Launch Vehicle," NASA Technical Memorandum 110296, Hampton, 1996.

[30] J. Shideler, H. Kelly, D. Avery, M. Blosser and H. Adelman, "Multiwall TPS An Emerging Concept," NASA Technical Memorandum 83133, Hampton, 1981.

[31] S. Johnson, M. Gasch, M. Stackpoole, J. Lawson and M. Gusman, "Recent developments in ultra high temperature ceramics at NASA Ames," in *16th AIAA/DLR/DGLR International Space Planes and Hypersonic Systems and Technologies Conference*, 2009.

[32] K. Wei, H. Rujie, C. Xiangmeng, Z. Rubing, P. Yongmao and F. Daining, "A lightweight, high compression strength ultra high temperature ceramic corrugated panel with potential for thermal protection system applications," *Materials & Design,* vol. 66, pp. 552-556, 2015.

[33] R. F. M. D. Savino, D. Paterna and M. Serpico, "Aerothermodynamic study of UHTC-based thermal protection systems," *Aerospace Science and Technology,* vol. 9, no. 2, pp. 151-160, 2005.

[34] E. Wuchina, E. Opila, W. Fahrenholtz and I. Talmy, "UHTCs: ultra-high temperature ceramic materials for extreme environment applications," *the electrochemical society interface,* vol. 16, pp. 30-36, 2007.

[35] S. Karlsdottir and J. Halloran, " Rapid Oxidation Characterization of Ultra-High Temperature Ceramics," *Journal of the American Ceramic Society,* vol. 90, no. 10, pp. 3233-3238, 2007.

[36] R. Savino, D. Fumo M.D.S: Paterna, A. Di Maso and F. Monteverde, "Arc-jet testing of ultra-high-temperature-ceramics," *Aerospace Science and Technology,* vol. 14, no. 3, pp. 178-187, 2010.

[37] B. Behrens and M. Muller, "Technologies for thermal protection systems applied," *Acta Astronautica,* vol. 55, pp. 529-536, 2004.

[38] J. I. Goldstein, D. E. Newbury, P. Echlin, D. C. Joy, C. Fiori and E. Lifshin, Scanning Electron Microscopy and X-Ray Microanalysis; a text for biologists, materials scientists, and geologists., New York: Plenum Press, 1981.

[39] J. F. Moulder, W. F. Stickle, P. E. Sobol and K. D. Bomben, Handbook of X-ray photoelectron Spectroscopy, J. Chastain, Ed., Perkin-Elmer Corporation, 1992.

[40] "Materials Characterization," in *ASM Handbook* , ASM International, 1986.

[41] J. J. Mecholsky, R. W. Rice and S. Freiman, "Prediction of fracture energy and flaw size in glasses from measurements of mirror size," *Journal of the American Ceramic Society,* vol. 57, no. 10, pp. 440-443, 1974.

[42] T. Ono and R. Allaire, *Fracture Analysis, a Basic Tool to Solve Breakage Issues,* Taiwan FPD Expo 2000, 2000.

[43] J. S. Coneille, J.-W. He and W. D. Goodman, "XPS characterization of ultra thin MgO films on a Mo (100) surface," *Surface Science,* vol. 306, pp. 269-278, 1994.

[44] "Columbia Crew Survival Investigation Report," NASA SP-2008-565, 2008.

[45] "Metallography and Microstructures," in *ASM Handbook*, Materials Park, OH: ASM International, 2004.

[46] R. Abbaschian, L. Abbaschian and R. E. Reed-Hill, Physical Metallurgy Principles, Cengage Learning, 2008.

[47] "Returning from Space: Re-entry," Federal Aviation Administration.

[48] "The Space Enviornment," Federal Aviation Administration.

[49] S. D. Cramer and B. S. Covino Jr, "ASM handbook volume 13b: corrosion: materials," in *ASM Handbook*, vol. 13, ASM International, 2005.

[50] J. D. Olivas, B. Mayeaux, P. Melroy and D. Cone, "Study of Ti Alloy Combustion Susceptibility in Simulated Entry Environments," in *Amaerican Institute of Aeronautics and Astronautics*, 2009.

[51] J. L. Buckner, *Investigation of Ti-6Al-4V Alloy Response to Atmospheric Re-Entry Exposure,* ProQuest 10239940, 2016.

[52] P. Brito, H. Pinto and A. Kistka, "The crystallographic template effect assisting the formation of stable α-Al2O3 during low temperature oxidation of Fe–Al alloys," *Corrosion Science,* vol. 105, pp. 100-108, 2016.

[53] F. C. Campel, Elements of metallurgy and engineering alloys, ASM International , 2008.

[54] A. Coats and J. Redfern, "Thermogravimetric analysis: A review," *Analyst,* vol. 88, no. 1053, pp. 906-924, 1963.

[55] J. Hyde, E. Christiansen and D. Lear, "Shuttle MMOD impact database," *Procedia Engineering ,* vol. 103, pp. 246-253, 2015.

[56] K. Cohen, N. E. Martian, R. M. Deacon and A. R. Marder, "Failure analysis of the Columbia space shuttle glass windshields," *Journal of Failure Analysis and Prevention ,* vol. 6, no. 1, pp. 61-66, 2006.

[57] A. Grosse and J. Conway, "Combusion of metals in oxygen," *Industrial & Engineering Chemistry ,* vol. 50, no. 4, pp. 663-672, 1958.

Vita

Brenda Arellano as born and raised in El Paso, TX. She earned her Bachelor of Engineering degree in Metallurgical and Materials Engineering in 2012. In the Fall of 2012, she joined the Materials Science and Engineering doctoral program. During graduate school, she was first appointed as a research assistant for an additive manufacturing based research for developing new 3D printed materials for Fused Deposition Modeling (FDM). A year later, she became appointed as a research assistant for the Center for the Advancement of Space Safety and Mission Assurance Research (CASSMAR).

While pursuing her undergraduate degree, she worked on research associated with high-temperature oxidation of Niobium-based alloys where she presented at international conferences; TMS 2012, MS&T 2011, and MS&T 2010. She also co-authored a publication for; *A comparison of the effect of Cr and Al additions on the oxidation behavior of alloys from the Nb–Cr–Si system*, Materials at High Temperatures 33, no. 2 (2016) 105-114.

During graduate school, she presented her project proposal to the materials group at the Kennedy Space Center in 2014. Afterwards, she secured a materials & process engineering intern position at KSC for the summer of 2015 where she was nominated by her mentor for NASA Intern of the Year. She also published and presented at the Great Minds in STEM HENAAC Conference in Fall 2016 and was a graduate student poster competition winner. In the same month, she published and presented her research at MS&T 2016. She has published a first author research paper of: "*Material Behavior of Window 7 Carrier Panel Tiles and Thermal Pane Glass Recovered from the Space Shuttle Columbia*," for Ceramic Transactions as part of the Thermal Protection Materials and Systems symposium of MS&T 2016. She is currently working on a second manuscript for Materials Characterization Journal. Recently, she has presented at the Southwest Emerging Technology Symposium 2017.

Permanent address: 3104 Glasgow Rd.

El Paso, TX, 79925

This thesis/dissertation was typed by Brenda R. Arellano.